Technische Universität Dresden
Fakultät Umweltwissenschaften
Institut für Grundwasserwirtschaft

Untersuchungen zur Steuerung der Mangankonzentration bei der Uferfiltration und Unterirdischen Enteisenung / Entmanganung

Dissertation
zur Erlangung des akademischen Grades
Doktor der Ingenieurwissenschaften (Dr.-Ing.)

Eingereicht von
Dipl.-Ing. (FH) Sebastian Paufler
geboren am 24.07.1990 in Pirna, Deutschland

Gutachter:
Prof. Dr. Rudolf Liedl
Prof. Dr.-Ing. Thomas Grischek
Prof. Dr. Mario Schirmer

Datum der Disputation: 19.02.2019

Europäische Union
Europa fördert Sachsen.
ESF
Europäischer Sozialfonds
Fördernummer 200031585

Erklärung zur Eröffnung des Promotionsverfahrens

1. Hiermit versichere ich, dass ich die vorliegende Arbeit ohne unzulässige Hilfe Dritter und ohne Benutzung anderer als der angegebenen Hilfsmittel angefertigt habe; die aus fremden Quellen direkt oder indirekt übernommenen Gedanken sind als solche kenntlich gemacht.
2. Bei der Auswahl und Auswertung des Materials sowie bei der Herstellung des Manuskripts habe ich Unterstützungsleistungen von folgenden Personen erhalten: Keine.
3. Weitere Personen waren an der geistigen Herstellung der vorliegenden Arbeit nicht beteiligt. Insbesondere habe ich nicht die Hilfe eines kommerziellen Promotionsberaters in Anspruch genommen. Dritte haben von mir weder unmittelbar noch mittelbar geldwerte Leistungen für Arbeiten erhalten, die im Zusammenhang mit dem Inhalt der vorgelegten Dissertation stehen.
4. Die Arbeit wurde bisher weder im Inland noch im Ausland in gleicher oder ähnlicher Form einer anderen Prüfungsbehörde vorgelegt und ist – sofern es sich nicht um eine kumulative Dissertation handelt – auch noch nicht veröffentlicht worden.
5. Sofern es sich um eine kumulative Dissertation gemäß § 10 Abs. 2 handelt, versichere ich die Einhaltung der dort genannten Bedingungen.
6. Ich bestätige, dass ich die Promotionsordnung der Fakultät Umweltwissenschaften der Technischen Universität Dresden anerkenne.

Dresden, 15.04.2019

(Unterschrift des Doktoranden)

Kurzfassung

Die Uferfiltration und die unterirdische Enteisenung / Entmanganung (UEE) sind bewährte Verfahren für die natürliche, unterirdische Voraufbereitung von Wasser. In Abhängigkeit von der Wasserbeschaffenheit und den geochemischen Eigenschaften des Grundwasserleiters können Redoxreaktionen, Sorptions- und Auflösungsprozesse oder eine ungünstige Bewirtschaftung der Brunnen bei beiden Verfahren zu erhöhten Mangankonzentrationen im Rohwasser führen. Erhöhte Mangankonzentrationen sind häufig für Verockerungsprozesse im Filterbereich der Brunnen und Ablagerungen in Pumpen und Steigleitungen verantwortlich. Diese beeinträchtigen den langfristigen Brunnenbetrieb und führen zu höheren Kosten der Wasseraufbereitung. Außerdem führt Mangan zur Färbung des Wassers und muss in der Trinkwasseraufbereitung auf < 0,05 mg/L verringert werden. Für Wasserwerksbetreiber ist die Kenntnis über die Ursache und das Verhalten von Mangan essentiell für einen optimalen Betrieb.

Die ägyptische Hauptstadt Kairo steht einem stark wachsenden Wasserbedarf gegenüber. Für die Bewertung einer möglichen Anwendung der Uferfiltration am Nil wurden vorhandene Versuchsbrunnen teufenabhängig beprobt und das Flusssohlsediment untersucht. Das Flusssohlsediment wies hohe Eisen- und Mangangehalte auf und wurde als Ursache für erhöhte Eisen-, Mangan- und Ammoniumkonzentrationen im Uferfiltrat identifiziert.

Für den Uferfiltrationsstandort Dresden-Tolkewitz wurde der Einfluss von Temperatur und Infiltrationsrate auf die Manganfreisetzung aus der Elbsohle untersucht. Betriebsdaten der Jahre 2006 bis 2016 und Säulenversuche bildeten die Grundlage. Die Manganfreisetzung wurde primär von der Temperatur kontrolliert, die Infiltrationsrate war weniger wichtig und verlor mit steigender Temperatur weiter an Bedeutung. Eine Manganfreisetzung wurde bei Wassertemperaturen von 20 °C und Infiltrationsraten von ≥ 0,3 $m^3/(m^2 \times d)$ ausgelöst.

Während der Inbetriebnahme eines UEE-Wasserwerks in Khabarovsk (Russland) wurde an einigen Brunnen eine intensive Manganfreisetzung beobachtet. Außerdem führte biologische Kolmation zu einem raschen Leistungsverlust und erforderte die Desinfektion der Brunnen. Die Auswertung der ersten 194 UEE-Zyklen eines Förderbrunnens und ergänzende Batchversuche ergaben, dass die Auflösung des im Grundwasserleiter vorhandenen, manganhaltigen Siderits die Ursache der Mn-Freisetzung war. Die Auflösungsprozesse hingen stark von der Korngröße des GWL-Materials und dem pH-Wert des Grundwassers ab. Die Filterkiesschüttung des Brunnens zehrte weniger als 1 % des infiltrierten Chlors und das Natriumhypochlorit drang ca. 2 bis 3,5 m in den Grundwasserleiter ein.

Das Wasserwerk Eggersdorf nutzt die UEE für die Voraufbereitung von eisenhaltigem Grundwasser und dient, entgegen den Empfehlungen für die UEE, der Abdeckung von Bedarfsspitzen. In einem Feldversuch wurde die mögliche Umnutzung der UEE-Brunnen für

die dauerhafte Grundwasserförderung getestet. Die dabei aufgetretene Manganfreisetzung wurde auf die chemische Reduktion von abgeschiedenen Mangan(hydr)oxiden durch eisenhaltiges Grundwasser zurückgeführt.

Abstract

Bank filtration and Subsurface Iron Removal (SIR) are proven technologies for the natural subsurface pre-treatment of water. Depending on the water quality and the geochemical properties of the aquifer, redox reactions, sorption and dissolution or unfavorable well management can lead to increased manganese concentrations in both treatment options. Increased manganese concentrations often cause filter screen clogging of the well or deposits in pumps and standpipes. This can affect the long-term well operation and lead to higher costs of water treatment. Furthermore, increased manganese concentrations can cause a coloring of the water and must be lowered to < 0.05 mg/l during drinking water treatment. For waterworks operators, the knowledge about the source and the behavior of manganese is essential for an optimal operation.

The Egyptian capital Cairo faces a growing water demand. To evaluate a potential riverbank filtration site, depth-dependent sampling at existing test wells was carried out and sediment samples from the Nile riverbed were taken. The riverbed sediment showed elevated iron and manganese contents and was identified as cause of increased iron, manganese and ammonium concentrations in the riverbank filtrate.

For the bank filtration site Dresden-Tolkewitz, the impact of temperature and infiltration rate on the manganese release from the riverbed sediment of the Elbe river was investigated. The investigations were based on monitoring data of the years 2006 to 2016 and column experiments. The manganese release was primarily controlled by temperature, the infiltration rate was less important. With increasing temperature, the infiltration rate became even less critical. Manganese was released at water temperatures of 20 °C and infiltration rates of ≥ 0.3 $m^3/(m^2 \times d)$.

During the start-up phase of a SIR waterworks in Khabarovsk, Russia, an intense manganese release was observed in several wells. In addition, biological clogging led to a rapid performance loss of the wells and required well disinfection. The evaluation of the first 194 SIR cycles of a production well and accompanying batch experiments indicated that the dissolution of the manganese-bearing siderite, which was present in the aquifer, caused the Mn release. The dissolution heavily depended on the grain size of the aquifer material and the pH of the groundwater. The filter gravel pack of the well consumed less than 1 % of the infiltrated chlorine and the sodium hypochlorite approximately penetrated between 2 and 3.5 m into the aquifer.

The waterworks Eggersdorf has been using SIR for the pre-treatment of ferrous groundwater and, contrary to general recommendations for SIR well operation, served for covering peaks in water demand. In a field trial, the possible conversion of the SIR wells for permanent groundwater extraction was tested. An observed manganese release was attributed to the chemical reduction of former precipitated Mn(hydr)oxides by iron-containing groundwater.

Danksagung

Die Dissertation wurde an der Hochschule für Technik und Wirtschaft Dresden (HTW Dresden), Lehrgebiet Wasserwesen, und in Kooperation mit dem Institut für Grundwasserwirtschaft der Technischen Universität Dresden (TU Dresden) durchgeführt. Die Dissertation wurde durch die Förderung des Europäischen Sozialfonds (ESF, Fördernummer 200031585) und der Abschluss durch die Förderung der Graduiertenakademie der TU Dresden (PSP-Element F-003661-553-Ü2A-2330000) ermöglicht.

Mein ganz besonderer Dank gilt Prof. Thomas Grischek, meinem Doktorvater und Betreuer seitens der HTW Dresden, für die Initiierung der ESF-Antragstellung, für die spannenden praxisnahen Teilaufgaben sowie das Vertrauen und die Freiräume bei der Bearbeitung. Die konstruktiven Diskussionen waren stets eine persönliche und fachliche Bereicherung.

Weiterhin gilt mein Dank meinem Betreuer seitens der TU Dresden, Prof. Rudolf Liedl, für die freundliche Unterstützung und die wertvollen Hinweise zur Struktur und Gestaltung der Arbeit.

Ein großer Dank gebührt auch der Arbeitsgruppe des Lehrgebiets Wasserwesen an der HTW Dresden. Rico Bartak danke ich für zahlreichen konstruktiven Gespräche und die Hinweise bei der Modellierung. Außerdem danke ich Fabian Musche für die lehrreichen Feldeinsätze in der Lausitz und Thomas Voltz für die große Hilfsbereitschaft bei der Verbesserung der englischsprachigen Artikel. Außerdem gilt mein Dank Prof. Ulrike Feistel, Dr. Cornelius Sandhu, Jakob Ebermann und Wolfgang Macheleidt. Die angenehme Atmosphäre hat die Arbeit sehr erleichtert. Die Fakultät Bauingenieurwesen stellte einen Arbeitsplatz und erforderliche Messtechnik zur Verfügung.

Danken möchte ich auch Yasmin Adomat, Nadine Seidel, Britta Weber, Marcos Benso und André Exner für die Unterstützung der Laborarbeiten.

Des Weiteren gilt mein Dank Prof. Jörg Feller (Bereich Chemieingenieurwesen, HTW Dresden) und Dr. Hilmar Börnick (Institut für Wasserchemie, TU Dresden) für die stets schnelle und zuverlässige Analyse der zahlreichen Proben.

Ebenfalls danke ich dem Team der Arcadis Germany GmbH: Dr.-Ing. Jobst Herlitzius für die Möglichkeit, in Khabarovsk zu arbeiten, Igor Leonhardt für die Hilfe vor Ort und Karsten Hiller für die zuverlässige Mitbetreuung der Säulenversuche in Khabarovsk.

Weiterhin bedanke ich mich bei Martin Ruppert und Lars Patzke vom Wasserverband Strausberg-Erkner für die Möglichkeit, das interessante Projekt im WW Eggersdorf zu begleiten und für die zuverlässige Probennahme.

Außerdem gilt mein Dank Thomas Fischer von der DREWAG Netz AG für die Unterstützung der Untersuchungen in Dresden-Tolkewitz.

Meiner Freundin Melanie danke ich für ihre Geduld und die Unterstützung bei der Anfertigung dieser Dissertation.

Inhaltsverzeichnis

Abkürzungsverzeichnis

Abkürzungen

AP	Außenpegel
BG	Bestimmungsgrenze
Br.	Brunnen
CWW	Containerwasserwerk
EGK	Ergiebigkeitskoeffizient
el. LF	elektrische Leitfähigkeit
FOK	Filteroberkante
FUK	Filterunterkante
GW	Grundwasser
GWL	Grundwasserleiter
GWM	Grundwassermessstelle
IP	Innenpegel
k_f-Wert	hydraulische Durchlässigkeit
$k_{f,Kol}$	hydraulische Durchlässigkeit einer Kolmationsschicht
k_{ox}, k_{nit}, k_{mn}	Reduktionskonstante unter Sauerstoff-, Nitrat-, und Mangan-reduzierenden Bedingungen
NMW	mittlerer niedrigster Wert der Wasserstände in einer Zeitspanne
OFW	Oberflächenwasser
Q	Durchfluss
T	Wassertemperatur
t_a	Aufenthaltszeit
UEE	Unterirdische Enteisenung und Entmanganung
UF	Uferfiltrat
v_a	Abstandsgeschwindigkeit
$V_{FÖR}$	Fördervolumen
V_{INF}	Infiltrationsvolumen
WW	Wasserwerk

Chemische Stoffe

Al	Aluminium
As	Arsen
Ca^{2+}	Calcium
Cl^-	Chlor
Cr	Chrom
Cu	Kupfer
Fe(II, III)	Eisen, ggf. zweiwertiges bzw. dreiwertiges Eisen
Fe^{2+}	Eisen(II)-Ion, gelöstes Eisen
K^+	Kalium
Mg^{2+}	Magnesium
Mn(II, IV)	Mangan, ggf. zweiwertiges bzw. vierwertiges Mangan
Mn^{2+}	Mangan(II)-Ion, gelöstes Mangan
Na^+	Natrium
NaClO	Natriumhypochlorit
NO_2^-	Nitrit
NO_3^-	Nitrat
O_2	Sauerstoff, zweiwertig
Pb	Blei
SO_4^{2-}	Sulfat
Zn	Zink

1 Einleitung

1.1 Ausgangssituation

Die Uferfiltration wird in vielen Ländern Europas (Bourg & Bertin, 1993; Grischek et al., 2002), den USA (Ray et al., 2003; Regnery et al., 2015), Afrika (Shamrukh & Abdel-Wahab, 2008; Blanford et al., 2010) und Asien (Hu et al., 2016, Sandhu et al., 2011) erfolgreich für die natürliche und kostengünstige Wassergewinnung eingesetzt. Neben der natürlichen Uferfiltration kann die Infiltration des Flusswassers durch die Wasserentnahme aus flussnahen Brunnen induziert werden. Der Pumpvorgang erzeugt einen hydraulischen Potenzial-gradienten vom Fluss in Richtung der Brunnen. Im Unterschied zur direkten Entnahme von Oberflächenwasser (OFW) finden bei der Uferfiltration entlang des Fließweges im Grundwasserleiter (GWL) vielfältige natürliche Reinigungsprozesse statt. So werden pathogene Mikroorganismen und andere Partikel weitgehend zurückgehalten, abbaubare organische Stoffe entfernt und gelöste Spurenmetalle durch Sorption bzw. Fällung teilweise immobilisiert (Gimbel et al., 2004; Hiscock & Grischek, 2002). Eine Reihe von Redoxprozessen entlang des Fließweges kann die Beschaffenheit des Uferfiltrats (UF) beeinträchtigen (Abb. 1).

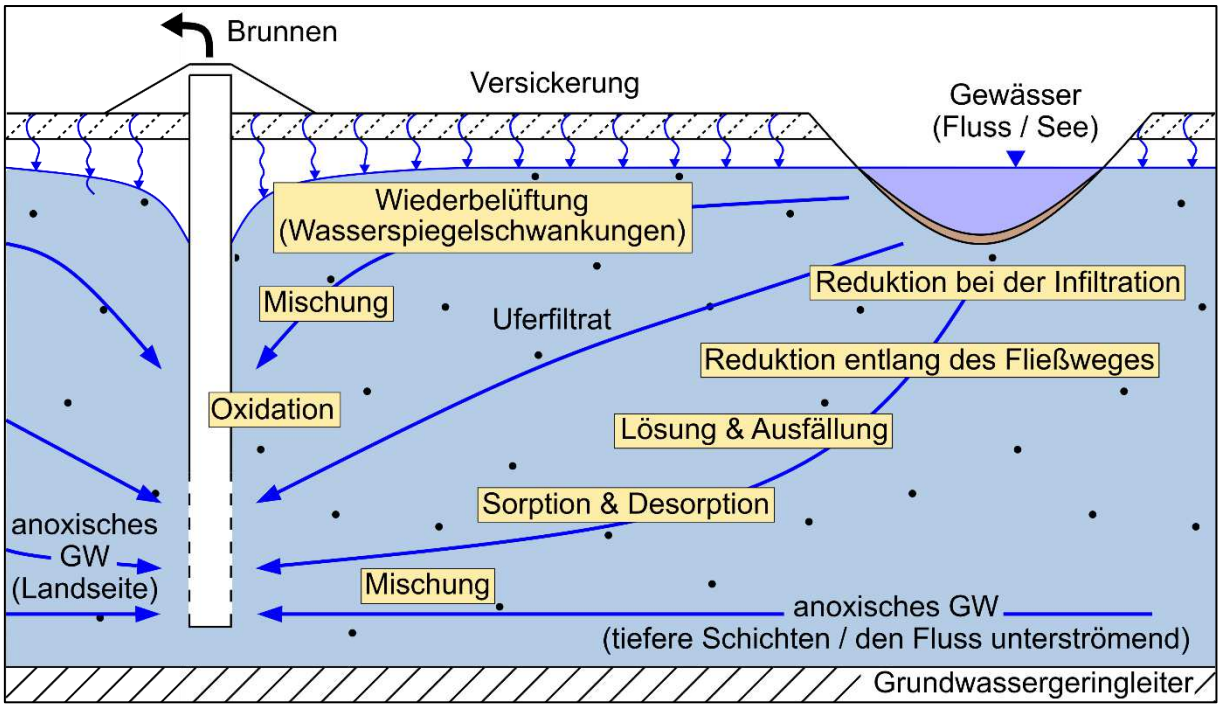

Abb. 1: Schema der Uferfiltration und den Mangangehalt beeinflussende Prozesse

Die Zehrung von gelöstem Sauerstoff (O_2), die Denitrifikation und die Reduktion von Mangan (Mn)-Verbindungen in der Flusssohle und im GWL kann zu erhöhten Mn-Konzentrationen im Uferfiltrat führen. In einem stärker anoxischen Milieu kann es auch zur Reduktion von Eisen (Fe)-Verbindungen und Sulfat (SO_4^{2-}) und zur Methanbildung kommen (Grischek, 2003; Stuyfzand, 2011). Die resultierende Mn-Konzentration im Uferfiltrat hängt von verschiedenen Randbedingungen ab, z. B. der Aufenthaltszeit (t_a), der Wassertemperatur (T) oder der Ausbildung einer Kolmationsschicht im Gewässer.

Eine weitere Technik der naturnahen Voraufbereitung ist die unterirdische Enteisenung und Entmanganung (UEE). Die UEE wird häufig für die Erschließung von eisen- bzw. mangan-reichen Grundwasservorkommen genutzt (Hallberg & Martinell, 1976; Rott et al., 2002) und kann mit der Uferfiltration gekoppelt werden (Ghodeif, 2011; Grischek et al., 2013). Bei der UEE wird mit Sauerstoff angereichertes Wasser in einen anoxischen GWL infiltriert (Abb. 2). Dadurch wird eine sogenannte Oxidations- oder Reaktionszone geformt (Abb. 3). Innerhalb dieser Zone werden gelöstes und adsorbiertes Fe(II) und Mn(II) zu Fe(III) und Mn(IV) oxidiert und als Metall(hydr)oxide abgeschieden (Abb. 4). Nach einer kurzen Ruhezeit von wenigen Stunden oder Tagen kann das Wasser zurückgepumpt werden. Aufgrund der großen Austauschkapazität der zuvor abgeschiedenen Metall(hydr)oxidschichten adsorbieren gelöstes Fe^{2+} oder Mn^{2+} an den Metall(hydr)oxidoberflächen und das Förderwasser ist weitgehend eisen- und manganfrei (Abb. 5, Rott et al., 2002; van Halem et al., 2012). Im Gegensatz zu herkömmlichen oberirdischen Wasseraufbereitungsanlagen bleiben die Oxidationsprodukte von Fe und Mn im GWL, eine kostenintensive Entsorgung oder Behandlung von Abfallprodukten entfällt. Außerdem haben UEE-Anlagen oft geringere Investitions- und Betriebskosten als oberirdische Aufbereitungsanlagen (Rott et al., 2002).

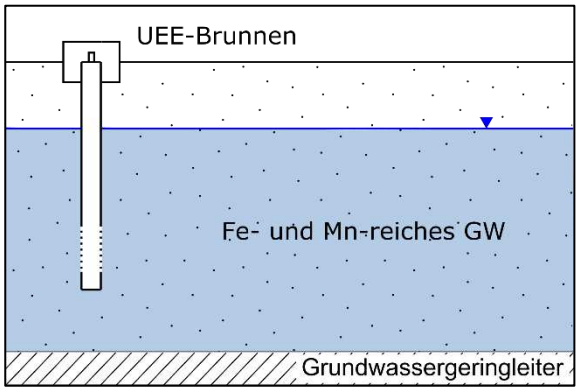

Abb. 2: Ausgangszustand vor der Inbetriebnahme eines UEE-Brunnens mit Fe- und Mn-reichem GW in einem anoxischen GWL

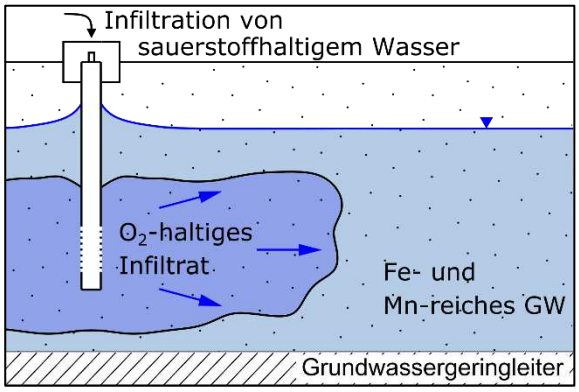

Abb. 3: Die Infiltration von sauerstoffhaltigem Wasser in den anoxischen GWL führt zu Bildung der Reaktionzone

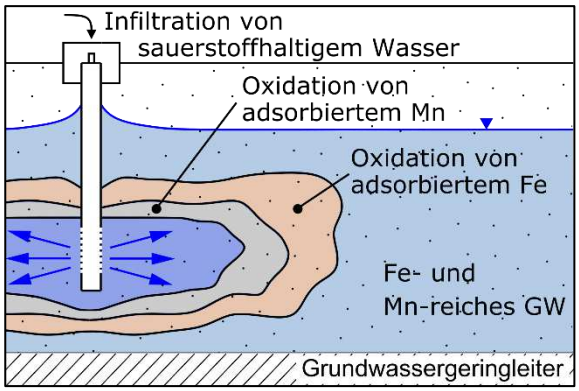

Abb. 4: Oxidation des an das GWL-Material adsorbierten Fe und Mn während der Infiltration

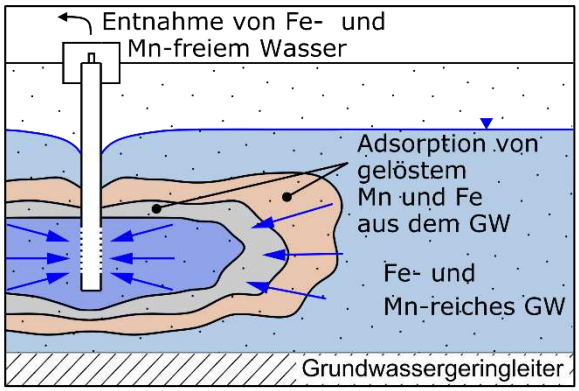

Abb. 5: Adsorption des Fe und Mn aus dem GW an die zuvor abgeschiedenen Fe- und Mn-(Hydr-)Oxide während der Entnahme

Erhöhte Mangankonzentrationen können zu Verockerungsprozessen im Filterbereich und zu Ablagerungen in Pumpen und Steigleitungen führen und den langfristigen Brunnenbetrieb beeinträchtigen. Außerdem führen erhöhte Mangangehalte im Rohwasser zu höheren Kosten der Wasseraufbereitung und sind auch bei Einhaltung der Trinkwassergrenzwerte für zeitweise Braunwasserbildung im Verteilungsnetz mit verantwortlich. Deshalb streben die erforderlichen Aufbereitungsschritte im Wasserwerk die Einhaltung des technisch begründeten Trinkwasser-Grenzwertes von 0,05 mg/L Mn an (TrinkwV, 2018). Die konventionelle, oberirdische Enteisenung und Entmanganung erfolgt häufig durch Oxidation, Flockung, Sedimentation und Filtration (Mutschmann & Stimmelmayr, 2007).

1.2 Motivation und Ziele

Aktuelle Prognosen deuten darauf hin, dass die Weltbevölkerung von heute ca. 7,5 Milliarden bis zum Jahr 2100 auf über 11 Milliarden Menschen ansteigen wird. Während für Europa ein leichter Bevölkerungsrückgang erwartet wird, wächst die Bevölkerung in anderen Regionen weiter und soll sich zum Beispiel in Afrika fast vervierfachen (UN, 2017). Bereits heutzutage verzeichnet die ägyptische Hauptstadt Kairo ein enormes Wachstum und leidet zunehmend unter der steigenden Bevölkerungsdichte. Um den dadurch steigenden Wasserbedarf decken zu können, möchte der Wasserversorger ein bestehendes Wasserwerk mit Oberflächenwasserentnahme im Stadtteil Embaba um Uferfiltrationsbrunnen erweitern. Im Jahr 2015 gebohrte Versuchsbrunnen wiesen erhöhte Mangankonzentrationen auf. Die Aufbereitung des manganhaltigen Uferfiltrats war mit der vorhandenen Aufbereitungstechnik für Oberflächenwasser aus dem Nil nicht erfolgreich. Auf Grundlage einer langjährigen Kooperation bat der Wasserversorger um Mithilfe bei der Ursachenfindung und Lösung des Problems.

Die gegenwärtigen Klimaprognosen deuten darauf hin, dass der Anstieg der Klimaextreme in manchen Regionen in Europa anhalten wird (EEA, 2016). Eine mögliche Folge dieser Klimaextreme können Änderungen der Mangankonzentration im Uferfiltrat sein (Diem, 2013; von Rohr, 2014; Sprenger et al., 2011). Im Wasserwerk Dresden-Tolkewitz werden erhöhte Mangankonzentrationen im Uferfiltrat der Elbe gemessen. Vorangegangene Untersuchungen wiesen darauf hin, dass die Mangankonzentration vom Wasserstand der Elbe beeinflusst wird (Paufler, 2015). Eine Bewertung bzw. Prognose der Mangankonzentration im Uferfiltrat, unter Berücksichtigung der möglichen Zunahme der Klimaextreme, ist bisher nicht möglich und würde zu einer Betriebsoptimierung beitragen.

Bei erhöhten Mangankonzentrationen im Rohwasser ist eine nachfolgende Entmanganung unerlässlich. Die UEE bietet Vorteile gegenüber der konventionellen oberirdischen Aufbereitung und erfordert vor allem bei der Inbetriebnahme eine gewissenhafte Betreuung. Die Einfahrphase und die Bildung und Position der Reaktionszone bestimmen den späteren Aufbereitungserfolg der UEE. Die Einfahrphase für die unterirdische Enteisenung kann nach

wenigen Tagen oder Wochen abgeschlossen sein, während die Einfahrphase für die unterirdische Entmanganung mehrere Monate dauern kann (Rott & Friedle, 2000, Rott et al., 2002). Im russischen Khabarovsk wird seit 2010 ein neues Wasserwerk für die Anwendung der UEE gebaut. Aufgrund von unerwarteter biologischer Kolmation ließ die Leistungsfähigkeit einiger Brunnen nach kurzer Zeit in Betrieb nach (Herlitzius, 2015; Braun et al., 2017). Um die Leistungsminderung zu begrenzen, wird das Infiltrationswasser chloriert, aber der tatsächliche Wirkungsradius des Chlors ist nicht bekannt. Darüber hinaus kam es während der Infiltrations- und insbesondere während der Förderphasen zu einer starken Freisetzung von Mangan aus der Reaktionszone. Das Wissen über die Ursache der Manganfreisetzung und über den Wirkungsradius der Desinfektion war die Voraussetzung für eine Prozessoptimierung.

Der demografische Wandel und der weiter rückläufige Wasserbedarf in vielen ländlichen Regionen in Deutschland sind eine Herausforderung bei der Erhaltung bzw. beim Umbau der Infrastruktur in der Wasserwirtschaft. Dies betrifft auch den Umbau von Uferfiltrat- und Grundwasserfassungsanlagen, den Rück- und Neubau von Brunnen und die Anpassung des Brunnenbetriebes. Im Fall des UEE-Wasserwerks Eggersdorf führen häufige Bedarfsspitzen zu einer ungleichmäßigen Auslastung und Nutzung der Brunnen, was den Empfehlungen für die Anwendung der UEE widerspricht. Die Umnutzung der UEE-Brunnen für die dauerhafte Förderung ist im Zuge einer geplanten Sanierung möglich und könnte einen wirtschaftlicheren Betrieb des Wasserwerks ermöglichen. Bisher sind in der Literatur keine Standortbeispiele für die dauerhafte Umstellung von UEE-Brunnen auf kontinuierliche Förderung dokumentiert, welche die Abschätzung einer möglichen Freisetzung von Mangan oder anderen Schwermetallen aus der ehemaligen Reaktionszone erlauben.

Aus den genannten praktischen Problemen in der Wasserwirtschaft ergeben sich folgende Ziele der Dissertation:

- Für den potenziellen Uferfiltrationsstandort in Embaba (Kairo) soll eine detaillierte Standorterkundung zur Ursachenermittlung der Manganfreisetzung beitragen. Auf Grundlage dessen soll die Anwendbarkeit der Uferfiltration am Standort beurteilt werden.
- Am Uferfiltrationsstandort Dresden-Tolkewitz soll der Einfluss der Temperatur und der Infiltrationsrate auf die Manganfreisetzung aus der Elbsohle bewertet werden.
- Für das neu gebaute UEE-Wasserwerk in Khabarovsk soll die Ursache für die Manganfreisetzung aus dem Reaktionsraum ermittelt werden. Weiterhin soll die effektive Reichweite des Desinfektionsmittels im Grundwasserleiter abgeschätzt werden.
- Für die geplante Sanierung des UEE-Wasserwerks in Eggersdorf soll die mögliche Manganfreisetzung bei einer Umstellung der Brunnen auf eine dauerhafte Förderung bewertet werden.

1.3 Gliederung der Arbeit

Die Dissertation ist wie folgt gegliedert: Der thematische Schwerpunkt der Kapitel 2-4 ist die Uferfiltration. Kapitel 2 beschreibt das Auftreten und Verhalten von Mangan bei der Uferfiltration. Anhand von weltweiten Standortbeispielen werden mögliche Eintragspfade von Mangan in das Uferfiltrat beschrieben. Darüber hinaus werden Einflussgrößen und mögliche Steuerungsgrößen des Mangangehalts im Uferfiltrat zusammengefasst. Im Kapitel 3 werden die Ergebnisse einer 5-tägigen Standorterkundung des potenziellen Uferfiltrationsstandortes in Kairo beschrieben. Kapitel 4 stellt die Ergebnisse der Untersuchungen zum Einfluss der Wassertemperatur und der Infiltrationsrate auf die Freisetzung von Mangan aus der Gewässersohle in Dresden-Tolkewitz dar.

Die Kapitel 5 & 6 befassen sich mit der unterirdischen Enteisenung und Entmanganung. Im Kapitel 5 werden die Ergebnisse von Untersuchungen zur Manganfreisetzung nach der Inbetriebnahme der UEE-Brunnen in Khabarovsk beschrieben. Darüber hinaus werden die Ergebnisse zur Untersuchung der Chlorzehrung bzw. zur Reichweite des Chlors in Khabarovsk zusammengefasst. Im Kapitel 6 werden die Erkenntnisse aus Untersuchungen zur Umnutzung der UEE-Brunnen im WW Eggersdorf dargestellt.

Abschließend werden im Kapitel 7 die Hauptergebnisse der Dissertation zusammengefasst und ein Ausblick auf den zukünftigen Forschungsbedarf gegeben.

Die vorliegende Dissertation ist eine Zusammenfassung von bereits veröffentlichten Artikeln in nationalen und internationalen wissenschaftlichen Zeitschriften. Die relevanten Publikationen sind der Arbeit beigelegt. Alle Publikationen durchliefen ein Gutachterverfahren (peer-review). Verweise auf beiliegende Publikationen sind mit [P] gekennzeichnet. Eine Liste der Publikationen ist ab Seite 29 zu finden.

2 Auftreten und Verhalten von Mangan bei der Uferfiltration

2.1 Eintragspfade von Mangan in das Uferfiltrat

Das Rohwasser von Brunnen für die Uferfiltration besteht aus drei Wässern, welche meist verschiedene Beschaffenheiten aufweisen. Das Uferfiltrat, als Synonym für das infiltrierende Flusswasser, und landseitig zuströmendes Grundwasser sind an den meisten Standorten die Hauptkomponenten des Rohwassers. Den Fluss unterströmendes Grundwasser hat oft den geringsten Anteil und ist an vielen Uferfiltrationsstandorten gar nicht vorhanden (Abb. 1, Paufler & Grischek, 2018) [P1]. Infolge einer Reihe von Redoxreaktionen werden an Uferfiltrationsstandorten auf der ganzen Welt erhöhte Eisen- und Mangankonzentrationen im Rohwasser der Brunnen gemessen (z.B. Bourg & Richard-Raymond, 1994; Henzler et al., 2016; von Gunten et al., 1991). Das Wissen über die Herkunft und das Verhalten von Eisen und Mangan ist für Wasserwerksbetreiber Voraussetzung für eine Prognose der Rohwasserkonzentration und für die Betriebsoptimierung (Grischek & Paufler, 2017) [P2].

Die Beschaffenheit des Rohwassers bei der Uferfiltration wird primär durch vier Faktoren gesteuert: (1) Reduktionsprozesse in der Flusssohle und in Ufernähe, (2) Adsorptions- und Desorptionsprozesse, (3) Auflösung und Ausfällung von Mineralen im Grundwasserleiter und (4) Oxidationsprozesse in der Umgebung der Brunnen (Farnsworth & Hering, 2011).

Der Übersichtbeitrag von Paufler & Grischek (2018) [P1] zeigt, dass die rein chemische Reduktion von Manganoxiden bei der Uferfiltration kaum relevant ist. Die mikrobielle Reduktion ist fast immer Ursache der Manganfreisetzung. Entlang des Fließweges vom Fluss zu den Brunnen kann das mobilisierte Mn durch Ausfällung als Mangancarbonat ($MnCO_3$, Rhodochrosit) wieder festgelegt werden. Dies wird oft bei langen Fließstrecken und Aufenthaltszeiten angenommen. Die Annahme beruht meist auf der Beobachtung einer übersättigten Lösung im Hinblick auf $MnCO_3$ (Massmann et al., 2004) und nicht auf tatsächlich vorgefundenen Ausfällungsprodukten. Da die Ausfällung als Rhodochrosit sehr langsam abläuft (Jensen et al., 2002), beeinflusst diese Reaktion die Mn-Konzentration nicht in den ersten Monaten nach Inbetriebnahme einer Uferfiltratfassung. Jensen et al. (2002) zeigen auch, dass die Übersättigung nicht zwangsläufig eine Ausfällung als $MnCO_3$ zur Folge hat. Beispielsweise kann die Bildung von organischen Komplexen gelöstes Mn in Lösung halten.

Im Grundwasserleiter vorhandene Oxide können gelöstes Mn durch Adsorption und eine darauffolgende Oxidation immobilisieren. Die Sorptionsvorgänge laufen häufig unter Ionenaustausch ab und sind innerhalb weniger Stunden abgeschlossen. Die Adsorption von Mn^{2+} an MnO_2 bewirkt eine Oxidation über Autokatalyse und ist teilweise umkehrbar. Durch die Autokatalyse verläuft die Festlegung des Mangans schneller. Da die chemische Oxidation durch Sauerstoff bei pH < 8 langsam verläuft, ist diese für die Uferfiltration irrelevant.

2.2 Einflussgrößen auf den Mangangehalt im Uferfiltrat

Der Vergleich weltweiter Uferfiltrationsstandorte in Paufler & Grischek (2018) [P1] zeigt, dass Mn-Konzentrationen zwischen 0,4 und 1,6 mg/L typisch für viele Uferfiltrationsstandorte sind. Folgende Faktoren steuern maßgeblich die Mangankonzentration im Rohwasser von Uferfiltratbrunnen (Abb. 6, Paufler & Grischek, 2018) [P1]:

- **Das Redoxmilieu.** An den meisten Standorten stellt sich ein anoxisches Redoxmilieu ein, selten wird eine Sulfatreduktion beobachtet. Erhöhte Mn-Konzentrationen im Uferfiltrat werden fast immer auf die Reduktion von Mangan(hydr)oxiden zurückgeführt.
- **Die Entfernung zwischen Gewässer und Brunnen.** An vielen Uferfiltrationsbrunnen befinden sich die Brunnen 30 bis 260 m vom Fluss entfernt. Bis zu einer Entfernung von 75 m zum Fluss sind Mn-Konzentrationen zwischen 0,3 und 1,1 mg/L im Rohwasser üblich. Brunnen, die weiter als 75 m entfernt vom Gewässer gebaut wurden, weisen oft Konzentrationen von 0,5 bis 1,8 mg/L Mn auf.
- **Die Aufenthaltszeit.** Aufenthaltszeiten zwischen 15 und 165 Tagen sind typisch für viele Uferfiltrationsstandorte. Fließwege bis zu 5 km und Aufenthaltszeiten von fast 100 Jahren, wie beispielsweise in Poldergebieten, führen zu stark reduzierenden Verhältnissen und bis 9 mg/L Mn im Rohwasser (Massmann et al., 2004).
- **Der Zustrom von landseitigem Grundwasser.** Die Mischung und Verdünnung von manganhaltigem Uferfiltrat mit manganarmem Grundwasser können zu einer Verringerung der Mn-Konzentration führen. Wenn das landseitige GW einen hohen Mn-Gehalt aufweist, kann die Verdünnung durch manganärmeres Uferfiltrat die Rohwasserqualität verbessern. Die Kolmation der Gewässersohle, der Abstand zwischen dem Gewässer und den Brunnen, die Pumpraten der Brunnen und die Mächtigkeit des GWL beeinflussen den Uferfiltratanteil sowie die Aufenthaltszeiten. Über die Festlegung der Brunnenstandorte und der Pumpraten kann somit die Rohwasserqualität gesteuert werden.
- **Sauerstoffgehalt, pH-Wert und Temperatur des Oberflächenwassers.** Bei einem Sauerstoffgehalt von mehr als 10 mg/L und einem pH-Wert > 7,8 des Oberflächenwassers wurden an vielen Standorten geringere Mangankonzentrationen gemessen als an sauerstoffärmeren und saureren Gewässern. Saisonal höhere Temperaturen führen häufig zu einer stärkeren Manganfreisetzung während der warmen Sommermonate.
- **Brunnenbetrieb und Betriebsdauer**. Bei erhöhten Mn-Konzentrationen im Uferfiltrat kann eine gesteigerte Pumprate den Uferfiltratanteil erhöhen und die Mn-Konzentration im Rohwasser verzögert ansteigen. An Seen kann die Eutrophierung zu reduzierenden Verhältnissen in und unter der Gewässersohle führen und die Mn-Konzentration im Uferfiltrat verzögert ansteigen.

  Nach mehreren Jahrzehnten mit kontinuierlichem Brunnenbetrieb wurde an einem Uferfiltrationsstandort an der Elbe eine Verringerung der Mn- und Fe-Konzentration im

Rohwasser beobachtet (Grischek & Paufler, 2017) [P2]. Wenn das landseitige GW erhöhte Mn-Konzentrationen aufweist und der Brunnen temporär außer Betrieb genommen wird, kann das GW den Brunnen überströmen und nach der Wiederinbetriebnahme zu anfangs erhöhten Konzentrationen führen.

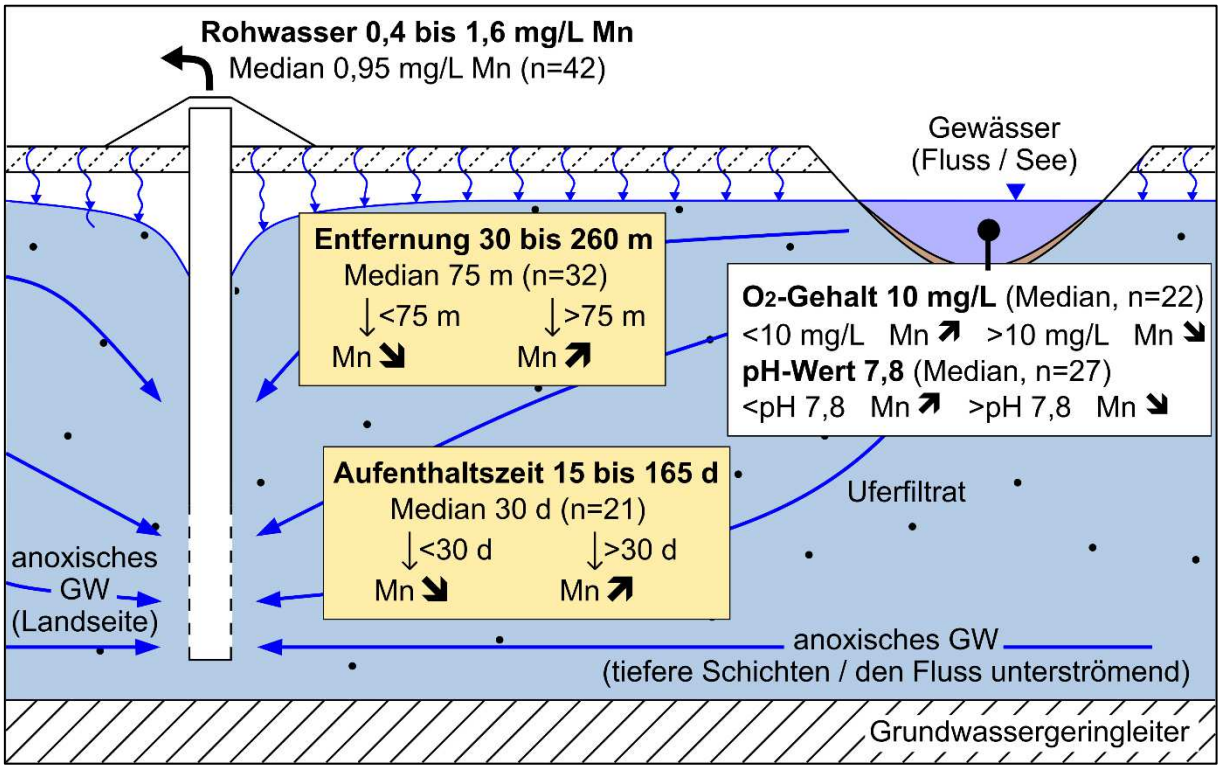

Abb. 6: Einflussgrößen auf den Mangangehalt im Rohwasser von Uferfiltrationsbrunnen (nach Paufler & Grischek, 2018) [P1]

3 Erkundung eines neuen Uferfiltrationsstandortes in Embaba

3.1 Einleitung und Standortbeschreibung

Die ägyptische Hauptstadt Kairo verzeichnet ein enormes Wachstum und leidet zunehmend unter der steigenden Bevölkerungsdichte. Der Wasserbedarf von Kairo wird momentan durch Oberflächenwasser (OFW) aus dem Nil gedeckt. Eines der größten Wasserwerke in Kairo befindet sich im Stadtteil Embaba und wird von der Holding Company for Water and Wastewater (HCWW) betrieben (Abb. 1 in Ghodeif et al., 2018) [P3]. In Embaba werden täglich ca. 1,2 Millionen m³ OFW aus dem Nil entnommen und durch Filtration, Vorchlorung, Flockung, Sedimentation, Schnellsandfiltration und Desinfektion aufbereitet.

Um den steigenden Wasserbedarf von Kairo zu decken, soll das bestehende Wasserwerk in Embaba erweitert werden und zusätzlich 200.000 m³/d Trinkwasser produzieren. Aufgrund des hydraulischen Gefälles zum Landesinneren infiltriert das Nilwasser natürlicherweise in den GWL. Für die Untersuchung der Anwendbarkeit der (induzierten) Uferfiltration für die Erweiterung des WW in Embaba wurde der Standort erstmals im Jahr 2012 erkundet (Bartak et al., 2014). Proben des Grund- und Nilwassers sowie vom Flusssohlsediment wiesen auf ungünstige Bedingungen für die Anwendung der Uferfiltration hin. Die Ablagerung von Feinsediment hinter dem Einlass für die OFW-Entnahme aus dem Nil und eine daraus resultierende Kolmation der Flusssohle wurde als Hauptproblem identifiziert. Da die Kolmation einer Flusssohle häufig die Qualität sowie die gewinnbare Wassermenge beeinträchtigt (Schubert, 2002; Grischek & Bartak, 2016), wurde der Bau eines Versuchsbrunnens empfohlen. Im Jahr 2015 wurden sechs Brunnen entlang des Nils gebohrt, um die Anwendbarkeit der Uferfiltration in Embaba zu untersuchen (Abb. 2 in Paufler et al., 2018b) [P4]. Ghodeif et al. (2018) [P3] beschreiben die hydrogeologischen Verhältnisse sowie den Ausbau der 6 Versuchsbrunnen in Embaba. In Paufler et al. (2018b) [P4] werden die Ergebnisse einer 5-tägigen Felduntersuchung mit einem Stufenpumpversuch und einer teufenabhängigen Probennahme während des laufenden Pumpenbetriebes dargestellt. Ein vereinfachtes Grundwasserströmungsmodell half, die Eignung von Embaba als Uferfiltrationsstandort zu bewerten.

3.2 Teufenabhängige Probennahme während des regulären Betriebes

Für das reguläre Monitoring der Versuchsbrunnen in Embaba werden die Wasserproben am Ende der Steigleitung an einem Probennahmehahn entnommen. Das heißt, jede Wasserprobe ist eine Mischprobe aus Uferfiltrat und Grundwasser, welches in den 24 m langen Filter eintritt. Eine teufenabhängige Probennahme ermöglicht es, bestimmte Abschnitte mit unterschiedlichen Wasserqualitäten entlang des Filterbereiches zu lokalisieren (z.B. Landon et al., 2010). Für die teufenabhängige Probennahme in Embaba wurde ein Kunststoffschlauch (d = 3 mm) mit einem Sinterfilter (200 µm) bestückt und an eine Peristaltikpumpe angeschlossen. Um den Betrieb der Brunnen nicht zu unterbrechen, wurde der Schlauch mit

dem Sinterfilter durch den Innenpegel (IP) an der Pumpe vorbeigeführt. Die Wasserproben wurden von Filterunterkante (FUK) bis zur Filteroberkante (FOK) im Abstand von 5 m entnommen. Die Abb. 5 in Paufler et al. (2018b) [P4] zeigt die Ergebnisse der teufenabhängigen Probennahme für einen Brunnen in der Mitte der Wasserfassung (Br. 3) und einen der äußeren Brunnen (Br. 6).

Entlang der unteren 20 m des Filterbereiches von Br. 3 und Br. 6 variierte die Mangankonzentration zwischen 0,60 und 0,71 mg/L. Die Eisenkonzentration zeigte einen deutlichen Anstieg um etwa 0,5 mg/L im Abstand von 5 m über der FUK und verringerte sich in Richtung der FOK. Entlang der oberen 5 m des Filterbereiches von Br. 3 stiegen Fe und Mn auf 0,45 und 0,97 mg/L an. Mangan entlang des Filterbereiches von Br. 6 blieb mit 0,62-0,64 mg/L nahezu stabil. Mischungsrechnungen berücksichtigten die einströmenden Wassermengen und stützten die Ergebnisse (Abb. 6 in Paufler et al., 2018b) [P4]. Ammonium (NH_4^+) im Rohwasser der Brunnen war generell erhöht (Tab. 2 in Paufler et al., 2018b) [P4].

Die Ergebnisse der teufenabhängigen Probennahme trugen zum Verständnis der hydrogeologischen und hydrogeochemischen Verhältnisse in Embaba bei und wurden beispielsweise auch erfolgreich im Uferfiltrat-Wasserwerk in Dresden-Hosterwitz angewendet (Paufler, 2015). Ein Vorteil der vorgestellten Technik gegenüber herkömmlichen Methoden für die teufenabhängige Probennahme (Packer) ist der geringere Zeit- und Materialaufwand. Das aufwändige Ziehen der Steigleitung und der Pumpe entfällt. Darüber hinaus werden die stationären Anströmverhältnisse während des regulären Brunnenbetriebes nicht gestört.

3.3 Ursache der Manganfreisetzung und Bewirtschaftung des Standortes

Die Ergebnisse der teufenabhängigen Probennahme während des regulären Brunnenbetriebes und von zusätzlichen Sedimentprobennahmen weisen auf die Flusssohle des Nils als Quelle für das Mangan im Uferfiltrat hin. Außerdem ist die Organik-reiche Flusssohle eine potenzielle Quelle für die erhöhten Eisen- und Ammoniumkonzentrationen im Uferfiltrat.

Mit Hilfe eines vereinfachten Grundwasserströmungsmodells wurden Szenarien für die Kolmation der Flusssohle und den Ausbau der Brunnen simuliert. Die kalibrierte hydraulische Durchlässigkeit der Kolmationsschicht ($k_{f,Kol}$) betrug 5×10^{-6} m/s. Der Vergleich mit anderen UF-Standorten, z.B. Dresden (Grischek & Bartak, 2017), zeigte, dass die kalibrierte $k_{f,Kol}$ für Embaba optimistisch geschätzt ist und die tatsächliche hydraulische Durchlässigkeit wahrscheinlich geringer ist.

Die Erkenntnisse aus der Modellierung können wie folgt zusammengefasst werden:

1. Die Aufenthaltszeiten vom Nil zu den Brunnen sind wahrscheinlich bis zu 4-mal länger als die kalibrierten Aufenthaltszeiten von 11 bis 22 Tagen.

2. Auf Grundlage der Modellergebnisse und unter Berücksichtigung der tiefen Filterposition sowie der Ergebnisse der teufenabhängigen Probennahmen wird ein Grundwasserzustrom vom anderen Ufer des Nils vermutet (Unterströmung).
3. Diese Unterströmung trägt zu den erhöhten Eisenkonzentrationen im Rohwasser bei.
4. Auch wenn in Embaba eine natürliche Uferfiltration auftritt, ist der Uferfiltratanteil wahrscheinlich geringer als 60 %. Das Uferfiltrat wird mit dem den Nil unterströmenden Grundwasser gemischt.
5. Ein nur 5 m langer und etwa 10 m höherer Filterbereich würde den Uferfiltratanteil nur geringfügig erhöhen und wäre nicht sinnvoll. Grischek (2003) kam zu einer ähnlichen Schlussfolgerung für Uferfiltratwasserwerke in Dresden-Tolekwitz, Meißen-Siebeneichen und Torgau.
6. Das Ausbaggern des stark kolmatierten Bereiches hinter dem Einlass des OFW mit einem vorhandenen Schiffsbagger kann zu einer besseren Beschaffenheit des Uferfiltrats beitragen. Das Ausbaggern würde die wahrscheinliche Quelle der erhöhten Mn-Konzentrationen entfernen und die hydraulische Durchlässigkeit der Flusssohle verbessern.

4 Einfluss der Infiltrationsrate und der Temperatur auf die Manganfreisetzung aus der Elbsohle in Dresden

4.1 Einleitung und Standortbeschreibung

Aktuelle Klimaprognosen sind für viele Uferfiltrationsstandorte besorgniserregend (Diem, 2013; Sprenger et al., 2016). Langanhaltende Trockenperioden verringern den Durchfluss in Flüssen, führen zu längeren Aufenthaltszeiten des Uferfiltrats und fördern anaerobe Bedingungen entlang des Fließweges. Überschwemmungen führen oft zu verkürzten Aufenthaltszeiten und ggf. zu Durchbrüchen von Krankheitserregern und organischen Spurenstoffen. Die Europäische Umweltagentur vermutet, dass der Anstieg der Klimaextreme in Europa in einigen Regionen anhalten wird. Diese sind geprägt durch häufigere Hitzewellen, langanhaltende Trockenperioden, Starkniederschlagsereignisse und Überschwemmungen (EEA, 2016).

Das Wasserwerk Dresden-Tolkewitz liegt an der oberen Elbe in Sachsen, Deutschland (Abb. 1 in Paufler et al., 2018c) [P5]. Drei Heberleitungen mit 72 Brunnen liefern bis zu 36.000 m³ Rohwasser pro Tag. Der Uferfiltratanteil beträgt etwa 83 % bei Mittelwasser und 70 % bis 75 % bei Niedrigwasser der Elbe. Die Aufenthaltszeit liegt bei 24 bis 30 Tagen (Ahrns, 2008). Im Fokus der Untersuchungen stand eine 95 m lange Stromröhre zwischen der Elbe und dem Heber III des WW Dresden-Tolkewitz. In der Stromröhre befinden sich drei Grundwassermessstellen, die in je drei Teufen verfiltert sind. Paufler et al. (2018c) [P5] beschreiben die Ergebnisse der Untersuchungen zum Einfluss der Wassertemperatur und der durchflussabhängigen Infiltrationsrate auf die Manganfreisetzung aus der Flusssohle der Elbe in Dresden-Tolkewitz. Beschaffenheitsdaten der Jahre 2006 bis 2016 von den GWM entlang der Stromröhre waren die Grundlage der Untersuchungen. Weiterhin wurde die Manganfreisetzung aus der Flusssohle durch Säulenversuche für vier Wassertemperaturen der Elbe (10, 20, 30 und 35 °C) und drei Infiltrationsraten (0,3, 0,6 und 1,1 m³/(m²×d)) quantifiziert.

4.2 Einfluss der Temperatur auf die Manganfreisetzung

Die Wassertemperatur der Elbe und die meisten relevanten Redoxparameter entlang der Stromröhre zeigten starke saisonale Schwankungen (Abb. 2 & 3 in Paufler et al., 2018c) [P5]. Die Mn-Konzentration entlang der Stromröhre variierte vor allem in der flussnächsten GWM am Messpunkt der obersten Teufe (GWM1-1 in Paufler et al., 2018c) [P5]. Im Winter war die Mn-Konzentration in der GWM 1-1 sehr niedrig, stieg aber im Sommer auf bis zu 0,42 mg/L an. An fast allen anderen Messpunkten entlang der Stromröhre zeigte die Mn-Konzentration kaum saisonale Schwankungen. Die Mn-Konzentration war immer > 0,1 mg/L und meist < 0,35 mg/L (Tab. S4 in Paufler et al., 2018c) [P5]. An Uferfiltrationsstandorten in Frankreich und der Schweiz wurden ähnliche Trends in flussnahen Messstellen beobachtet (Bourg & Bertin, 1994; von Gunten et al., 1994).

Die Ergebnisse der Säulenversuche wiesen auf eine starke Temperaturabhängigkeit der Mn-Freisetzung hin (Abb. 7). Bei konstanten Infiltrationsraten (0,3 bis 1,1 m³/(m²×d)) nahm die Mn-Konzentration mit steigender Temperatur zu (auch Abb. 5 in Paufler et al., 2018c) [P5]. Bei hohen Infiltrationsraten (1,1 m³/(m²×d)) stieg die Mn-Konzentration von << 0,2 auf > 0,5 mg/L an, nachdem die Temperatur von 30 auf 35 °C anstieg. Bei mittleren und niedrigen Infiltrationsraten (0,6 und 0,3 m³/(m²×d)) stieg die Mn-Konzentration an, nachdem die Wassertemperatur von 20 auf 30 °C anstieg.

Im Anschluss an die Säulenversuche wurden die Reduktionskonstanten für Sauerstoff (k_{ox}), Nitrat (k_{nit}) und Mangan (k_{mn}) durch chemische Modellierung mit PHREEQC (Parkhurst & Appelo, 2013) bestimmt. Für hohe Infiltrationsraten zeigte die kalibrierte Reduktionskonstante k_{mn} einen 20-fachen Anstieg von 30 auf 35 °C und spiegelt die Ergebnisse der Säulenversuche wider. Bei mittleren und niedrigen Infiltrationsraten war k_{mn} 15- und 17-mal höher, nachdem die Temperatur von 20 auf 30 °C anstieg (Tab. 3 in Paufler et al., 2018c) [P5].

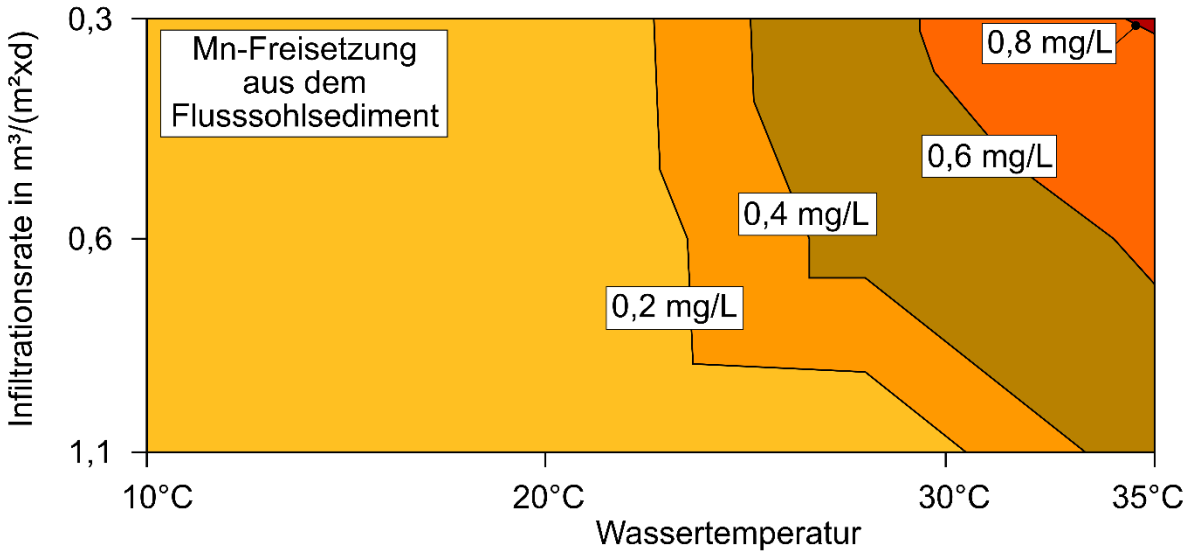

Abb. 7: Manganfreisetzung aus dem Sediment der Elbsohle in Abhängigkeit der Infiltrationsrate und Wassertemperatur während der Säulenversuche

4.3 Einfluss der Infiltrationsrate auf die Manganfreisetzung

An den meisten Uferfiltrationsstandorten hängen die Infiltrationsraten von den Entnahmeraten der Brunnen und der Kolmation der Flusssohle ab. Weiterhin beeinflussen der Flusswasserstand, die Entfernung zwischen dem Fluss und den Brunnen sowie die Infiltrationsfläche die Infiltrationsraten und somit die Manganfreisetzung.

Der Pegel der Elbe zeigt starke saisonale Schwankungen, ähnlich der Wassertemperatur. Niedrigwasserverhältnisse der Elbe sind gekennzeichnet durch einen Wasserstand von 0,75 m am Pegel Augustusbrücke und sind selten (NMW, WSV, 2018). Während des Auswertungszeitraumes von 2006 bis 2016 unterschritt der Elbpegel viermal den NMW. Die Mn-Konzentration an den Messpunkten der GWM entlang der Stromröhre korrelierte nur schwach

und nicht signifikant mit dem Elbe-Wasserspiegel. Niedrige Wasserstände und Durchflüsse der Elbe treten meist in den warmen Sommermonaten mit steigenden Wassertemperaturen auf. Um eine mögliche Temperaturabhängigkeit auszugleichen, wurde die Korrelation zwischen dem Wasserspiegel und der Mn-Konzentration entlang der Stromröhre für Wassertemperaturen unter und über 20 °C getestet, zeigte jedoch keine signifikante Korrelation.

Während der Säulenversuche mit Elbsohlsediment bei Wassertemperaturen von 10 °C und 20 °C war die Manganfreisetzung für alle drei Infiltrationsraten gering (Abb. 5 in Paufler et al., 2018c) [P5]. Bei Wassertemperaturen von 30 und 35 °C stieg die Mn-Konzentration mit abnehmender Infiltrationsrate.

Die Ergebnisse des Monitorings der Stromröhre im WW Dresden-Tolkewitz und aus den Säulenversuchen mit Elbsohlsediment waren mehrdeutig. Aktuelle Studien (von Rohr et al., 2014) und die Ergebnisse der Säulenversuche wiesen darauf hin, dass langanhaltende Trockenperioden mit geringem Durchfluss zu erhöhten Mn-Konzentrationen im Uferfiltrat führten. Mögliche Ursachen waren geringere Infiltrationsraten und längere Aufenthaltszeiten. Im Gegensatz dazu zeigte Diem (2013), dass ein höherer Durchfluss mit einer stärkeren Sauerstoffzehrung in der Flusssohle korrelierte. Ergebnisse der chemischen Modellierung von Diem (2013) und die Modellergebnisse von Paufler et al. (2018c) [P5] stützen dieses Ergebnis. Da eine höhere Sauerstoffzehrung häufig mit steigenden Mn-Konzentrationen im Uferfiltrat zusammenhängt (Bourg & Bertin, 1993), können höhere Durchflüsse eine Manganfreisetzung verursachen. Kürzere Aufenthaltszeiten im GWL bei hohen Durchflüssen und entsprechend hohen Wasserständen wirken dem entgegen. Außerdem zeigten die Ergebnisse der Säulenversuche, dass der Temperatureffekt diese Durchflussabhängigkeit verzerrte.

Die Temperatur ist eine entscheidende Größe für die Manganfreisetzung aus dem Flusssohlsediment, die Infiltrationsrate spielt eine untergeordnete Rolle. Niedrige Infiltrationsraten von 0,3 $m^3/(m^2 \times d)$ erforderten Temperaturen über 20 ºC, um Mn aus dem Sediment freizusetzen. Mit steigender Temperatur wurde die Infiltrationsrate weniger bedeutend. Bei Temperaturen von 30 °C verursachten Infiltrationsraten von ≈0,6 $m^3/(m^2 \times d)$ bereits eine starke Mn-Freisetzung aus dem Flusssohlsediment.

In der gemäßigten Klimazone sind Oberflächenwassertemperaturen von > 30 °C selten. Saisonale Flüsse weisen bei geringen Durchflüssen oft die höchsten Wassertemperaturen auf (van Vliet et al., 2013). Dies kann dazu beitragen, dass Uferfiltrationsstandorte in der gemäßigten Klimazone an Flüssen mit großen saisonalen Durchflussschwankungen zukünftig mit steigenden Mn-Konzentrationen rechnen müssen. An Standorten in trockenen oder tropischen Klimazonen, wie Ägypten oder Vietnam, ist auch bei hohen Infiltrationsraten eine verstärkte Mn-Freisetzung aus dem Flussbett zu erwarten.

5 Freisetzung von Mangan beim Start einer UEE in Khabarovsk

5.1 Einleitung und Standortbeschreibung

Die Stadt Khabarovsk befindet sich im Fernen Osten Russlands im zentralen Amur-Becken am Zusammenfluss der Flüsse Ussuri und Amur (Abb. 1 in Paufler et al., 2019a) [P6]. Für die Trinkwassergewinnung wird Grundwasser aus dem 400 km^2 großen Tungusska-Becken genutzt. Siderit ($FeCO_3$) ist das dominierende Carbonatmineral im Grundwasserleiter. Dieses ist wahrscheinlich mit Mn und Ca "kontaminiert" und hat die ungefähre Zusammensetzung $(Ca_{0,15}Mn_{0,08}Fe_{0,77})CO_3$ (Bilek, 2016). Das Grundwasser enthält 26 ± 3 mg/L Fe, 1 bis 3 mg/L Mn und hat einen niedrigen pH-Wert von 5,9 (Tab. 1 in Paufler et al., 2019a) [P6]. Außerdem hat das GW eine geringe Pufferkapazität von 150 bis 165 mg/L HCO_3^- und weist eine hohe CO_2-Konzentration von 155 bis 215 mg/L auf.

Für die Trinkwasserbereitstellung wird das Grundwasser durch unterirdische Enteisenung und Entmanganung voraufbereitet (UEE, Subterra-Technik) (Herlitzius, 2015; Braun et al., 2017). Alle Brunnen dienen abwechselnd als Infiltrations- und Förderbrunnen. Ein UEE-Zyklus besteht aus einer Infiltrationsphase und der anschließenden Förderphase. Grundwasser aus früheren Förderphasen dient als Infiltrat. Vor der Infiltration wurde das GW mit technischem Sauerstoff auf bis zu 25 mg/L O_2 angereichert und mit Natriumhypochlorit (NaClO) chloriert (Paufler et al., 2018a) [P7]. Die Infiltrationszeit betrug 48 h bei einer Infiltrationsrate von 80 m³/h. Die Förderdauer betrug zunächst 48 h und wurde auf 72 h erhöht. Die Förderrate betrug 160 m³/h (Abb. 2 in Paufler et al., 2019a) [P6].

Nachdem die Enteisenung und teilweise die Entmanganung an mehr als 25 Brunnen erfolgreich startete, wurde eine unerwartete Freisetzung von Mn während der Infiltrations- und insbesondere während der Förderphasen an mehreren Brunnen beobachtet. Die resultierende Mn-Konzentration war teilweise doppelt so hoch wie die Hintergrundkonzentration im GW. In Paufler et al. (2019a) [P6] werden die Ergebnisse der Untersuchungen zur Ursache der Manganfreisetzung zusammengefasst. Für die Begrenzung der kolmationsbedingten Leistungsabnahme in manchen Brunnen wird das Infiltrat chloriert. In Paufler et al. (2018a) [P7] sind die Ergebnisse der Untersuchungen zur Brunnendesinfektion in Khabarovsk dargestellt.

5.2 Untersuchungen zur Ursache der Manganfreisetzung

Von dem regulären Monitoring wurden die Wasserbeschaffenheitsdaten der ersten 194 UEE-Zyklen (650 Tage) eines Förderbrunnens und von dessen drei Grundwassermessstellen ausgewertet. GWM 1 war 6 m, GWM 2 war 12 m und GWM 3 war 18 m von dem Brunnen entfernt. Batchversuche dienten der weiteren Untersuchung einer möglichen Auflösung von Mn-reichem Siderit als Ursache der Mn-Freisetzung während der Förderphasen. Weiterhin

wurde die Mn-Freisetzung bei einem geringen pH-Wert durch einen Kleinsäulenversuch mit einer 0,5 m -langen Säule mit GWL-Material simuliert.

Die Ergebnisse des regulären Monitorings zeigten, dass der Reaktionsraum für die Fe-Entfernung nach 25 UEE-Zyklen fast vollständig entwickelt war. Nach 25 UEE-Zyklen wurden fast 99 % der ≈ 20 mg/L Fe im Grundwasser zwischen GWM 3 und GWM 2 zurückgehalten. In den Brunnennahraum bis zur GWM 1 (6 m entfernt) drang kein Fe^{2+} mehr ein.

Obwohl die Enteisenung rasch einsetzte, passierte Mangan auch nach 194 UEE-Zyklen den Reaktionsraum nahezu ungehindert (Abb. 6 in Paufler et al., 2019a) [P6]. Innerhalb der ersten 6 UEE-Zyklen des untersuchten Brunnens wurde der Ergiebigkeitskoeffizient (EGK) auf > 1 angehoben (Abb. 5 in Paufler et al., 2019a) [P6]. Der Vergleich mit Beobachtungen an anderen UEE-Standorten (z.B. Rott et al., 2002; Rössner et al., 2017) weist darauf hin, dass das frühzeitige Anheben des EGK eine Ursache der ausgebliebenen Entmanganung war.

Die beobachtete Mn-Freisetzung wurde auf die Auflösung von Mn-haltigen Carbonatmineralen zurückgeführt, welche als unreines Siderit im GWL-Material vorhanden sind. Die Auflösung von Mn-haltigen Carbonatmineralen kann auch die zunehmende Härte und Säurekapazität entlang des Fließweges erklären. Eine permanente Untersättigung des Grundwassers gegenüber Siderit (und Rhodochrosit) verstärken diese These.

Die Ergebnisse der Batchversuche zeigten erwartungsgemäß, dass die Mn-Freisetzung aus dem GWL-Material stark von der Korngröße und vom pH-Wert abhängt. Bei dem pH-Wert des Grundwassers während der Förderphasen von ca. pH 6 setzte die Korngröße < 4 mm mehr als 1 mg/L Mn frei. Die Mn-Freisetzung aus den Feinanteilen des GWL-Materials (< 0,063 mm) lag bei > 2 mg/L. In dem Kleinsäulenversuch mit Grundwasser mit einem pH-Wert von 5 wurden bis zu 1,7 mg/L Mn freigesetzt. Basierend auf den Ergebnissen einer sequentiellen Extraktion und der gegenwärtigen Entwicklung von Mn im Förderwasser des Brunnens wurde die Zeitspanne für eine mögliche Auslaugung des Mn-Pools abgeschätzt. Beide Ansätze weisen auf eine Erschöpfung des Mn-Carbonat-Pools innerhalb von 13 bis 15 Jahren hin.

5.3 Begrenzung der Leistungsabnahme der UEE-Brunnen

Innerhalb von mehreren Monaten in Betrieb nahm die spezifische Ergiebigkeit einiger Brunnen in Khabarovsk stark ab und fiel innerhalb eines Jahres auf fast die Hälfte des Wertes bei der Inbetriebnahme. Laut Herlitzius (2014) ist dieser Rückgang hauptsächlich auf die Akkumulation von Biomasse von Eisen-, Mangan- und Methan-oxidierenden Bakterien im Brunnen und in der Filterkiesschüttung zurückzuführen. Um die Leistungsabnahme zu begrenzen, wird dem Infiltrationswasser Natriumhypochlorit (NaClO) zugesetzt. Das NaClO erreichte nicht die nächstliegende GWM 1 im Abstand von 6 m, und die tatsächliche Reichweite des NaClO war unbekannt. Für die Untersuchung der Reichweite des NaClO wurden insgesamt 4 Säulen mit GWL-Material oder Filterkies befüllt und in Anlehnung an die

Infiltrations- und Förderzyklen der Brunnen mit dem chlorhaltigen Infiltrat der Brunnen und Grundwasser beschickt (Paufler et al., 2019a) [P6]. Darüber hinaus wurde die Chlorzehrung des Filtermaterials, von Ton und dem GWL-Material in Batchversuchen bestimmt.

Die Batchversuche zeigten niedrige Chlorzehrungsraten für Filterkies und -sand von 0,005 mg/g/d. Die Chlorzehrung von Ton und dem natürlichen GWL-Material war mit 0,030 und 0,054 mg/g/d deutlich größer. Kleinere Korngrößen < 1 mm zeigten innerhalb der ersten Stunde in Kontakt mit chlorhaltigem Wasser 10- bis 70-fach höhere Chlorzehrungsraten als die Medianwerte der Chlorzehrungsraten. Bei längeren Kontaktzeiten wurde die Korngröße weniger wichtig. Die anfängliche Chlorkonzentration beeinflusst wahrscheinlich nicht die Desinfektionsfähigkeit des Materials für Korngrößen > 1 mm, kann jedoch zu einer effektiveren Desinfektion von Korngrößen < 1 mm führen. Dies gilt insbesondere bei sehr feinen Materialien mit Korngrößen < 0,063 mm.

Die Ergebnisse der Säulenversuche bestätigten die Ergebnisse der Batchversuche. Die ermittelten Zehrungskonstanten für eine Chlorzehrung 1. Ordnung waren niedrig für das Filtermaterial (16 d^{-1}) und mit 254 d^{-1} deutlich höher für das GWL-Material.

Für die Abschätzung der Reichweite des NaClO an den Brunnen in Khabarovsk wurden drei Berechnungsansätze verwendet. Alle Ansätze zeigten übereinstimmend, dass die Filterkiesschüttung eines Brunnens weniger als 1 % des infiltrierten Chlors verbrauchte. Die Desinfektionszone um den Brunnen erstreckte sich etwa 2 m (> 90 % der Chlormasse) und maximal 3,5 m in den Grundwasserleiter. Eine Chlordosierung von mehr als 10 mg/L hätte den Desinfektionsradius nicht erhöht. Eine effizientere Desinfektion wäre durch ein größeres Infiltrationsvolumen oder eine längere Infiltrationszeit möglich gewesen.

6 Manganfreisetzung bei der geplanten Umstellung des UEE-Wasserwerks Eggersdorf auf kontinuierliche Förderung

6.1 Einleitung und Standortbeschreibung

Der demografische Wandel, die Abwanderung der Bevölkerung in Ballungsräume und bisher unvorhersehbare Klimaextreme erschweren die Planung für viele Wasserversorger. Das Wasserwerk (WW) Eggersdorf des Wasserverbandes Strausberg-Erkner (WSE) ist seit etwa 40 Jahren in Betrieb und soll saniert werden. Das WW liegt südlich von Eggersdorf in einem Waldstück am Stienitzsee bei Berlin (Abb. 1 in Paufler et al., 2019b) [P8]. Die 16 Brunnen des WW produzieren bei Bedarf ca. 16.000 m³/d (max. 19.500 m³/d) mit Hilfe des UNEIS-Verfahrens (Eichhorn, 1985). Um eisen- und manganhaltiges Grundwasser unterirdisch aufzubereiten, werden die Brunnen abwechselnd als Infiltrations- und Förderbrunnen betrieben. Das GW enthält ca. 1 mg/L Fe, 0,2 mg/L Mn und ist mit einer Säurekapazität ($K_{S4,3}$) von 3-4 mmol/L gut gepuffert (Tab. 1 in Paufler et al., 2019b) [P8].

Da das WW Eggersdorf inzwischen als Spitzenstunden-WW genutzt werden muss, werden die Brunnen unregelmäßig ausgelastet. Dies widerspricht den Empfehlungen für die Anwendung der unterirdischen UEE. Für den Wasserversorger kommen nach der Sanierung zwei Varianten für den Betrieb in Frage: die weitere Nutzung des UNEIS-Verfahrens oder die Umstellung des Brunnenbetriebes auf ausschließliche Grundwasserförderung mit nachgeschalteter oberirdischer Aufbereitung. Paufler et al. (2019b) [P8] beschreiben die Ergebnisse eines Feldversuchs für die Umstellung eines UNEIS-Brunnens im WW Eggersdorf auf eine dauerhafte Förderung von eisen- und manganhaltigem GW.

6.2 Umstellung eines UEE-Brunnens auf dauerhafte Förderung

Um die Auswirkungen einer Umstellung von unterirdischer Enteisenung auf kontinuierliche Förderung zu untersuchen, wurde über 250 Tage ein Feldversuch am Brunnen 12 des WW Eggersdorf durchgeführt. Vorher wurde der Br. 12 viele Jahre als UNEIS-Brunnen betrieben. Im regulären UNEIS-Betrieb wurde Trinkwasser mit einem Sauerstoffgehalt von etwa 10 mg/L O_2 in den Br. 12 infiltriert. Das Infiltrationsvolumen betrug 2.000 m³ bei einer Infiltrationsrate von ca. 30 m³/h. Das Fördervolumen betrug 14.000 m³, die Förderrate lag bei 60 bis 70 m³/h. Daraus ergab sich ein Ergiebigkeitskoeffzient von 7 (EGK = Förder-volumen $V_{För}$ / Infiltrationsvolumen V_{Inf}). Für den Feldversuch förderte Br. 12 kontinuierlich Grundwasser zu einem Containerwasserwerk (CWW). In dem CWW fand die notwendige oberirdische Enteisenung des Grundwassers statt. Bis zum Versuchsende wurden rund 120.000 m³ Grundwasser gefördert. Dies entsprach einem EGK von 65.

Die Mangankonzentration im Förderwasser stieg ab EGK 30 bis zum Versuchsende bei EGK 65 auf bis zu 0,72 mg/L an (Abb. 3 in Paufler et al., 2019b) [P8]. Damit war die Mn-Konzentration im Förderwasser etwa 3,5-mal höher als die Hintergrundkonzentration im

Grundwasser. Ab EGK 7 stieg die Eisen-Konzentration von < 0,01 auf max. 0,15 mg/L an und blieb danach konstant. Die Konzentrationen der Hauptkationen Ca^{2+}, Mg^{2+}, Na^{+} und K^{+} schwankten nur geringfügig um die jeweiligen Medianwerte (Tab. 2 in Paufler et al., 2019b) [P8]. Mit dem Anstieg der Mn-Konzentration stieg die Ca-Konzentration temporär um 10 mg/L an. Aufgrund des Anstiegs der Mn-Konzentration wurde das Analysespektrum um Al, As, Cr, Cu, Pb und Zn erweitert. Die Konzentrationen von fast allen analysierten Schwermetallen blieben unter der jeweiligen Bestimmungsgrenze (BG). Nur Zn überstieg mit einem Medianwert von 0,005 mg/L und maximal 0,22 mg/L die BG. Der pH-Wert stieg kontinuierlich über die gesamte Versuchsdauer von etwa pH 6,9 auf pH 7,6 an (Abb. 4 in Paufler et al., 2019b) [P8].

Abb. 7 in Paufler et al. (2019b) [P8] zeigt, dass mit dem Anstieg von Zn auch Fe kurzzeitig auf bis zu 0,44 mg/L anstieg. Die Ursache war vermutlich eine geplante, plötzliche Steigerung der Förderrate. Durch die höheren Fließgeschwindigkeiten wurde möglicherweise partikuläres Eisen aus der unmittelbaren Umgebung des Brunnens mobilisiert. Auf Grundlage der Ergebnisse wurde das Risiko für einen zusätzlichen Aufbereitungsaufwand für die analysierten Schwermetalle bei dauerhafter Förderung, auch bei einer anhaltenden Mn-Freisetzung, als sehr gering eingeschätzt.

6.3 Ursache der Manganfreisetzung aus dem ehemaligen Reaktionsraum

Mit dem Anstieg der Mn-Konzentration auf bis zu 0,72 mg/L überstieg Mn den Hintergrundwert im GW von 0,19 mg/L um bis zu 0,53 mg/L. Infolge von temporär erhöhten EGK oder während „Crashtests“ wurde an anderen UEE-Standorten ein qualitativ ähnliches Verhalten von Mn beobachtet (Rott et al., 2002, Rössner et al., 2017).

Basierend auf den Ganglinien der Ca-, Fe- und Mn-Konzentration und unter Berücksichtigung des Verlaufs des pH-Wertes wurde die Ursache der Manganfreisetzung im WW Eggersdorf am Br. 12 wie folgt erklärt (Abb. 7 in Paufler et al., 2019b) [P8]:

(1) Bei Infiltrationsende bzw. vor Beginn der Förderung war das Korngerüst innerhalb der Reaktionszone mit einer Schicht aus Fe- und Mn-Oxiden überzogen und die freien Adsorptionsplätze vor allem durch Ca-, Mg- oder K-Ionen besetzt.
(2) Mit dem Zurückpumpen des Infiltrats (Beginn der Förderung) drang eisen- und mangan-reicheres GW in die Reaktionszone ein. Zunächst adsorbierte gelöstes Mn^{2+}, wurde aber anschließend durch Fe^{2+} verdrängt.
(3) Die Adsorptionskapazität nahm entlang des Fließweges ab und eine Sättigungsfront für Fe^{2+} und Mn^{2+} wanderte nach innen.
(4) Das Eindringen von Fe^{2+} in den inneren Bereich der Reaktionszone führte zur Reduktion abgeschiedener Mn-Oxide. Die hohe Reaktionsgeschwindigkeit führte zu einem schnellen Anstieg der Mn-Konzentration (Gl. 1 in Paufler et al., 2019b) [P8].

(5) Entstandene Fe-(Hydr)oxide passivierten die Mn-Oxide, die reaktive Oberfläche der Mn-Oxide wurde geringer. Die Passivierung und der steigende pH-Wert verlangsamten die Reaktion (Villinski et al., 2003). Außerdem stieg die Adsorptionskapazität der Fe- und Mn-(Hydr)oxide mit dem höheren pH-Wert an, sodass möglicherweise freigesetztes Mn^{2+} teilweise wieder adsorbierte. Da davon ausgegangen werden kann, dass die Mn-(Hydr)oxide im Überschuss im Vergleich zu Fe^{2+} vorhanden waren, war bis zum Versuchsende kein Durchbruch von Fe^{2+} messbar.

7 Zusammenfassung und Ausblick

Die vorliegende Dissertation befasst sich mit den Eintragspfaden und dem Verhalten von Mangan bei der Uferfiltration und der unterirdischen Enteisenung / Entmanganung und Möglichkeiten der technischen Steuerung der Mn-Konzentration im geförderten Wasser. Die vier Hauptziele der Arbeit waren 1. die Bewertung eines potenziellen Uferfiltrationsstandortes in Embaba (Kairo), 2. die Abschätzung der Manganfreisetzung aus der Elbsohle für den Uferfiltrationsstandort Dresden-Tolkewitz in Abhängigkeit der Klimavariablen Temperatur und Infiltrationsrate, 3. die Untersuchung der Ursache der Manganfreisetzung kurz nach dem Start einer UEE in Khabarovsk und 4. die Beurteilung der Umstellung von UEE-Brunnen für die dauerhafte Förderung von Grundwasser als mögliche Sanierungsvariante für das WW Eggersdorf.

Mangankonzentrationen zwischen 0,4 und 1,6 mg/L sind typisch für viele Uferfiltrationsstandorte. Die Mn-Konzentration im Rohwasser von Uferfiltrationsbrunnen hängt von dem Verhältnis und dem Mangangehalt der Rohwasserkomponenten Uferfiltrat, landseitig zuströmendes und den Fluss unterströmendes Grundwasser, ab. Durch Reduktion und die Auflösung von Manganverbindungen in der Flusssohle oder dem Grundwasserleiter kann Mangan freigesetzt werden. Entlang des Fließweges vom Gewässer zu den Brunnen können Sorptions-, Fällungs- und Oxidationsreaktionen Mangan wieder immobilisieren. Durch Festlegung der Position der Brunnen und des Betriebsregimes kann die Mangankonzentration im Rohwasser über die Änderung der Aufenthaltszeit und die Anteile der Rohwasserkomponenten technisch gesteuert werden. Der Sauerstoffgehalt, pH-Wert und die Temperatur des Oberflächenwassers beeinflussen das Redoxmilieu entlang des Fließweges und damit ebenfalls den Mangangehalt.

Eine teufenabhängige Probennahme während des regulären Brunnenbetriebes, Sedimentproben und nachfolgende Wasser- und Feststoffanalysen dienten der Bewertung des potenziellen Uferfiltrationsstandortes in Embaba. Die Ergebnisse wiesen auf die Flusssohle als Quelle für die erhöhten Eisen-, Mangan- und Ammoniumkonzentrationen im Uferfiltrat hin.

Der Einfluss von Temperatur und Infiltrationsrate auf die Manganfreisetzung aus der Elbsohle wurde anhand von Beschaffenheitsdaten von drei GWM entlang einer Stromröhre in Dresden-Tolkewitz untersucht. Mit Hilfe von Säulenversuchen wurde die Manganfreisetzung aus dem Flusssohlsediment für drei Infiltrationsraten und vier Temperaturregime quantifiziert. Die Ergebnisse zeigten, dass die Temperatur die Mn-Freisetzung stärker beeinflusst als die Infiltrationsrate. Bei niedrigen Infiltrationsraten von $< 0{,}3$ m³/(m²×d) erfolgt die Manganfreisetzung erst bei Temperaturen über 20 °C. Mit steigenden Temperaturen wurde die Infiltrationsrate weniger wichtig. Bei Infiltrationsraten von ca. 0,6 m³/(m²×d) können Temperaturen von 30 °C zu einer starken Mn-Freisetzung aus dem Flussbett führen.

Für die Untersuchung der Manganfreisetzung während der Inbetriebnahme des UEE-Wasserwerks in Khabarovsk wurden Wasserbeschaffenheitsdaten der ersten 194 UEE-Zyklen (650 Tage) eines Förderbrunnens ausgewertet. Ergänzende Batchversuche dienten der Bewertung einer möglichen Auflösung von Mn-reichem Siderit als Ursache der Mn-Freisetzung. Die Auflösung des im GWL vorhandenen manganhaltigen Siderits wurde als Ursache der Mn-Freisetzung identifiziert. Die Batchversuche zeigten eine starke Korngrößen- und pH-Abhängigkeit der Mn-Freisetzung aus dem GWL-Material. Die Abschätzung der Reichweite des Natriumhypochlorits zur Brunnendesinfektion erfolgte auf Grundlage von Säulenversuchen an den Brunnen in Khabarovsk und Batchversuchen im Labor. Die Ergebnisse wiesen darauf hin, dass die Filterkiesschüttung des Brunnens weniger als 1 % des infiltrierten Chlors zehrte. Die Reichweite des Natriumhypochlorits im Grundwasserleiter wurde mit 2 bis 3,5 m berechnet.

Die mögliche Umnutzung der UEE-Brunnen im WW Eggersdorf für die dauerhafte Grundwasserförderung wurde durch einen Feldversuch bewertet. Ab einem Ergiebigkeits-koeffizienten von 30 führte die chemische Reduktion von abgeschiedenen Mangan(hydr)oxiden durch Fe-haltiges Grundwasser zu einer Freisetzung von Mangan aus dem ehemaligen Reaktionsraum. Bis zum Versuchsende bei EGK 65 wurden keine weiteren Schwermetalle freigesetzt.

Im Rahmen der vorliegenden Dissertation wurden Ansatzpunkte für zukünftige Untersuchungen deutlich. Diese werden wie folgt zusammengefasst:

- Die teufenabhängige Probennahme an den Brunnen in Embaba führte zu belastbaren Ergebnissen für die Beurteilung der Zustromverhältnisse (Paufler et al., 2018b) [P4] und wurde erfolgreich an anderen Standorten angewendet. Die Richtung der Probennahme (N-S-O-W) war unbekannt. Das Wissen über die Zustromrichtung würde eine genauere Beschreibung des einströmenden Wassers (Grundwasser, Uferfiltrat) ermöglichen.
- Vorangegangene Untersuchungen an Uferfiltrationsstandorten in Torgau und Dresden (Grischek & Paufler, 2017) [P2] wiesen auf eine mögliche „Auswaschung“ des Fe- und Mn-Pools in der Flusssohle und dem GWL hin. Paufler et al. (2018c) [P5] zeigten, dass eine Auswaschung des Mn-Pools der Flusssohle auch bei Berücksichtigung einer Nachlieferung von partikulärem Mn durch das Flusswasser möglich ist. Langzeitversuche mit Flusssohlsediment und GWL-Material können dazu beitragen, diesen Effekt zu quantifizieren.
- Paufler et al. (2018c) [P5] quantifizierten die Manganfreisetzung aus der Elbsohle in Dresden in Abhängigkeit der Temperatur und Infiltrationsrate. Aufgrund der weiteren Beeinflussung des freigesetzten Mn entlang des Fließweges vom Fluss zu den Brunnen sind diese Ergebnisse nicht für eine Prognose der zu erwartenden Mn-Konzentration im Rohwasser nutzbar. Die Identifizierung weiterer Einflussgrößen würde zu einer Prognose

der Rohwasserkonzentrationen beitragen. Vor allem sollte die Relevanz der Rhodochrosit-Ausfällung geprüft werden. Mehrere Studien weisen auf die Möglichkeit der $MnCO_3$-Ausfällung als Mn-Senke hin (z.B. Bourg & Bertin, 1993; Massmann et al., 2004), beruhen aber auf theoretischen Betrachtungen.

- Die Auflösung von Mn-haltigen Siderit wurde als Hauptursache der Mn-Freisetzung in Khabarovsk identifiziert (Paufler et al., 2019a) [P6]. Die Prozesse der Carbonatbildung und -auflösung sind für UEE-Standorte (Mettler et al., 2001) und Uferfiltrationsstandorte (Massmann et al., 2004) relevant, aber können bisher nicht quantifiziert werden. Eine genauere Untersuchung der Prozesse kann zur Optimierung von beiden unterirdischen Ausbereitungsverfahren beitragen. Außerdem sollte die Übertragbarkeit der Ergebnisse einer sequentiellen Extraktion auf reale Standortbedingungen genauer untersucht werden. Bisher kann nicht abgeschätzt werden, wie hoch der Anteil des im GWL freisetzbaren Mangan im Vergleich zur leicht löslichen bzw. leicht reduzierbaren Fraktion solcher Batchversuche ist.
- Die Übertragbarkeit der Ergebnisse zur Abschätzung der Reichweite des Natriumhypochlorits (Paufler et al., 2018a) [P7] bei der Brunnendesinfektion sollte für Standorte mit anderen Zusammensetzungen des GWL-Materials geprüft werden. Da die Dissoziation von Chlor temperaturabhängig ist, sollte dies bei der Anwendung in anderen Klimazonen berücksichtigt werden.

In der vorliegenden Dissertation wurde auf der Grundlage einer Recherche zu 42 Uferfiltrationsstandorten, sowie durch exemplarische Untersuchungen an zwei Uferfiltratfassungen herausgearbeitet, dass Mangan bei der Uferfiltration überwiegend durch das Uferfiltrat in das Rohwasser eingetragen wird. Die Freisetzung von Mangan findet vor allem in der Gewässersohle statt und wird primär durch die Temperatur kontrolliert. Der Einfluss der Temperatur und der Infiltrationsrate auf die Manganfreisetzung aus der Gewässersohle konnte quantifiziert werden. Sowohl bei der Uferfiltration als auch bei der Unterirdischen Enteisenung / Entmanganung wird die Manganfreisetzung im GWL durch die Bildung und Auflösung carbonatischer Mineralphasen kontrolliert.

Literaturverzeichnis

Ahrns, J. (2008) Modellierung des Austausches zwischen Oberflächenwasser und Grundwasser mit Hilfe des Umwelttracers Temperatur. Diplomarbeit, Hochschule für Technik und Wirtschaft Dresden, Fakultät für Bauingenieurwesen und Architektur, Lehrgebiet Wasserwesen, 93 S.

Bartak, R., Grischek, T., Herlitzius, J. (2014) Bank filtration under arid conditions for drinking water supply at low cost. Abschlussbericht BMBF Forschungsprojekt GEF10-186, FKZ 01DH12012A, 164 S.

Bilek, F. (2016) Begleitung des Feldtests zur Infiltration von Wasser mit erhöhter O_2-Konzentration durch Auswertung der geochemisch-mineralogischen Untersuchungsergebnisse. Wissenschaftlich-technischer Bericht, GFI Grundwasser-Consulting-Institut GmbH Dresden, unveröffentlicht, 47 S.

Blanford, W., Boving, T., Al-Ghazawi, Z., Shawaqfah, M., Al-Rashdan, J., Saadoun, I., Schijven, J., Ababneh, Q. (2010) River bank filtration for protection of Jordanian surface and groundwater. Proceedings of the World Environmental and Water Resources Congress 2010: Challenges of Change. ASCE, Providence RI, 776-781.

Bourg, A.C.M., Bertin, C. (1993) Biogeochemical processes during the infiltration of river water into an alluvial aquifer. Environ. Sci. Technol. 27(4), 661-666. doi: 10.1021/es00041a009.

Bourg, A.C.M., Bertin, C. (1994) Seasonal and spatial trends in manganese solubility in an alluvial aquifer. Environ. Sci. Technol. 28(5), 868-876. doi: 10.1021/es00054a018.

Bourg, A.C.M., Richard-Raymond, F. (1994) Spatial and temporal variability in the water redox chemistry of the M27 experimental site in the Drac river calcareous alluvial aquifer (Grenoble, France). J. Contam. Hydrol. 15(1-2), 93-105. doi: 10.1016/0169-7722(94)90012-4.

Braun, B., Schröder, J., Knecht, H., Szewzyk, U. (2016) Unraveling the microbial community of a cold groundwater catchment system. Water Res. 107, 113-126. doi: 10.1016/ j.watres.2016.10.040.

Diem, S. (2013) Riverbank Filtration within the Context of River Restoration and Climate Change. Dissertation, Universität Neuenburg, Zentrum für Hydrogeologie und Geothermie, Neuenburg, Schweiz, 144 S.

EEA (2016) European Environment Agency. Climate change, impacts and vulnerability in Europe 2016. An indicator-based report. Publications Office of the European Union, Luxembourg, 2017. ISBN 978-92-9213-835-6.

Eichhorn, D. (1985) Beitrag zur Theorie der Eisenelimination bei der Untergrundwasseraufbereitung. Dissertation, Fakultät für Bau-, Wasser- und Forstwesen, TU Dresden.

Farnsworth, C.E., Hering, J.G. (2011) Inorganic geochemistry and redox dynamics in bank filtration settings. Environ. Sci. Technol. 45(12), 5079-5087. doi: 10.1021/es2001612.

Ghodeif, K.O. (2011) Removal of iron and manganese within the aquifer using enhanced riverbank filtration technique under arid conditions. In: Ray, C., Shamrukh, M. (Eds.) Riverbank filtration for water security in desert countries. Dordrecht: Springer, 235-253.

Ghodeif, K.O., Paufler, S., Grischek, T., Wahaab, R., Souaya, E., Bakr, M., Abogabal, A. (2018) Riverbank filtration in Cairo, Egypt - Part I: Installation of a new riverbank filtration site and first monitoring results. Environ. Earth Sci. 77, 270. doi: 10.1007/s12665-018-7450-2.

Gimbel, R., Jekel, M., Ließfeld, R. (2004) Wasseraufbereitung - Grundlagen und Verfahren. DVGW Lehr- und Handbuch Wasserversorgung. Oldenbourg: Oldenbourg Industrie-Verlag. ISBN: 978-3835663657.

Grischek, T. (2003) Zur Bewirtschaftung von Uferfiltratfassungen an der Elbe. Dissertation, TU Dresden, Institut für Grundwasserwirtschaft. Mitteilungen des Instituts für Grundwasser-wirtschaft 4, Dresden, 252 S.

Grischek, T., Ahrns, J., Kuehne, M., Bartak, R., Herlitzius, J., Ghodeif, K., Wahaab, R.A. (2013) Coupling riverbank filtration and subsurface iron removal. Proc. Int. Symp. on Managed Aquifer Recharge, 15.-18.10.2013, Peking, 1-8.

Grischek, T., Bartak, R. (2016) Riverbed clogging and sustainability of riverbank filtration. Water 8(12), 604. https ://doi.org/10.3390/w8120 604.

Grischek, T., Paufler, S. (2017) Prediction of iron release during riverbank filtration. Water 9, 317, 1-13, doi: 10.3390/w9050317.

Grischek, T., Schoenheinz, D., Worch, E., Hiscock, K. (2002) Bank filtration in Europe – An overview of aquifer conditions and hydraulic controls. In: Dillon, P. (Ed.) Management of Aquifer Recharge for Sustainability. Lisse, The Netherlands: Balkema Publ., 485-488.

Hallberg, R.O., Martinell, R. (1976) Vyredox - In Situ Purification of Ground Water. Ground Water 14(2), 88-93. doi: 10.1111/j.1745-6584.1976.tb03638.x.

Henzler, A.F., Greskowiak, J., Massmann, G. (2016) Seasonality of temperatures and redox zonations during bank filtration – A modeling approach. J. Hydrol. 535, 282-292. doi: 10.1016/j.jhydrol.2016.01.044.

Herlitzius, J. (Hrsg.) (2014) Mikrobiologische Forschungen zur Ausarbeitung von Kontroll-methoden der mikrobiologischen Situation und Maßnahmen zur Vorbeugung der möglichen Förderleistungsminderung von Brunnen der ersten Sektion des Tungusskavorkommens der Stadt Khabarovsk. Wissenschaftlich-technischer Bericht, Arcadis Germany GmbH, unveröffentlicht, 219 S.

Herlitzius, J. (Hrsg.) (2015) Begründung der Bedingungen zur Bildung von Biofilm und technische Lösungen zur Vorbeugung der Biofilmbildung auf der technologischen Ausrüstung der Wasserfassung im Tungusskavorkommen. Wissenschaftlich-technischer Bericht, Arcadis Germany GmbH, unveröffentlicht, 24 S.

Hiscock, K.M., Grischek, T. (2002) Attenuation of groundwater pollution by bank filtration. J. Hydrol. 266(3-4), 139-144. doi: 10.1016/S0022-1694(02)00158-0.

Hu, B., Teng, Y., Zhai, Y., Zuo, R., Li, J., Chen, H. (2016) Riverbank filtration in China: A review and perspective. J. Hydrol. 541, 914-927. doi: 10.1016/j.jhydrol.2016.08.004.

Jensen, D.L., Boddum, J.K., Tjell, J.C., Christensen, T.H. (2002) The solubility of rhodochrosite ($MnCO_3$) and siderite ($FeCO_3$) in anaerobic aquatic environments. Applied Geochemistry 17(4), 503-511. doi: 10.1016/S0883-2927(01)00118-4.

Landon, M.K., Jurgens, B.C., Katz, B.G., Eberts, S.M., Burow, K.R., Crandall, C.A. (2010) Depth-dependent sampling to identify short-circuit pathways to public-supply wells in multiple aquifer settings in the United States. Hydrogeol. J. 18(3), 577-593. doi: 10.1007/s10040-009-0531-2.

Massmann, G., Pekdeger, A., Merz, C. (2004) Redox processes in the Oderbruch polder groundwater flow system in Germany. Appl. Geochem. 19(6), 863-886. doi: 10.1016/j.apgeochem.2003.11.006.

Mettler, S., Abdelmoula, M., Hoehn, E., Schoenenberger, R., Weidler, P., von Gunten, U. (2001) Characterization of iron and manganese precipitates from an in-situ ground water treatment plant. Ground Water 39(6), 921-930. doi: 10.1111/j.1745-6584.2001.tb02480.x.

Mutschmann, J., Stimmelmayr, F. (2007) Taschenbuch der Wasserversorgung. 14. Aufl., Wiesbaden: Vieweg & Sohn Verlag / GWV Fachverlage GmbH.

Parkhurst, D.L., Appelo, C.A.J. (2013) Description of input and examples for PHREEQC version 3: A computer program for speciation, batch-reaction, one-dimensional transport, and inverse geochemical calculations. U.S. Geological Survey Techniques and Methods, book 6, chap. A43. Available only at http://pubs.usgs.gov/tm/06/a43.

Paufler, S. (2015) Bewirtschaftung von Uferfiltratfassungen zur Verringerung der Mangan-gehalte im Rohwasser. Diplomarbeit, Hochschule für Technik und Wirtschaft Dresden, Fakultät für Bauingenieurwesen und Architektur, Lehrgebiet Wasserwesen, 157 S.

Paufler, S., Grischek, T. (2018) Herkunft und Verhalten von Mangan bei der Uferfiltration. Grundwasser 23(4), 277-296. doi: 10.1007/s00767-018-0401-8.

Paufler, S., Grischek, T., Adomat, Y., Herlitzius, J., Hiller, K., Metelica, Y. (2018a) Effective range of chlorine transport in an aquifer during disinfection of wells: from laboratory experiments to field application. J. Hydrol. 559, 711-720. doi: 10.1016/j.jhydrol.2018.02.054.

Paufler, S., Grischek, T., Bartak, R., Ghodeif, K., Wahaab, R., Boernick, H. (2018b) Riverbank filtration in Cairo, Egypt - Part II: Detailed investigation of a new riverbank filtration site with a focus on manganese. Environ. Earth Sci. 77, 318. doi: 10.1007/s12665-018-7500-9.

Paufler, S., Grischek, T., Benso, M., Seidel, N., Fischer, T. (2018c) The impact of river discharge and water temperature on manganese release from the riverbed during riverbank filtration – A case study from Dresden, Germany. Water 10(10), 1476. doi: 10.3390/w10101476.

Paufler, S., Grischek, T., Herlitzius, J., Feller, J., Kulakov, V.V. (2019a) Manganese release linked to carbonate dissolution during the start-up phase of a subsurface iron removal well in Khabarovsk, Russia. Sci. Total Environ. 650(2), 1722-1733. doi: 10.1016/j.scitotenv.2018.09.319.

Paufler, S., Grischek, T., Ruppert, M. (2019b) Freisetzung von Mangan nach Umstellung von Brunnen mit unterirdischer Enteisenung auf Dauerbetrieb. gwf Wasser / Abwasser 1(160), 55-65.

Ray, C., Melin, G., Linsky, R.B. (2002) Riverbank filtration - improving source water quality. Dordrecht: Kluwer, 364 S.

Regnery, J., Barringer, J., Wing, A.D., Hoppe-Jones, C., Teerlink, J., Drewes, J.E. (2015) Start-up performance of a full-scale riverbank filtration site regarding removal of DOC, nutrients, and trace organic chemicals. Chemosphere 127, 136-142. doi: 10.1016/j.chemosphere.2014.12.076.

Rott, U, Friedle, M (2000) 25 Jahre unterirdische Wasseraufbereitung in Deutschland - Rückblick und Perspektiven. gwf Wasser Abwasser 141(13), 99-107.

Rott, U., Meyer, C., Friedle, M. (2002) Residue-free removal of arsenic, iron, manganese and ammonia from groundwater. Wat. Sci. Technol. - Water Supply 2(1), 17-24.

Rössner, U., Sailer, C., Langert, J., Plaßmann, C. (2017) Einfahrbetrieb der Unterirdischen Enteisenung und Entmanganung an der Wassergewinnung Kaldenkirchen (Niederrhein). ewp Energie-Wasser-Praxis 12, 92-95.

Sandhu, C., Grischek, T., Kumar, P., Ray, C. (2011) Potential for riverbank filtration in India. Clean Technol. Environ. Policy 13(2), 295-316. doi: 10.1007/s10098-010-0298-0.

Schubert, J. (2002) Hydraulic aspects of riverbank filtration-field studies. J. Hydrol. 266(3–4), 145-161. doi: 10.1016/S0022-1694(02)00159 -2.

Shamrukh, M., Abdel-Wahab, A. (2008) Riverbank filtration for sustainable water supply: application to a large-scale facility on the Nile River. Clean Techn. Environ. Policy 10(4), 351-358.

Sprenger, C., Lorenzen, G., Hulshoff, I., Gruetzmacher, G., Ronghang, M., Pekdeger, A. (2011) Vulnerability of bank filtration systems to climate change. Sci. Total Environ. 409(4), 655-663. doi: 10.1016/j.scitotenv.2010.11.002.

Stuyfzand, P.J. (2011) Hydrogeochemical processes during riverbank filtration and artificial recharge of polluted surface waters: Zonation, identification, and quantification. In: Ray, C., Shamrukh, M. (Hrsg.) Riverbank filtration for water security in desert countries. Dordrecht: Springer, 97-128.

TrinkwV (2018) Trinkwasserverordnung in der Fassung der Bekanntmachung vom 10. März 2016 (BGBl. I S. 459), die zuletzt durch Artikel 1 der Verordnung vom 3. Januar 2018 (BGBl. I S. 99) geändert worden ist, 45 S.

UN (2017) United Nations, Department of Economic and Social Affairs, Population Division. World Population Prospects: The 2017 Revision, Key Findings and Advance Tables. Working Paper No. ESA/P/WP/248.

van Halem, D., Moed, D.H., Verberk, J.Q.J.C., Amy, G.L., van Dijk, J.C. (2012) Cation exchange during subsurface iron removal. Wat. Res. 46(12), 307-315. doi: 10.1016/ j.watres.2011.10.015.

van Vliet, M.T.H., Franssen, W.H.P., Yearsley, J.R., Ludwig, F., Haddeland, I., Lettenmaier, D.P., Kabat, P. (2013) Global river discharge and water temperature under climate change. Glob. Environ. Chang. 23(2), 450-464. doi: 10.1016/j.gloenvcha.2012.11.002.

Villinski, J.E., Saiers, J.E., Conklin, M.H. (2003) The Effects of Reaction-Product Formation on the Reductive Dissolution of MnO_2 by Fe(II). Environ. Sci. Technol. 37(24), 5589-5596. doi: 10.1021/es034060r.

von Gunten, H.R., Karametaxas, G., Keil, R. (1994) Chemical processes in infiltrated riverbed sediments. Environ. Sci. Technol. 28(12), 2087-2093. doi: 10.1021/es00061a017.

von Gunten, H.R., Karametaxas, G., Krähenbühl, U., Kuslys, M., Giovanoli, R., Hoehn, E., Keil, R. (1991) Seasonal biogeochemical cycles in riverborne groundwater. Geochim. Cosmochim. Acta 55(12), 3597-3609. doi: 10.1016/0016-7037(91)90058-D.

von Rohr, R.M., Hering, J.G., Kohler, H.P., von Gunten, U. (2014) Column studies to assess the effects of climate variables on redox processes during riverbank filtration. Water Res. 61, 263-275. doi: 10.1016/j.watres.2014.05.018.

WSV (2018) Wasserstraßen- und Schifffahrtsverwaltung des Bundes. Hydrologisches Informationssystem. Online verfügbar unter www.wsv.de (letzter Zugriff am 31.07.2018).

Beiliegende Publikationen

[P1] **Paufler, S.**, Grischek, T. (2018) Herkunft und Verhalten von Mangan bei der Uferfiltration. Grundwasser 23(4), 277-296. doi: 10.1007/s00767-018-0401-8.

[P2] Grischek, T., **Paufler, S.** (2017) Prediction of iron release during riverbank filtration. Water 9, 317, 1-13. doi: 10.3390/w9050317.

[P3] Ghodeif, K.O., **Paufler, S.**, Grischek, T., Wahaab, R., Souaya, E., Bakr, M., Abogabal, A. (2018) Riverbank filtration in Cairo, Egypt - Part I: Installation of a new riverbank filtration site and first monitoring results. Environ. Earth Sci. 77, 270. doi: 10.1007/s12665-018-7450-2.

[P4] **Paufler, S.**, Grischek, T., Bartak, R., Ghodeif, K., Wahaab, R., Boernick, H. (2018) Riverbank filtration in Cairo, Egypt - Part II: Detailed investigation of a new riverbank filtration site with a focus on manganese. Environ. Earth Sci. 77, 318. doi: 10.1007/s12665-018-7500-9.

[P5] **Paufler, S.**, Grischek, T., Benso, M., Seidel, N., Fischer, T. (2018) The impact of river discharge and water temperature on manganese release from the riverbed during riverbank filtration – A case study from Dresden, Germany. Water 10(10), 1476. doi: 10.3390/w10101476.

[P6] **Paufler, S.**, Grischek, T., Herlitzius, J., Feller, J., Kulakov, V.V. (2019) Manganese release linked to carbonate dissolution during the start-up phase of a subsurface iron removal well in Khabarovsk, Russia. Sci. Total Environ. 650(2), 1722-1733. doi: 10.1016/j.scitotenv.2018.09.319.

[P7] **Paufler, S.**, Grischek, T., Adomat, Y., Herlitzius, J., Hiller, K., Metelica, Y. (2018) Effective range of chlorine transport in an aquifer during disinfection of wells: from laboratory experiments to field application. J. Hydrol. 559, 711-720. doi: 10.1016/j.jhydrol.2018.02.054.

[P8] **Paufler, S.**, Grischek, T., Ruppert, M. (2019) Freisetzung von Mangan nach Umstellung von Brunnen mit unterirdischer Enteisenung auf Dauerbetrieb. gwf Wasser / Abwasser 1(160), 55-65.

Beiliegende Publikation 1

Paufler, S., Grischek, T. (2018) Herkunft und Verhalten von Mangan bei der Uferfiltration. Grundwasser 23(4), 277-296. doi: 10.1007/s00767-018-0401-8.

Beiliegende Publikation 2

Grischek, T., **Paufler, S.** (2017) Prediction of iron release during riverbank filtration. Water 9, 317, 1-13, doi: 10.3390/w9050317.

water

MDPI

Article

Prediction of Iron Release during Riverbank Filtration

Thomas Grischek * and Sebastian Paufler

Division of Water Sciences, Faculty of Civil Engineering & Architecture, Dresden University of Applied Sciences, 01069 Dresden, Germany; sebastian.paufler@htw-dresden.de

* Correspondence: thomas.grischek@htw-dresden.de; Tel.: +49-351-462-3350

Academic Editor: Pieter J. Stuyfzand

Received: 19 February 2017; Accepted: 24 April 2017; Published: 30 April 2017

Abstract: At many sites, anoxic conditions and dissolution of iron and manganese are already present, or are likely to develop during riverbank filtration (RBF). A prediction of iron and manganese mobilization during riverbank filtration is required to evaluate the need for further water treatment. Different methods have been tested at RBF sites in Germany: water and sediment analysis, batch and column experiments using river water, sequential extraction, and the mass balance approach. At these sites, a "wash out" effect was observed, resulting in a gradual decrease in iron concentrations between the riverbank and the abstraction well over two decades. Hydrogeochemical exchange processes in the aquifer can cause a long-term release of iron and manganese even if the organics concentration in the river water is low. Contrary to common expectations, high iron concentrations are often dominated by the portion of landside groundwater, whereas iron concentrations in bank filtrate often undergo a long-term decline.

Keywords: riverbank filtration; iron; manganese; remobilization

1. Introduction

Riverbank filtration (RBF) is a natural or technically-induced process during which surface water is subjected to subsurface flow prior to extraction from vertical or horizontal wells, caisson wells, or drain pipes. The raw water abstracted from the pumping well consists of a mixture of infiltrated river water and groundwater recharged in the landside catchment (Figure 1).

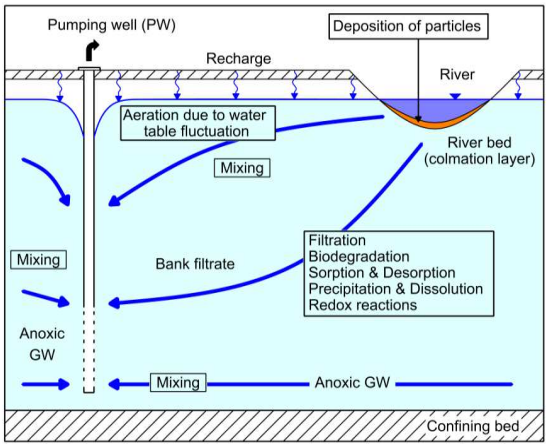

Figure 1. Schematic diagram of processes affecting iron and manganese concentration during riverbank filtration.

From a water resources perspective, RBF is normally characterized by improved water quality [1,2]. Therefore, RBF is a well-proven treatment step which, at numerous sites, is part of a multi-barrier approach to the drinking water supply. The positive effects of RBF arise primarily in the mixing, sorption, and degradation processes. The whole process can be thought of as occurring in two distinct steps:

(1) the highly biologically active colmation (clogging) zone in the riverbed, in which intensive filtration, degradation, and sorption processes take place over short flow paths and residence times; and
(2) the subsequent subsurface aquifer passage with more moderate degradation and sorption rates, and also the increasing effects of mixing processes.

Many organic, especially nonpolar water substances, are completely retained during RBF, while poorly-degradable polar compounds are hardly removed at all. A synoptic evaluation of the elimination processes at RBF sites in the Netherlands revealed a strong and sustainable removal of polycyclic aromatic hydrocarbons, polychlorinated biphenyls, organochlorine pesticides, bromoform, nitrobenzene, nitrotoluene, and chloronitrobenzene, regardless of redox conditions [3]. Anoxic conditions bring about a thorough removal of pesticides, like atrazine, diuron, and simazine, which are hardly broken down under aerobic conditions. During RBF on the Rhine River, concentrations of dissolved organic carbon (DOC), adsorbable organic halogen or sulfur compounds (AOX or AOS) were reduced, on average, by more than 50% after a residence time of 6–8 weeks. An overview of the removal of organic and inorganic water substances with respect to redox conditions is offered by Stuyfzand [3] and Ray et al. [4].

Depending on the quality of the surface water, redox conditions can already change quickly in the riverbed or along the subsequent flow path in the aquifer. This depends especially on organic carbon, oxygen, and nitrate concentrations, and temperature. If riverbed and/or aquifer sediments contain iron and/or manganese minerals/(hydr)oxides, these can be reduced and dissolved. The resulting increases in dissolved iron and/or manganese concentrations can create problems for drinking water supply.

Precipitation of iron and manganese can cause incrustations in pipes, which are relevant for flow hydraulics and offering surfaces for microbial growth, which can cause increased turbidity and a brown color in the water during times of increased flow velocities in networks. It will also adversely affect the taste of the water. Thus, using the abstracted water as drinking water, but also for industrial and agricultural purposes, requires adequate treatment, which is commonly performed after abstraction e.g., by aeration and filtration. As a result, iron and manganese removal is required as a further treatment step, making RBF more costly and representing a drawback that may limit its wider use as an alternative to direct surface water abstraction and treatment. Thus, prediction of iron and manganese release during riverbank filtration is required.

If the biodegradable portion of total organic carbon (TOC) in river water is relatively high, biodegradation processes can consume all dissolved oxygen, and often nitrate as well [5]. This, again, can cause anoxic environments in the aquifer (especially in aquifers that exhibit low hydraulic conductivity and/or confined conditions) and dissolution of iron and manganese. Such a case is shown in principle in Figure 2, where the iron concentration in the pumped water increases as a result of redox and/or dissolution processes in the riverbed and/or aquifer. A simple DOC analysis is not sufficient because particulate organic matter (the difference between TOC and DOC) often accumulates in the riverbed and consumes oxygen and nitrate. Even autochthonous production of TOC at the sediment-water interface has been observed at RBF sites [6].

At many sites, anoxic conditions are already present (Figure 3) and dissolution of iron and manganese would develop during RBF. Although this paper will focus on iron and manganese, at a few sites such dissolution can also be observed for arsenic as a result of a reduction of As(V) to As(III) having a higher solubility or related to dissolution of iron (hydr)oxides containing previously-adsorbed or co-precipitated As. Recent findings on As removal during RBF are published by Postma et al. [7].

Continuous pumping and low(er) iron and manganese concentrations in bank filtrate would change the local equilibria in the aquifer and result in dissolution and/or desorption of iron and manganese. Figures 4 and 5 demonstrate the principal, time-dependent change in Fe concentration between the river and the pumping well (PW). If the portion of bank filtrate (BF) in the pumped water is high, e.g. 80%, the expected decrease in the iron concentration in the pumped water will be stronger during the same time Δt (Figure 6). It must be mentioned that a prediction of the iron concentration is not straightforward, as the river stage and well operation will affect the portion of BF (Figure 7, higher portion during floods, lower portion after non-operational periods of wells) and the landside groundwater quality has some dynamics.

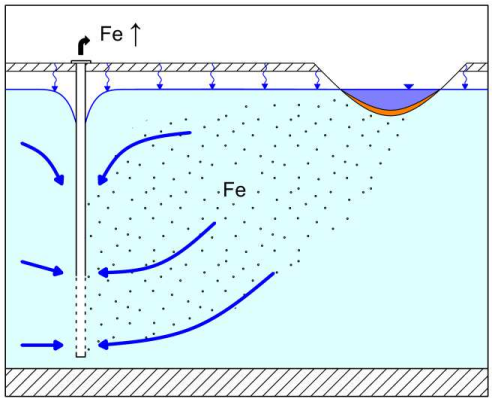

Figure 2. Case A—Low iron conc. in GW, increase due to RBF processes in riverbed and aquifer.

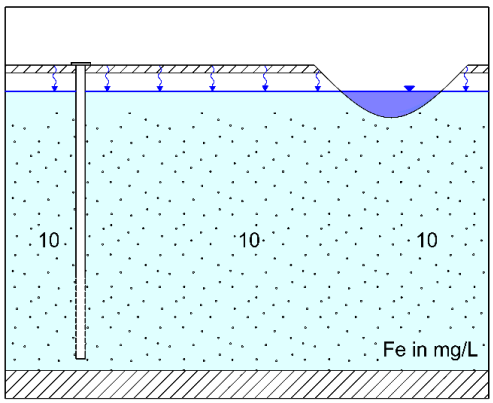

Figure 3. Case B—High iron-conc. in GW feeding the river, low iron conc. near groundwater surface.

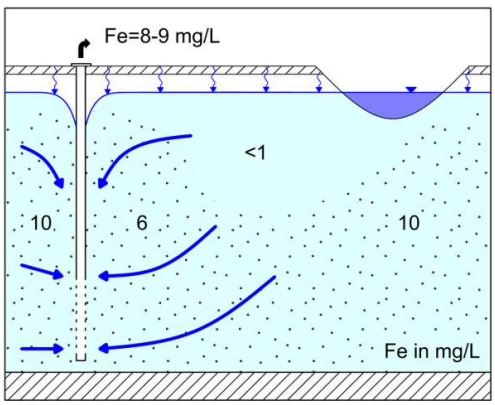

Figure 4. Case B—Infiltration of river water resulting low iron conc. in bank filtrate.

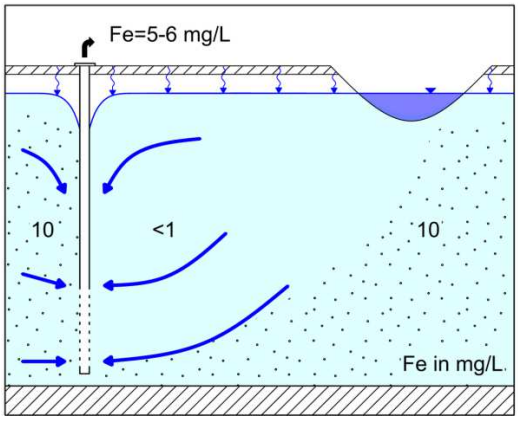

Figure 5. Case B—Significant decrease in iron conc. in in pumped water after years or decades.

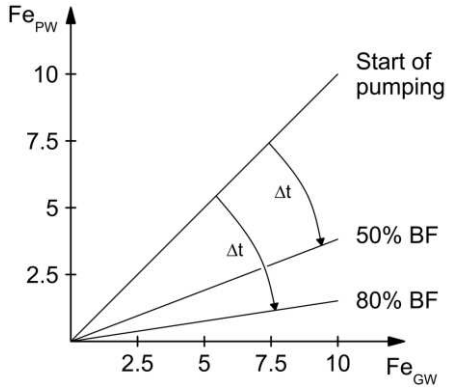

Figure 6. Change in iron conc. in pumped water (PW) with time depending on iron conc. in GW.

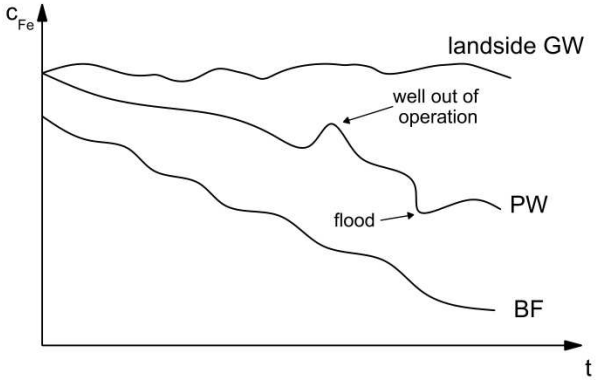

Figure 7. Expected change in iron conc. in pumpedwater (PW) and bank filtrate (BF) for Case B.

Based on field site investigations along the Elbe River in Germany, long-term water quality changes will be discussed together with accompanying laboratory experiments.

2. Materials and Methods

2.1. Water Quality Investigation at RBF Site at Torgau

The source water catchment of the RBF waterworks at Torgau is located along the left bank of the Elbe River (Figure 8). There are 42 vertical wells arranged in 9 groups of 3–7 wells, at an average distance from the riverbank of 300 m, over a river reach about 15 km long. Abstraction rates of

approximately 150 m^3/h per well provide a total waterworks capacity of around 150,000 m^3/d. Well screens have a length of 15–20 m and are located at a depth of 30–50 m below ground level inside a zone of coarse to medium sand layers. The total thickness of the aquifer does not exceed 55 m.

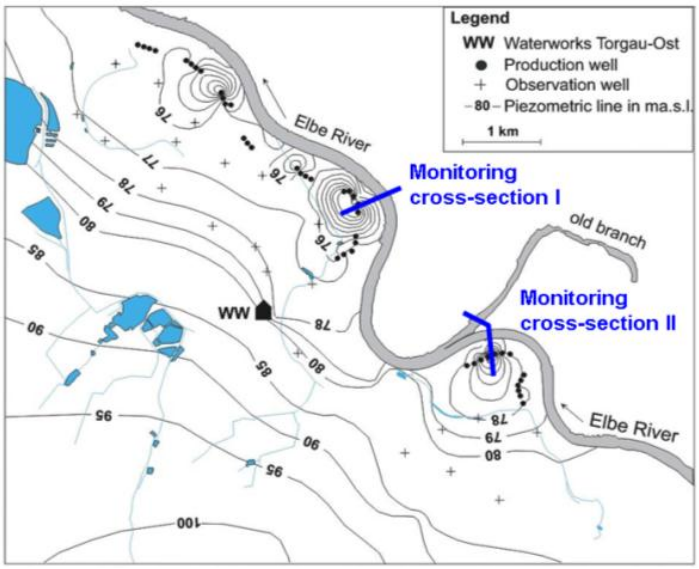

Figure 8. Location map of RBF site Torgau along the River Elbe, showing cross-sections I and II.

Groundwater samples were taken at least monthly from cross-sections, including several observation wells at different distances from the riverbank and different depths between 1995 and 1997, later with lower frequency during routine sampling campaigns of the water company. Groundwater was obtained using either a mobile submersible pump lowered into observation wells or from in situ membrane pumps used to sample from directly below the riverbed. Chemical analyses included major ions, iron, and manganese, and were carried out according to German guidelines and DIN methods (e.g., DIN 38401 for iron analysis [8,9]).

2.2. Laboratory Experiments

To properly estimate the magnitude of iron and manganese released from the sediment, the source of the high iron concentrations, especially in the landside groundwater, must be identified. The total iron content, as well as the chemical speciation of iron were, therefore, determined by running tests on the soil. By using a variety of extraction methods, it is possible to quantify the fractions of a certain metal (e.g., iron) in its different species, since the stability of the different species largely depends on the respective dominant redox and pH conditions. In this way, stepwise (sequential) changes in these conditions revealed how much each fraction contributed to the total iron content.

Preliminary tests were conducted with sediment samples from drill cores from observation well (OW) I-6. The total iron concentration in the grain size fraction <2 mm decreased from 3500 mg/kg in the unsaturated zone to a relatively constant level of 1500 mg/kg below 69 meters above sea level (masl). This decrease was corroborated by the observation of strong surface deposits of red iron hydroxides on the quartz grains in the unsaturated zone. In the deepest part of the aquifer, the total iron content was higher than in the middle layers. The portion of easily extractable iron made up 41% $\pm$ 11.5% of the total iron content. No crystalline iron minerals were found using X-ray diffraction analysis in any samples. An iron content of 6400 mg/kg was extracted from a soil sample from a depth of 48.5 masl, which contained lignite particles.

Soil samples A and B were taken from OW II-6 immediately next to well 33 on the land side, from depths of 22–25 m below ground level (mbgl) and 40–43 mbgl, respectively. These were used in a batch experiment following the method of sequential extraction according to Brand [10]. In the first three

steps for the determination of well soluble iron salts, exchangeable ions and carbonate-bound phases, it was possible to extract 70 mg/kg from the soil. The fourth extraction step using hydroxylammonium chloride solution at a pH of 2 revealed high iron concentrations. Since repeated batch experiment trials all yielded high iron concentrations, a large-scale experimental approach was taken.

In January 1994, four columns were setup to run in a closed loop with extraction chemicals, each containing 1000 g of air-dried soil, sieved to below 2 mm. The iron content of the soil samples was in the range of 0.2%–0.4%, typical for Quaternary medium sand. In the first three extraction steps a total of only 5 mg/kg of iron was released. The fourth extraction step with hydroxylammonium chloride solution allowed a repeated extraction of iron at concentrations between 20 and 26 mg/L iron, virtually without end. Therefore, the solutions were renewed weekly in the beginning, later every two weeks, to continue the iron extraction and to quantify the easily-reducible iron fraction. Two experiments with two columns in parallel ran over 511 days, and two other columns over a total of 873 days.

3. Results

3.1. Field Observations

Much of the biodegradable portion of particulate organic matter, DOC, and biodegradable single organic compounds are swiftly attenuated in the riverbed, which has a high organic carbon content. For DOC and many single compounds, up to a 50% decrease in concentration occurred along the first few centimeters of the flow path [5]. Accordingly, oxygen is completely consumed along the first decimeters of the flow path. At the RBF site at Torgau, with retention times of the bank filtrate in the aquifer between 50 and 300 days [9], the nitrate concentration decreased from 22 to <1 mg/L as a result of heterotrophic and autotrophic denitrification (Table 1). Mass balance calculations and laboratory experiments showed that the input of biodegradable organic carbon during riverbank filtration is lower than the stoichiometric demand for oxygen consumption and denitrification [5,9,11]. The oxidation of 1 mg/L DOC requires about 1.2 mg/L O_2 and the oxidation of 1 mg/L NH_4^+ requires about 3.6 mg/L O_2. These observations implied that particulate organic carbon, which forms an organic rich layer in the upper centimeters of the riverbed (proven by analyses of TOC in sediment samples from different depths), acts as a reducing agent for O_2 and nitrate in the bank filtrate. The resulting Fe(II) concentration in bank filtrate at OW I-6/3 is slightly increased compared to river water, but is much lower than in landside groundwater.

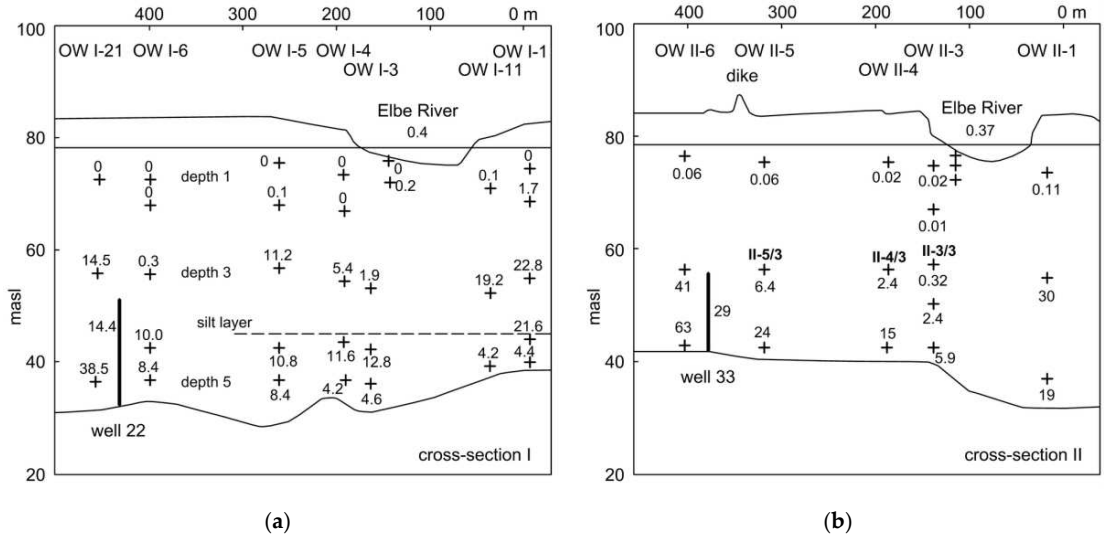

(**a**) (**b**)

Figure 9. Mean total iron concentrations in mg/L at (**a**) cross-section I and (**b**) cross-section II in Torgau, 1995-97 (n > 12), looking downstream.

Table 1. Hydrochemical parameters of Elbe River water, bank filtrate (BF) near the river at OW I-4/2 and near the pumping well at OW I-6/3, pumped water from Well 22, and landside groundwater at OW I-21/3 at the RBF site in Torgau, Germany (median values for the period 1995-97, n > 36; location of OW see Figure 9).

	Elbe River	Bank filtrate		Well 22	Landside GW	Change from River to BF
Parameter		OW I-4/2	OW I-6/3		OW I-21/3	OW I-6/3
pH	7.5	7.0	6.9	6.6	6.1	-
EC in µS/cm	479	475	466	581	761	-
O_2 in mg/L	10	<0.1	<0.1	<0.1	<0.1	down >99%
DOC in mg/L	5.5	3.2	2.8	2.2	1.6	down 49%
NH_4^+ in mg/L	0.4	0.02	0.06	0.16	0.02	down 85%
NO_3^- in mg/L	22.1	16.1	<1	1.6	<1	down >95%
Fe^{2+} in mg/L	<0.1	<0.1	0.3	14.4	14.5	up >200%
Mn in mg/L	0.11	0.14	0.08	0.63	0.59	down 27%
Cl^- in mg/L	26.5	27.2	27.0	33.4	42.9	-
SO_4^{2-} in mg/L	85	91	104	162	257	up 22%
Ca^{2+} in mg/L	56.6	49.5	54.1	65.3	76.3	-
Mg^{2+} in mg/L	11.0	10.1	10.3	11.9	15.2	-
Na^+ in mg/L	22.9	23.8	22.4	22.7	25.6	-

The iron concentration in the abstracted water of the wells in the whole catchment covers a wide range, with an average value of 17 mg/L for the observed wells. Additionally, large variations of iron concentration (from 0 to over 100 mg/L) can be observed over the vertical expanse of the aquifer [10]. In the bank filtrate the median Fe(II) concentrations increased very slightly by 0.25 mg/L, up to the OW nearest to the Elbe River. In the shallow depths, no increase in Fe(II) concentration was found, as expected in the presence of nitrate. In cross-section I a decrease in iron concentrations was found below the silt layer, likely due to the infiltration of groundwater from the right-hand side of the Elbe River. The old groundwater at the greatest depth showed iron concentrations of about 4 mg/L.

Figure 9 provides an overview of the distribution of the total iron concentrations. As Fe(III) is only slightly soluble at neutral pH, the total iron concentration at values above 1 mg/L can be primarily attributed to the Fe(II) concentrations.

Given the lack of oxygen and nitrate and the availability of biodegradable organic compounds, reduction of Fe(III) was expected at the medium depth. However, as well operation continued, a decrease in Fe(II) concentrations in bank filtrate was found in both cross-sections. This change was most pronounced in cross-section II. Figure 10 shows the decrease in iron concentrations at OW II-3/3, II-4/3, II-5/3, and well 33.

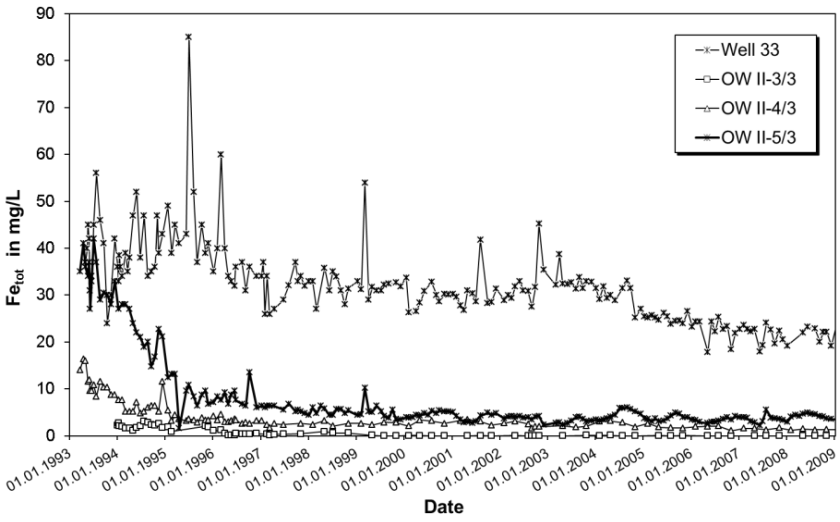

Figure 10. Progression of total iron concentrations in mg/L, medium depth, and cross-section II in Torgau.

Before well 33 was put into operation in 1993, the water sampled from OW II-5/3 was under the strong influence of landside groundwater, which showed iron concentrations as high as 100 mg/L. Depending on the water level in the river, iron-rich landside groundwater can enter the region between the wells and the river, during times when well 33 is operating at a low flow rate or the well gallery is not in operation. This water is subsequently extracted from the wells, leading to iron concentration peaks in the raw water. The augmented flow of bank filtrate, brought about by the steady operation of wells, led to a drastic reduction in median iron concentrations during the period from 1993 to 1998 from 34 mg/L to 4.4 mg/L at OW II-5/3 (bank filtrate) and from 1993 to 2009 from 40 mg/L to 20 mg/L at well 33 (mixture of bank filtrate and groundwater), as well as manganese concentrations from 1.6 mg/L to 0.1 mg/L at OW II-5/3 and from 1.6 mg/L to 0.9 mg/L at well 33 during the same periods. The decreasing iron and manganese concentrations could be explained as a result of leaching of the most reactive $Fe(OH)_3$ phase in the aquifer between the river and the well.

3.2. Laboratory Experiments

Figure 11 shows the cumulative mass curves of the iron extracted during the column experiments. Soil sample A yielded 2470 mg/kg of extract out of a total 3550 mg/kg, and 400 mg/kg was found in the subsequent soil analysis. Soil sample B yielded 2000 mg/kg of extract out of a total 2470 mg/kg, and 130 mg/kg was measured in the subsequent soil analysis. The portion of extracted iron made up 70% and 81% of the total iron content, respectively. These figures are underestimates, as the cumulative mass curves showed a clear upward trend, and more iron would have been extracted had the experiments been continued. It can be concluded from these results that the vast majority of iron in the soil is present in the form of amorphous iron hydroxides and iron oxides.

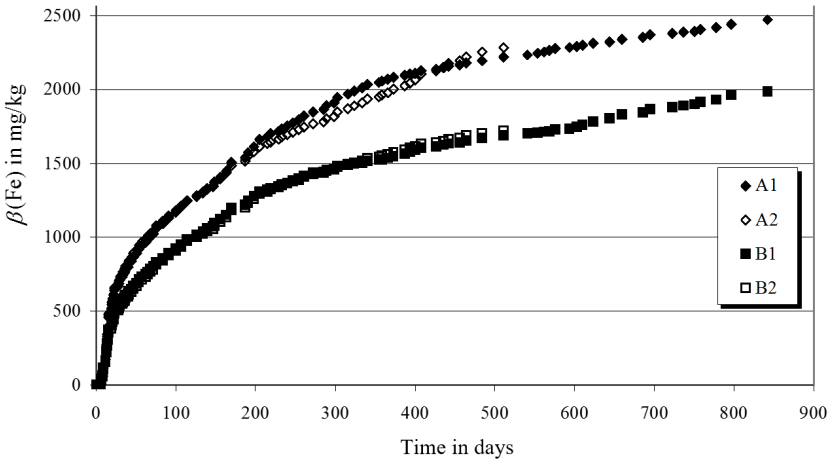

Figure 11. Cumulative mass curves of the iron extracted from the soil samples from OW II-6.

Mineralogical tests of the soil samples from the groundwater aquifer indicated the presence of quartz, feldspar, and iron-rich chlorite [12], probably Thuringite. The chlorite comes from alluvially-deposited fragments of mica slate and from the weathering of biotite, which is contained in granodiorite boulders. In some isolated cases magnetite was found in grain sizes below 100 µm, but was generally found below 2 mm throughout the entire depth, as determined by suspension experiments and with the help of magnets.

4. Discussion

4.1. Control of Iron Concentration at an Existing RBF Site at Torgau

Steady operation of the wells led to a displacement of groundwater through bank filtrate and to a slow reduction in iron concentrations in the raw water. This conclusion has been supported

by the analysis of raw water data from other wells. In the time between 1986 and 1994 there was a gradual decrease in iron concentrations of about 1 mg/L per year for all wells near cross-section I. From 1995–1997 to 2007, the mean iron concentration at well 22 decreased from 14.4 mg/L by about 50% and remained stable between 6 and 8 mg/L during the period from 2007 to 2016 as a result of high iron concentrations in landside groundwater. Which iron concentrations should be expected in the bank filtrate in the long term? In the Elbe valley at Torgau, the steady operation of the wells is likely to cause a continued displacement of the iron-rich pore water and eventually lead to iron concentrations below 3 mg/L in bank filtrate, even at cross-section II, which had a high initial iron concentration in the groundwater. In 2006, the mean iron concentrations in OW II-5/3 and well 33 were 3.2 mg/L (n = 7) and 23.1 mg/L (n = 9), respectively. Later on, sampling was reduced to specific observation wells. Pumping from well 33 was stopped in 2009 due to a decreasing water demand and the option to pump water with lower iron concentrations from other wells. Thus, the further development of iron concentrations could not be investigated.

The Fe(II) concentrations in the bank filtrate continue to fall as the well galleries operate over the years, as Figure 7 shows in principle, and are hardly influenced anymore by reductive processes. The increased portion of bank filtrate in the raw water caused by higher pumping rates is causing a decrease in the iron concentration of the raw water down to a threshold value that is determined by the influx of landside groundwater. The well galleries are designed for long-term continuous operation. This creates a continuous replacement of the iron-rich water in the area between the wells and the river.

Before the well galleries started operating, the Elbe valley at Torgau was characterized by unusually high iron concentrations between 10 and 100 mg/L in the middle and lower depths of the aquifers, mainly as a result of pyrite oxidation. At the majority of the OW, the highest iron concentrations were found at medium depths (20 to 30 m below the water table) together with high sulphate concentrations (see Table 1, OW I-21/3). The high iron concentrations of the landside groundwater are not likely to decrease in the coming decades due to a very low flow velocity of less than 0.1 m/d. Even at a 60%–65% portion of bank filtrate, with its ever-decreasing iron concentrations, 10 mg/L is the lowest concentration that is likely to be achieved in the raw water.

The location of wells 22 and 33 within well groups allowed an estimation of the region of the aquifer from which they receive water if all wells are active. Figure 12 shows the principle of fixing the catchment area, which is much more difficult for single wells. If data on the bank filtrate portion, flow conditions, thickness of the aquifer, and easily-reducible fraction of iron in the aquifer material are available, and an input concentration of iron beneath the riverbed can be neglected, a simple calculation can be done to theoretically estimate the time at which the available iron in the aquifer between the wells is mainly removed.

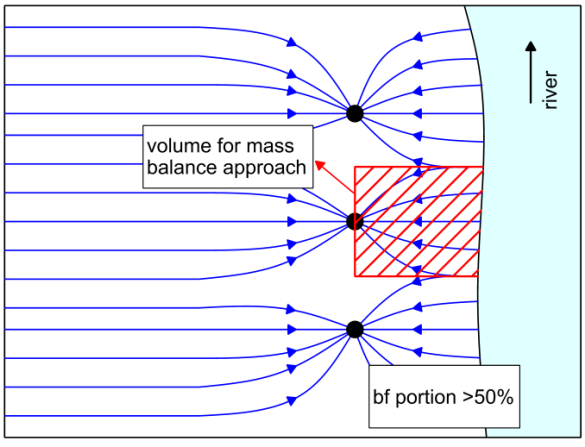

Figure 12. Approach to determine the aquifer volume from which iron could be released.

For cross-section II in Torgau, a pool of >2.5 million kg iron was calculated for the actively-used part of the aquifer based on about 2500 mg/kg soluble iron in the lab experiments (Figure 11). At a pumping rate of about 150 m^3/h, a portion of bank filtrate of 50% and a starting iron concentration in the bank filtrate of about 40 mg/L (optimistic approach with start concentration, Figure 10), a removal of 26,280 kg iron per year can be calculated. Assuming a stable removal rate despite the observed decrease in iron concentrations in bank filtrate due to different flow paths in the aquifer, a complete iron removal would be achieved within 95 years. This is much longer than the field observations indicate. Reasons for such overestimation of time are neglecting lower iron concentrations in the aquifer in the upper layer and near the river due to surface water–groundwater interaction before installation of the RBF scheme, optimistic observations along cross-section II at the centre of the defined area presenting the shortest travel times, and different flow velocities in different aquifer layers resulting in faster "wash out" along preferred flow paths in layers having a higher hydraulic conductivity. On the other hand, this explains the slow response of the iron concentration in well water (Figure 10). In summary, the mass balance approach gave a rough and more pessimistic estimate for the time required for rendering the aquifer section between the well and the river becoming iron-free.

4.2. Control of Iron Concentration as an Aspect of Planning New RBF Sites

In designing new RBF sites, the first step should be a comparison with existing sites with similar boundary conditions. Field experiments using observation wells to study the removal efficiency and to obtain parameters for the design of large RBF facilities are only useful if the pumping rates are high and the experiments are carried out for a long time (years). Such field studies should be accompanied by batch and/or column experiments in the laboratory using actual river water and sediments from the riverbed and aquifer at the site in question. These experiments could be completed within six months. After installation of abstraction wells, a minimum of two observation wells should be placed between the riverbank and the wells and one on the land side of the wells, each with sampling points at different depths depending on the thickness of the aquifer. If frequent sampling is difficult to manage, e.g., during long winter periods, a continuous automated measurement of water temperature and electrical conductivity in the observation wells using probes and data loggers is advised [13].

The occurrence of iron in groundwater is a common problem that constrains wide groundwater use for drinking water supplies worldwide. For example, in Egypt, a baseline national water quality monitoring report [14] indicated a high level of iron and manganese in some observation wells in the Nile delta. Iron concentrations in the Quaternary aquifer of the Nile delta exceed the Egyptian drinking water standards of 0.3 mg/L in about 20% of wells sampled [15] with a maximum value of 1.7 mg/L [16]. There is great potential for RBF in Egpyt [17]. However, elevated iron concentrations in landside groundwater indicate that the part of the aquifer between the riverbank and the newly-planned pumping well could release iron in the long term, even if the biodegradable portion of DOC of the river water is low and redox processes are limited. Control of iron concentration by specific well operation will be marginal. Design parameters of an RBF scheme, such as the number and pumping rates of wells and the distance between the wells and the riverbank, are the most important. If RBF is mainly used to remove particles and pathogens, and to achieve some pre-treatment, the wells might be placed near to the riverbank (Figure 13), thereby pumping a higher portion of bank filtrate and achieving lower iron concentrations in raw water after several months or years. Therefore, it is necessary to understand flow conditions, especially if test wells are operated.

Intermittent operation of the wells, or the entire gallery, should be avoided, since this would allow the iron-rich landside groundwater to spill over the wells into the area between the river and the wells, erasing the positive effects on total iron concentration in the raw water achieved through the continuous extraction of bank filtrate (Figure 7).

In some cases, the pumping rate of a test well has been too low compared to the distance to the riverbank, or it was not continuously pumped [13]. In such cases (Figure 14), the portion of bank filtrate would be very low and no "wash out" effect for iron would be observed.

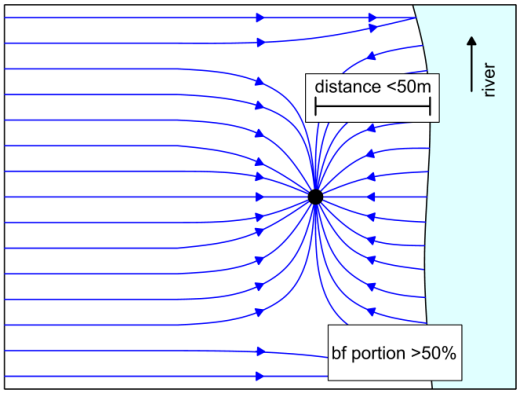

Figure 13. Well placed near the riverbank, pumping more than 50% bank filtrate (bf).

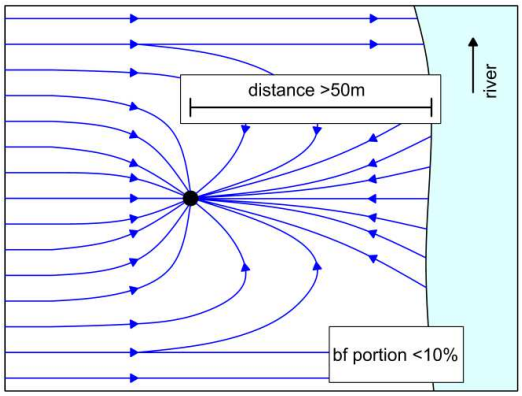

Figure 14. Well placed too far from riverbank pumping less than 10% bank filtrate (bf).

A high portion of bank filtrate, which could be achieved by locating wells on an island or in a meander, could be advantageous for preventing the necessity of iron removal in post-treatment. As the composition and clogging of the riverbed are of major importance, the potential of iron, manganese, and arsenic remobilization within the riverbed should be investigated in detail, e.g., using column experiments with original riverbed sediment and river water.

4.3. Further Issues Related to Manganese Release

If redox processes cause remobilization of metals along the flow path of bank filtrate, an increase in manganese is frequently also observed, which is more difficult to handle than iron during post-treatment. Possibilities of influencing the manganese concentration in mixed raw water were investigated at two sites in Germany by altering the operation of bank filtration wells. Success depends on the boundary conditions affecting the release of manganese, as well as the operational demands with respect to the choice, operating time, and discharge rates of the wells. The change in manganese concentration during bank filtration fundamentally depends on the groundwater flow velocity (residence time), temperature, pH, the presence and thickness of a clogging layer on the bank of the surface water body, and the degree of oxygen consumption. The evaluation of data from bank filtration sites in Meissen and Dresden along the Elbe River show that manganese concentrations in pumped raw water are most influenced by the mode of operation of the wells and the resulting mixture ratio. Depth-dependent sampling in individual pumping and observation wells was a precondition to distinguish between mixing and redox processes. A mass balance study of manganese in riverbed sediment and aquifer material showed that manganese can be released over a period of many decades during an anoxic subsurface passage of bank filtrate [18]. Finally, it has to be mentioned that the

remobilization of manganese is more difficult to predict, as observed in aquifer storage and recovery studies in The Netherlands [19,20] and at a lake bank filtration site in Berlin, Germany [21].

5. Conclusions

Current guidelines do not exist to support engineers in identifying appropriate sites for RBF. A complex and comprehensive assessment of hydrological, hydrogeological, and hydrochemical aspects, together with information about country- and state-specific regulations, land use, cost, and other issues, are necessary for optimal RBF siting [9,22]. It is essential to have a clear understanding of how RBF will be utilized (e.g., as a means of pre-treatment or as a primary treatment) prior to commencing site location planning studies, as certain conditions may be likely to arise that demand additional technical measures.

At the RBF site at Torgau, a long-term "wash out" effect was observed, resulting in a slow, but steady decrease in iron concentrations between the riverbank and the abstraction well. Exchange processes in the aquifer can cause a long-term release of iron and manganese even if the DOC concentration is low. A combination of the sequential extraction of aquifer sediments and the mass balance approach proved that iron release can last several decades. Thus, at some sites, a short distance between the riverbank and the wells would be advantageous in lowering costs for further treatment.

Coupling of RBF and subsurface iron removal (SIR) is an interesting option and has been used for many years at Linz in Austria, Boker Heide in Germany, and Khabarovsk in Russia [23,24]. Results from a five-month field experiment coupling RBF and SIR in Torgau, Germany, showed satisfying iron removal which partly exceeded the expectations by far [24]. However, the results from the Torgau experiments cannot be simply transferred to other sites because of numerous factors affecting the chemical processes involved. The relatively large distance between the Elbe River and the pumping wells cause equilibration of concentrations and water levels to a higher degree than observed at other RBF sites.

Acknowledgments: The authors are grateful to the BMBF for funding the projects "NIRWINDU" (02WCL1356A) and "FHproUnt2012: Optimization of bank filtration and subsurface removal of iron and manganese" (03FH042PX2). Manganese data analysis was supported by an ESF grant (no. 200031585) to S. Paufler. The authors thank Fernwasserversorgung Elbaue-Ostharz GmbH and DREWAG Netz GmbH for providing data and supporting sampling campaigns.

Author Contributions: T.G. reviewed data from the Torgau RBF site, conducted samplings and lab experiments within his PhD work and later projects, S.P. reviewed literature on manganese dissolution and conducted field experiments at the Hosterwitz RBF site 2015–2016.

Conflicts of Interest: The authors declare no conflict of interest. The founding sponsors had no role in the design of the study; in the collection, analyses, or interpretation of data; in the writing of the manuscript, and in the decision to publish the results.

References

1. Hiscock, K.; Grischek, T. Attenuation of groundwater pollution by bank filtration. *J. Hydrol.* **2002**, *266*, 139–144. [CrossRef]
2. Kuehn, W.; Mueller, U. River bank filtration—An overview. *J. AWWA* **2000**, *92*, 60–69.
3. Stuyfzand, P.J. Fate of pollutants during artificial recharge and bank filtration in the Netherlands. In *Artificial Recharge of Groundwater*; Peters, Ed.; Balkema: Rotterdam, The Netherlands, 1998; pp. 119–125.
4. Ray, C.; Melin, G.; Linsky, R.B. *Riverbank Filtration–Improving Source Water Quality*; Kluwer Academic Publishers: Dordrecht, The Netherlands, 2003; p. 364.
5. Grischek, T.; Hiscock, K.M.; Metschies, T.; Dennis, P.; Nestler, W. Factors affecting denitrification during infiltration of river water into a sand and gravel aquifer in Saxony, Germany. *J. Water Res.* **1998**, *32*, 450–460. [CrossRef]
6. Diem, S.; Rudolf von Rohr, M.; Hering, J.G.; Kohler, H.P.; Schirmer, M.; von Gunten, U. NOM degradation during river infiltration: Effects of the climate variables temperature and discharge. *J. Water Res.* **2013**, *47*, 6585–6595. [CrossRef] [PubMed]

7. Postma, D.; Mai, N.T.; Lan, V.N.; Trang, P.T.; Sø, H.U.; Nhan, P.Q.; Larsen, F.; Viet, P.H.; Jakobsen, R. Fate of arsenic during Red River water infiltration into aquifers beneath Hanoi, Vietnam. *Environ. Sci. Technol.* **2017**, *51*, 838–845. [CrossRef] [PubMed]
8. *German Standard Methods for the Examination of Water, Waste Water and Sludge; Cations (Group E); Determination of Iron (E1)*; DIN 38406-1; Beuth Verlag GmbH: Berlin, Germany, 1983.
9. Grischek, T. Management of Bank Filtration Sites along the Elbe River. Ph.D. Thesis, Communication of the Institute for Groundwater Management, TU Dresden, Dresden, Germany, 2003; p. 252.
10. Brand, K. Investigation of precipitation and remobilization of heavy metals Pb, Cd, Cu and Zn during bank filtration. In *Schriftenreihe Angewandte Geologie Karlsruhe*; Angewandte Geologie Karlsruhe: TH Karlsruhe, Germany, 1989; Volume 6, pp. 73–77. (In German)
11. Nestler, W.; Walther, W.; Jacobs, F.; Trettin, R.; Freyer, K. *Water Production in Alluvial Aquifers along the River Elbe*; UFZ-Research Report 7; Helmholtz Centre for Environmental Research: Leipzig, Germany, 1998; p. 203. (In German)
12. Clayton, R.G. Geochemical modelling of an unconfined aquifer adjacent to the River Elbe, Dresden. Master's Thesis, NRG Fossil Fuels and Environmental Geochemistry, University of Newcastle, Callaghan, NSW, Australia, 1993.
13. Bartak, R.; Grischek, T.; Ghodeif, K.O.; Wahaab, R.A. Shortcomings of the RBF pilot site in Dishna. *Egypt. J. Hydro. Eng.* **2015**, *20*. [CrossRef]
14. NWRC. *National Water Quality Monitoring Component: National Water Quality and Availability Management (NAWQAM) Project*; National Water Research Center: Cairo, Egypt, 2003.
15. El Arabi, N. Problems of groundwater quality related to the urban environment in Greater Cairo. In *Impacts of Urban Growth on Surface Water and Groundwater Quality*; IAHS Publ. No. 259; IASH Press: Wallingford, UK, 1999; pp. 29–38.
16. Emara, M.M.; El Sabagh, I.; Kotb, A.; Turkey, A.S.; Husseen, D. Evaluation of drinking groundwater for the rural areas adjacent to the nearby desert of Giza governorate of Greater Cairo, Egypt. In *Environmental Security in Harbors and Coastal Areas*; Linkov, I., Kiker, G.A., Wenning, R.J., Eds.; Springer: Berlin, Germany, 2007; pp. 379–394.
17. Ghodeif, K.; Grischek, T.; Bartak, R.; Wahaab, R.; Herlitzius, J. Potential of river bank filtration (RBF) in Egypt. *Environ. Earth Sci.* **2016**, *75*. [CrossRef]
18. Paufler, S.; Grischek, T. Sources and behavior of manganese during riverbank filtration. In Proceedings of the 42nd IAH Congress AQUA 2015, Rome, Italy, 13–18 September 2015; p. 246.
19. Antoniou, E.A.; Stuyfzand, P.J.; van Breukelen, B.M. Reactive transport modeling of an aquifer storage and recovery (ASR) pilot to assess long-term water quality improvements and potential solutions. *Appl. Geochem.* **2013**, *35*, 173–186. [CrossRef]
20. Antoniou, E.A.; van Breukelen, B.M.; Putters, B.; Stuyfzand, P.J. Hydrogeochemical patterns, processes and mass transfers during aquifer storage and recovery (ASR) in an anoxic sandy aquifer. *Appl. Geochem.* **2012**, *27*, 2435–2452. [CrossRef]
21. Henzler, A.; Greskowiak, J.; Massmann, G. Seasonality of temperatures and redox zonations during bank filtration – A modeling approach. *J. Hydrol.* **2016**, *535*, 282–292. [CrossRef]
22. Sandhu, C. A Concept for the Investigation of Riverbank Filtration Sites for Potable Water Supply in India. Ph.D. Thesis, Faculty of Civil Engineering and Architecture, Dresden University of Applied Sciences, and Faculty of Environmental Sciences, Dresden, Germany, 2015.
23. Herlitzius, J.; Sumpf, H.; Grischek, T. German-Russian cooperation for clean drinking water. *Int. J. Water Manag. Bluefacts* **2012**, 76–81.
24. Ahrns, J.; Klügel, S.; Schoenheinz, D.; Eichhorn, D.; Grischek, T. Subsurface iron removal at river bank filtration sites. In Proceedings of the IWA Eastern European Regional Young Water Professionals Conference, Minsk, Belarus, 21–22 May 2009; pp. 290–297.

Beiliegende Publikation 3

Ghodeif, K.O., **Paufler, S.**, Grischek, T., Wahaab, R., Souaya, E., Bakr, M., Abogabal, A. (2018) Riverbank filtration in Cairo, Egypt - Part I: Installation of a new riverbank filtration site and first monitoring results. Environ. Earth Sci. 77, 270. doi: 10.1007/s12665-018-7450-2.

Beiliegende Publikation 4

Paufler, S., Grischek, T., Bartak, R., Ghodeif, K., Wahaab, R., Boernick, H. (2018): Riverbank filtration in Cairo, Egypt - Part II: Detailed investigation of a new riverbank filtration site with a focus on manganese. Environ. Earth Sci. 77, 318. doi: 10.1007/s12665-018-7500-9.

Beiliegende Publikation 5

Paufler, S., Grischek, T., Benso, M., Seidel, N., Fischer, T. (2018) The impact of river discharge and water temperature on manganese release from the riverbed during riverbank filtration – A case study from Dresden, Germany. Water 10(10), 1476. doi: 10.3390/w10101476.

water

MDPI

Article

The Impact of River Discharge and Water Temperature on Manganese Release from the Riverbed during Riverbank Filtration: A Case Study from Dresden, Germany

Sebastian Paufler [1,*], Thomas Grischek [1], Marcos Roberto Benso [1], Nadine Seidel [1] and Thomas Fischer [2]

[1] Dresden University of Applied Sciences, Friedrich-List-Platz 1, 01069 Dresden, Germany; thomas.grischek@htw-dresden.de (T.G.); marcosbenso@hotmail.com (M.R.B.); nadine_85@msn.com (N.S.)
[2] DREWAG Netz GmbH Dresden, Kohlenstraße 23, 01189 Dresden, Germany; Thomas_Fischer@drewag-netz.de
* Correspondence: sebastian.paufler@htw-dresden.de; Tel.: +4-935-1463-2631

Received: 19 July 2018; Accepted: 15 October 2018; Published: 19 October 2018

Abstract: The climate-related variables, river discharge, and water temperature, are the main factors controlling the quality of the bank filtrate by affecting infiltration rates, travel times, and redox conditions. The impact of temperature and discharge on manganese release from a riverbed were assessed by water quality data from a monitoring transect at a riverbank filtration site in Dresden-Tolkewitz. Column experiments with riverbed material were used to assess the Mn release for four temperature and three discharge conditions, represented by varying infiltration rates. The observed Mn release was modeled as kinetic reactions via Monod-type rate formulations in PHREEQC. The temperature had a bigger impact than the infiltration rates on the Mn release. Infiltration rates of <0.3 $m^3/(m^2 \cdot d)$ required temperatures >20 °C to trigger the Mn release. With increasing temperatures, the infiltration rates became less important. The modeled consumption rates of dissolved oxygen are in agreement with results from other bank filtration sites and are potentially suited for the further application of the given conditions. The determined Mn reduction rate constants were appropriate to simulate Mn release from the riverbed sediments but seemed not to be suited for simulations in which Mn reduction is likely to occur within the aquifer. Sequential extractions revealed a decrease of easily reducible Mn up to 25%, which was found to reflect the natural stratification within the riverbed, rather than a depletion of the Mn reservoir.

Keywords: riverbank filtration; organic matter degradation; manganese; riverbed; climate change; floods; droughts; column experiments; PHREEQC

1. Introduction

Riverbank filtration (RBF) has been successfully used as a natural and cost-efficient water treatment method in many countries in Europe [1,2], the USA [3,4], Africa [5,6], and Asia [7,8]. RBF can naturally occur or can be induced by pumping, whereby wells are placed adjacent to the river that creates a hydraulic potential gradient from the river towards the wells. RBF triggers a variety of natural attenuation processes that can largely improve the water quality of the bank filtrate (BF) and lower the post-treatment effort [9,10]. For example, some organic micropollutants are effectively removed within the first meter of infiltration under oxic conditions [11]. A series of redox processes along the flow path of the infiltrate can adversely affect the BF quality. Depletion of dissolved oxygen

(DO), followed by denitrification and the reduction of manganese (Mn) minerals in the riverbed and the aquifer can cause elevated Mn concentrations, which require subsequent treatment [12–14].

However, the resulting Mn concentration depends on various factors, including residence time and water temperature [15]. Assuming a steady well operation, the residence time can change due to river water level fluctuations, which are usually connected to river discharge variations (floods/droughts). For example, decreasing water levels usually lower the hydraulic gradient and prolong the distance between the river and the RBF wells. The lowered hydraulic gradient also affects the infiltration rate. Additionally, the infiltration rate is impacted by a usually smaller infiltration area at lower water levels. Water temperature variations affect the viscosity of the water and, therefore, also affect the residence times and infiltration rates. Additionally, according to the rule of Van 't Hoff [16], increasing temperatures lead to increased biological degradation rates, whereby Mn release is considered to be largely biologically mediated.

Current climate forecasts are thought-provoking at many RBF sites [17–19]. Droughts potentially lower the river discharge, extend travel times, and promote anaerobic conditions along the flow path, while floods can shorten travel times or cause, for example, breakthroughs of pathogens and organic micropollutants. The current increase of climate extremes in Europe is expected to continue, with a higher frequency of heat waves, long-lasting droughts in some regions, heavy precipitation events and river floods [20]. For the German state of Saxony, the air temperature is projected to increase by 3–3.5 °C and the mean summer rainfall is to decrease by 20–25% by the year 2100 [21].

The Waterworks (WW) Dresden-Tolkewitz (Saxony, Germany) was built in 1898 and is one of the oldest RBF schemes in Europe. This study investigated the impact of the climate-related variables, temperature and discharge, on the BF quality. Water quality data of a 10-year time span from a monitoring transect were examined to identify discharge- and temperature-related patterns. To assess the potential Mn release from the riverbed in Dresden-Tolkewitz, three columns filled with riverbed sediment from the Elbe river emulated three infiltration rates and four temperature conditions. In order to use the results from the column experiment for a planned modeling of the transect, the observed Mn release was reproduced by hydrogeochemical modeling with PHREEQC. Additionally, a sequential extraction procedure was applied to the riverbed sediment from the columns after the experiment. Based on that data, the implications of the results to the redox-related BF quality in a potentially changing climate are discussed with a focus on Mn.

2. Materials and Methods

2.1. Description of the RBF Waterworks Dresden-Tolkewitz

The WW Dresden-Tolkewitz is located at the upper Elbe river in Germany (Figure 1). Three siphon well galleries with 72 vertical wells abstract up to 1500 m^3/h (36,000 m^3/d). The portion of riverbank filtrate is around 83% during mean flow and 70–75% during low flow conditions [22]. The focus of this study was a 95 m wide transect between the Elbe river and a production well (PW), which already was the focus of previous riverbed clogging studies [22]. The PW fully penetrates the aquifer and the 4 m long filter screen is located directly above the aquitard. The transect has three observation wells (OW 1, 2 and 3). Each OW has sampling points at three depths (upper, middle, lower = OW i-1, i-2, i-3). During the mean flow, the nearest OW (OW 1) is around 21–30 m apart from the riverbank. OW 2 and OW 3 are around 40 and 80 m apart from the bank during mean flow. The average travel time along the transect is between 24 and 30 days [23].

The mean discharge of the Elbe river in Dresden is 332 m^3/s (at 1.84 m river stage). The discharge varies during the mean low and high flow periods between 110 m^3/s (0.75 m) and 1700 m^3/s at a water level of 5.47 m [22]. The climate in Dresden is humid continental with warm summers. The alluvial aquifer is unconfined, composed of gravel and coarse sand with a saturated thickness of 11–14 m and has a hydraulic conductivity of 1–2 $\times$ 10^{-3} m/s [22].

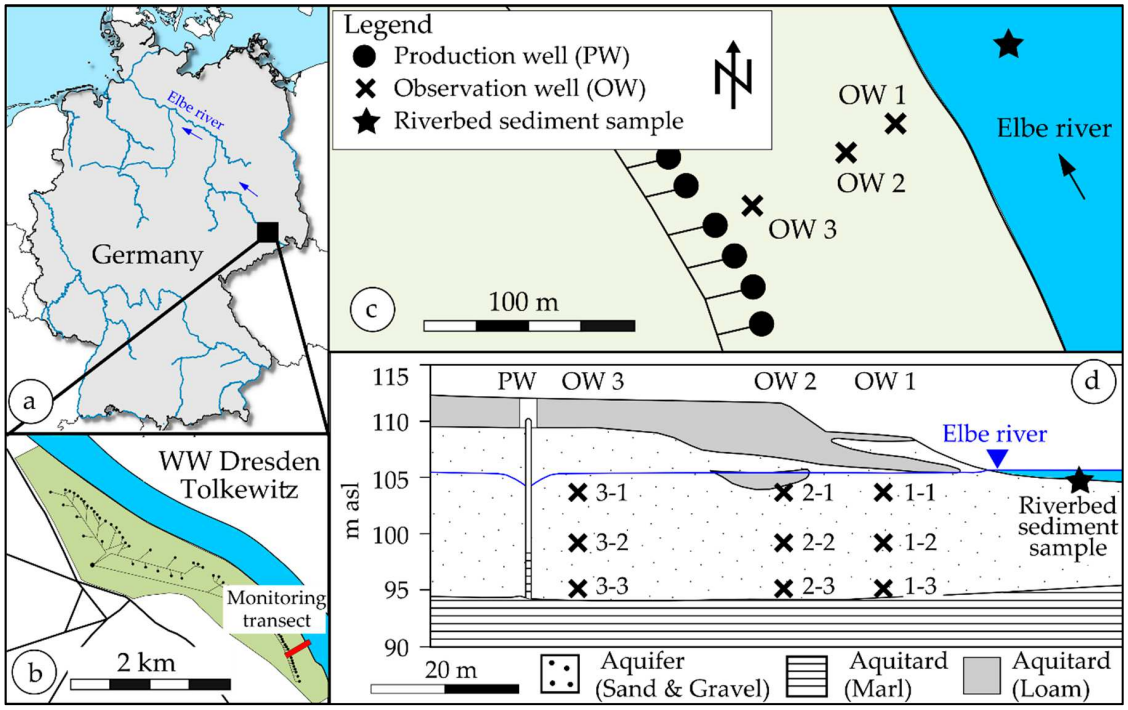

Figure 1. (**a**) The location of the RBF Waterworks Dresden-Tolkewitz, (**b**) Observed transect between the Elbe river and the pumping well (PW), (**c**) Location of the observation wells within the transect and sampling point of the riverbed sediment for the column experiment, (**d**) cross-section of the transect and locations of the observation points for each observation well (OW).

2.2. Regular Monitoring in Dresden-Tolkewitz

In this study, the evaluation period of the water quality data from the WW Dresden-Tolkewitz was a 10-year time span from 1 January 2006 to 31 December 2016. Regular samples were taken twice a year from all sampling points of each OW by the waterworks staff. Additional event-based samples were taken during low flow periods and, if possible, during high flow periods. Sampling was carried out according to DVGW [24] and corresponding to earlier guidelines. Water quality data for the Elbe river were taken from the database of the Saxon state ministry [25]. The relevant sampling point is located at river km 43.5, around 3 km upstream of the WW. Water levels in this study refer to the federal water level "Dresden Augustusbruecke" at river km 55.63 [26].

2.3. Set-Up of the Column Experiments

To understand the behavior of Mn at the RBF site in Dresden-Tolkewitz, three columns with riverbed sediments were set up in the laboratory of the University of Applied Sciences Dresden (Figure S1). Each column was 1 m long, had an inner diameter of 0.08 m, and was made up of galvanized steel. The filling material was riverbed sediment from the Elbe River. The riverbed material was collected in front of the investigated monitoring cross-section of the RBF Waterworks Dresden-Tolkewitz (Figure 1). The riverbed sediment was recovered around 20 m apart from the riverbank during a low discharge period. Due to the very low gradient of the riverbed towards the riverbank, the area around the sampling point was already flooded at slightly higher water levels, which still would occur during mean low flow conditions. Hence, the area around the sampling point can be considered as a potential infiltration area. Because of the relatively coarse riverbed, undisturbed sampling was not possible. Thus, the upper 5 cm of the riverbed where scratched first to represent the clogging layer. Subsequently, the deeper riverbed material was dug out layer-wise and sieved in place to a grain size <4 mm. Immediately after transporting it to the lab, the wet riverbed material was filled into columns in ≈0.1 m thick, separately compacted layers with the clogging layer on top.

During the filling of the columns, the sediment mass was measured using a balance to calculate the bulk density and assess the compaction of the material in the columns. The mean travel time (t_a) and effective porosity (n_e) for both columns were determined from electrical conductivity (NaCl) breakthrough curves from tracer experiments performed before start-up.

To adjust the temperature regiment, all three columns with riverbed material were stored in a thermostatic cabinet. A second thermostatic cabinet contained three storage containers with Elbe river water, collected in Dresden once per week. The outflow of the columns flowed into three additional containers within the second cabinet. The investigated temperatures were 10, 20, 30, and 35 °C (Table 1).

Table 1. The experimental design of the column experiment.

Column	**1, 2, and 3**											
Temperature in °C	**10**			**20**			**30**			**35**		
Flow in mL/min	1	2	4	1	2	4	1	2	4	1	2	4
n Samples/event	3	3	3	3	3	3	3	3	3	3	3	3

Temperature (T), dissolved oxygen (DO), the pH-value, and electrical conductivity (EC) were determined using WTW Multi 3430 and appropriate electrodes (WTW, Weilheim, Germany) before the columns in the storage containers and after the columns in a flow-through cell. A series of valves allowed sending the outflow of each column separately through the cell.

At most RBF sites, the infiltration rates depend for example on abstraction rates of the wells, clogging of the riverbed, distance between the river and the wells and the infiltrating area, and are therefore very site specific. To represent the low, mean, and high infiltration rates of 0.3, 0.6 and 1.1 $m^3/(m^2 \cdot d)$, the flow through the columns was adjusted to 1, 2, and 4 mL/min. The flow rate was adjusted individually for each column using ProMinent Beta diaphragm pumps (ProMinent, Heidelberg, Germany). Each of the 12 possible flow and temperature conditions run until 15 to 20 pore volumes (PV) of every column were exchanged. Sampling started after around 5 PV and continued until at least 10 and 15 PV. Up to three intermediate samples were taken if possible (e.g., weekends were skipped). At one sampling event, the water samples from all three columns were taken at separate sampling taps after the columns before the outflow container. Thus, the presented results for each temperature and flow rate represent the mean value of three similarly prepared, and independently operated columns. Samples from the storage containers (=inflow) were taken once per week. Alkalinity was determined at every sampling event by alkalimetric titrations with 0.1 M hydrochloric acid (HCl).

2.4. Water Analysis

Water samples of the regular monitoring at the OW's in Dresden-Tolkewwitz were analyzed for >100 parameters in the lab of DREWAG Netz GmbH (DIN EN ISO/IEC 17025 certified). Water samples from the column experiment were filtered immediately after sampling through 0.45 µm membrane filters (VWR International GmbH, Darmstadt, Germany). The samples for cation analysis were preserved with 0.1 M nitric acid (HNO_3). Major cations K^+, Na^+, Ca^{2+}, Mg^{2+} and dissolved metals As, Fe, Mn, Si, and Sr were measured with ICP-OES (Optima 4300 DV, PerkinElmer, Waltham, MA, USA). Br^-, Cl^-, F^-, $NO_2{}^-$, $NO_3{}^-$, $PO_4{}^{3-}$, and $SO_4{}^{2-}$ were determined with ion-chromatography (autosampler AS50, eluent generator EG50, gradient pump GP50, electrochemical detector ED50, separation column AS19, all from Dionex) at the Institute for Water Chemistry, TU Dresden, Germany.

2.5. Sequential Extraction of the Riverbed Sediment

To estimate the mobilization behavior of Mn and to assess the mineralogical composition, a 4-step sequential extraction procedure was applied to the filling material of the columns after the experiment

(Table S1). Rauret et al. [27] and Sutherland and Tack [28] described the applied procedure in detail. The total extractable Mn was determined by microwave acid digestion with HNO_3 for separate samples from the same sampling points. Samples were taken after 0.05 m (below the clogging layer), and at 0.3, 0.6, and 0.9 m along the columns, before being immediately filled into airtight sample containers and stored at 4 °C before analysis.

2.6. Estimation of Reduction Constants for the Elbe Riverbed with PHREEQC

Elevated Mn concentrations at many bank filtration sites are linked to the microbiological reduction of Mn minerals within the riverbed and the aquifer [1,29]. The degradation (oxidation) of organic matter (OM, simplified CH_2O) is the driving force for the associated redox reactions (Equations (1)–(3)).

$$\text{Aerobic respiration}: \ CH_2O + O_2 \rightarrow CO_2 + H_2O \quad (1)$$

$$\text{Denitrification}: \ 5CH_2O + 4NO_3^- + 4H^+ \rightarrow 5CO_2 + 2N_2 + 7H_2O \quad (2)$$

$$\text{Mn(IV) reduction}: \ CH_2O + 2MnO_2(s) + 4H^+ \rightarrow 2Mn^{2+} + 3H_2O + CO_2 \quad (3)$$

The results from the column experiments are considered to represent the potential Mn release from the riverbed. In order to use the results for a planned modeling of the transect, the observed Mn release was reproduced by chemical modeling with PHREEQC [30]. By applying the approach of Henzler et al. [14], the relevant redox reactions were modeled as kinetic reactions using Monod-type rate formulations (Equations (4)–(7)). Because neither increasing Fe concentrations nor decreasing sulfate concentrations were observed along the transect, additional redox reactions accounting for iron and sulfate reduction were excluded.

$$r_{ox} = -f_{reac} \times {Y_{ox}}^{-1} \times k_{ox} \times \left(\frac{C_{ox}}{C_{ox} + K_{ox}} \right) \times f_T \quad (4)$$

$$r_{nit} = -f_{reac} \times {Y_{nit}}^{-1} \times k_{nit} \times \left(\frac{C_{nit}}{C_{nit} + K_{nit}} \right) \times \left(\frac{K^{ox}_{inhb_{nit}}}{C_{ox} + K^{ox}_{inhb_{nit}}} \right) \times f_T \quad (5)$$

$$r_{mn} = f_{reac} \times {Y_{mn}}^{-1} \times k_{mn} \times \left(\frac{K^{ox}_{inhb_{mn}}}{C_{ox} + K^{ox}_{inhb_{mn}}} \right) \times \left(\frac{K^{nit}_{inhb_{mn}}}{C_{ox} + K^{nit}_{inhb_{mn}}} \right) \times f_T \quad (6)$$

$$r_{OM} = Y_{ox} \times r_{ox} + Y_{nit} \times r_{nit} - Y_{mn} \times r_{mn} \quad (7)$$

The parameters r_{ox}, r_{nit} and r_{mn} denote the production and consumption rates (positive and negative) of dissolved O_2, ${NO_3}^-$, and Mn^{2+}. Rate constants for OM degradation under oxic, nitrate and manganese reducing condition are represented by k_{ox}, k_{nit} and k_{mn}. C_{ox} and C_{nit} are the dissolved oxygen and nitrate concentrations. K_{ox} and K_{nit} denote Monod-half saturation constants. The inhibition of nitrate and manganese reduction under oxic conditions was implemented by the inhibition constants $K^{ox}_{inhb_{nit}}$ and $K^{nit}_{inhb_{mn}}$. Accordingly, $K^{nit}_{inhb_{mn}}$ represents the inhibition constant for manganese reduction under nitrate-reducing conditions. The overall turnover rate of OM r_{OM} (Equation (7)) is the sum of the reaction rates r_{ox}, r_{nit}, and r_{mn} that are multiplied with the stoichiometric coefficients Y_{ox}, Y_{nit}, and Y_{mn} corresponding to the redox reactions (Equations (1)–(3)). Following a similar modeling approach of Greskowiak et al. [31], the parameter f_{reac} was included to simulate a zone of increased reactivity at the first section of the infiltration path [14]. The application of Equations (4)–(7) implied two assumptions. First, MnO_2 was present in excess. Hence, MnO_2 was not rate limiting and the implementation of a Monod-half saturation constant for Mn was not necessary in Equation 6. Second, the OM content was assumed to be infinitely available (or redelivered by the river) and would not be exhausted during the simulation period.

Similar to Diem et al. [32], Greskowiak et al. [31], and Sharma et al. [33], an additional temperature factor f_T was implemented that accounted for the impact of temperature changes on the degradation rates (Equation (8)).

$$f_T = exp\left[\alpha + \beta \times T \times \left(1 - 0.5 \times \frac{T}{T_{opt}}\right)\right] \quad (8)$$

T_{opt} denotes the optimal temperature for a maximal degradation rate and α as well as β are fitting parameters. Applying the results from Diem et al. [32], Henzler et al. [14], Greskowiak et al. [33] and Sharma et al. [33], none of the three parameters were to be changed from the initial data set.

In PHREEQC, a 1 m long column was represented by 50 cells with a length of each of them being 0.02 m (Table S2). Porosity and pore velocity were known from the tracer test. The dispersion and diffusion coefficients for the model were calibrated for the NaCl breakthrough curves from the tracer tests and non-reactive transport. Subsequently, the data from Henzler et al. [14] for the rate constants k_{ox}, k_{nit}, and k_{mn}, as well as for the inhibition constants $K^{ox}_{inhb_{nit}}$, $K^{ox}_{inhb_{mn}}$, and $K^{nit}_{inhb_{mn}}$, were used as the initial parameter set for reactive modeling. Calibration was initially carried out with PEST [34]. Since the inhibition constants $K^{ox}_{inhb_{nit}}$, $K^{ox}_{inhb_{mn}}$ and $K^{nit}_{inhb_{mn}}$ did not change during the initial calibration runs, and in order to speed up the calibration, the inhibition constants were held fixed at the initial values during further calibration. The following calibration of the rate constants k_{ox}, k_{nit} and k_{mn} was first carried out by adjusting the parameters for best fit by hand (trial-and-error). Afterward, the trial-and-error results were checked with PEST.

The calibration targets were the determined median values of pH, DO, NO_3^- and Mn^{2+} in the outflow water of the columns for each of the three flow and four temperature conditions. Hence, the calibration each resulted in 12 values for k_{ox}, k_{nit}, and k_{mn}.

3. Results

3.1. Seasonal Fluctuation of Redox-Sensitive Parameters Close to the Riverbank

Most relevant redox parameters of the Elbe river undergo strong seasonal fluctuations (Table S3). The median value for water temperature was 10.9 °C (3.0–21.3 °C, 10–90%ile, n = 267) during the entire 10-year observation period. Median values for DO, NO_3^-, DOC, TOC, and Mn were 10.8 mg/L (8.4–13.8 mg/L, n = 269), 15.0 mg/L (12.0–20.0 mg/L, n = 279), 5.2 mg/L (4.6–6.0 mg/L, n = 325), 6.3 mg/L (5.2–8.2 mg/L, n = 292), and 0.01 mg/L (0.01–0.03 mg/L, n = 278). During the cold winter season (December–March), the water temperature decreased down to 3 °C and the TOC concentration to <6 mg/L, whereas DO and NO_3^- increased to around 13 and 19 mg/L. During hot summer months (June–September), the water temperature increased to >21 °C and the TOC concentration to >7 mg/L, whereas DO and NO_3^- usually decreased to ≈8.5 mg/L and ≈13 mg/L. Mn in the Elbe river showed no noticeable seasonal fluctuations.

Along the transect from the Elbe river towards the PW seasonal fluctuations were also noticeable (Table S4). As expected, OW 1-1 and 2-1 in the upper aquifer showed the strongest variations. The temperatures at both observation points varied from winter to summer from 6.1 to 20.0 °C and 8.3 to 19.9 °C (Figures 2 and 3). Temperature fluctuations at the deeper observation points OW 1-2 and 2-2 were in the same order of magnitude. At the lowest observation points OW 1-3 and 2-3, as well as further along the flow path at OW 3, the temperature variations were ±3 °C compared to the median values.

DO showed similar patterns during the year. The higher DO concentration in the Elbe river in winter resulted in >6.5 mg/L at OW 1-1, >2.5 mg/L at OW 1-2 and >1.0 mg/L at OW 2-1. Further, along the flow path, DO was mostly found <0.5 mg/L. During summer, the DO was almost depleted at OW 1-1. Nitrate showed a similar behavior. During winter, NO_3^- concentrations were >20 mg/L at OW 1-1, >7 mg/L at OW 1-2 and >13 mg/L at OW 2-1, whereas in summer, the nitrate was with <1.0, <0.5 and <3.0 mg/L almost neglectable.

Mn concentration varied primary at OW 1-1 during the year. In winter, the Mn concentration was very low at OW 1-1, but increased up to 0.42 mg/L during summer time. At all other observation points, variations were found but without distinct patterns. Along the entire flow path after OW 1-1, the Mn concentration was always >0.1 mg/L and mostly below 0.35 mg/L (Table S4).

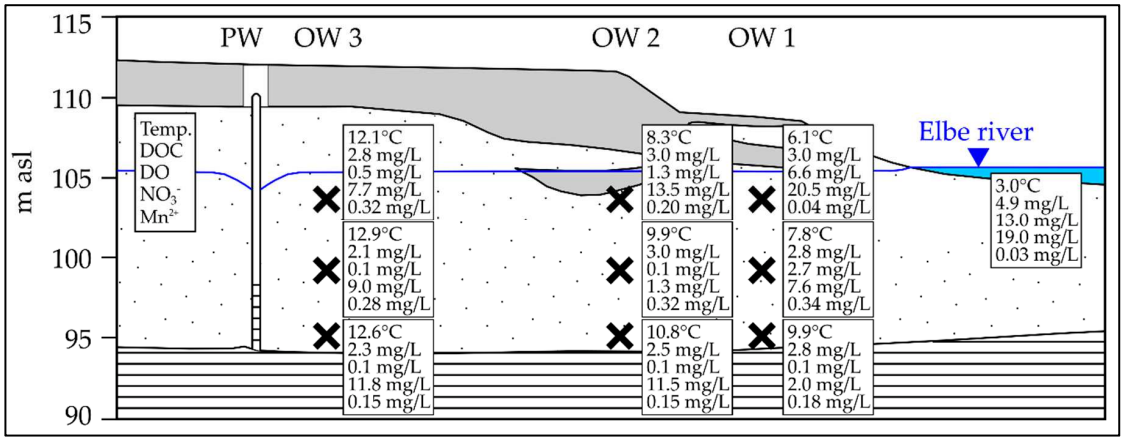

Figure 2. The mean values (n = 2) of the relevant redox parameters along the transect in February (Table S4).

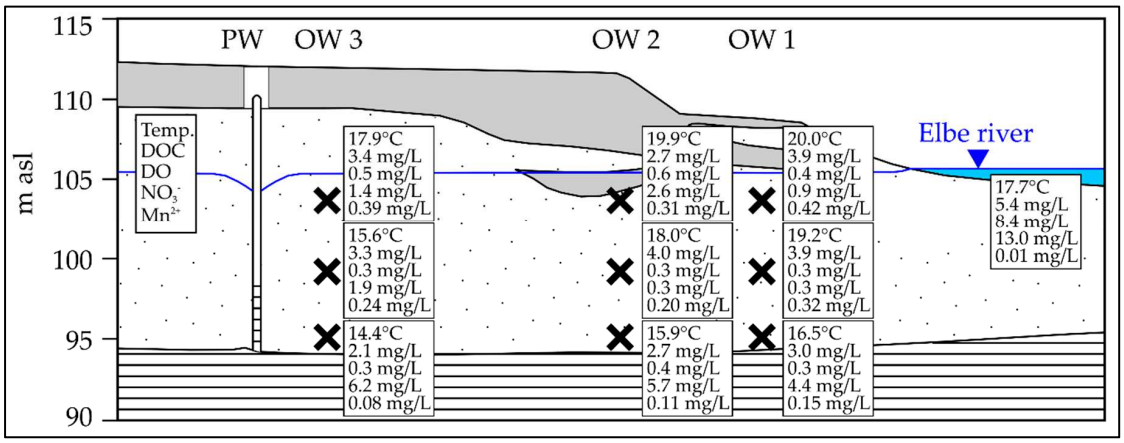

Figure 3. The mean values (n = 2) of the relevant redox parameters along the transect in September (Table S4).

3.2. Mn Release During Low Discharge Periods of the Elbe River

The water level of the Elbe river shows strong annual fluctuations. Long-lasting mean low discharge conditions are represented by a water level of ≤0.75 m and are rare. From 1998 to 2006, the Elbe water level was between 0.7 and 0.8 m only in 2003 (for almost 3 months). During the observation period from 2006 onwards, the Elbe river decreased to mean low discharge conditions in 2008, 2009, and 2016, which lasted for two weeks at maximum. In 2015, the latest low discharge period was observed that lasted for more than 3 months and the water level dropped to as low as 0.5 m [26].

During this 153 day long low discharge period in 2015, the median water level was 0.74 m (0.62–1.05 m, 10–90%ile, n = 153) and the mean water temperature 20.1 °C (11.0–24.6 °C, n = 153, Table S5). The Mn concentration at OW 1-1 increased up to 0.69 mg/L (median 0.19 mg/L, n = 6, Table S5) after the water temperature already fell below 20 °C (Figure 4). At the two deeper OW 1-2 and OW 1-3, the Mn concentration did not change noticeably. Further, along the flow path at OW 2-1, Mn increased up to 0.42 mg/L (median 0.23 mg/L, n = 6, Figure S2) and at OW 3-1 up to 0.39 mg/L

(median 0.26 mg/L, n = 6, Figure S3). At OW 2-2, 2-3, 3-2, and 3-3, the Mn concentration remained almost constant.

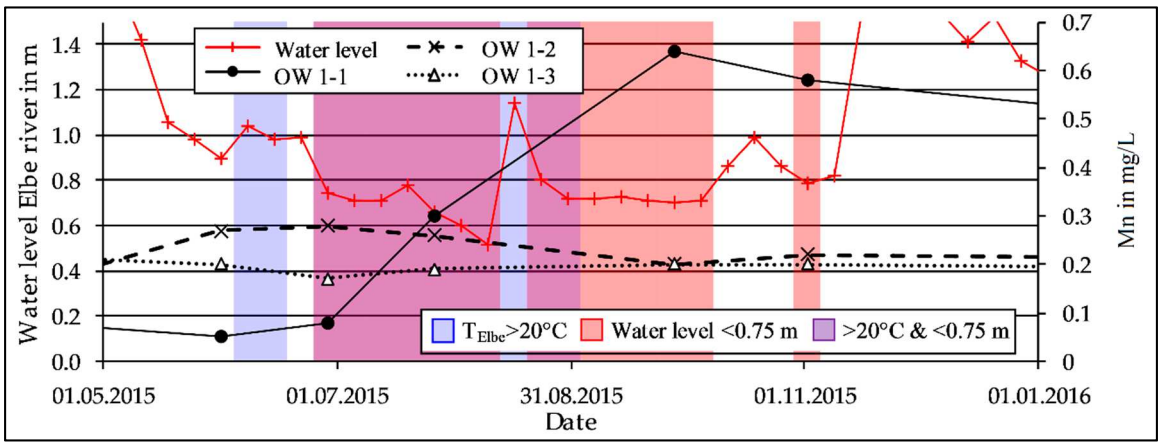

Figure 4. The Mn concentration at OW 1 during a low discharge period in 2015.

3.3. Mn Release Depending on the Temperature and Infiltration Rate During the Column Experiments

To investigate the effect of varying temperature to the Mn release from the riverbed, three columns filled with riverbed sediments run at 10, 20, 30, and 35 °C. Varying flow rates of 1, 2, and 4 mL/min represented low, mean and high infiltration rates for all four temperature regimes.

After changing temperature and/or flow, the Mn concentration changed within 5 pore volumes (PV) and was stable after 8–10 PV (e.g., Figure S4). At high infiltration rates (4 mL/min, pore velocity $v_a = 3.44 \cdot 10^{-5}$ m/s, residence time t_R = 8.1 h) and water temperatures of 10 and 20 °C, the median Mn release was <<0.01 mg/L (n = 9 and 12) and almost neglectable (Figure 5, Table S6). At 30 °C, the Mn concentration increased in the outflow slightly to around 0.03 mg/L (median, n = 21). Only at 35 °C was Mn released (median of 0.51 mg/L).

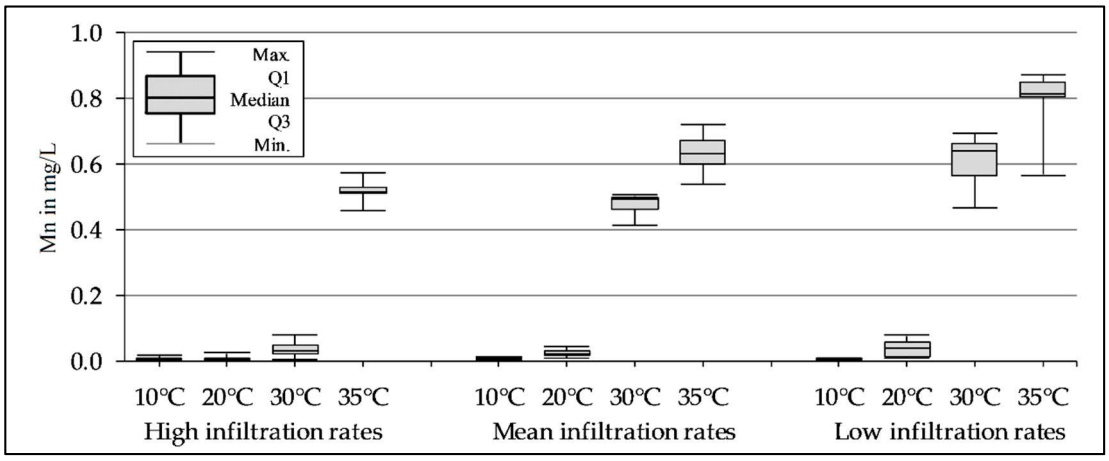

Figure 5. The mean Mn concentration in the outflow of the columns with riverbed sediment for high, mean, and low infiltration rates (4, 2 and 1 mL/min) at different temperatures (see Table S6 for no. of samples), Q_1 and Q_3 correspond to the 1st and 3rd quartile.

At mean infiltration rates (2 mL/min, $v_a = 1.72 \cdot 10^{-5}$ m/s, t_R = 16.2 h), a minor Mn release was observed at 10 and 20 °C with median values of 0.01 and 0.02 mg/L, respectively. With increasing temperature, the Mn release increased to 0.49 mg/L at 30 °C (median, n = 9) and 0.63 mg/L at 35 °C (median, n = 15).

For low infiltration rates (1 mL/min, $v_a = 8.60 \cdot 10^{-6}$ m/s, $t_R = 32.4$ h) at 10 °C, no Mn release was observed. The Mn concentration in the outflow increased already at 20 °C and stabilized around 0.04 mg/L (median, $n = 21$). After the temperature rose to 30 °C, Mn increased sharply to ≈0.64 mg/L (median, $n = 18$, Figure S4). The subsequent temperature increase to 35 °C led to around 0.81 mg/L Mn (median, $n = 15$).

The Mn concentration in the feed water maximally was 0.02 mg/L (median <LOD, limit of detection 0.005 mg/L Mn, $n = 23$).

3.4. Reduction Constants of O_2, NO_3^- and Mn(IV) as Electron Acceptors

The observed Mn release was reproduced by chemical modeling with PHREEQC using Monod-type rate formulations and the reduction rate constants k_{ox}, k_{nit}, and k_{mn} as calibration parameters. The reduction rate constant k_{ox} showed the highest value at high infiltration rates and at a temperature of 10 °C (1.8×10^{-9} mol/(L·s)). With increasing temperature, k_{ox} decreased down to 4.3×10^{-10} mol/(L·s) (Table 2, Figure S5). For mean and low infiltration rates, a similar behavior was found. The lowest k_{ox} of 9.7×10^{-11} mol/(L·s) was determined at low infiltration rates and a temperature of 35 °C.

Table 2. The calibrated reduction constants of this study compared to the literature data.

This Study					
Temperature	v_a	k_{ox}	k_{nit}	k_{mn}	**Notes**
	m/s	**mol/(L·s)**	**mol/(L·s)**	**mol/(L·s)**	
10 °C	8.60×10^{-6}	5.18×10^{-10}	2.00×10^{-12}	2.50×10^{-10}	Low infiltration rate (1 mL/min)
	1.72×10^{-5}	8.65×10^{-10}	7.00×10^{-12}	2.00×10^{-10}	Mean infiltration rate (2 mL/min)
	3.44×10^{-5}	1.80×10^{-9}	5.00×10^{-12}	1.00×10^{-10}	High infiltration rate (4 mL/min)
20 °C	8.60×10^{-6}	2.17×10^{-10}	1.53×10^{-10}	1.10×10^{-10}	Low infiltration rate (1 mL/min)
	1.72×10^{-5}	4.50×10^{-10}	5.50×10^{-11}	1.50×10^{-10}	Mean infiltration rate (2 mL/min)
	3.44×10^{-5}	8.90×10^{-10}	5.00×10^{-12}	1.00×10^{-10}	High infiltration rate (4 mL/min)
30 °C	8.60×10^{-6}	1.02×10^{-10}	1.88×10^{-10}	1.90×10^{-9}	Low infiltration rate (1 mL/min)
	1.72×10^{-5}	2.14×10^{-10}	2.80×10^{-10}	2.20×10^{-9}	Mean infiltration rate (2 mL/min)
	3.44×10^{-5}	4.70×10^{-10}	5.00×10^{-12}	1.00×10^{-10}	High infiltration rate (4 mL/min)
35 °C	8.60×10^{-6}	9.70×10^{-11}	1.35×10^{-10}	1.62×10^{-9}	Low infiltration rate (1 mL/min)
	1.72×10^{-5}	2.14×10^{-10}	3.50×10^{-11}	1.40×10^{-9}	Mean infiltration rate (2 mL/min)
	3.44×10^{-5}	4.28×10^{-10}	5.00×10^{-12}	1.95×10^{-9}	High infiltration rate (4 mL/min)
10%ile		1.13×10^{-10}	5.00×10^{-12}	1.00×10^{-10}	
Median		$\mathbf{4.39 \times 10^{-10}}$	$\mathbf{2.10 \times 10^{-11}}$	$\mathbf{2.25 \times 10^{-10}}$	
90%ile		8.88×10^{-10}	1.85×10^{-10}	1.95×10^{-9}	
n		12	12	12	
Literature Data					
Temperature	v_a	k_{ox}	k_{nit}	k_{mn}	**Source**
	m/s	**mol/(L·s)**	**mol/(L·s)**	**mol/(L·s)**	
Variable	Variable	1.52×10^{-10}	3.81×10^{-11}	8.91×10^{-13}	[31]
Variable	Variable	2.00×10^{-10}	1.00×10^{-10}	1.70×10^{-12}	[14]
22 °C	7.60×10^{-6}	3.50×10^{-8}	3.40×10^{-8}	3.00×10^{-13}	[35]
n.a.	n.a.	3.98×10^{-10}	3.98×10^{-11}	6.31×10^{-14}	[36]
Variable	Variable	1.57×10^{-9}	1.00×10^{-11}	n.a.	[37]
Variable	Variable	1.30×10^{-9}	8.00×10^{-10}	n.a.	[33] for DOC
Variable	Variable	1.90×10^{-11}	1.20×10^{-11}	n.a.	[33] for SOM

n.a.—not available, v_a—pore velocity.

For the reduction rate constant k_{nit}, no distinct pattern was found. At high infiltration rates, k_{nit} remained constant at 5.0×10^{-12} mol/(L·s). For mean and low infiltration rates at 10 °C, k_{nit} was in the same order of magnitude (7.0 and 2.0×10^{-12} mol/(L·s)). With increasing temperatures of 20 °C and 30 °C, k_{nit} increased up to 2.8×10^{-10} mol/(L·s). At 35 °C, k_{nit} decreased again at the mean and low infiltration rates.

The reduction rate constant k_{mn} at 10 °C and 20 °C for high, mean and low infiltration rates were in the order of magnitude of 1.0 to 2.5×10^{-10} mol/(L·s). At 30 °C and high infiltration rates, k_{mn} remained in this range. For mean and low infiltration rates at 30 °C and 35 °C, k_{mn} increased to 1.4–2.0×10^{-9} mol/(L·s).

With a percental error of −2.4% compared to the measured values (median, −6.7–0.2%, 10–90%ile, n = 12), the simulated DO concentrations showed the largest errors of relevant redox parameters (Table S7). The error for NO_3^- with a median of 0.4% and a span of −0.6 to 1.1% (10 to 90%ile, n = 12) was lower. With an error of 0.2%, the simulated Mn^{2+} concentrations showed the smallest median deviation but a comparable large span of −15.7 to 8.5% (n = 12). The median error for the simulated pH was −1.0% with a span of −8.7 to 1.7% (n = 12).

3.5. The Decrease of Easily Reducible Mn Along the Flow Path

To estimate the mobilization behavior of Mn, a 4-step sequential extraction procedure was applied to the filling material of the three columns after the experiment. All three columns showed qualitatively similar results and all the following values represent median values with n = 3 (Table S8). The total Mn mass (Mn_{tot}, as the sum of all 4 extracted fractions) was around 270 mg/kg at the inlet after 0.05 m (Figure 6). Further along the flow path, the total Mn mass decreased to ≈150 mg/kg down to a minimum of ≈125 mg/kg the minimum at the outlet after 0.9 m. The total extractable Mn (microwave acid digestion) was around 112 mg/kg at the inlet and increased to 133, 250, and 473 mg/kg at the outlet (Table S8).

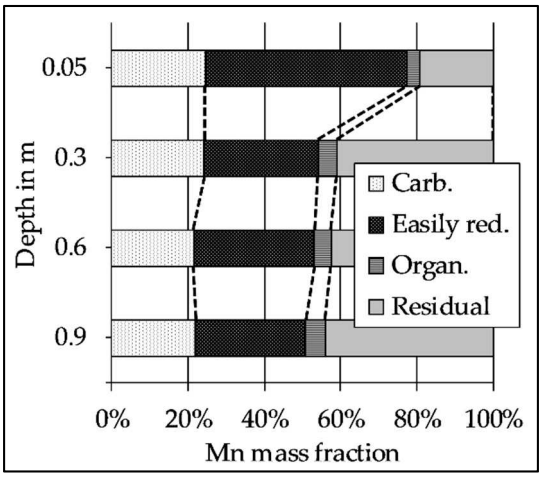

Figure 6. The median values (n = 3) of the absolute Mn mass fractions along the column.

The mass fraction of soluble and carbonate bound Mn ("Carb.") decreased from around 65 mg/kg to 30 mg/kg along the flow path. On a percentage base, the soluble and carbonate bound Mn always remained between 21–24% (Figure 7). Easily reducible Mn dropped from around 140 mg/kg (53% of the total mass) at the inlet to 36 mg/kg (<30%) after 0.9 m. Organically bound Mn ("Organ.") remained stable between 6–9 mg/kg (3–5%). The residual Mn fraction was found almost constant at 51–64 mg/kg, but the percentage increased from around 20 to >40%.

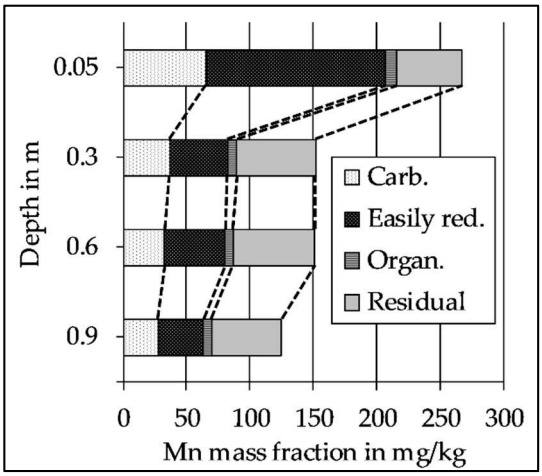

Figure 7. The median values (n = 3) of percentage Mn mass fractions along the columns.

4. Discussion

4.1. The Significance of the Calibrated Degradation Rate Constants

In order to use the results from the column experiment for a planned modeling of the transect, the observed Mn release was simulated using PHREEQC, focusing on relevant redox reactions. During an initial automated calibration with PEST, the inhibition constants $K^{ox}{}_{inhb\_nit}$, $K^{ox}{}_{inhb\_mn}$, and $K^{nit}{}_{inhb\_mn}$ did not change and were held fixed at the initial values during further calibration. Hence, only the reduction rate constants k_{ox}, k_{nit} and k_{mn} were used for calibration.

The calibrated k_{ox} had an overall median value of 4.4×10^{-10} mol/(L·s) (n = 12, Table 2). These results are in fair agreement with results of Henzler et al. [14], who determined a k_{ox} of 2.0×10^{-10} mol/(L·s) for a bank filtration site at Lake Tegel in Berlin, Germany. Greskowiak et al. [31] used a k_{ox} of 1.52×10^{-10} mol/(L s) to simulate the consumption of DO at an infiltration pond in Berlin. Sharma et al. [33] used a more than ten times higher degradation rate with $k_{ox} = 1.30 \times 10^{-9}$ mol/(L·s) to simulate a transect at the RBF Waterworks Flehe in Düsseldorf, Germany. The average water temperature in their study was 13.5 °C and the BF traversed the ≈60 m wide stretch from the riverbank to the well within 60 days [33]. This corresponds to a pore velocity (v_a) of $\approx 1.2 \times 10^{-5}$ m/s. Comparing this with the results of this study of $k_{ox} = 8.65 \times 10^{-10}$ mol/(L·s) at 10 °C and $v_a \approx 1.72 \times 10^{-5}$ m/s, shows a good agreement, too.

The overall median value for the calibrated k_{nit} was 2.1×10^{-11} mol/(L·s) (n = 12, Table 2). This is about five times lower than a reported k_{nit} of 1.0×10^{-10} mol/(L·s) by Henzler et al. [14] and 40-times lower than what Sharma et al. [33] reported with a $k_{nit} = 8.0 \times 10^{-10}$ mol/(L·s). Prommer and Stuyfzand [37] and Greskowiak et al. [31] reported a k_{nit} of 1.0 and 3.8×10^{-11} mol/(L·s), which correspond to the values of this study.

For k_{mn}, the overall median value was 2.3×10^{-10} mol/(L·s) (n = 12, Table 2). This is ≈100- to 1000-times higher than the reported data of $k_{mn} = 1.7 \times 10^{-12}$ mol/(L·s) [14], 8.9×10^{-13} mol/(L·s) [31] or 3.0×10^{-13} mol/(L·s) [35]. Matsunga et al. [35] modeled a column experiment and included the precipitation of Rhodochrosite ($MnCO_3$) as a sink for Mn^{2+}. The precipitation of $MnCO_3$ as a sink for Mn^{2+} has also been shown at other bank filtration sites [38]. Taking the average water quality of the outflow from the columns at 20 °C (pH 8, 50 mg/L Ca^{2+}, 120 mg/L HCO_3^-) and mean infiltration rates for equilibrium in PHREEQC, the water would be supersaturated with respect to $MnCO_3$ with around 0.1 mg/L Mn^{2+} in equilibrium (saturation index 0.77). Thus, the precipitation of$MnCO_3$ would probably control the Mn concentration for longer residence times but did not along the columns due to slow reaction kinetics [39]. As a consequence, the given k_{mn} seem to be representative in simulating an Mn release from a (highly reactive) riverbed, but are not suited for simulations of longer transects,

in which an Mn reduction is likely to occur within the aquifer and can be controlled by $MnCO_3$ precipitation, for example.

4.2. Impact of the Discharge on the Observed Redox Patterns

River discharge indirectly affects the quality of the BF in multiple ways. Low river discharge and related low water levels are often associated with less dilution of wastewater effluent, higher loads of dissolved organic matter (DOM), prolonged travel times, and they are expected to promote DO consumption [19]. Low discharge periods further result in reduced shear stress at the riverbed and more intense clogging at the bottom of the water body, which can also promote anoxic conditions [40,41]. High discharge conditions/floods can cause a partial removal of the clogging layer, resulting in a better hydraulic conductivity of the riverbed and higher water levels lead to higher infiltration rates [18]. Increased flow velocities combined with shorter flow paths cause shorter travel times. Furthermore, high flow conditions and shorter travel times were linked to an increased input of TOC (total organic carbon) [42,43].

To the authors' knowledge, very few researchers have addressed the impact of river discharge to Mn release from the riverbed or the Mn concentration in the BF. Previous work has focused on the impact of discharge on the degradation of natural organic matter (NOM) and DO consumption. In a column experiment, von Rohr et al. [44] evaluated the role of discharge on NOM degradation during RBF. The experiment was set up at 20 °C and with four flow rates, resulting in residence times (t_R) of 40, 20, 12, and 4 h. At residence times of 4 h, oxic conditions persisted through the entire column. With a residence time of 20 h, anoxic conditions were observed within 20 cm along the flow path. Results from the column experiment in this study confirm the flow/infiltration rate dependency of oxygen depletion. At 20 °C and at high infiltration rates (t_R = 8.1 h), the columns remained oxic, but became anoxic at residence times of 16–32 h (Table S9). Diem et al. [32] found river discharge to be correlated with an enhanced POM input and higher DO consumption during flood events. Due to a generally higher DO consumption at temperatures >15 °C, the correlation was only found to be true for temperatures below 15 °C [17]. Diem et al. [32] successfully modeled these observations using higher DO consumption for higher discharges. In this study, rates for DO consumption (k_{ox}) in PHREEQC were highest at high infiltration rates and decreased at mean and low infiltration rates, which is in agreement with the findings of Diem et al. [32].

Groffman and Crossey [45] found slightly increasing Mn concentrations within the upper aquifer section during periods with lower discharge at Rio Calaveras (New Mexico, USA). The observations from the transect in Dresden-Tolkewitz did not reveal a clear discharge/water level dependency. Figure 4 indicates an increasing Mn concentration at OW 1-1 during a long-lasting low discharge period of the Elbe River in 2015. In addition, Mn at OW 2-1 and 3-1 increased during this period (Figures S2 and S3). Contrary to this, at OW 1-1 Mn, already decreased when the water level was still low, whereas Mn further increased at OW 2-1 and 3-1. Hence, the field observations did not indicate a mere discharge-dependency of Mn along the transect.

Manganese release during the column experiment with riverbed material was low at 10 °C and 20 °C for the high, mean, and low infiltration rates (Figure 5). At 30 and 35 °C, Mn increased from high to mean and again to low infiltration rates. Correlation coefficients of −0.99 for 30 °C and −0.87 for 35 °C were very high and significant ($p < 0.05$, data not shown).

The relation between river discharge and the release of Mn from the riverbed is ambiguous. On the one hand, the literature data [44] and the results from the column experiments in this study suggest that periods of low discharge lead to elevated Mn concentrations due to lower infiltration rates and longer residence times. Contrary to that, e.g., Diem et al. [17] found higher river discharge to be correlated with higher DO consumption, which was also reinforced by modeling [32]. Since higher DO consumption is often related to increasing Mn concentrations during RBF [1], periods of higher discharge may cause Mn release. Shorter travel times during periods of high river discharge would

interfere with this. In addition, the results of the column experiment in this study showed that the temperature effect distorts this discharge dependency (see the following paragraph).

4.3. Manganese Release Controlled by Temperature

A temperature-dependent fluctuation of the Mn concentration has been shown at many bank filtration sites [1,15,38,46–50].

Manganese along the transect in Dresden-Tolkewitz varied the most at OW 1-1, 2-1, and 2-2 (Figures 4 and S2), which are closest to the Elbe river (≈20 m). Furthermore, those observation points showed the largest temperature fluctuations (Figures 2 and 3). Especially the Mn concentration at OW 1-1, which is closest to the riverbank, responded to higher water temperatures during low and mean flow conditions (Figures S6–S8). However, at the more distant observation points (OW 1-3, 2-3 and OW 3), Mn was comparably stable during the year. This can partially be attributed to extended travel times (compared to the average travel times), especially towards the deeper observation points. Similar observations were made at RBF sites at the Lot river in France [51] and at the Glatt river in Switzerland [50]. Both found a seasonal trend for Mn, with elevated concentrations during the warm summer months and lower concentrations during the winter season. For the RBF site in Dresden-Tolkewitz, no seasonal trend for Mn was observed at any OW, which is probably due to the long sampling interval. Temperature seems to be a very important factor controlling initial Mn release from the riverbed in Dresden-Tolkewitz, but more research is needed in order to assess this parameter quantitatively. Since the assessment is only possible during temporary constant, low water levels [23], future research must focus on the rare long-lasting low discharge periods.

Results from the column experiments indicate a high-temperature dependency of Mn release. At constant infiltration rates (high, mean, or low), the Mn concentration increased with increasing temperature (Figure 5). At high infiltration rates (residence time t_R = 8.1 h), the Mn concentration increased in the outflow sharply from 0.03 to 0.51 mg/L at higher temperatures of 30 and 35 °C. For mean and low infiltration rates (t_R = 16.2 and 32.4 h), a similar Mn increase happened after water temperature increased from 20 to 30 °C. The calibrated k_{mn} in this study reflects the sharp increases, showing a 20-fold increase from 30 to 35 °C at high infiltration rates as well as a 15- and 17-times higher k_{mn} after temperature raised from 20 to 30 °C at mean and low infiltration rates (Table 2).

Bourg and Bertin [51] reported a threshold water temperature of 10 °C to trigger a microbiologically mediated Mn reduction. Hoehn et al. [52] observed extensive denitrification, stronger reducing conditions, and elevated Mn concentrations at water temperatures above 14 °C. The findings of the column experiment support these observations. At water temperatures of 10 °C, the Mn release was neglectable for all infiltration rates. In addition, the results from the column experiment and the determined reduction constants can expand these statements for Mn containing riverbeds. For high infiltration rates of 1.1 $m^3/(m^2 \cdot d)$ and above, Mn release from the riverbed is unlikely for surface water temperatures that are typical in temperate climate zones (≤30 °C). If the BF infiltrates at infiltration rates in the order of magnitude of 0.6 $m^3/(m^2 \cdot d)$ and below, water temperatures >20 °C are sufficient to trigger extensive Mn release from the riverbed.

4.4. Depletion of the Mn Reservoir Within the Riverbank

After the column experiments were finished, a sequential extraction procedure was applied to the riverbed sediment (Figures 6 and 7).

Manganese contents in the riverbed sediments are very site-specific and cannot be limited to regional or climatic differences [53]. Moreover, the Mn content depends highly on the grain size. Jain and Ram [54] and Jain and Sharma [55] found 230–650 mg/kg Mn in the grain size fraction with the highest mass fraction (36%, d = 0.21–0.25 mm), whereas the grain size fraction with the lowest mass fraction of only 2% (d < 0.075 mm) contained up to 2800 mg/kg Mn.

However, the order of magnitude of ≈150–300 mg/kg Mn was low compared to many other riverbed sediments, e.g., 960 mg/kg Mn in the Rhine sediment [56] or 1700 mg/kg Mn in the

Garonne [53]. Nonetheless, the values are in agreement with the former analysis of the riverbed sediment from the Elbe river. Grischek et al. [57] determined ≈50 mg/kg Mn_{tot} (n = 3) in riverbed sediment at Torgau around 100 km downstream of Dresden. In Dresden-Tolkewitz at the same transect, Paufler [58] determined around 250 mg/kg Mn_{tot} (n = 3) for the upper 5 cm of the riverbed and only ≈80 mg/kg Mn_{tot} (n = 6) for the depths 5–30 cm.

At the Glatt river in Switzerland, von Gunten et al. [13] hypothesized that the repetitive exhaustion of Mn deposits in the river sediments towards the fall season could be one reason for seasonal Mn variations.

Integrating the released Mn from one column over the entire experimental time in this study (all four infiltration rates and three temperature regimes), this results in an overall mass output of approx. 140 mg Mn (data not shown). After the experiment, the total Mn mass was around 1600 mg within a column (Figure 7, ≈10 kg of sediment, calculated dry weight). Considering the large deviations from the total extractable Mn (Table S8), and the potential error of sequential extraction procedures [59], conclusions about a possible exhaustion of Mn during the column experiment would not be reasonable. Taking the observations of Paufler [58] into account, the observed steps along the columns in this study may reflect the natural stratification within the riverbed, rather than a depletion of the Mn reservoir.

With around 5 mg/L of filterable substances and a Mn content of 3500 mg/kg of the suspended matter (both median, n > 100 [25]), the Elbe river water contains approximately 0.04 mg/L Mn, which is bound to suspended solids. Considering the mean abstraction of 22,000 m^3/d in Dresden-Tolkewitz and a bank filtrate portion of 70%, about 15,500 m^3 BF are abstracted per day. Assuming an even distribution of suspended solids in the infiltrating river water, the Elbe river delivers around 6×10^5 mg Mn per day into the riverbed, which is probably not entirely reducible. With the same BF portion and the observed Mn release of 0.1 to 0.8 mg/L, the Mn output from the riverbed into the BF would be 1.5×10^6 to 1.2×10^7 mg/d. Thus, a depletion of the Mn reservoir seems to be possible but more research is needed to evaluate this conclusively.

4.5. Implications for (River-)Bank Filtration Sites

Current climate forecasts show an increase in river discharge seasonality, with increasing high discharges and decreasing low discharges. Furthermore, global mean river water temperatures are projected to increase by 0.8–1.6 °C by 2100 with Europe, the United States, parts of southern Africa, Australia and eastern China facing the largest changes [60].

The results of this study showed stronger Mn release for low infiltration rates compared to high infiltration rates when the temperature was equal. RBF sites in regions with a colder climate probably will not notice different Mn concentrations in the future, since Mn release was neglectable at water temperatures of 10 °C for all infiltration rates. In regions with a temperate climate, Mn release from the riverbed is unlikely during high discharge events with infiltration rates ≥1.1 $m^3/(m^2 \cdot d)$. At infiltration rates of around 0.6 $m^3/(m^2 \cdot d)$ and below, water temperatures >20 °C are sufficient to trigger extensive Mn release from the riverbed. Thus, RBF sites in temperate climate zones at rivers with large seasonal discharge fluctuations may have to deal with increasing Mn concentrations in the future. Additionally, the effect of seasonal rivers showing the highest water temperatures during low discharge periods [60] may intensify this effect. Surface water temperatures of >30 °C are rare in the temperate climate zone.

Typically, rivers in dry/arid or tropical climates like the Nile river [61] or the Mekong river [62] show temperatures in this order of magnitude. Thus, the results of this study suggest that RBF sites in arid or tropical climate zones should be aware of an intensified Mn release from the riverbed in the future, which can distort the quality of the BF even at high infiltration velocities. In such cases, biological post-treatment could be a viable option to remove Mn from the BF [63].

Nonetheless, elevated temperatures are not necessarily causing elevated Mn concentrations during RBF. During the summer in 2003, maximum river water temperatures of 25 °C were observed at the RBF site at the Rhine river in Germany. No elevated Mn concentrations were detected, although anaerobic conditions developed within the aquifer [64].

The field observations in Dresden-Tolkewitz and at other RBF sites prove that an actual high Mn release from the riverbed must not necessarily lead to elevated Mn concentrations in the pumped raw water [1,47]. Sorption, (re-)oxidation, and precipitation along the flow path are potential sinks for Mn released from a riverbed. Especially if the aquifer material contains Mn(hydr)oxides, Mn concentrations of the BF can change largely along the flow path due to the high affinity of Mn^{2+} for Mn(hydr)oxides [63]. Thus, a long distance between the riverbank and the pumping wells could be of advantage to buffer elevated Mn concentrations and temperature. However, such an advantage may have to be checked against a lower portion of abstracted bank filtrate and a higher portion of potentially Fe- and Mn-rich landside groundwater [65].

For the RBF site in Dresden-Tolkewitz, the temperature was found to be the driving force for Mn release from the riverbed and high discharge and infiltration rates limit the release at lower temperatures. In Dresden-Tolkewitz, the mean infiltration rate is around 0.2 $m^3/(m^2 \cdot d)$, which corresponds to the infiltration rate that was found to be sustainable for RBF sites along the River Rhine, Elbe, and other European Rivers [66]. After Soares [67], an infiltration rate of 0.32 $m^3/(m^2 \cdot d)$ would be still sustainable for this RBF site. Ahrns [23] observed infiltration rates up to 0.95 $m^3/(m^2 \cdot d)$ in Dresden-Tolkewitz. Thus, the investigated low infiltration rate of 0.3 $m^3/(m^2 \cdot d)$ in this study represents the mean infiltration rate in Dresden-Tolkewitz. Such low infiltration rates must go in hand with temperatures above 20 °C to trigger a Mn release. With increasing temperatures, the infiltration rate becomes less important and at water temperatures around 30 °C, an extensive Mn release from the riverbed can be expected even at mean infiltration rates.

5. Conclusions

Current climate forecasts project increasing river discharge seasonality and water temperatures and thus, are thought-provoking at many (river)bank filtration sites. Water quality data of a 10-year time span from a monitoring transect at the RBF site Dresden-Tolkewitz and accompanying column experiments were used to assess the potential Mn release from the riverbed with respect to the climate-related variables, temperature and discharge. Temperature was found to be more important than discharge. Low infiltration rates 0.3 $m^3/(m^2 \cdot d)$ required temperatures above 20 °C to trigger Mn release. With an increasing temperature, the discharge becomes less important and at 30 °C, the infiltration rates of ≈0.6 $m^3/(m^2 \cdot d)$ can already cause an extensive Mn release from the riverbed. The subsequent modeling of the column experiment with PHREEQC resulted in degradation rates for DO that are applicable at other RBF sites for several water temperatures and flow velocities. The determined Mn reduction rate constants are appropriate to simulate an Mn release from riverbed sediments but are not suited for simulations in which Mn reduction is likely to occur within the aquifer and the Mn concentrations can be limited by precipitation, for example.

Supplementary Materials: The following are available online at http://www.mdpi.com/2073-4441/10/10/1476/s1,

- Figure S1: The flow scheme of the column experiments inside the thermostatic cabinets;
- Figure S2: The Mn concentration at OW 2 during a low discharge period in 2015;
- Figure S3: The Mn concentration at OW 3 during a low discharge period in 2015;
- Figure S4: The increase of the Mn concentration within the first 5 PV at 30 °C and 1 mL/min after lowering from 2 mL/min, Median, 10- and 90-%ile (each n = 3);
- Figure S5: The calibrated reduction rate constants for the column experiment;
- Figure S6: The Mn concentration at OW 1 during a low discharge period in 2007;
- Figure S7: The Mn concentration at OW 2 during a low discharge period in 2007;
- Figure S8: The Mn concentration at OW 3 during a low discharge period in 2007;
- Table S1: The chemical reagents and analytical conditions for the optimized BCR sequential extraction procedure [27,28];
- Table S2: The input data of the column in PHREEQC;
- Table S3: The statistical data of the Elbe river at Dresden for the entire observation period 2006–2016 [25];
- Table S4: The monthly and 10-year median values of selected parameters along all three OW's of the transect in the WW Dresden-Tolkewitz for the entire observation period 2006–2016;
- Table S5: The statistical data for the low flow period in 2015;

- Table S6: The statistical data for Mn release during the column experiment with riverbed sediment from the Elbe river in Dresden-Tolkewitz, Q_1 and Q_3 correspond to the 1st and 3rd quartile;
- Table S7: The comparison of the measured parameter values during the column experiment and the modeled parameters from PHREEQC;
- Table S8: The results and statistical data of the sequential extraction of the riverbed sediment after the column experiment (n = 3 for each statistical data);
- Table S9: The median concentration of DO in the outflow during the column experiment.

Author Contributions: Data curation, M.B., N.S. and T.F.; Investigation, S.P. and T.G.; Methodology, S.P. and T.G.; Project administration, T.G.; Modeling, S.P.; Supervision, S.P. and T.G.; Writing—original draft, S.P.; Writing—review & editing, S.P., T.G., M.B., N.S. and T.F.

Funding: This research received no external funding.

Acknowledgments: This work was performed as cooperation between DREWAG Netz GmbH and the Division of Water Sciences at the University of Applied Sciences Dresden. The authors are grateful to the ESF for the financial support to S. Paufler (grant no. 200031585). The paper was completed by further analysis supported by the AquaNES project, which has received funding from the European Union's Horizon 2020 research and innovation programme under grant agreement No. 689450.

Conflicts of Interest: The authors declare no conflict of interest. The founding sponsors had no role in the design of the study; in the collection, analyses, or interpretation of data; in the writing of the manuscript, and in the decision to publish the results.

References

1. Bourg, A.C.M.; Bertin, C. Biogeochemical processes during the infiltration of river water into an alluvial aquifer. *Environ. Sci. Technol.* **1993**, *27*, 661–666. [CrossRef]
2. Grischek, T.; Schoenheinz, D.; Worch, E.; Hiscock, K. Bank filtration in Europe – An overview of aquifer conditions and hydraulic controls. In *Management of Aquifer Recharge for Sustainability*; Dillon, P., Ed.; Balkema Publ.: Lisse, The Netherlands, 2002; pp. 485–488.
3. Ray, C.; Melin, G.; Linsky, R.B. *Riverbank Filtration—Improving Source Water Quality*; Kluwer: Dordrecht, The Netherlands, 2003; 364p.
4. Regnery, J.; Barringer, J.; Wing, A.D.; Hoppe-Jones, C.; Teerlink, J.; Drewes, J.E. Start-up performance of a full-scale riverbank filtration site regarding removal of DOC, nutrients, and trace organic chemicals. *Chemosphere* **2015**, *127*, 136–142. [CrossRef] [PubMed]
5. Blanford, W.; Boving, T.; Al-Ghazawi, Z.; Shawaqfah, M.; Al-Rashdan, J.; Saadoun, I.; Schijven, J.; Ababneh, Q. River bank filtration for protection of Jordanian surface and groundwater. In Proceedings of the World Environmental and Water Resources Congress 2010: Challenges of Change; ASCE: Providence, RI, USA, 2010; pp. 776–781.
6. Ghodeif, K.; Paufler, S.; Grischek, T.; Wahaab, R.; Souaya, E.; Bakr, M.; Abogabal, A. Riverbank filtration in Cairo, Egypt—Part I: Installation of a new riverbank filtration site and first monitoring results. *Environ. Earth. Sci.* **2018**, *77*, 270. [CrossRef]
7. Hu, B.; Teng, Y.; Zhai, Y.; Zuo, R.; Li, J.; Chen, H. Riverbank filtration in China: A review and perspective. *J. Hydrol.* **2016**, *541*, 914–927. [CrossRef]
8. Sandhu, C.; Grischek, T.; Kumar, P.; Ray, C. Potential for riverbank filtration in India. *Clean Technol. Environ. Policy* **2011**, *13*, 295–316. [CrossRef]
9. Hiscock, K.M.; Grischek, T. Attenuation of groundwater pollution by bank filtration. *J. Hydrol.* **2002**, *266*, 139–144. [CrossRef]
10. Kuehn, W.; Mueller, U. Riverbank filtration—An overview. *J. Am. Water Works Assoc.* **2000**, *92*, 60–69. [CrossRef]
11. Bertelkamp, C.; Reungoat, J.; Cornelissen, E.R.; Singhal, N.; Reynisson, J.; Cabo, A.J.; van der Hoek, J.P.; Verliefde, A.R.D. Sorption and biodegradation of organic micropollutants during river bank filtration: A laboratory column study. *Water Res.* **2014**, *52*, 231–241. [CrossRef] [PubMed]
12. Bourg, A.C.M.; Richard-Raymond, F. Spatial and temporal variability in the water redox chemistry of the M27 experimental site in the Drac river calcareous alluvial aquifer (Grenoble, France). *J. Contam. Hydrol.* **1994**, *15*, 93–105. [CrossRef]

13. Von Gunten, H.R.; Karametaxas, G.; Krähenbühl, U.; Kuslys, M.; Giovanoli, R.; Hoehn, E.; Keil, R. Seasonal biogeochemical cycles in riverborne groundwater. *Geochim. Cosmochim. Acta* **1991**, *55*, 3597–3609. [CrossRef]
14. Henzler, A.F.; Greskowiak, J.; Massmann, G. Seasonality of temperatures and redox zonations during bank filtration—A modeling approach. *J. Hydrol.* **2016**, *535*, 282–292. [CrossRef]
15. Gross-Wittke, A.; Gunkel, G.; Hoffmann, A. Temperature effects on bank filtration: Redox conditions and physical–chemical parameters of pore water at Lake Tegel, Berlin, Germany. *J. Water Clim. Chang.* **2010**, *1*, 55–66. [CrossRef]
16. Van't Hoff, J.H.; Cohen, E. *Studies on Chemical Dynamics*; Studien zur chemischen Dynamik, Etudes de dynamique chemique; Frederik Muller & Co.: Amsterdam, The Netherlands, 1896; p. 128.
17. Diem, S.; von Rohr, M.R.; Hering, J.G.; Kohler, H.-P.E.; Schirmer, M.; von Gunten, U. NOM degradation during river infiltration: Effects of the climate variables temperature and discharge. *Water Res.* **2013**, *47*, 6585–6595. [CrossRef] [PubMed]
18. Schoenheinz, D.; Grischek, T. Behavior of dissolved organic carbon during bank filtration under extreme climate conditions. In *Riverbank Filtration for Water Security in Desert Countries*; Shamrukh, M., Ed.; NATO Science for Peace and Security Series C: Environmental Security; Springer: Dordrecht, The Netherlands, 2011; pp. 151–168, ISBN 978-94-007-0025-3.
19. Sprenger, C.; Lorenzen, G.; Hulshoff, I.; Gruetzmacher, G.; Ronghang, M.; Pekdeger, A. Vulnerability of bank filtration systems to climate change. *Sci. Total Environ.* **2011**, *409*, 655–663. [CrossRef] [PubMed]
20. EEA European Environment Agency. *Climate Change, Impacts and Vulnerability in Europe 2016*; An Indicator-Based Report; Publications Office of the European Union: Luxembourg, 2017; ISBN 978-92-9213-835-6.
21. Kreienkamp, F.; Spekat, A.; Enke, W. *WEREX V: Provision of an Ensemble of Regional Climate Projections for Saxony*, 1st ed.; Saxon State Office for the Environment, Agriculture and Geology: Dresden, Germany, 2011; 71p. (In German)
22. Grischek, T.; Bartak, R. Riverbed clogging and sustainability of riverbank filtration. *Water* **2016**, *8*, 604. [CrossRef]
23. Ahrns, J. Modeling the Exchange between Surface Water and Groundwater Using Temperature as Tracer. Diploma Thesis, Dresden University of Applied Sciences, Dresden, Germany, 2008. (In German)
24. DVGW German Technical and Scientific Association for Gas and Water. *Guideline DVGW W 112 (A), Principles of Groundwater Sampling from Groundwater Monitoring Wells*; WVGW: Bonn, Germany, 2011; ISSN 0176-3504. (In German)
25. SMUL Saxon State Ministry for Environment and Agriculture. Water Quality Data for the Elbe River. 2018. Available online: www.umwelt.sachsen.de/umwelt/wasser/ (accessed on 15 June 2018).
26. WSV Federal Waterways and Shipping Administration. Hydrological Information System. 2018. Available online: www.wsv.de (accessed on 14 June 2018).
27. Rauret, G.; López-Sánchez, J.F.; Sahuquillo, A.; Rubio, R.; Davidson, C.; Ure, A.; Quevauviller, P. Improvement of the BCR three step sequential extraction procedure prior to the certification of new sediment and soil reference materials. *J. Environ. Monit.* **1999**, *1*, 57–61. [CrossRef] [PubMed]
28. Sutherland, R.A.; Tack, F.M.G. Determination of Al, Cu, Fe, Mn, Pb and Zn in certified reference materials using the optimized BCR sequential extraction procedure. *Anal. Chim. Acta* **2002**, *454*, 249–257. [CrossRef]
29. Farnsworth, C.E.; Hering, J.G. Inorganic geochemistry and redox dynamics in bank filtration settings. *Environ. Sci. Technol.* **2011**, *45*, 5079–5087. [CrossRef] [PubMed]
30. Parkhurst, D.L.; Appelo, C.A.J. Description of Input and Examples for Phreeqc Version 3: A Computer Program for Speciation, Batch-Reaction, One-Dimensional Transport, and Inverse Geochemical Calculations. U.S. Geological Survey Techniques and Methods, book 6, chap. A43; 2013. Available online: http://pubs.usgs.gov/tm/06/a43 (accessed on 14 June 2018).
31. Greskowiak, J.; Prommer, H.; Massmann, G.; Nutzmann, G. Modeling seasonal redox dynamics and the corresponding fate of the pharmaceutical residue phenazone during artificial recharge of groundwater. *Environ. Sci. Technol.* **2006**, *40*, 6615–6621. [CrossRef] [PubMed]
32. Diem, S.; Cirpka, O.A.; Schirmer, M. Modeling the dynamics of oxygen consumption upon riverbank filtration by a stochastic–convective approach. *J. Hydrol.* **2013**, *505*, 352–363. [CrossRef]
33. Sharma, L.; Greskowiak, J.; Ray, C.; Eckert, P.; Prommer, H. Elucidating the effects on seasonal variations of biogeochemical turnover rates during riverbank filtration. *J. Contam. Hydrol.* **2012**, *428–429*, 104–115. [CrossRef]

34. Doherty, J. *PEST. Model-Independent Parameter Estimation*, 7th ed.; Watermark Numerical Computing: Brisbane, Australia, 2018.
35. Matsunaga, T.; Karametaxas, G.; von Gunten, H.R.; Lichtner, P.C. Redox chemistry of iron and manganese minerals in river-recharged aquifers: A model interpretation of a column experiment. *Geochim. Cosmochim. Acta* **1993**, *57*, 1691–1704. [CrossRef]
36. Mayer, K.U.; Benner, S.G.; Frind, E.O.; Thornton, S.F.; Lerner, D.N. Reactive transport modeling of processes controlling the distribution and natural attenuation of phenolic compounds in a deep sandstone aquifer. *J. Contam. Hydrol.* **2001**, *53*, 341–368. [CrossRef]
37. Prommer, H.; Stuyfzand, P.J. Identification of temperature-dependent water quality changes during a deep well injection experiment in a pyritic aquifer. *Environ. Sci. Technol.* **2005**, *39*, 2200–2209. [CrossRef] [PubMed]
38. Massmann, G.; Pekdeger, A.; Merz, C. Redox processes in the Oderbruch polder groundwater flow system in Germany. *Appl. Geochem.* **2004**, *19*, 863–886. [CrossRef]
39. Jensen, D.L.; Boddum, J.K.; Tjell, J.C.; Christensen, T.H. The solubility of rhodochrosite ($MnCO_3$) and siderite ($FeCO_3$) in anaerobic aquatic environments. *Appl. Geochem.* **2002**, *17*, 503–511. [CrossRef]
40. Heeger, D. Investigation of Clogging in Rivers. Ph.D. Thesis, Dresden University of Technology, Dresden, Germany, 1987. (In German)
41. Grischek, T. Management of bank filtration sites along the Elbe River. Ph.D. Thesis, Faculty of Forestry, Geo and Hydro Sciences, Dresden University of Technology, Dresden, Germany, 2003. (In German)
42. Eckert, P.; Rohns, H.P.; Irmscher, R. Dynamic processes during bank filtration and their impact on raw water quality. In Proceedings of the Aquifer Recharge, Recharge Systems for Protecting and Enhancing Groundwater Resources, Berlin, Germany, 11–16 June 2005; pp. 17–22.
43. Eckert, P.; Irmscher, R. Over 130 years of experience with riverbank filtration in Düsseldorf, Germany. *Aqua* **2006**, *55*, 283–291. [CrossRef]
44. Von Rohr, R.M.; Hering, J.G.; Kohler, H.P.; von Gunten, U. Column studies to assess the effects of climate variables on redox processes during riverbank filtration. *Water Res.* **2014**, *61*, 263–275. [CrossRef] [PubMed]
45. Groffman, A.R.; Crossey, L.J. Transient redox regimes in a shallow alluvial aquifer. *Chem. Geol.* **1999**, *161*, 415–442. [CrossRef]
46. Bourg, A.C.M.; Darmendrail, D.; Ricour, J. Geochemical filtration of riverbank and migration of heavy metals between the Deûle River and the Ansereuilles alluvion-chalk aquifer (Nord, France). *Geoderma* **1989**, *44*, 229–244. [CrossRef]
47. Jacobs, L.A.; von Gunten, H.R.; Keil, R.; Kuslys, M. Geochemical changes along a river-groundwater infiltration flow path: Glattfelden, Switzerland. *Geochim. Cosmochim. Acta* **1988**, *52*, 2693–2706. [CrossRef]
48. Kedziorek, M.; Geoffriau, S.; Bourg, A.C.M. Organic matter and modeling redox reactions during river bank filtration in an alluvial aquifer of the Lot River, France. *Environ. Sci. Technol.* **2008**, *42*, 2793–2798. [CrossRef] [PubMed]
49. Maeng, S.K.; Ameda, E.; Sharma, S.K.; Grützmacher, G.; Amy, G.L. Organic micro-pollutant removal from wastewater effluent-impacted drinking water sources during bank filtration and artificial recharge. *Water Res.* **2010**, *44*, 4003–4014. [CrossRef] [PubMed]
50. Von Gunten, H.R.; Karametaxas, G.; Keil, R. Chemical processes in infiltrated riverbed sediments. *Environ. Sci. Technol.* **1994**, *28*, 2087–2093. [CrossRef] [PubMed]
51. Bourg, A.C.M.; Bertin, C. Seasonal and spatial trends in manganese solubility in an alluvial aquifer. *Environ. Sci. Technol.* **1994**, *28*, 868–876. [CrossRef] [PubMed]
52. Hoehn, E.; Zobrist, J.; Schwarzenbach, R.P. Infiltration of river water into groundwater—Hydrogeological and hydrochemical investigations in the Glattal. *Gas Wasser Abwasser* **1983**, *63*, 401–410. (In German)
53. Martin, J.M.; Meybeck, M. Elemental mass-balance of material carried by major world rivers. *Mar. Chem.* **1979**, *7*, 173–206. [CrossRef]
54. Jain, C.K.; Ram, D. Adsorption of lead and zinc on bed sediments of the river Kali. *Water Res.* **1997**, *31*, 154–162. [CrossRef]
55. Jain, C.K.; Sharma, M.K. Adsorption of Cadmium on bed sediments of River Hindon: Adsorption models and kinetics. *Water Air Soil Poll.* **2001**, *137*, 1–19. [CrossRef]
56. Förstner, U.; Salomons, W. Trace metal analysis on polluted sediments, II. Evaluation of environmental impact. *Environ. Technol. Lett.* **1980**, *1*, 506–517. [CrossRef]

57. Grischek, T.; Dehnert, J.; Nestler, W.; Treutler, H.C.; Freyer, K. Description of system conditions during bank filtration through accompanying drilling core investigations. In Proceedings of the 2nd Dresdner Grundwasserforschungstage, Dresden, Germany, 25 March 1993; pp. 207–220. (In German)
58. Paufler, S. Management of Riverbank Filtration Sites to Reduce Manganese Concentrations in Raw Water. Diploma Thesis, Dresden University of Applied Sciences, Dresden, Germany, 2015. (In German)
59. Nirel, P.M.V.; Morel, F.M.M. Pitfalls of sequential extractions. *Water Res.* **1990**, *24*, 1055–1056. [CrossRef]
60. Van Vliet, M.T.H.; Franssen, W.H.P.; Yearsley, J.R.; Ludwig, F.; Haddeland, I.; Lettenmaier, D.P.; Kabat, P. Global river discharge and water temperature under climate change. *Glob. Environ. Chang.* **2013**, *23*, 450–464. [CrossRef]
61. Abdalla, F.A.; Shamrukh, M. Quantification of river Nile/Quaternary aquifer exchanges via riverbank filtration by hydrochemical and biological indicators, Assiut, Egypt. *J. Earth Syst. Sci.* **2016**, *125*, 1697–1711. [CrossRef]
62. Buschmann, J.; Berg, M.; Stengel, C.; Sampson, M.L. Arsenic and manganese contamination of drinking water resources in Cambodia: Coincidence of risk areas with low relief topography. *Environ. Sci. Technol.* **2007**, *41*, 2146–2152. [CrossRef] [PubMed]
63. Brandhuber, P.; Clark, S.; Knocke, W.; Tobiason, J. (Eds.) *Guidance for the Treatment of Manganese*; Water Research Foundation: Denver, Colorado, 2013; 148p, ISBN 978-1-60573-187-2.
64. Rohns, H.P.; Forner, C.; Eckert, P.; Irmscher, R. Efficiency of riverbank filtration considering the removal of pathogenic microorganisms of the River Rhine. In *Recent Progress in Slow Sand and Alternative Biofiltration Processes*; Gimbel, R., Graham, N.J.D., Collins, M.R., Eds.; IWA Publishing: London, UK, 2006; pp. 539–546, ISBN 9781843391203.
65. Grischek, T.; Paufler, S. Prediction of iron release during riverbank filtration. *Water* **2017**, *9*, 317. [CrossRef]
66. Grischek, T.; Schoenheinz, D.; Eckert, P.; Ray, C. Sustainability of river bank filtration: Examples from Germany. In *Groundwater Quality Sustainability*; Maloszewski, P., Witczak, S., Malina, G., Eds.; Taylor & Francis Group: London, UK, 2012; pp. 213–227.
67. Soares, M. The influence of high infiltration rates, suspended sediment concentration and sediment grain size on river and lake bed clogging. Ph.D. Thesis, Technical University of Berlin, Berlin, Germany, 2015.

water

MDPI

Article -Supplementary material

The impact of river discharge and water temperature on manganese release from the riverbed during riverbank filtration – A case study from Dresden, Germany

Sebastian Paufler[1]*, Thomas Grischek[2], Marcos Benso[3], Nadine Seidel[4], Thomas Fischer[5]

[1] Dresden University of Applied Sciences, Friedrich-List-Platz 1, 01069 Dresden, Germany; sebastian.paufler@htw-dresden.de; Tel.: +49351/463-2631.
[2] Dresden University of Applied Sciences, Friedrich-List-Platz 1, 01069 Dresden, Germany; thomas.grischek@htw-dresden.de
[3] Dresden University of Applied Sciences, Friedrich-List-Platz 1, 01069 Dresden, Germany; marcosbenso@hotmail.com
[4] Dresden University of Applied Sciences, Friedrich-List-Platz 1, 01069 Dresden, Germany; nadine_85@msn.com
[5] DREWAG Dresden, Kohlenstraße 23, 01189 Dresden, Germany; Thomas_Fischer@drewag-netz.de

Received: date; Accepted: date; Published: date

Supplementary material

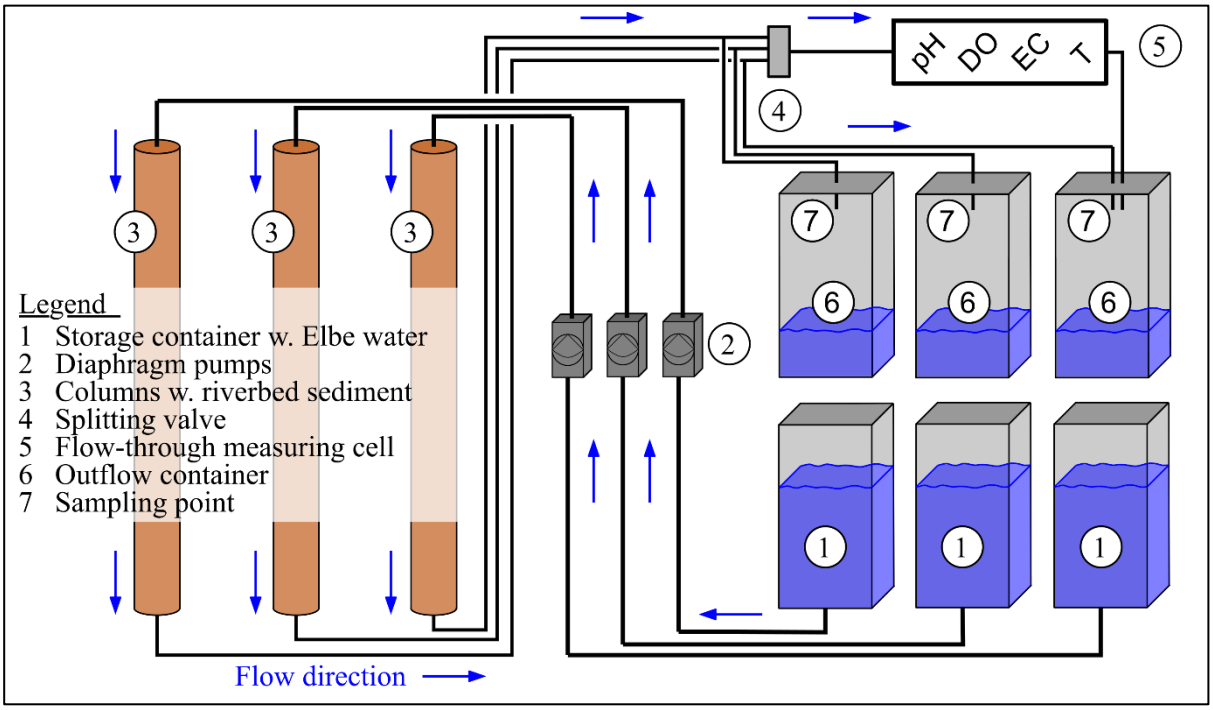

Figure S1: Flow scheme of the column experiments inside the thermostatic cabinets

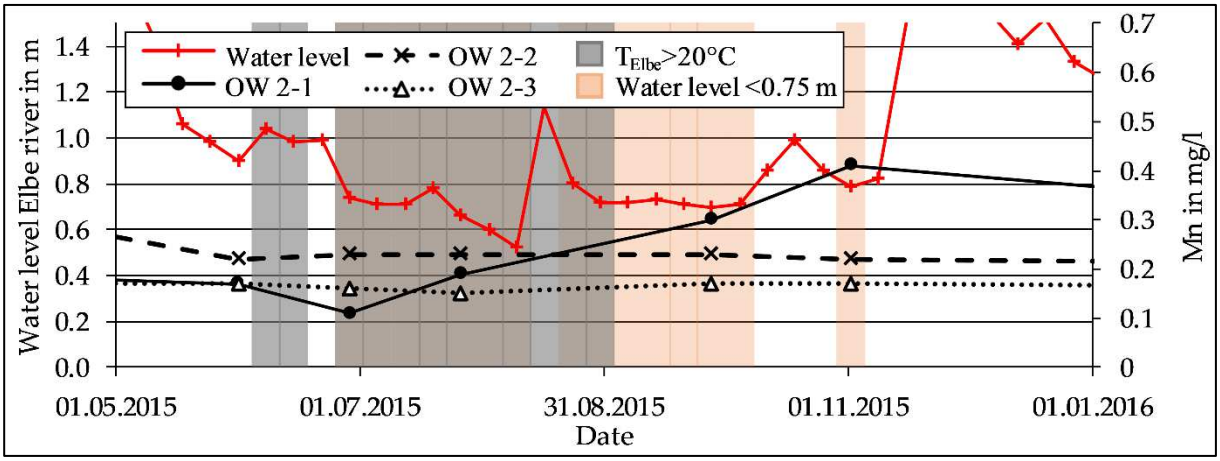

Figure S2: Mn concentration at OW 2 during a low discharge period in 2015

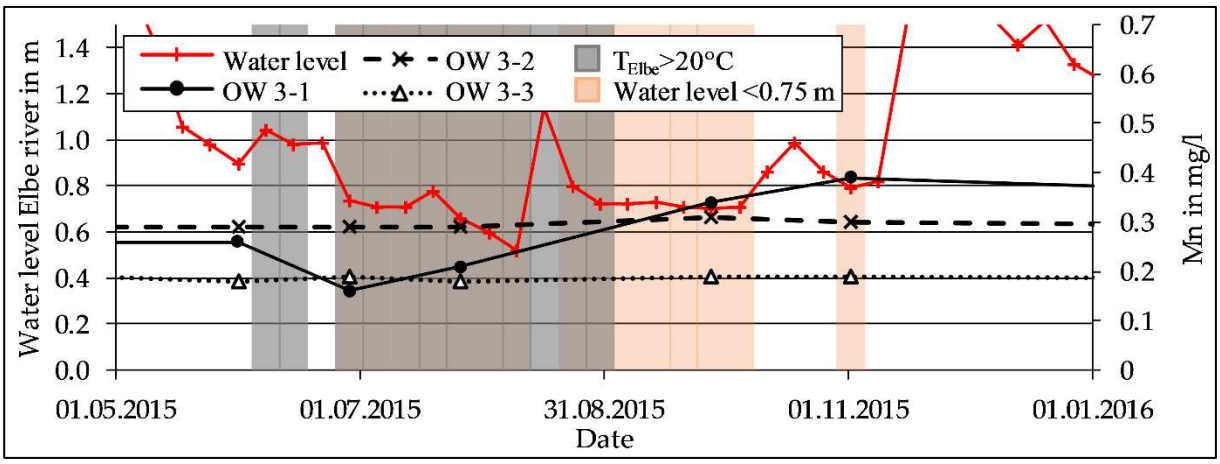

Figure S3: Mn concentration at OW 3 during a low discharge period in 2015

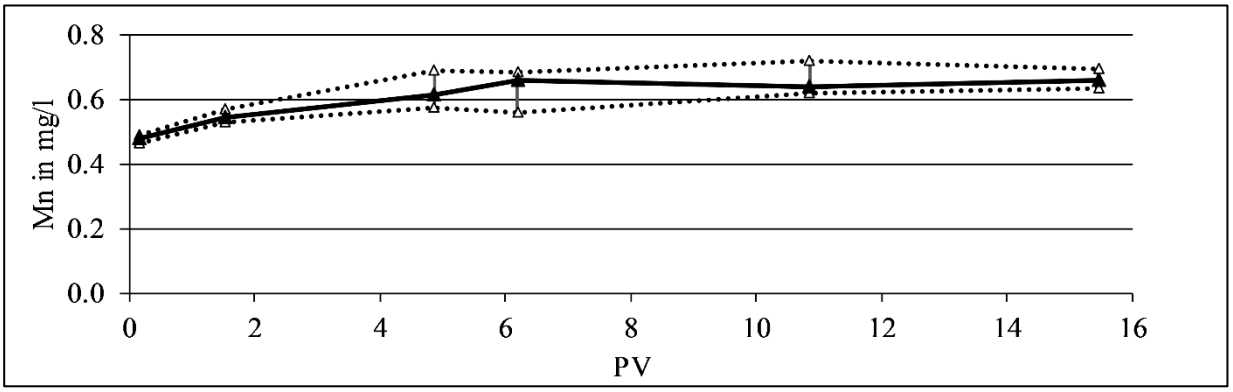

Figure S4: Increase of the Mn concentration within the first 5 PV at 30°C and 1 ml/min after lowering from 2 ml/min, Median, 10- and 90-%ile (each n=3)

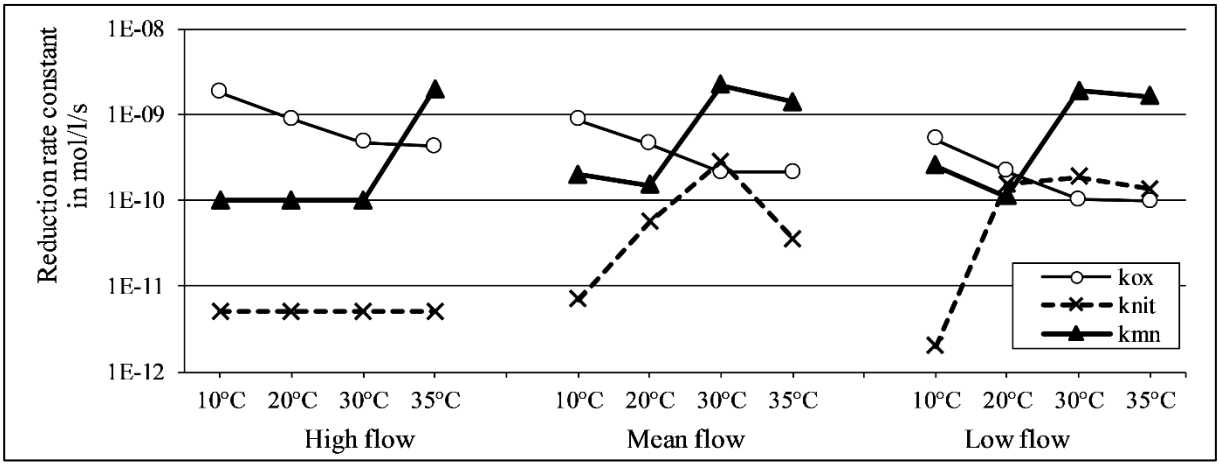

Figure S5: Calibrated reduction rate constants for the column experiment

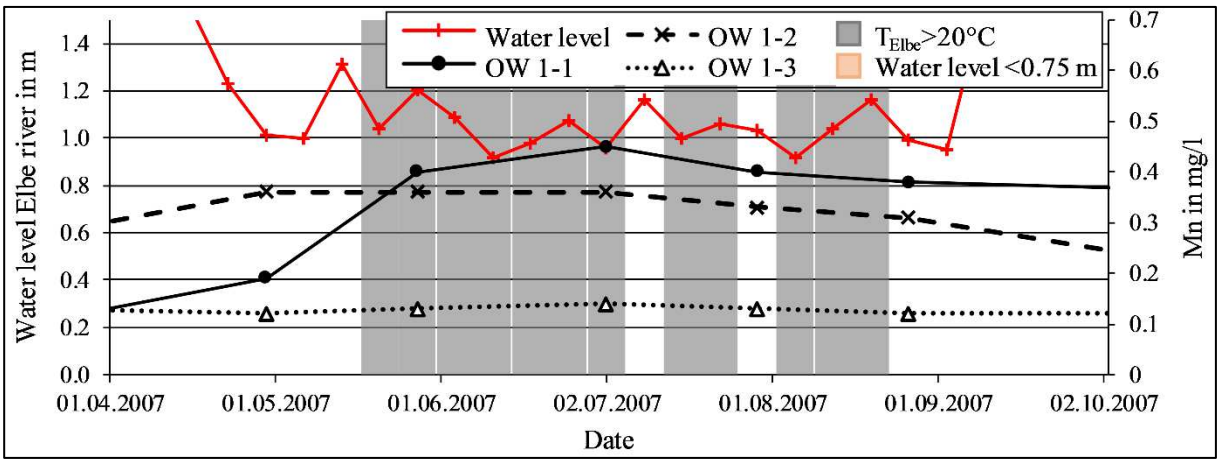

Figure S6: Mn concentration at OW 1 during a low discharge period in 2007

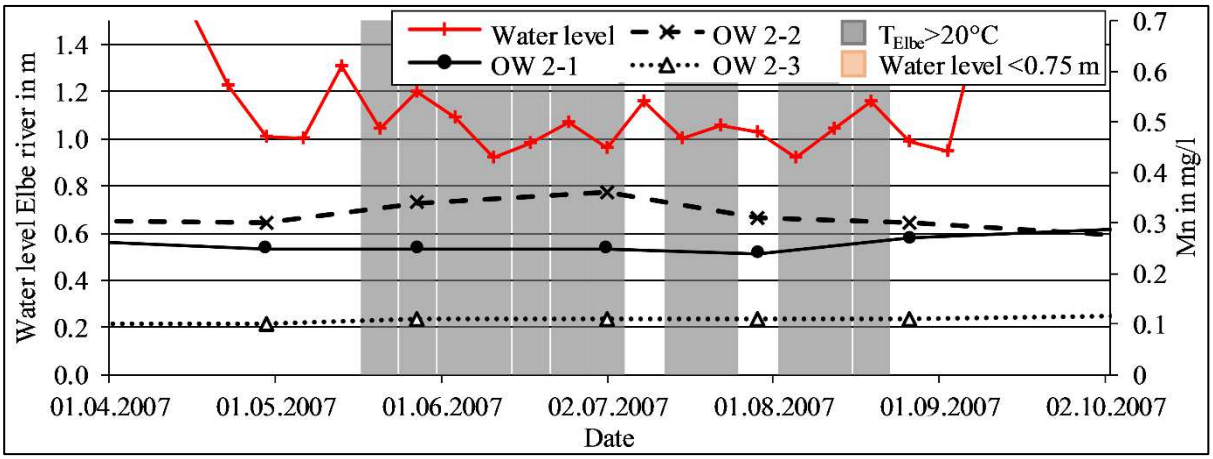

Figure S7: Mn concentration at OW 2 during a low discharge period in 2007

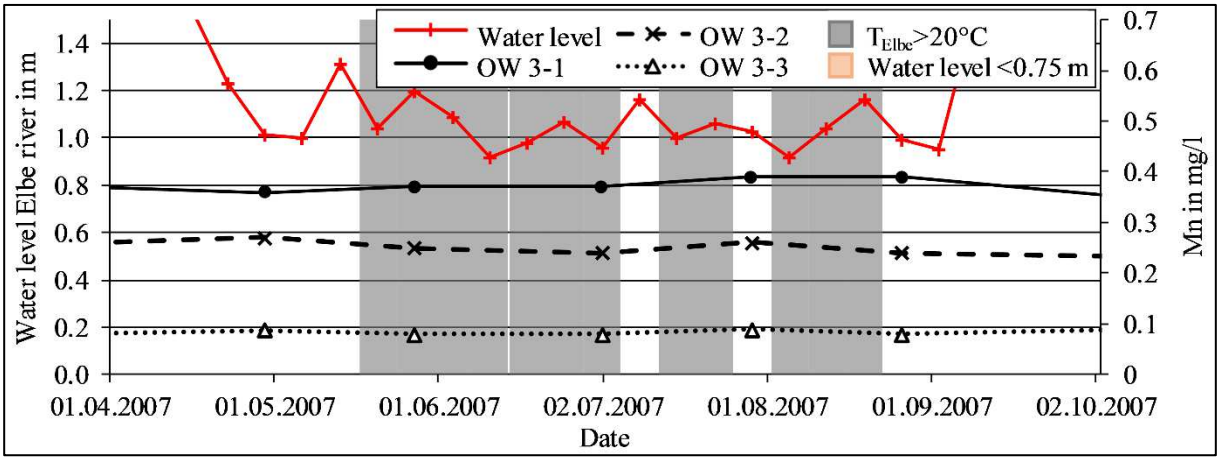

Figure S8: Mn concentration at OW 3 during a low discharge period in 2007

Table S1: Chemical reagents and analytical conditions for the optimized BCR sequential extraction procedure after Rauret et al. (1999) / Sutherland & Tack (2002)

Step	Extracted phase	Chemical reagents*1 and conditions
1	Acid extractable Exchangeable Carbonate	1 g aliquot, 40 ml 0.11 M CH_3COOH Shake for 16 h at 22±5 °C Separate extract from the solid by centrifugation at 3000 U/min for 20 min
2	Reducible	To step 1 residue: 40 ml 0.5 M $NH_2OH{\cdot}HCl$ (pH≈1.5) Shake for 16 h at 22±5 °C Centrifuge extract as per step 1
3	Oxidizable	To step 2 residue: 10 ml of 30 % H_2O_2 (pH 2–3) Keep at 85±2 °C for 1 h Add further 10 ml of 30 % H_2O_2 (pH 2–3) Keep at 85±2 °C for 1 h Add 50 ml; 1 M NH_4OAc (pH 2) Shake for 16 h at 22±5 °C Centrifuge extract as per step 1
4	Residual *2	To step 3 residue: 15 ml HNO_3 with 5 ml $HClO_4$ Keep at 70-80 °C for 1 h Add further 5 ml HNO_3 with 1 ml $HClO_4$ Keep at 120 °C for 1 h Centrifuge extract as per step 1

*1 CH_3COOH (Acetic acid), $NH_2OH{\cdot}HCl$ (Hydroxylammonium-hydrochloride), H_2O_2 (Hydrogen peroxide), NH_4OAc (Ammonium acetate), HNO_3 (Nitric acid), $HClO_4$ (Perchloric acid)

*2 Extraction of the residual phase differed slightly from Rauret et al. (1999) due to lab restrictions.

Note: Results were checked against a total extraction that was parallel conducted with separate samples by direct application of step 4.

Table S2: Input data of the column in PHREEQC

Parameter	Value
Cells	50
Lengths	0.02
Dispersivity	0.01
Diffusion coefficient	$1 \cdot 10^{-9}$
Porosities	0.34
Bcond	flux flux
Flow direction	forward
Shifts	depending on simulated infiltration rate
Time	depending on simulated infiltration rate

Table S3: Statistical data of the Elbe river at Dresden for the entire observation period 2006-2016 (SMUL, 2018)

Month	EC	pH	T	DO	NO_3^-	DOC	TOC	Mn
Jan.	427	7.8	3.0	13.1	19.0	5.1	5.8	0.02
Feb.	443	7.8	3.0	13.0	19.0	4.9	5.6	0.03
Mar.	466	7.85	4.9	13.5	19.0	5.1	6.5	0.03
Apr.	365	7.9	9.5	12.1	18.0	4.9	6.2	0.01
May	413	8.9	14.9	11.8	13.0	5.0	7.4	0.01
June	429	7.9	19.0	9.7	14.0	5.1	7.1	0.01
July	427	7.9	21.6	8.5	12.0	5.2	6.3	0.01
Aug.	407	7.8	21.0	8.5	13.0	5.8	6.7	0.01
Sept.	447	7.7	17.7	8.4	13.0	5.4	6.0	0.01
Oct.	467	7.8	14.0	9.5	14.0	5.4	6.0	0.01
Nov.	446	7.8	9.7	10.6	15.0	5.4	6.1	0.01
Dec.	463	7.8	5.6	11.7	16.0	5.1	5.2	0.02
Min	255	7.5	0.0	7.0	9.7	4.0	4.4	<0.01
10%ile	355	7.7	3.0	8.4	12.0	4.5	5.2	0.01
Median	435	7.8	10.9	10.8	15.0	5.2	6.3	0.01
90%ile	492	8.6	21.3	13.8	20.0	6.0	8.2	0.03
Max	549	9.4	26.0	19.0	32.0	7.0	17.0	0.07
n	279	300	267	269	279	325	292	278

Table S4: Monthly median and 10-year median values of selected parameters along all three OW's of the transect in the WW Dresden-Tolkewitz for the entire observation period 2006-2016

Parameter	OW	Month												10-year
		Jan.	Feb.	Mar.	Apr.	May	June	July	Aug.	Sept.	Oct.	Nov.	Dec.	Median
EC in µS/cm	1-1	451	474	474	465	399	436	470	468	397	467	433	410	463
	1-2	470	449	486	478	423	428	464	446	407	465	435	410	464
	1-3	431	441	508	452	449	441	436	441	417	469	435	410	452
	2-1	471	465	468	526	415	436	458	448	396	462	429	414	460
	2-2	455	440	468	481	449	428	439	446	399	461	428	420	452
	2-3	420	442	509	447	443	448	434	434	417	467	470	413	449
	3-1	449	446	465	462	426	420	433	439	429	458	421	424	453
	3-2	415	439	456	438	441	447	429	433	430	458	459	396	453
	3-3	423	445	505	439	442	452	442	446	422	518	470	420	465
pH	1-1	6.8	6.9	6.8	7.0	7.0	7.1	7.0	6.9	7.0	7.0	7.1	6.9	7.0
	1-2	7.0	7.0	7.0	7.0	7.1	7.2	7.1	7.1	7.1	7.2	7.1	7.1	7.1
	1-3	7.1	7.0	7.1	7.1	7.1	7.0	7.1	7.0	6.9	7.1	7.1	7.0	7.0
	2-1	7.0	7.1	7.0	7.1	7.1	7.1	6.9	7.0	7.0	7.0	7.1	7.1	7.0
	2-2	7.2	7.2	7.2	7.2	7.2	7.2	7.1	7.1	7.1	7.1	7.1	7.1	7.1
	2-3	7.1	7.0	7.1	7.0	7.1	7.1	7.1	7.0	6.9	7.0	7.0	7.0	7.0
	3-1	7.0	7.0	7.0	7.1	7.1	7.1	7.1	7.0	7.0	7.0	7.1	7.0	7.0
	3-2	7.1	7.1	7.1	7.1	7.1	7.2	7.1	7.1	7.0	7.1	7.1	7.1	7.1
	3-3	7.1	6.9	7.1	7.0	7.1	7.1	7.1	7.0	6.8	7.0	7.0	7.0	7.0
T in °C	1-1	7.8	6.1	6.3	6.2	8.6	13.8	17.4	19.2	20.0	18.3	15.8	12.6	14.1
	1-2	10.5	7.8	7.3	6.5	8.3	10.9	14.2	16.0	19.2	17.2	16.5	14.5	12.1
	1-3	11.8	9.9	9.2	8.8	9.4	10.7	11.8	13.8	16.5	15.3	15.2	13.7	14.4
	2-1	11.7	8.3	8.6	6.1	7.8	10.6	14.2	16.3	19.9	17.6	17.1	15.1	12.6
	2-2	13.0	9.9	10.1	8.3	8.5	9.5	11.3	13.9	18.0	16.2	16.5	14.9	11.8
	2-3	12.8	10.8	10.7	9.4	9.7	10.1	11.0	12.7	15.9	14.6	15.0	14.1	11.7
	3-1	15.0	12.1	10.4	11.6	9.1	8.7	9.2	11.8	17.9	15.9	16.9	14.2	11.7
	3-2	15.2	12.9	10.8	12.2	10.2	9.4	8.8	10.8	15.6	13.1	15.7	12.8	11.5
	3-3	14.4	12.6	11.5	12.2	10.9	10.2	9.3	10.8	14.4	13.3	14.6	12.1	14.1
DO in mg/l	1-1	8.2	6.6	7.1	3.2	0.9	0.7	1.7	0.7	0.4	0.5	2.9	1.7	1.3
	1-2	2.0	2.7	2.2	1.1	0.4	0.3	0.4	0.3	0.3	0.4	1.6	0.3	0.4
	1-3	0.7	0.1	0.2	0.2	0.2	0.4	0.4	0.3	0.3	0.4	1.2	0.2	0.2
	2-1	2.9	1.3	2.2	1.2	0.5	0.5	0.5	0.3	0.6	0.4	1.3	0.2	0.5
	2-2	0.8	0.1	0.2	0.1	0.2	0.3	0.3	0.6	0.3	0.4	1.1	0.2	0.2
	2-3	1.0	0.1	0.2	0.1	0.2	0.3	0.4	0.3	0.4	0.4	1.1	0.3	0.3
	3-1	2.5	0.5	2.1	1.2	1.5	1.0	1.2	1.0	0.5	0.8	1.8	0.7	1.1
	3-2	0.8	0.1	0.1	0.1	0.2	0.3	0.4	0.3	0.3	0.4	1.2	0.2	0.2
	3-3	0.9	0.1	0.2	0.1	0.2	0.3	0.4	0.3	0.3	0.4	1.1	0.2	0.2
NO_3^- in mg/l	1-1	28.2	20.5	31.8	10.8	8.9	0.7	5.3	10.2	0.9	1.7	6.0	9.9	5.3
	1-2	5.9	7.6	11.6	4.8	2.0	0.3	0.3	0.3	0.3	0.3	0.3	1.1	0.3
	1-3	6.5	10.1	11.0	9.2	12.2	11.4	9.5	8.3	4.4	4.0	5.3	5.5	8.9
	2-1	18.9	13.5	13.4	5.6	7.2	2.2	2.9	5.5	2.6	3.1	4.0	4.1	4.1
	2-2	0.6	1.3	0.7	0.9	2.0	2.5	0.6	0.6	0.3	0.3	1.3	0.5	0.7
	2-3	8.4	11.5	13.4	10.7	14.8	13.6	11.4	10.6	5.7	6.8	6.3	7.9	10.8
	3-1	7.8	7.7	8.2	6.5	6.4	4.0	2.6	2.0	1.4	3.4	3.0	2.3	4.0
	3-2	3.7	9.0	5.2	9.9	6.9	5.9	7.0	3.3	1.9	1.6	3.8	4.7	5.2
	3-3	6.9	11.8	14.9	11.6	15.3	15.1	14.8	12.1	6.2	10.0	6.7	11.0	12.0

Continued: Table S4: Monthly median and 10-year median values of selected parameters along all three OW's of the transect in the WW Dresden-Tolkewitz for the entire observation period

Parameter	OW	Month												10-year
		Jan.	Feb.	Mar.	Apr.	May	June	July	Aug.	Sept.	Oct.	Nov.	Dec.	Median
DOC in mg/l	1-1	3.3	3.0	3.4	3.2	2.9	3.6	3.6	3.5	3.9	3.4	3.2	3.2	3.4
	1-2	3.4	2.8	3.1	3.4	3.1	3.6	3.7	3.9	3.9	3.6	3.3	3.7	3.5
	1-3	2.9	2.8	2.8	3.0	3.0	2.9	2.9	3.2	3.0	3.2	3.1	3.0	3.0
	2-1	3.4	3.0	3.1	2.8	3.0	3.5	3.1	3.6	3.7	3.5	3.3	3.6	3.4
	2-2	3.4	3.0	2.9	3.1	2.8	3.3	3.3	3.8	4.0	3.8	3.5	3.9	3.5
	2-3	2.7	2.5	2.7	2.9	2.7	2.8	2.9	2.8	2.7	2.9	3.0	3.0	2.8
	3-1	2.9	2.8	2.9	2.9	2.7	2.9	3.0	3.3	3.4	3.3	3.4	3.5	3.0
	3-2	3.3	3.1	3.1	3.4	3.1	3.0	3.0	3.2	3.3	3.4	3.4	3.4	3.2
	3-3	2.7	2.3	2.5	2.6	2.7	2.5	2.6	2.6	2.1	2.6	2.7	2.5	2.6
Mn in mg/l	1-1	0.01	0.04	0.01	0.14	0.05	0.05	0.08	0.18	0.42	0.31	0.04	0.22	0.06
	1-2	0.33	0.34	0.25	0.30	0.28	0.32	0.41	0.36	0.32	0.27	0.26	0.31	0.32
	1-3	0.20	0.18	0.24	0.19	0.19	0.18	0.25	0.21	0.15	0.21	0.20	0.17	0.20
	2-1	0.17	0.20	0.22	0.17	0.16	0.18	0.21	0.22	0.31	0.24	0.22	0.32	0.21
	2-2	0.30	0.32	0.35	0.33	0.29	0.28	0.30	0.28	0.30	0.28	0.25	0.31	0.30
	2-3	0.16	0.15	0.18	0.16	0.16	0.16	0.17	0.16	0.11	0.18	0.17	0.13	0.17
	3-1	0.22	0.32	0.31	0.35	0.29	0.24	0.28	0.23	0.39	0.30	0.33	0.43	0.30
	3-2	0.30	0.28	0.32	0.26	0.29	0.29	0.28	0.28	0.24	0.31	0.29	0.25	0.29
	3-3	0.22	0.15	0.21	0.15	0.19	0.18	0.20	0.20	0.18	0.24	0.19	0.13	0.19
n	1-1	1	2	2	2	4	4	5	4	2	5	5	2	38
	1-2	1	2	2	2	4	4	5	4	2	5	5	2	38
	1-3	1	2	2	2	4	4	5	4	2	5	5	2	38
	2-1	1	2	2	1	4	4	5	4	2	5	5	2	37
	2-2	1	2	2	2	4	4	5	4	2	5	5	2	38
	2-3	1	2	2	2	4	4	5	4	2	5	5	2	38
	3-1	1	2	2	2	4	4	5	4	2	5	5	2	38
	3-2	1	2	2	2	4	4	5	4	2	5	5	2	38
	3-3	1	2	2	2	4	4	5	4	2	5	5	2	38

Table S5: Statistical data for the low flow period in 2015

	Elbe river		OW 1-1	OW 1-2	OW 1-3	OW 2-1	OW 2-2	OW 2-3	OW 3-1	OW 3-2	OW 3-3
	T in °C	Water level in m	Mn in mg/l								
10%ile	11.0	0.62	0.06	0.20	0.18	0.14	0.22	0.16	0.19	0.29	0.18
Median	20.1	0.74	0.19	0.24	0.20	0.19	0.23	0.17	0.26	0.29	0.19
90%ile	24.6	1.05	0.61	0.28	0.21	0.36	0.25	0.17	0.37	0.31	0.19
n	153	153	6	6	6	6	6	6	6	6	6

Table S6: Statistical data for Mn release during the column experiment with riverbed sediment from the Elbe river in Dresden-Tolkewitz, Q_1 & Q_3 correspond to the 1st & 3rd quartile

Flow rate		10°C	20°C	30°C	35°C
4 ml/min (High flow)	Min.	0.001	0.000	0.000	0.457
	Q1	0.001	0.000	0.019	0.508
	Median	0.002	0.001	0.029	0.512
	Q3	0.008	0.006	0.045	0.526
	Max.	0.014	0.020	0.076	0.569
	n	9	12	21	12
2 ml/min (Mean flow)	Min.	0.002	0.005	0.410	0.537
	Q1	0.005	0.013	0.462	0.596
	Median	0.007	0.018	0.491	0.627
	Q3	0.007	0.029	0.496	0.670
	Max.	0.007	0.041	0.500	0.717
	n	9	9	9	15
1 ml/min (Low low)	Min.	0.000	0.005	0.465	0.564
	Q1	0.002	0.011	0.562	0.802
	Median	0.002	0.038	0.636	0.812
	Q3	0.002	0.057	0.658	0.847
	Max.	0.003	0.074	0.691	0.868
	n	6	21	18	15

Table S7: Comparison of the measured parameter values during the column experiment and the modeled parameters from PHREEQC

Temperature	Flow rate	% Error between the measured and the calibrated value			
		DO	NO_3^-	Mn^{2+}	pH
10°C	1 ml/min	0.1	0.3	8.7	6.2
	2 ml/min	0.2	0.4	6.9	1.6
	4 ml/min	-0.9	0.3	-1.4	-2.2
20°C	1 ml/min	0.2	-0.2	1.8	-2.8
	2 ml/min	-5.3	1.1	-36.6	0.2
	4 ml/min	-3.3	0.5	-17.3	1.5
30°C	1 ml/min	-6.7	4.4	0.1	-9.3
	2 ml/min	-16.6	-1.7	4.8	-8.7
	4 ml/min	-5.4	0.8	8.8	-5.1
35°C	1 ml/min	0.2	-0.7	0.3	-8.7
	2 ml/min	-1.6	-0.1	-1.5	1.2
	4 ml/min	-6.6	0.9	-1.6	1.7
10%ile		-6.7	-0.6	-15.7	-8.7
Median		**-2.4**	**0.4**	**0.2**	**-1.0**
90%ile		0.2	1.1	8.5	1.7
n		12	12	12	12

Table S8: Results and statistical data of the sequential extraction of the riverbed sediment after the column experiment (n=3 for each statistical data)

Column	Depth	Carb.	Easily red.	Organ.	Residual	Sum	Total Extr.
no.	in m	in mg/kg	in mg/kg	in mg/kg	in mg/kg	in mg/kg	in mg/kg
1	0.05	61	149	15	51	277	213
	0.3	30	55	8	53	146	98
	0.6	33	48	7	70	158	112
	0.9	28	36	7	55	125	110
2	0.05	79	115	9	46	249	251
	0.3	47	46	7	62	162	133
	0.6	57	42	7	63	168	331
	0.9	30	34	6	46	116	111
3	0.05	65	142	9	54	270	250
	0.3	37	44	6	64	151	106
	0.6	28	48	6	64	146	705
	0.9	21	38	6	64	129	476
10%ile	0.05	62	121	9	47	253	101
Median		65	142	9	51	270	112
90%ile		76	148	14	53	275	192
10%ile	0.3	32	45	6	54	147	114
Median		37	46	7	62	151	133
90%ile		45	53	8	64	160	228
10%ile	0.6	29	43	6	63	148	138
Median		33	48	7	64	158	250
90%ile		52	48	7	69	166	315
10%ile	0.9	22	34	6	48	118	180
Median		28	36	6	55	125	476
90%ile		30	38	7	62	128	659

Table S9: Median concentration of DO in the outflow during the column experiment

Flow	Residence time	Temperature			
		10°C	20°C	30°C	35°C
4 ml/min	8.1 h	5.4	1.8	0.2	0.2
		n=9	n=12	n=21	n=12
2 ml/min	16.2 h	5.1	0.6	0.2	0.2
		n=9	n=9	n=9	n=15
1 ml/min	32.4 h	4.2	0.2	0.2	0.2
		n=6	n=21	n=18	n=15

Beiliegende Publikation 6

Paufler, S., Grischek, T., Herlitzius, J., Feller, J., Kulakov, V.V. (2019) Manganese release linked to carbonate dissolution during the start-up phase of a subsurface iron removal well in Khabarovsk, Russia. Sci. Total Environ. 650(2), 1722-1733. doi: 10.1016/j.scitotenv.2018.09.319.

Science of the Total Environment 650 (2019) 1722–1733

Contents lists available at ScienceDirect

Science of the Total Environment

journal homepage: www.elsevier.com/locate/scitotenv

Manganese release linked to carbonate dissolution during the start-up phase of a subsurface iron removal well in Khabarovsk, Russia

S. Paufler [a,*], T. Grischek [a], J. Herlitzius [b], J. Feller [a], V.V. Kulakov [c]

[a] Dresden University of Applied Sciences, Friedrich-List-Platz 1, 01069 Dresden, Germany
[b] Arcadis Germany GmbH, EUREF-Campus 10, 10829 Berlin, Germany
[c] Institute of Water and Ecological Problems, FEB RAS, 680000 Khabarovsk, Russia

HIGHLIGHTS

- An unexpected Mn release was observed during the start-up phase of a SIR well.
- Water quality data of the first 194 infiltration & extraction phases were evaluated.
- Column-experiments & closed-bottle batch tests with aquifer sediment were conducted.
- Aquifer materials' grain size and groundwater pH primary controlled the Mn release.
- Dissolution of Mn-bearing carbonate minerals was identified as primary Mn source.

GRAPHICAL ABSTRACT

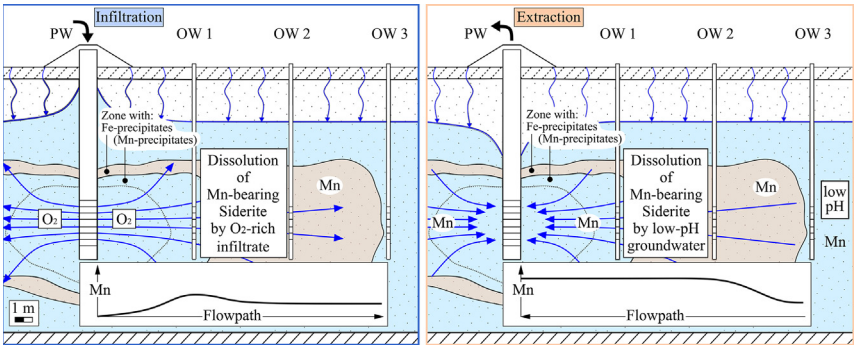

ARTICLE INFO

Article history:
Received 16 July 2018
Received in revised form 24 September 2018
Accepted 24 September 2018
Available online 25 September 2018

Editor: José Virgílio Cruz

Keywords:
Subsurface iron removal
Start-up phase
Manganese release
Carbonate dissolution
Russia

ABSTRACT

Subsurface iron removal (SIR) is a proven pre-treatment technology for removing dissolved iron and manganese from groundwater. The start-up phase of a SIR well and the proper development of the reaction zone around the well are crucial for its subsequent performance. This study evaluates the start-up phase of a SIR production well in Khabarovsk, Russia during the first 194 SIR cycles. A strong release of manganese was observed, which led to concentrations twice as high as the background value of the pristine groundwater. Regular monitoring of the production well and its three adjacent observation wells showed that iron removal began immediately after start-up and that the reaction zone was completely formed within 25 SIR cycles. Closed-bottle batch tests and a flow-through leaching test revealed that the grain size of the aquifer material and groundwater pH are the primary controls on manganese release. During infiltration phases the dissolution of manganese-bearing carbonate minerals was caused by direct oxidation by O_2, whereas the low groundwater pH of 6 seemed to be responsible for the manganese release during extraction.

1. Introduction

Subsurface iron removal (SIR) is a widely used and proven pre-treatment technology for removing dissolved iron and manganese from groundwater (Hallberg and Martinell, 1976; Rott et al., 2002). The principle is that aerated water is injected into an anoxic aquifer to form a so-called oxidation or reaction zone. Within this zone, dissolved and adsorbed iron, Fe(II), and manganese, Mn(II), are oxidized to Fe(III) and Mn(IV) and deposited as metal(hydr)oxides. After a short storage period of a few hours or days, the water can be recovered. Due to the large exchange capacity of the previously

* Corresponding author.
E-mail address: sebastian.paufler@htw-dresden.de (S. Paufler).

https://doi.org/10.1016/j.scitotenv.2018.09.319
0048-9697/

formed metal(hydr)oxide layers, dissolved Fe or Mn are going to adsorb at the metal(hydr)oxide surfaces and the water can be extracted without containing dissolved iron and manganese (Rott et al., 2002; van Halem et al., 2012).

One major advantage of the SIR process is the avoidance of any waste products above the surface. Contrary to conventional above-ground water treatment plants, where Fe and Mn are removed by e.g. aeration, flocculation and filtration, the oxidation products of iron and manganese remain in the aquifer. Hence, no cost-intensive disposal or treatment of waste products is required and SIR is often considered to have lower investment and operating costs (Rott et al., 2002). In addition, due to the aging-related conversion of the hydrous hydroxide precipitates to less voluminous oxides and oxide hydrates and comparably small amount of precipitates, clogging of aquifer pores will not lower the SIR efficiency in the long term (Mettler et al., 2001; Rott et al., 2002). Nonetheless, to ensure a satisfying treatment effectiveness of this technique, the initial start-up phase and the formation and position of the reaction zone are of major importance. Several studies showed that iron removal started within a few infiltration phases, whereas several months or years passed until manganese removal was completed (e.g. Meyerhoff, 1996; Rott and Friedle, 2000b; Roessner et al., 2017).

Problems that interrupt the SIR process were observed when the reaction zone was insufficiently developed and/or the extracted volume was increased too early, such that the existing treatment capacity was exceeded. The consequence was a breakthrough of Mn that surpassed the background concentration of the groundwater (Meyerhoff, 1996; Roessner et al., 2017). Furthermore, the periodic precipitation and dissolution of (Mn-)bearing carbonate minerals was found to impact the manganese concentration during SIR (Mettler et al., 2001). Antoniou et al. (2012, 2014) observed that the infiltration of oxygen-rich water caused the release of Mn from (Mn-)bearing carbonates by direct oxidation from O_2 and indirectly by pyrite oxidation, which forces buffering reactions of the (Mn-bearing) carbonate minerals. Also, since Fe^{2+} can chemically reduce existing Mn(hydr)oxides, incomplete iron removal can cause the release of Mn and lead to a delayed start of Mn removal (Meyerhoff, 1996).

In the city of Khabarovsk, SIR is used as pre-treatment at a recently built waterworks. After Fe removal and partial Mn removal were successfully initiated at >25 wells, an unexpected release of Mn was observed during the infiltration and (especially) the extraction phases at several production wells (PW). This study evaluates the initial start-up of a SIR production well during the first 194 SIR cycles, which took 650 days altogether. At this particular well a strong release of Mn was observed, resulting in Mn concentrations twice as high as the background concentration in the pristine groundwater. Based on a detailed evaluation of data from the regular monitoring of the PW and three adjacent observation wells (OW), the spatial and temporal formation of the reaction zone is described and the primary Mn source is identified. The resulting characterization is reinforced by results of additional column experiments, closed-bottle batch tests and a flow-through leaching test. Finally, results of a sequential extraction of aquifer sediments and from regular monitoring were used to estimate the expected future time span for Mn release.

2. Materials & methods

2.1. Field site Khabarovsk

The city of Khabarovsk is located in the Far East of Russia within the Central Amur River Basin at the confluence of the Ussuri and Amur Rivers (Fig. 1). Groundwater from the 400 km^2 large Tungusska reservoir is used for drinking water production. The base of the Central Amur River Basin begins at 120 m depth and consists of silt layers, silicate rock, sand, argillite and aleurolite (Neumann, 2007). A 50 to 70 m thick layer of low diagenized, carbonaceous rocks overlies the base. The upper part is formed by Pliocene-Quaternary unconsolidated rocks and is 50 to 60 m thick. Within the unconsolidated rocks are water-bearing layers of medium to coarse sand. These have a thickness of 40 to 50 m and are covered by a 5 to 7 m thick clay layer. Solid material analysis identified siderite ($FeCO_3$) as dominant carbonate mineral. This is probably "contaminated" with Mn and Ca and has the approximate composition $(Ca_{0.15}Mn_{0.08}Fe_{0.77})CO_3$ (Bilek, 2016). Rhodochrosite ($MnCO_3$) was not found as pure mineral. In addition, pyrite (FeS_2) was not found in noticeable amounts within the aquifer (Neumann, 2007). The pristine groundwater contains 26 ± 3 mg/l Fe, 1 to 3 mg/l Mn and has a low pH of 5.9 (Table 1). It also has a low to medium high buffer capacity with 150 to 165 mg/l bicarbonate and a high CO_2 concentration (155 to 215 mg/l).

To control elevated Fe concentrations in the pristine groundwater, SIR (Subterra technique) is applied as a pre-treatment step (Kulakov et al., 2011; Kulakov, 2013; Herlitzius et al., 2012; Herlitzius, 2015; Braun et al., 2016). All production wells (PW) alternately serve as infiltration and extraction wells. The efficiency coefficient assesses the effectiveness of the process and reflects the ratio of extracted water volume (V_{extr}) to (re-)infiltrated water volume (V_{inf}). Depending on the aquifer and raw water conditions the efficiency coefficient can reach values between 2 and 12 (Rott et al., 2002). This study focuses on one particular PW, where a strong release of Mn was observed already at an efficiency coefficient of 3. The PW was equipped with three observation wells (OW), which were located 6 m (OW 1), 12 m (OW 2) and 18 m (OW 3) apart from the well. The PW had a casing diameter of 0.35 m, a 0.1-m-thick filter gravel pack and a filter screen height of 5 m. The infiltration time was 48 h at an infiltration rate of 80 m^3/h (Fig. 2). Pretreated groundwater (aerated, chlorinated) from previous extraction phases served as infiltrate. To increase the treatment capacity, the infiltrate was enriched by technical oxygen up to a dissolved oxygen concentration of ≈25 mg/l. Extraction time was initially 48 h and increased after up to 72 h at a rate of 160 m^3/h. After 165 completed SIR cycles (450 days, observation period 1) with continuous operation the PW was shut down due to operational issues (Fig. 2). Following a 100 days lasting rest period the PW was restarted and further monitored for another 27 SIR cycles (observation period 2). Additional column experiments were conducted during observation period 2.

2.2. Regular monitoring

During infiltration phases, relevant water samples for this study were taken after total infiltrated volumes of 200, 2000 and 3840 m^3. Sampling during extraction phases was conducted after total extracted volumes of initially 100, 1000 and 4000 m^3 (48 h extraction) as well as after 8840 and 11,520 m^3 at 72 h extraction. Temperature (T), dissolved oxygen (O_2), pH and electrical conductivity (EC) were determined using a WTW Multi 3430 and appropriate electrodes (WTW, Weilheim, Germany) in a flow-through cell during water sampling.

2.3. Calculation of saturation indices and alkalinity

Because the infiltrate at the PW has roughly pH 8, precipitation of Mn as its divalent carbonate mineral rhodochrosite ($MnCO_3$) could occur (Mettler et al., 2001). To check saturation of Mn^{2+} with respect to $MnCO_3$ (Eq. (1), Table 2), saturation indices (SI) for rhodochrosite were determined with PHREEQC (Parkhurst and Appelo, 2013). Because solid material analysis identified $FeCO_3$ as dominant carbonate mineral, SI were determined for siderite, too (Eq. (2.1), Table 2). Since the equilibrium constant of the mineral actually present in Khabarovsk is unknown, Eq. (2.2) was not used for saturation calculations. SI were calculated for all observation points after infiltrated volumes of 200 m^3 (start) and 3840 m^3 (end) as well as after extracted volumes

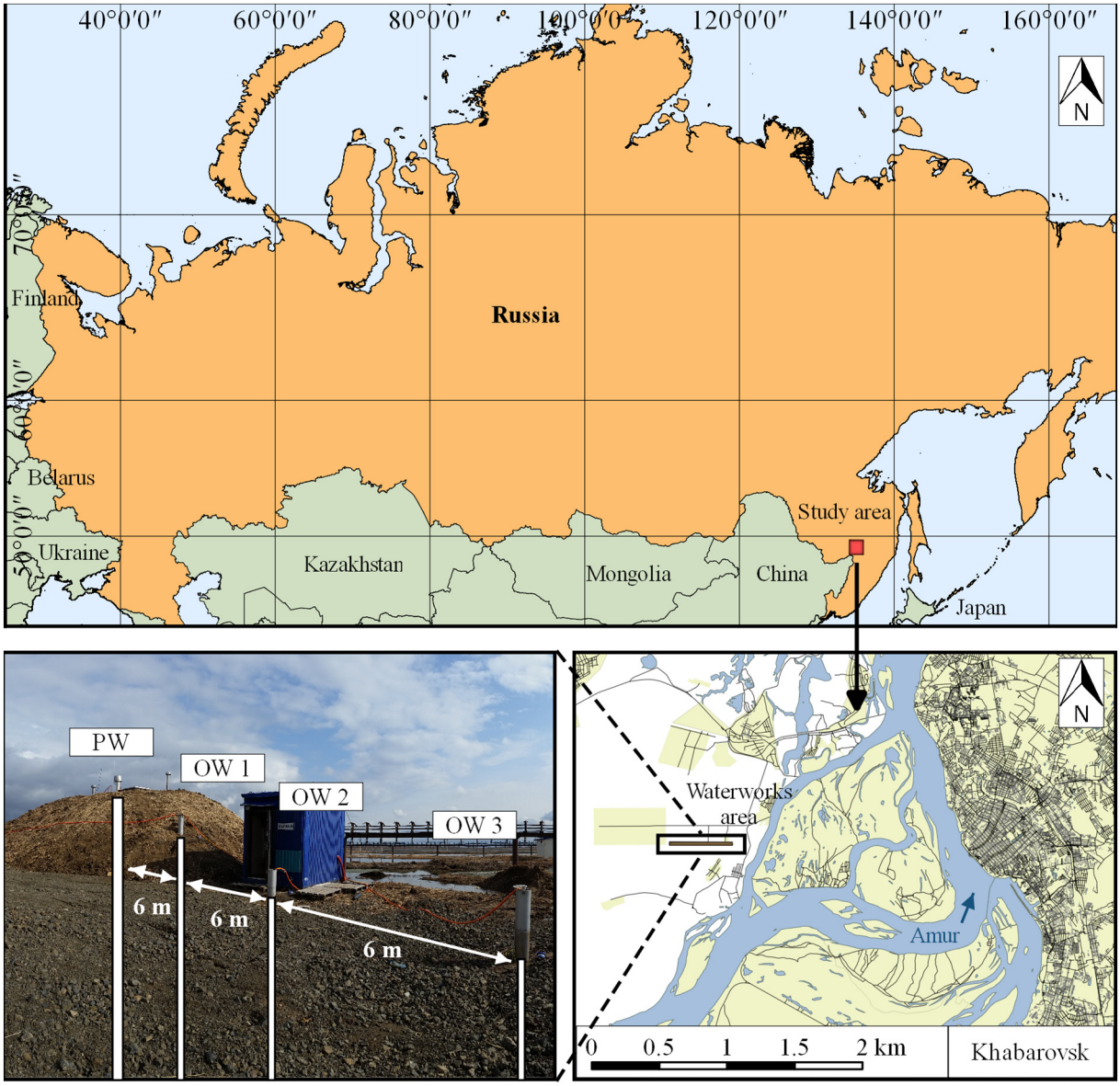

Fig. 1. Location of the study area.

of 100 (start), 1000, 4000 and 11,520 m^3 (end). Input values were median values for each observation point and the related volume during the entire observation period. Because calcium (Ca) was not measured during regular monitoring, the relation of Ca to the total hardness (1°dH = 7.15 mg/l Ca, Worch, 2015) was used to calculate Ca for the input data set. Subsequently, the total concentration of relevant Mn (II) species in equilibrium with $MnCO_3$ (SI = 0) was calculated after Eq. (1), as described by von Rohr et al. (2014).

Because alkalinity was determined only irregularly during monitoring by alkalimetric titration, the measured total hardness served as basis for an estimation of alkalinity within the aquifer zone by assuming a linear relationship between total hardness and alkalinity. This assumption implied that the measured carbonate hardness was nearly equal to total hardness (Worch, 2015).

2.4. Column experiments

To simulate the aquifer zone from OW 1 to the PW, two columns (column SI & SII) with aquifer material were set up in a container near to a PW (Fig. S1). The columns run according to the infiltration (48 h) and extraction phases (72 h) of the PW after the well was shut down for 100 d (second observation period, Fig. 2). Two diaphragm pumps (delta opto-drive, ProMinent, Heidelberg, Germany) pumped infiltrate from the PW (infiltration phases) or groundwater (GW, extraction

Table 1
Water quality of the pristine groundwater from the Tungusska reservoir.

Temp. °C	O_2 mg/l	pH	EC µS/cm	HCO_3^- mg/l	CO_2 mg/l	Fe^{2+} mg/l	Mn mg/l	NH_4^+ mg/l	SO_4^{2-} mg/l	NO_3^- mg/l	Hardness °dH
6	0–1	5.9	230	150–165	155–215	23–29	1–3	0.4–0.7	3–12	0.3–1.1	2–3

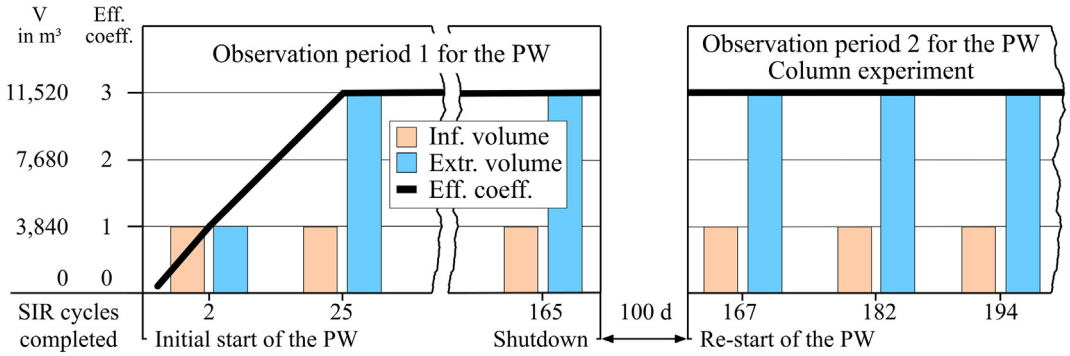

Fig. 2. Timeline of the study period. One completed SIR phase is equal to one infiltration phase and the subsequent extraction phase.

phases) from OW 1 into the columns. Flow direction in all columns was from bottom to top during infiltration and vice versa during extraction. To emulate different pumping rates during infiltration and extraction at the PW, flow rates through the columns were adjusted to 80 and 110 ml/min for infiltration and extraction. Both flow rates resulted in pore velocities of 5 to 8×10^{-4} m/s corresponding to estimated pore velocities in the aquifer at a distance of 10 to 4 m apart from the PW. Since the OW 1 was drilled at the inner edge of the reaction zone of the PW, actual SIR processes were assumed to be completed and thus not simulated in the columns.

During extraction, Mn was measured before the columns and at sampling ports at 0.05 m and subsequently every 0.5 m along the columns (Fig. S1). For subsequent lab analysis (see below), 10 ml water samples were taken after random time intervals but from all sampling ports on one sampling event. Temperature (T), O_2, pH and EC were determined using a WTW Multi 3430 and appropriate electrodes (WTW, Weilheim, Germany) in flow-through cells before and after the columns. Pressure was measured with digital pressure gauges (DM 01, BD Sensors, Germany). An inductive flow meter (IFM, MAG 5000, Siemens, Germany) was installed for flow measurements after the columns.

Each column had an inner diameter of 0.1 m, a length of 2 m and was made up of opaque PVC. Aquifer material for filling was obtained from a core drilling outside of the reaction zone of the PW. Only material from the depths of the actual filter screen position of the PW was used as filling material and sieved to a grain size <4 mm before filling. During filling of the columns, the sediment mass was measured using a balance to calculate the bulk density and assess the compaction of the material in the columns. Mean travel time (t_a) and porosity (n_e) for both columns were determined from EC breakthrough curves from tracer experiments with NaCl performed before start-up. Flow rate and head loss were taken to calculate hydraulic conductivity by applying Darcy's law.

2.5. Manganese leaching

2.5.1. Closed-bottle batch test

To further assess the dissolution of siderite-rich minerals as potential source for Mn during the extraction phases, a closed-bottle batch test with the aquifer sediments used in the column experiments was conducted. In order to reproduce the actual aquifer conditions as realistically as possible, the batch tests were conducted with groundwater from OW 1, taken during an extraction phase. Material with a grain size of <4 mm or <0.063 mm was filled into glass-stoppered conical flasks and mixed with water adjusted to pH 5, 6 or 6.9 (Table S1). Mixing water for samples 1, 2, 5 and 6 with pH 6 represented the lowest observed pH within the actual reaction zone. Sample 9 with pH 6.9 represented conditions at OW 1 during the column experiments, after switching from infiltration to extraction in which no Mn was released. Samples 3, 4, 7 and 8 with pH 5 were used to evaluate the impact of a further possible pH drop. The pH of the mixing water was adjusted with hydrochloric acid (HCl). For airtight sealing of the flasks, water was slightly overflowing when the ground-glass stoppers were plugged in. All flasks were hand-shaken before storage. Samples were stored for 24 h. Storage temperature was 15 to 20 °C and the flasks were protected from incident light. After 24 h storage, 10 ml water samples were taken from every bottle and analyzed in the lab for major anions and cations (see below).

2.5.2. Flow-through test

Based on the results of the batch test, a third, 0.5 m long column (SIII) was filled with aquifer material (<4 mm) and continuously fed with groundwater from OW 1. Iron-free, low manganese-containing and almost oxygen-free groundwater (<0.8 mg/l O_2) of the OW 1 was filled into a tub and pumped through column SIII. The pH of the feed water was adjusted to pH 5 with HCl. Temperature, O_2, pH and EC were determined using a WTW Multi 3430 and appropriate electrodes (WTW, Weilheim, Germany) in the tub and a flow-through cell after the column. During the test, Mn after column SIII was measured after 15, 30, 45, 60 and subsequently every 30 min until the Mn concentration plateaued. For subsequent lab analysis (see below), 10 ml water samples were taken accordingly.

2.6. Sediments analysis

To assess the mineralogical structure and to estimate mobilization behavior of Fe and Mn, a 4-step sequential extraction procedure was

Table 2
Chemical reactions considered to explain the observed Mn release.

$MnCO_3 \rightleftharpoons Mn^{2+} + CO_3^{2-}$ with $\log k = -10.39$ (Stumm and Morgan, 1996)	(1)
$FeCO_3 \rightleftharpoons Fe^{2+} + CO_3^{2-}$ with $\log k = -10.89$ (Stumm and Morgan, 1996)	(2.1)
$(Ca_{0.15}Mn_{0.08}Fe_{0.77})CO_3 \rightleftharpoons 0.08Ca^{2+} + 0.08Mn^{2+} + 0.84Fe^{2+} + CO_3^{2-}$	(2.2)
$4Fe^{2+} + 10H_2O + O_2 \rightarrow 4Fe(OH)_3 + 8H^+$	(3)
$CO_2 + H_2O \rightleftharpoons HCO_3^- + H^+$	(4)
$(1-x)O_2 + 4Fe_{(1-x)}Mn_xCO_3 + (6-2x)H_2O \rightarrow (4-4x)Fe(OH)_3 + 4xMn^{2+} + (4-8x)CO_2 + 8xHCO_3^-$	(5)
$FeS_2 + 4HCO_3^- + 3.75O_2 \rightarrow Fe(OH)_3 + 2SO_4^{2-} + 4CO_2 + 0.5H_2O$	(6)
$MnO_2 + 2Fe^{2+} + 4H_2O \longrightarrow Mn^{2+} + 2Fe(OH)_3 + 2H^+$	(7)

applied to the filling material of columns SI & SII (Table S2). The filling material was analyzed before and after the experiment. Thus, results represent the natural and the potentially operationally altered material composition. Details regarding the procedure are described in Rauret et al. (1999) and Sutherland and Tack (2002). Samples were taken after 0.05, 0.10, 0.25, 0.50, 0.75, 1.0, 1.5 and 2.0 m along the columns. The material was recovered by a rinsed scoop, immediately filled into sterile sample containers and stored at 4 °C before analysis.

2.7. Water analysis

Water quality during regular monitoring of the PW in Khabarovsk was assessed with Macherey-Nagel Visocolor® Eco Test Kits (Macherey-Nagel, Omnilab GmbH & Co. KG, Bremen, Germany). Manganese along the column SI & SII during the experiment was determined with Merck MColortest® (Merck KGaA, Darmstadt, Germany). Additional water samples for subsequent lab analysis (10 ml) were filtered on-site through 0.45 μm membrane filters. Major cations K^+, Na^+, Ca^{2+}, Mg^{2+} and dissolved metals such as Fe, Mn, Ba, Sr and Si were measured with ICP-OES (Optima 4300 DV, Perkin Elmer, Waltham, MA, USA). Anions such as Br^-, Cl^-, F^-, NO_2^-, NO_3^-, PO_4^{3-} and SO_4^{2-} were determined with ion-chromatography (autosampler AS50, eluent generator EG50, gradient pump GP50, electrochemical detector ED50, separation column AS19, all from Dionex) at the Institute for Water Chemistry, TU Dresden, Germany.

3. Results

3.1. Formation of the reaction zone and onset of iron removal

3.1.1. Changes in oxygen and iron concentrations during infiltration

After 2 complete SIR cycles (1 cycle = infiltration followed by extraction), the O_2 concentration at the end of the infiltration phases (infiltrated volume, V_{inf} 3840 m^3) at OW 1 at a distance of 6 m from the PW increased up to 19 mg/l (Fig. 3). At OW 2 (12 m distance) around 5 mg/l O_2 were measured, and traces of O_2 were measured at OW 3, which is around 18 m apart from the PW. Within 25 SIR cycles, the O_2 concentration after V_{inf} of 3840 m^3 at OW 1 reached the concentration of the PW and at OW 2 around 20 mg/l O_2 were measured. At OW 3 O_2 increased up to ≈1 mg/l. Before the PW was shut down after 165 SIR cycles, O_2 at the end of the infiltration phases at OW 2 and OW 3 further increased up to 22 mg/l and 6 mg/l respectively. After the shutdown, the O_2 concentration during the first infiltration phases still reached OW 3 (V_{inf} 3840 m^3) with around 9.6 mg/l. During further operation the spatial and temporal O_2 distribution did not change noticeably and reached around 4 mg/l at OW 3.

The Fe concentration during the infiltration phase of the second SIR cycle increased from 0 mg/l at the PW to around 10 mg/l at OW 3 (Fig. S2). During further operation Fe was only detectable along the aquifer zone from OW 2 to 3. The development of the pH during the infiltration phases qualitatively reflects the development of the O_2 concentration (Fig. S3). The high pH of the infiltrate led progressively to an elevated pH at OW 1 and OW 2. At OW 3 no noticeably change in pH was measured. Hardness during infiltration decreased within the first 2 SIR cycles from above 2.5°dH at the PW to <1°dH at OW 3 (Fig. S5). During further operation, hardness was generally slightly increased along the entire aquifer zone but still decreased from the PW to OW 3.

3.1.2. Changes in iron concentration, pH during extraction

During the first 2 SIR cycles around 0.1 mg/l Fe was measured at OW 1 at the end of the extraction phase and no Fe reached the PW (Fig. S6). At the initial start-up the extracted volume was approximately equal to the infiltrated volume and increased within 25 SIR cycles to 3-times of the infiltrated volume (efficiency coefficient 3, Fig. 2). After 25 complete SIR cycles and at an extracted volume of 11,520 m^3 the Fe concentration was around 0.3 mg/l at OW 2 and <0.01 mg/l at OW 1. After the shutdown (167 SIR cycles, observation period 2) the Fe concentration reached 0.4 to 0.8 mg/l at OW 2, around 0.1 mg/l at OW 1 and was always 0 mg/l at the PW until the end of the extraction phases. The pH during the extraction phases decreased at all observation wells and the PW and showed no obvious spatial patterns (Fig. S7). After shutdown of the PW no noticeable change of the pH pattern was measured. Total hardness did generally increase along the flow path from OW 3 towards the PW (Fig. S9). With ongoing operation time hardness at OW 3 increased to >1°dH at the beginning of extraction to around 2.5°dH at

SIR cycles	V_{inf} in m^3	PW	← 6 m →		OW 1	← 6 m →		OW 2	← 6 m →		OW 3
2	200	25.7	18.1	10.5	3.0	2.0	1.0	0.0	0.0	0.0	0.0
	2,000	23.6	19.6	15.7	11.7	9.5	7.2	5.0	3.4	1.7	0.1
	3,840	26.0	23.7	21.3	19.0	13.6	8.2	2.8	1.9	0.9	0.0
25	200	25.0	18.0	10.9	3.9	2.6	1.3	0.1	0.1	0.1	0.1
	2,000	25.3	24.9	24.4	24.0	21.5	18.9	16.4	11.0	5.6	0.2
	3,840	24.0	24.4	24.8	25.2	23.3	21.5	19.6	13.3	7.1	0.8
165	200	25.7	18.8	11.8	4.9	3.2	1.6	0.0	0.0	0.0	0.0
	2,000	24.4	24.0	23.6	23.2	22.4	21.6	20.8	15.4	10.0	4.7
	3,840	24.3	23.9	23.5	23.2	22.7	22.3	21.8	16.6	11.4	6.2
167	200	27.2	21.8	16.4	11.1	8.4	5.8	3.2	3.0	2.8	2.6
	2,000	26.2	25.3	24.5	23.6	23.6	23.6	23.7	17.6	11.5	5.5
	3,840	31.5	30.0	28.6	27.1	26.9	26.7	26.5	20.9	15.2	9.6
182	200	21.1	18.3	15.6	12.8	8.8	4.7	0.7	0.5	0.3	0.2
	2,000	21.0	20.8	20.7	20.5	19.4	18.2	17.1	11.6	6.0	0.5
	3,840	24.9	23.8	22.7	21.6	20.8	20.0	19.2	14.0	8.8	3.6
194	200	22.8	20.1	17.3	14.6	9.9	5.3	0.7	0.5	0.3	0.0
	2,000	21.9	21.6	21.4	21.1	19.8	18.6	17.3	11.8	6.3	0.8
	3,840	22.1	22.0	21.9	21.8	20.9	20.0	19.1	14.0	8.9	3.9

Fig. 3. Median O_2 concentration in mg/l during infiltration between the PW and OW 3, diagonal lines mark the 100 d shutdown and split observation period 1 & 2 (see Fig. 2), intermediate values are calculated by linear interpolation (see Table S3 for number of samples).

SIR cycles	V_{inf} in m³	PW	← 6 m →		OW 1	← 6 m →		OW 2	← 6 m →		OW 3
2	200	0.4	0.4	0.3	0.3						
	2,000	0.4	0.3	0.3	0.3	0.3	0.3	0.3	0.3	0.3	0.4
	3,840	0.5	0.4	0.4	0.3	0.3	0.3	0.3	0.3	0.3	0.3
25	200	0.2	0.5	0.9	1.2						
	2,000	0.1	0.3	0.4	0.6	0.6	0.5	0.5	0.5	0.6	0.7
	3,840	0.1	0.3	0.5	0.7	0.6	0.6	0.5	0.5	0.4	0.4
165	200	0.0	0.4	0.7	1.1	1.0	1.0	0.9	0.8	0.8	0.7
	2,000	0.1	0.3	0.4	0.6	0.6	0.6	0.6	0.6	0.6	0.6
	3,840	0.1	0.2	0.4	0.5	0.6	0.6	0.6	0.6	0.5	0.5
167	200	0.1	0.3	0.6	0.9	0.9	0.9	1.0	0.9	0.8	0.8
	2,000	0.1	0.2	0.4	0.5	0.5	0.4	0.4	0.5	0.5	0.6
	3,840	0.1	0.2	0.4	0.5	0.5	0.4	0.4	0.4	0.4	0.4
182	200	0.1	0.2	0.4	0.6	0.7	0.9	1.0	0.9	0.8	0.7
	2,000	0.1	0.2	0.3	0.4	0.4	0.4	0.4	0.5	0.5	0.6
	3,840	0.1	0.2	0.3	0.4	0.4	0.4	0.4	0.5	0.6	0.8
194	200	0.1	0.3	0.4	0.6	0.7	0.9	1.0	0.9	0.8	0.8
	2,000	0.1	0.2	0.3	0.4	0.4	0.3	0.3	0.4	0.6	0.7
	3,840	0.1	0.2	0.3	0.4	0.4	0.4	0.4	0.5	0.5	0.6

Fig. 4. Median Mn concentration in mg/l during infiltration between the PW and OW 3, diagonal lines mark the 100 d shutdown and split observation period 1 & 2 (see Fig. 2), intermediate values are calculated by linear interpolation (see Table S3 for number of samples).

the end of extraction. Towards the PW, hardness increased further to approx. 4°dH.

3.2. Behavior of manganese along the aquifer zone between the PW and OW 3

3.2.1. Manganese release during infiltration

During the first infiltration phases the Mn concentration remained almost constant ≈0.4 mg/l (Fig. 4). With ongoing operation Mn increased along the flow path from the PW to OW 1 and decreased towards OW 3 (25 up to 165 SIR cycles). The peak at OW 1 flattened over the time period of each infiltration phase. After shutdown and 167 SIR cycles the Mn peak had shifted in the direction of OW 2.

3.2.2. Manganese release during extraction

During the extraction phases of the first two SIR cycles the Mn concentration was max. 0.8 mg/l at all observation points and in the order of magnitude of the pristine groundwater (Fig. 5). In order to maximally extend the reaction zone at the PW, around 9000 m^3 oxygen-enriched water was infiltrated and only 1000 m^3 extracted at the first SIR cycle (efficiency coefficient 0.1). At the second SIR cycle the efficiency coefficient was lifted to 1 and within 25 SIR cycles to 3. Within the same time period of 25 SIR cycles the Mn concentration increased along the flow path from 0.8 mg/l at OW 3 to max. 1.7 mg/l at the PW (extracted volume, V_{extr} 11,520 m^3), which was almost as double as the background value of the pristine groundwater (Fig. 6).

After 165 completed SIR cycles with continuous operation the Mn concentration still increased at the PW to max. 1.2 mg/l. After shutdown and 167 SIR cycles the spatial and temporal distribution of Mn did not change. With increasing operation time after shutdown (182 SIR cycles) the Mn concentration decreased at the end of the extraction phases. After 194 completed SIR cycles the Mn concentration increased along the flow path from ≈0.8 mg/l at OW 3 to just 1.1 mg/l at the PW.

3.3. Saturation indices and alkalinity

Because alkalinity was determined irregularly during monitoring, the measured total hardness was used to estimate alkalinity within the aquifer zone (Fig. S10). During the observation period alkalinity was determined 65-times by titration immediately after sampling. The comparison of the lab-determined total hardness and the titrated alkalinity resulted in a medium high linear correlation with $R^2 = 0.5$. Nonetheless, the resulting relation of alkalinity (mg/l) = 37.81 × total hardness (°dH) + 27.91 was applied to estimate alkalinity along the aquifer zone (Figs. S11 & S12).

Sampled water during infiltration as well as during extraction from the PW and all three OW's was always undersaturated with respect to $MnCO_3$ (SI $MnCO_3 < 0$, Fig. S15). At OW 1 and 2 the SI $MnCO_3$ increased slightly to maximally −0.36 during infiltration, whereas SI $MnCO_3$ at OW 3 remained almost constant at -1.5 ± 0.2. In addition, all water samples were also undersaturated with respect to siderite (SI $FeCO_3 <$ 0, Fig. S16). SI $FeCO_3$ remained at all observation points relatively

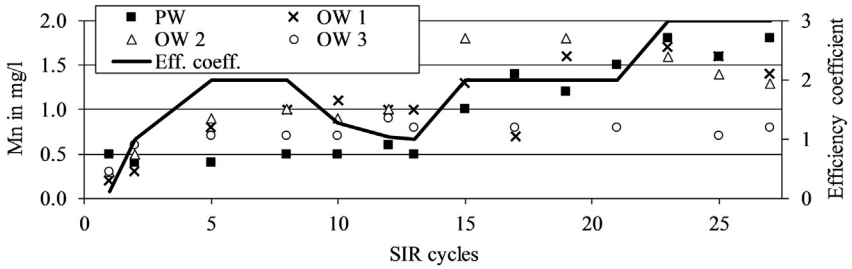

Fig. 5. Measured Mn concentration at the end of extraction and efficiency coefficients for the PW within the first 65 days of operation.

SIR cycles	V_{extr} in m³	PW	← 6 m →		OW 1	← 6 m →		OW 2	← 6 m →		OW 3
2	100	0.5	0.4	0.4	0.3	0.3	0.4	0.4	0.4	0.4	0.4
	1,000	0.5	0.4	0.3	0.3	0.3	0.3	0.3	0.4	0.5	0.6
	4,000	0.4	0.3	0.3	0.2	0.3	0.3	0.4	0.4	0.5	0.5
25	100	0.1	0.2	0.4	0.5	0.5	0.5	0.5	0.5	0.6	0.6
	1,000	0.2	0.3	0.4	0.5	0.5	0.6	0.6	0.7	0.7	0.8
	4,000	0.6	0.7	0.8	0.9	1.0	1.1	1.2	1.1	1.0	0.9
	8,840	1.7	1.7	1.7	1.7	1.7	1.7	1.7	1.4	1.1	0.8
	11,520	1.7	1.7	1.7	1.7	1.7	1.6	1.6	1.3	1.0	0.8
165	100	0.0	0.2	0.3	0.5	0.5	0.5	0.5	0.5	0.5	0.5
	1,000	0.0	0.2	0.4	0.6	0.6	0.6	0.6	0.6	0.6	0.6
	4,000	0.5	0.6	0.6	0.7	0.7	0.6	0.6	0.6	0.7	0.7
	8,840	1.1	1.0	1.0	0.9	0.9	0.9	0.9	0.9	0.8	0.8
	11,520	1.2	1.1	1.1	1.0	1.0	1.0	1.0	0.9	0.9	0.8
167	100	0.1	0.2	0.4	0.5	0.5	0.5	0.5	0.6	0.6	0.7
	1,000	0.5	0.5	0.5	0.5	0.5	0.4	0.4	0.5	0.5	0.6
	4,000	0.4	0.4	0.5	0.5	0.5	0.4	0.4	0.5	0.6	0.7
	8,840	0.8	0.8	0.8	0.8	0.8	0.8	0.8	0.8	0.8	0.8
	11,520	1.2	1.0	0.9	0.8	0.8	0.8	0.8	0.8	0.7	0.7
182	100	0.1	0.2	0.3	0.5	0.4	0.4	0.4	0.5	0.5	0.6
	1,000	0.5	0.5	0.4	0.4	0.4	0.4	0.4	0.5	0.6	0.7
	4,000	0.4	0.4	0.4	0.4	0.4	0.4	0.4	0.5	0.6	0.7
	8,840	0.8	0.8	0.8	0.8	0.8	0.7	0.7	0.7	0.8	0.8
	11,520	1.1	1.0	0.9	0.8	0.8	0.8	0.8	0.8	0.8	0.9
194	100	0.0	0.2	0.3	0.4	0.4	0.4	0.3	0.4	0.6	0.7
	1,000	0.1	0.2	0.3	0.5	0.4	0.4	0.3	0.4	0.4	0.5
	4,000										
	8,840										
	11,520	1.1	1.0	0.9	0.9	0.9	0.9	0.9	0.9	0.8	0.8

Fig. 6. Median Mn concentration in mg/l during extraction between the PW and OW 3, diagonal lines mark the 100 d shutdown and split observation period 1 & 2 (see Fig. 2), intermediate values are calculated by linear interpolation (see Table S3 for number of samples).

constant during infiltration and extraction. With SI $FeCO_3$ −0.45 ± 0.2 water from OW 3 showed noticeably higher SI $FeCO_3$ than samples from the PW, OW 1 and 3 (SI $FeCO_3 < -2$).

In order to check saturation of Mn^{2+} with respect to $MnCO_3$, the equilibrium concentration of Mn^{2+} with $MnCO_3$ was calculated for all observation points for infiltrated volumes of 200 and 3840 m^3 (Table S4). At the PW the equilibrium Mn concentration was calculated to 0.84 mg/l at the beginning of infiltration and 0.87 mg/l for the conditions at the end of infiltration. The equilibrium concentrations at OW 1 were 3.89 and 0.94 mg/l after 200 m^3 and 3840 m^3, respectively. Comparison of the calculated equilibrium concentrations with Fig. 4 shows, that the equilibrium concentration during infiltration was never exceeded at any observation point and observation time.

3.4. Manganese leaching at lower pH

A closed-bottle batch test with the material that was used in the column experiments aimed to assess the dissolution of siderite-rich minerals as potential source for Mn during the extraction phases. The water contained 0.77 mg/l Mn. Fig. 7 shows that at pH 6.9 (pH at the beginning of the extraction phase) approx. 0.3 mg/l Mn could be released from the sediment. At pH 6, the material released around 0.5 mg/l Mn. Mn release at pH 6 from sediment with higher portion of fine material (<0.063 mm) was ≈2 mg/l and more than twice as high as the Mn concentration of 0.77 mg/l in the water. Further reduction of the pH resulted in a Mn release >3.5 mg/l from the fines (<0.063 mm). The release from the grain fraction <4 mm remained largely unaffected by the lower pH value at about 1.7 mg/l. Ca^{2+}, K^+ and SO_4^{2-} increased similarly to Mn and no release of Fe^{2+} was observed when the pH was lowered.

After the batch tests indicated a potential release of Mn from the sediment, a 0.5 m long column (SIII) was filled with aquifer sediment (<4 mm) and continuously fed with groundwater from OW 1 adjusted to pH 5. Mn concentration started to increase after 1.5 pore volumes (PV, Fig. 8). After 9 PV the experiment indicated a plateau at 1.7 mg/l Mn and after five consecutive measurements of 1.7 mg/l the experiment was stopped. The lab analysis revealed that the Mn concentration increased to 1.99 mg/l, even after 14 PV. No other observed element

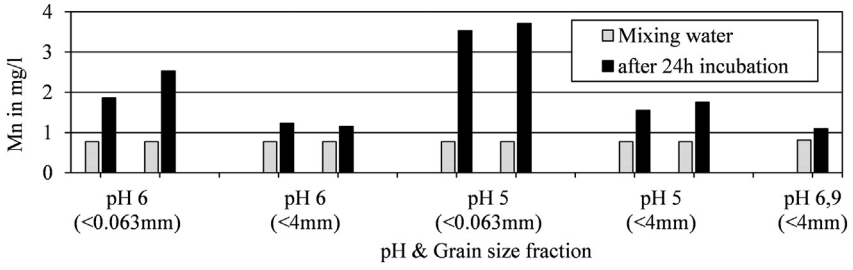

Fig. 7. Measured Mn concentration after 24 h depending on the grain size of the sediment material and the pH of the water.

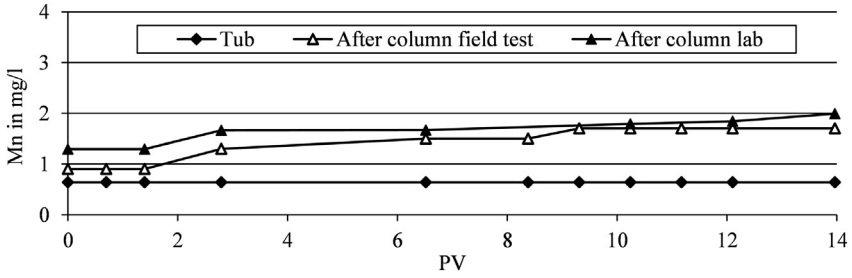

Fig. 8. Development of Mn concentration (field test and lab analysis) after the 0.5 m column SIII with aquifer material (<4 mm) during the leaching test with inflow water at pH 5.

concentration changed during the experiment (Table S6). After 7 PV the pH was equal to the inflow value of pH 5 and decreased further to pH 4.8 after 14 PV. EC remained almost constant at ≈200 μS/cm during the experiment. O_2 in the tub never exceeded 1.5 mg/l and increased from 0 to around 1.3 mg/l O_2 in the outflow of SIII (Table S6).

3.5. Simulation of the aquifer zone OW 1-PW in the column experiment

Two independently operated columns filled with aquifer material were set up in the SIR waterworks in Khabarovsk to emulate the aquifer zone from OW 1 to the PW (column SI & SII). Both columns run parallel and showed similar hydraulic properties and results (Table S7). During the extraction phases the median Mn concentration in the inflow water was 0.8 mg/l (Table S8). Since both columns were fed by groundwater from OW 1, the increase from 0.2 to 0.8 mg/l Mn over the time period of one extraction phase at OW 1 was also visible at the columns. Along the flow path of column SI from P5 to P1 the Mn concentration increased to around 0.9 mg/l and always remained below 1 mg/l (Fig. S17). The Mn concentration along SII behaved similarly (Fig. S18). Other observed elements did not show noticeably concentration changes along the columns.

After the column experiment was finished, a 4-step sequential extraction procedure was applied to the recovered filling material. The original filling material had a total Mn content of 1506 mg/kg, from which 13% were bound to carbonates, 64% were easily reducible Mn, 22% belonged to the oxidizable, and 1% to the residual fraction (Fig. 9). Following the flow path along the columns during extraction, the Mn fraction bound to carbonates increased from around 5% at the inlet to the initial value of 13% at the outlet. The distribution of all other Mn fractions did not show noticeable patterns along the flow path. The total Mn content (sum of all fractions) at the inlets in both flow directions was 300–600 mg/kg and less than the initial value of 1506 mg/kg (Fig. 10). The total Mn content within the columns was 1000–1500 mg/kg and in the order of magnitude determined for the original material. The total Fe content of the original filling material was 11,794 mg/kg and distributed among 4% bound to carbonates and 71%, 18% and 6% belonging to the easily reducible, oxidizable and residual fraction, respectively (Fig. S19). Around 3–4% of Fe was bound to carbonates and showed no clear trend along both columns. The total Fe content (sum of all fractions) at the inlets was 1000–5000 mg/kg in both flow directions and less than the initial value (Fig. S20). Along both columns the total Fe content was around 7500–13,500 mg/kg and in the order of magnitude for the original filling material.

4. Discussion

4.1. Formation of the reaction zone within 25 SIR cycles

Results of the regular monitoring showed that after two infiltration phases, dissolved oxygen was pushed beyond OW 2 and traces were measurable at OW 3 (Fig. 3). After 25 SIR cycles around 80% of the infiltrated O_2 reached OW 2 (19.6 mg/l) at the end of infiltration. This resulted in rapid development of the reaction zone for Fe and within 25 SIR cycles no more Fe^{2+} entered the zone from OW 1 to the PW (Fig. S6). Furthermore, almost 99% of ≈20 mg/l Fe in the groundwater was removed between OW 3 and OW 2. The rapid establishment of Fe removal in Khabarovsk confirms observations from other SIR plants, where Fe removal began following just the first infiltration phase (Rott et al., 2002; Roessner et al., 2017).

The median values for pH (Fig. S3) during infiltration reflected the extent of O_2 penetration into the aquifer. The oxidation of the adsorbed Fe^{2+} could explain the decreasing pH along the infiltration flow path. The oxidation of Fe^{2+} by O_2 causes the release of H^+ ions (Eq. (3), Table 2) and a decreasing HCO_3^- concentration (buffering, Eq. (4), Table 2). The median EC values during infiltration (Fig. S4) show the moving oxidation zone of Fe^{2+}, which adsorbed during the previous extraction phase. Considering the pH buffering by HCO_3^- (Eq. (4), Table 2) and a molar limiting conductivity of 44.3 S/cm^2/mol for HCO_3^- (Aqion, 2018), e.g. the loss of 50 mg/l HCO_3^- (Fig. S11) between OW 1 to 2 at the end of the second SIR cycle would cause an EC drop of 35 μS/cm. Both O_2 and the calculated HCO_3^- were only weakly linearly correlated to the EC (R^2 = 0.1–0.2), but both scatter plots indicated a dependency (Figs. S13 & S14). Thus, the oxidation of adsorbed Fe^{2+} can mostly explain the change in location of the minimum EC value from OW 1 after starting the infiltration towards OW 3 at the end of an infiltration phase.

The median values for EC (Fig. S8) during extraction underlined that most of the Fe was removed between OW 3 and 2. During extraction,

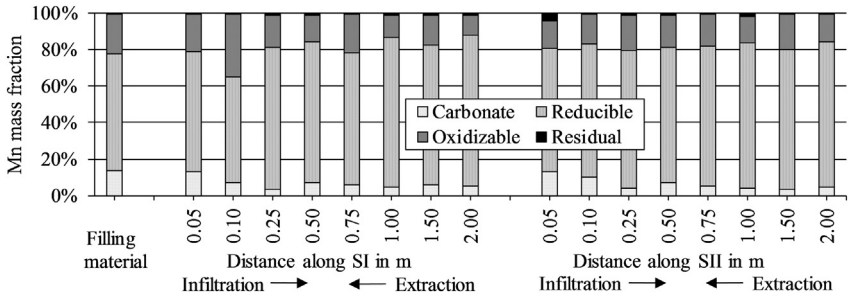

Fig. 9. Distribution of the Mn fractions along column SI & SII compared to the original filling material.

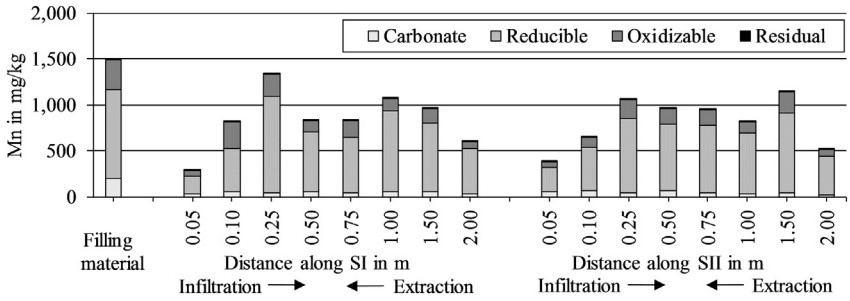

Fig. 10. Sum of the Mn fractions along column SI & SII compared to the original filling material.

around 20 mg/l Fe^{2+} (Fig. S6) were removed between OW 3 and 2. Considering a molar limiting conductivity of 108 S/cm²/mol for Fe^{2+} (Aqion, 2018), this would explain an EC drop of around 40 μS/cm, which is roughly in the observed order of magnitude. Taking the spatial and temporal distribution of O_2, pH and EC values into account, the reaction zone for Fe^{2+} is most probably located in the aquifer zone between OW 1 and OW 3 and thus, in a radius of about 6 to 18 m from the PW.

4.2. Sources for continuous Mn release

4.2.1. Operating scheme

While Fe was successfully removed within a few infiltration and extraction phases, Mn passed through the reaction zone unhindered (Fig. 6). Fig. 5 suggests that after the efficiency coefficient permanently rose above 1 (≈6 SIR cycles), the Mn concentration started to increase at the PW, OW 1 and 2. After several months of operation, the efficiency coefficient was temporarily increased to 6 and no further increase of Mn was observed (data not shown). Rott et al. (2002) noted an onset of Mn removal within 5 SIR cycles, and after 23 SIR cycles the Mn in the groundwater (0.35 mg/l) was lowered to <0.1 mg/l. During a "crash-test", Mn was released at an efficiency coefficient of 2 and Mn concentrations exceeded the background value of the groundwater. Roessner et al. (2017) observed an onset of Mn removal from ≈0.3 mg/l Mn to below 0.05 mg/l after 11 months at one well, whereas almost 20 months passed before the same result was achieved at a second well at the same location. A temporary increase of the efficiency coefficient from 3 to 4 and 5 was responsible for a release of Mn above the groundwater background value. At the well field Boker Heide, >30 SIR cycles were required until 0.3 mg/l Mn were lowered to <0.05 mg/l (Rott et al., 2003). To remove 0.8 mg/l Mn at the same location, another well had to be continuously operated for 90 SIR cycles. Rott and Friedle (2000a, 2000b) name several examples for SIR plants where Mn removal started after five month continuous operation and where operation schemes with efficiency coefficients of up to 11 did not cause a release of Fe or Mn. Hence, the efficiency coefficient of the PW in Khabarovsk was raised relatively early, which in conjunction with the relatively short total operation time may account for the lack of Mn removal.

4.2.2. Dissolution of Mn-bearing carbonate minerals

Solid material analysis identified $FeCO_3$ as the dominant carbonate mineral within the aquifer in Khabarovsk, which also could have been a potential source for Mn. Fig. 4 shows a Mn release up to 1.2 mg/l Mn during infiltration phases. According to Antoniou et al. (2012) dissolved oxygen can potentially oxidize Mn-siderite, which releases Mn^{2+} (Eq. (5), Table 2). Figs. 3 and 4 show that maximum Mn concentrations were measured at OW 1 & 2 after the sediment came into contact with the oxygen from the infiltrate. Instead of an expected continuous increase in Mn concentration with increasing O_2 transport range, Mn decreased after the maximum was reached, which indicates that Mn release may have been limited by other factors.

At an Aquifer Storage and Recovery (ASR) site in Herten, the Netherlands, the dissolution of Mn-bearing carbonate minerals (Mn-siderite) led to increased Mn^{2+} concentrations during infiltration and extraction and was linked to pyrite (FeS_2) oxidation (Antoniou et al., 2012, 2014). The authors observed that the oxygen-rich injection water oxidized naturally occurring pyrite. The released acidity (H^+) during pyrite oxidation was buffered by Mn-bearing carbonate minerals and led to a release of Mn during infiltration (Eqs. (4) & (6), Table 2).

Since no pyrite was found in the aquifer in Khabarovsk and no increase in sulfate concentration was observed during column experiments, reaction mechanism (6) was excluded to be responsible for the Mn release during infiltration. Nevertheless, the dissolution of potentially existing (Mn-)carbonate minerals by dissolved oxygen could potentially contribute to the Mn release during infiltration. Fig. S15 shows that the saturation index was never above 0 during infiltration and extraction. In addition, the measured Mn concentrations along the aquifer zone (Fig. 4) never exceeded the calculated equilibrium concentrations (Table S4). Hence, a periodic $MnCO_3$ or $FeCO_3$ precipitation that is limiting Mn release during infiltration, followed by a dissolution of the fresh precipitates as a Mn source during extraction, is not plausible.

During extraction phases a high release of Mn up to 1.7 mg/l was observed, which is twice as high as the background value of the pristine groundwater (Fig. 4). Results of the regular monitoring showed a generally increasing hardness from OW 3 to the PW during extraction. Considering hardness as the sum of Ca^{2+}-equivalents (1°dH = 7.15 mg/l Ca^{2+}, Worch, 2015), and taking the proposed composition of $(Ca_{0.15}Mn_{0.08}Fe_{0.77})CO_3$ (Eq. (2.2), Bilek, 2016) for the carbonate mineral, the increasing hardness along the flow path from OW 3 to the PW corresponds to the release of Ca^{2+} during dissolution of this mineral. Moreover, all water samples were undersaturated (SI < 0) with respect to $MnCO_3$ (Fig. S15, Table 2) and $FeCO_3$ (Fig. S16) during extraction phases. Taking the increasing hardness (Fig. S9) and alkalinity (Fig. S12) into account, all observations pointing towards a dissolution of potentially Mn-bearing carbonate minerals along the flow path from OW 3 to the PW during extraction (Fig. 11).

The results of the closed-bottle batch tests and a column flow-through test (SIII) indicate that the Mn release from the aquifer material is highly dependent on the grain size and is mainly controlled by the pH. With increasing extraction time, the pH of the water at the PW and around OW 1 decreases to approximately pH 6. In particular, the grain size fraction <0.063 mm already released more Mn at pH 6 (>2 mg/l) than actually measured at the well field. Since smaller grain size fractions usually show the highest heavy metal contents (Mettler et al., 2001; van Halem et al., 2011), higher Mn release was expected from this fraction. The lowest measured pH in Khabarovsk was around pH 5.8, yet with longer operation time of the SIR wells, a further drop of the pH is possible (Bartak et al., 2017). With a hardness of approx. 2 to 3°dH and ≈150 mg/l HCO_3^- in the pristine groundwater, the SIR plant in Khabarovsk is probably more prone to a potentially decreasing pH than other sites (e.g. Rott et al., 2003).

The results of the column flow-through test confirmed the results of the batch tests. During the test, the Mn concentration measured by the

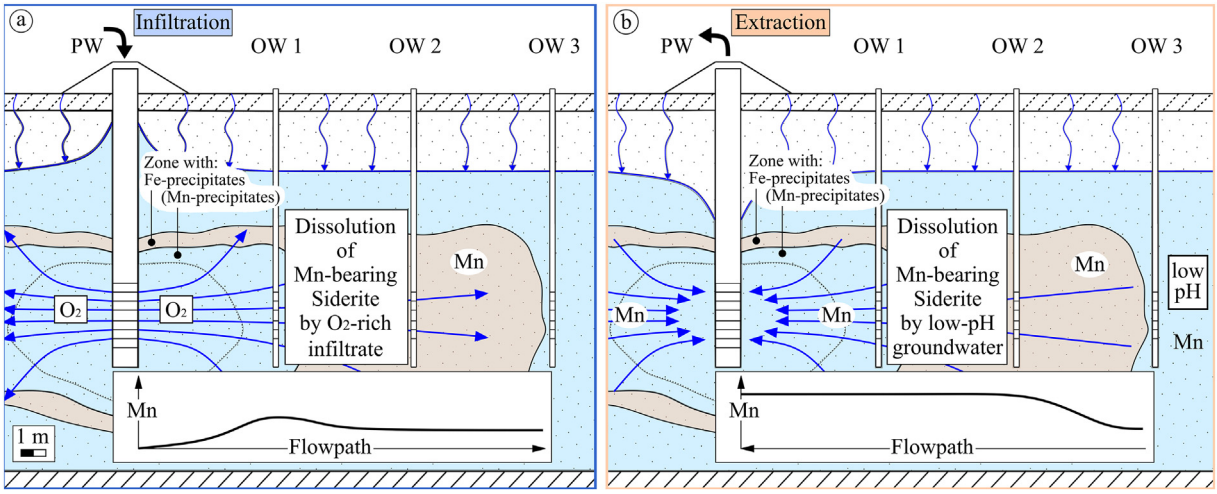

Fig. 11. Reaction mechanisms responsible for Mn release during infiltration (a) and extraction (b).

field test kit plateaued and the experiment was stopped after 5 subsequent samples showed the same results. The subsequent lab analysis revealed a still increasing Mn concentration. Thus, the determined Mn release of ≈2 mg/l probably does not represent the maximum release that would have been observed after longer experiment times. The experimental approach of the closed-bottle batch tests entailed that the entire material surface made contact with water. Along the columns, however, the porous soil matrix prevented the entire grain surface from coming into contact with water with a low pH. Moreover, on a macro-scale, preferential flow paths may have been established, leading to "dead-end" pores that further reduced the reactive surface. Considering a surface-dependent Mn release, observed Mn concentrations derived by closed-bottle batch tests represent the upper threshold and can be considered the worst case.

4.2.3. Ion exchange, biological & chemical reduction

Existing or former precipitated Mn(hydr)oxides can act as oxidants for Fe^{2+}, and Mn^{2+} could be released due to incomplete iron removal (Eq. (7), Table 2, Meyerhoff, 1996). Results of the regular monitoring showed that iron removal was completed by OW 2 and the aquifer zone from OW 2 to the PW only saw iron-free groundwater (Fig. S2). This corresponds to the increasing Mn concentration towards OW 2 (Fig. 6). Assuming that MnO_2 is present in excess and all Fe^{2+} was removed by MnO_2 according to Eq. (7), an increase of the Mn concentration would have been measurable. Considering almost equal molar weights of Fe and Mn, the removal of around 15…20 mg/l Fe^{2+} could potentially lead to a release of 7.5…10 mg/l Mn^{2+}. This would sufficiently explain the observed Mn^{2+} release. Conversely, after the entire Fe^{2+} in groundwater had been removed along the flow path by OW 2, the Mn^{2+} should reach a maximum at OW 2. Hence, this cannot explain the observed further increase in Mn^{2+} concentration after OW 2 and OW 1 to the PW. Additionally, within the time period of the column experiments (second observation period after the shutdown), Fe unfortunately reached OW 1 and entered column SI and SII (Table S8). After entering the columns, the Fe concentration decreased along the flow path. If Fe would be removed according to Eq. (7) and considering the almost equal molar weights of Fe and Mn, the removal of around 1.2 mg/l Fe should have led to an increase of around 0.6 mg/l Mn, which was not observed. Thus, chemical reduction of Mn(hydr)oxides by Fe^{2+} is evaluated to be very unlikely.

Results of the sequential extraction after the column experiments (SI & SII) indicated a decreasing trend for the carbonate-bound Mn fraction along the flow path during extraction. Since the extraction step for the carbonate-bound fraction also stripped off Mn that was acid extractable or exchangeable, the observed pattern could potentially be due to ion exchange. Possible exchange sites could be clay minerals and humic acids. During SIR, the removal of Fe^{2+} and Mn^{2+} has been linked to cation exchange with Na^+ (van Halem et al., 2012) or Ca^{2+} (Petrunic et al., 2005). Due to the limited analysis spectrum during regular monitoring, a potential cation exchange with Na^+ or Ca^{2+} cannot be directly evaluated. Considering hardness as sum of Ca^{2+}-equivalents (see above), the increase along the flow path from OW 3 towards the PW does not fit with an interpretation involving cation exchange. Along the columns that simulated the aquifer zone from OW 1 to the PW (SI & SII) no noteworthy cation exchange was observed, which corresponds to the general lack of Mn release along the columns (Table S8). Based on those results, cation exchange being responsible for the Mn release cannot be conclusively evaluated.

Often, the release of Mn is coupled to anoxic conditions that favor the reductive dissolution of Mn(hydr)oxides (Massmann et al., 2004; Greskowiak et al., 2006). Due to the lack of an easily degradable carbon source in the groundwater in Khabarovsk, Mn release by microbial reduction is not expected.

4.3. Forecast of the potential duration of Mn release

During extraction phases, the Mn concentration in the water extracted from the PW initially largely increased, but after 25 SIR cycles a continuous decrease started (Fig. 6). To forecast the behavior of Mn, the water quality of the PW is used as *first forecast approach*. Assuming a cylindrical shape of the extracted aquifer volume, a distance of 18 m between the PW and OW 3, and 5 m filter screen height, the aquifer volume from OW 3 to the PW is approx. 1300 m^3 (Fig. 12). The total pore volume (PV) is around 325 m^3 (effective porosity, $n_e = 0.25$) and the total aquifer mass around 2,276,084 kg ($\rho \approx 1750$ kg/m^3). Using the total volume extracted since the start-up, the PV has been exchanged about 9600-times during the extraction phases. When only extraction phases with extraction volumes of ≥9000 m^3 (highest Mn release) are considered, the maximum Mn concentration at the end of the extraction phases, $c(Mn_{END})$, can be linearly approximated by $c(Mn_{END}) = -4.36 \times 10^{-5}$ PV + 1.4 (Fig. S21). Applying the slope of -4.36×10^{-5} PV to the present $c(Mn_{END})$ of around 1.1 mg/l indicates that about 25,000 PV would have to be additionally exchanged until Mn would no longer be measurable in the pumped water (Fig. 13). Considering a time period of around 7 d to complete one SIR cycle, about 13 years would pass until the Mn concentration would meet the Russian drinking water standard of 0.1 mg/l Mn (SanPin, 2010).

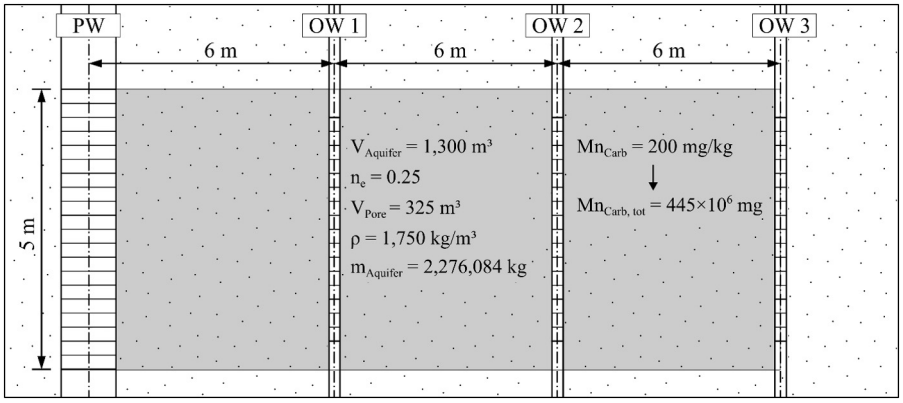

Fig. 12. Cross-section of the aquifer volume that was used for the forecast.

Since the results indicate that the Mn release can be mainly attributed to existing Mn-bearing carbonate minerals, the results of the sequential extraction can serve as *second forecast approach*. Taking the fraction of Mn bound to carbonates of the original aquifer material (<4 mm) of around 200 mg/kg (Fig. 9) and the aquifer mass of 2,276,084 kg between OW 3 and the PW, about 445 × 10^6 mg Mn are potentially available from this fraction. During the last observed extraction phases the Mn concentration increased from 0 mg/l (re-extraction of the infiltrate) to the approximate background value of 0.8 mg/l Mn and finally to around 1.1 mg/l. Because the groundwater enters the observed zone at OW 3 already with 0.8 mg/l, a carbonate mineral dissolution can only account for the additional increase of 0.3 mg/l Mn. Integrating the function of the increasing Mn concentration results in a mass of approx. 590,000 mg Mn that are extracted within one phase after 11,520 m^3 (not shown). This results in about 750 additional extraction phases to deplete the (Mn-bearing) carbonate pool, which are ≈26,700 PV and correspond to around 14 years of continuous operation (Fig. 13).

Since a few assumptions had to be made for both approaches, the forecasts are considered to be a rough estimation rather than an accurate prediction. The correlation of the maximum Mn concentration at the end of the extraction phases and total exchanged PV was quite weak, at $R^2 = 0.37$. If only the maximum concentration after exactly 11,520 m^3 extracted volume is considered, R^2 would be >0.6 and the resulting slope steeper (data not shown). Despite the weaker correlation, the taken trend line was preferred due to the larger sample size and most importantly, it represents more unfavorable conditions. The first limitation concerning the accuracy of the second forecast approach is probably the sequential extraction procedure itself (e.g. Nirel and Morel, 1990). Secondly, the approach does not include the impact of the background concentration and assumes that the Mn-bearing carbonate pool would be continuously depleted. Lastly, the second forecast is only valid assuming that Mn removal starts after the Mn-bearing carbonate pool is depleted. Despite those limitation, both approaches are independent from each other, but point towards a similar time span of 13 to 15 years, during which a further decreasing Mn concentration can be expected.

5. Conclusion

In Khabarovsk, subsurface iron removal (SIR) is used as pretreatment at a recently built waterworks. After Fe removal and partial Mn removal were successfully initiated at >25 wells, several production wells (PW) showed an anomalous behavior. An unexpected release of Mn during the infiltration and (especially) the extraction phases was observed. This study evaluated the entire start-up phase of one PW, where along an 18-m-wide aquifer zone up to 0.9 mg/l Mn were released in addition to the background concentration of around 0.8 mg/l Mn. Regular monitoring of the PW and three OW's showed that the formation of the Fe removal zone started immediately after two SIR cycles and was completed within 25 cycles. Based on the spatial and temporal distribution of dissolved oxygen, pH and EC values, the reaction zone for Fe^{2+} was identified within a radius of 6 to 18 m from the PW.

The observed release of Mn was linked to the dissolution of Mn-bearing carbonate minerals, which were found as impure siderite in the aquifer material. The dissolution of Mn-bearing carbonate minerals was found to be the primary source for Mn during extraction phases and can also account for the increasing hardness and alkalinity along the flow path. Permanent undersaturation of the groundwater with respect to rhodochrosite and siderite strengthen this theory. The lack of Mn removal in Khabarovsk can be partially attributed to the increased efficiency coefficient after around 5 SIR cycles and to a comparably short operation time.

Results of closed-bottle batch tests showed a strong grain-size- and pH-dependent release of Mn from the original aquifer material. At the presently observed pH ≈ 6 during extraction, the grain size <4 mm released >1 mg/l Mn and fines (<0.063 mm) >2 mg/l. Moreover, the grain size <0.063 mm released >3 mg/l Mn within 24 h at pH 5. A flow-through column leaching experiment showed a release of 1.7 mg/l Mn within 14 exchanged pore volumes using groundwater at pH 5, which

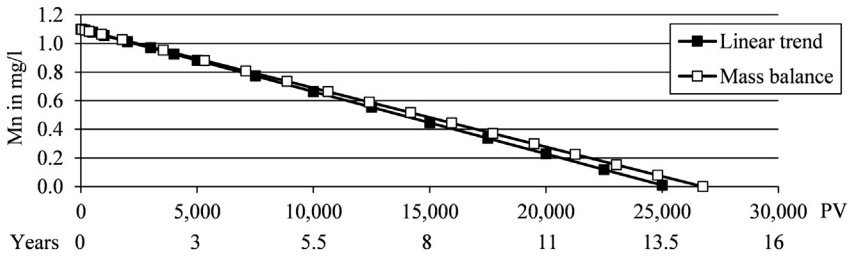

Fig. 13. Estimated Mn concentration in the pumped water from PW based on the observed decrease ("Linear trend") and a depletion of the Mn pool that is bound to carbonates ("Mass balance").

is equal to the maximum observed Mn concentration at the PW. Additionally, two independently operated columns containing aquifer material run in parallel with the PW, and a sequential extraction procedure was applied to the recovered filling material of the columns. Based on the results of the sequential extraction as well as the present development of Mn in the extracted water at the PW, the time span for the expected depletion of the Mn pool was estimated. Both approaches indicate that the Mn carbonate pool will probably be depleted within 13 to 15 years.

Acknowledgements

This work was performed as a cooperation between Arcadis Germany GmbH, Vodokanal Khabarovsk and the Division of Water Sciences at the University of Applied Sciences Dresden. The authors are grateful to the ESF for the financial support of S. Paufler (grant no. 200031585). We also thank N. Seidel for conducting the sequential extractions and the Institute of Water Chemistry at TU Dresden for additional water analyses.

Appendix A. Supplementary data

Supplementary data to this article can be found online at https://doi.org/10.1016/j.scitotenv.2018.09.319.

References

Antoniou, E.A., van Breukelen, B.M., Putters, B., Stuyfzand, P.J., 2012. Hydrogeochemical patterns, processes and mass transfers during aquifer storage and recovery (ASR) in an anoxic sandy aquifer. Appl. Geochem. 27 (12), 2435–2452. https://doi.org/10.1016/j.apgeochem.2012.09.006.

Antoniou, E.A., Hartog, N., van Breukelen, B.M., Stuyfzand, P.J., 2014. Aquifer pre-oxidation using permanganate to mitigate water quality deterioration during aquifer storage and recovery. Appl. Geochem. 50, 25–36. https://doi.org/10.1016/j.apgeochem.2014.08.006.

Aqion, 2018. Online manual, table of diffusion coefficients. http://www.aqion.de/site/194 (Cited 19th of January 2018).

Bartak, R., Macheleidt, W., Grischek, T., 2017. Controlling the formation of the reaction zone around an injection well during subsurface iron removal. Water 9 (2), 87 (1–13). https://doi.org/10.3390/w9020087.

Bilek, F., 2016. Begleitung des Feldtests zur Infiltration von Wasser mit erhöhter O_2-Konzentration durch Auswertung der geochemisch-mineralogischen Untersuchungsergebnisse [Supporting the field test for the infiltration of O_2-enriched water by evaluating the geochemical mineralogical investigation results]. Scientific-Technical Report. GFI Grundwasser-Consulting-Institut GmbH Dresden (unpublished, 47 p., In German).

Braun, B., Schröder, J., Knecht, H., Szewzyk, U., 2016. Unraveling the microbial community of a cold groundwater catchment system. Water Res. 107, 113–126. https://doi.org/10.1016/j.watres.2016.10.040.

Greskowiak, J., Prommer, H., Massmann, G., Nützmann, G., 2006. Modeling seasonal redox dynamics and the corresponding fate of the pharmaceutical residue phenazone during artificial recharge of groundwater. Environ. Sci. Technol. 40 (21), 6615–6621. https://doi.org/10.1021/es052506t.

Hallberg, R.O., Martinell, R., 1976. Vyredox - in situ purification of ground water. Ground Water 14 (2), 88–93. https://doi.org/10.1111/j.1745-6584.1976.tb03638.x.

Herlitzius, J., 2015. Begründung der Bedingungen zur Bildung von Biofilm und technische Lösungen zur Vorbeugung der Biofilmbildung auf der technologischen Ausrüstung der Wasserfassung im Tungusskavorkommen [Conditions for the formation of biofilm and technical solutions for the prevention of biofilm formation on the technological equipment of the water catchment in the Tungusska reservoir in Khabarovsk]. In: Herlitzius, J. (Ed.), Scientific-Technical Report. Arcadis Germany GmbH (unpublished, 24 p., In German).

Herlitzius, J., Sumpf, H., Grischek, T., 2012. German-Russian cooperation for clean drinking water. Int. J. Water Manag., bluefacts 2012, 76–81.

Kulakov, V.V., 2013. Technology of groundwater treatment in the aquifer for drinking water supplies. Proc. 35th IAHR World Congress, September 9–13, 2013, Chengdu, China, p. 432.

Kulakov, V.V., Fisher, N.K., Kondratieva, L.M., Grischek, T., 2011. Riverbank filtration as an alternative to surface water extraction for safe drinking water supply to the city of Khabarovsk, Russia. In: Ray, C., Shamrukh, M. (Eds.), Riverbank Filtration for Water Security in Desert Countries. Springer, Dordrecht, pp. 281–298.

Massmann, G., Pekdeger, A., Merz, C., 2004. Redox processes in the Oderbruch polder groundwater flow system in Germany. Appl. Geochem. 19 (6), 863–886. https://doi.org/10.1016/j.apgeochem.2003. 11.006.

Mettler, S., Abdelmoula, M., Hoehn, E., Schoenenberger, R., Weidler, P., von Gunten, U., 2001. Characterization of iron and manganese precipitates from an in situ ground water treatment plant. Ground Water 39 (6), 921–930. https://doi.org/10.1111/j.1745-6584.2001.tb02480.x.

Meyerhoff, R., 1996. Entwicklung von Planungs- und Anwendungskriterien für die in-situ-Aufbereitung eisen- und manganhaltiger Grundwässer [Development of planning and application criteria for the in-situ treatment of iron and manganese-containing groundwater]. (PhD Thesis). Stuttgarter Berichte zur Siedlungswasserwirtschaft. vol. 139 (233 p., In German).

Neumann, V., 2007. Pilotanlage Wasserversorgung Khabarovsk [Pilot plant for drinking water production in Khabarovsk]. Scientific-Technical Report. Arcadis Consult GmbH (unpublished, 31 p., In German).

Nirel, P.M.V., Morel, F.M.M., 1990. Pitfalls of sequential extractions. Water Res. 24 (8), 1055–1056. https://doi.org/10.1016/0043-1354(90)90129-T.

Parkhurst, D.L., Appelo, C.A.J., 2013. Description of input and examples for PHREEQC version 3: a computer program for speciation, batch-reaction, one-dimensional transport, and inverse geochemical calculations. U.S. Geological Survey Techniques and Methods available only at. http://pubs.usgs.gov/tm/06/a43 (book 6, chap. A43, 497 p.).

Petrunic, B.M., MacQuarrie, K.T.B., Al, T.A., 2005. Reductive dissolution of Mn oxides in river-recharged aquifers: a laboratory column study. J. Hydrol. 301, 163–181. https://doi.org/10.1016/j.jhydrol.2004.06.022.

Rauret, G., López-Sánchez, J.F., Sahuquillo, A., Rubio, R., Davidson, C., Ure, A., Quevauviller, P., 1999. Improvement of the BCR three step sequential extraction procedure prior to the certification of new sediment and soil reference materials. J. Environ. Monit. 1 (1), 57–61. https://doi.org/10.1039/A807854H.

Roessner, U., Sailer, C., Langert, J., Plaßmann, C., 2017. Einfahrbetrieb der Unterirdischen Enteisenung und Entmanganung an der Wassergewinnung Kaldenkirchen (Niederrhein) [Start-up of a Subsurface Iron Removal plant in Kaldenkirchen (Niederrhein)]. ewp Energie-Wasser-Praxis. vol. 12 pp. 92–95 (In German).

Rott, U., Friedle, M., 2000a. Eco-friendly and cost-efficient removal of arsenic, iron and manganese by means of subterranean ground-water treatment. Water Supply 18, 632–636.

Rott, U., Friedle, M., 2000b. 25 Jahre unterirdische Wasseraufbereitung in Deutschland - Rückblick und Perspektiven [25 years of subterranean groundwater treatment in Germany - review and perspectives]. gwf Wasser Abwasser 141 (13), 99–107 (In German).

Rott, U., Meyer, C., Friedle, M., 2002. Residue-free removal of arsenic, iron, manganese and ammonia from groundwater. Water Sci. Technol. Water Supply 2 (1), 17–24.

Rott, U., Kauffmann, H., Meyer, C., 2003. Simultane Trinkwassergewinnung und -aufbereitung in Kombination mit Horizontalfilterbrunnen [Simultaneous drinking water extraction and treatment in combination with horizontal collector wells]. Wasser und Abfall. vol. 9, pp. 22–25 (In German).

SanPin, 2010. SanPin 2.4.2.2821-10. Potable Water. Hygienic Requirements for Water Quality for Centralized Drinking Water Supply Systems. Gosstroy Rossii, Moscow.

Stumm, W., Morgan, J.J., 1996. Aquatic Chemistry. Chemical Equilibria and Rates in Natural Waters. 3rd ed. Wiley interscience, New York.

Sutherland, R.A., Tack, F.M.G., 2002. Determination of Al, Cu, Fe, Mn, Pb and Zn in certified reference materials using the optimized BCR sequential extraction procedure. Anal. Chim. Acta 454, 249–257. https://doi.org/10.1016/S0003-2670(01)01553-7.

van Halem, D., De Vet, W., Verberk, J., Amy, G., van Dijk, H., 2011. Characterization of accumulated precipitates during subsurface iron removal. Appl. Geochem. 26, 116–124. https://doi.org/10.1016/j.apgeochem.2010.11.008.

van Halem, D., Moed, D.H., Verberk, J.Q.J.C., Amy, G.L., van Dijk, J.C., 2012. Cation exchange during subsurface iron removal. Water Res. 46 (12), 307–315. https://doi.org/10.1016/j.watres.2011.10.015.

von Rohr, R.M., Hering, J.G., Kohler, H.P., von Gunten, U., 2014. Column studies to assess the effects of climate variables on redox processes during riverbank filtration. Water Res. 61, 263–275. https://doi.org/10.1016/j.watres.2014.05.018.

Worch, E., 2015. Hydrochemistry: Basic Concepts and Exercises. 1st ed. De Gruyter, Berlin (ISBN 978-3110315530).

Supplementary material

Manganese release linked to carbonate dissolution during the start-up phase of a subsurface iron removal well in Khabarovsk, Russia

Paufler, S[a], Grischek, T[a], Herlitzius, J[b], Feller, J.[a], Kulakov, V.V.[c]

[a] Dresden University of Applied Sciences, Friedrich-List-Platz 1, 01069 Dresden, Germany

[b] Arcadis Germany GmbH, EUREF-Campus 10, 10829 Berlin, Germany

[c] Institute of Water and Ecological Problems, FEB RAS, 680000 Khabarovsk, Russia

Corresponding author:

S. Paufler

Dresden University of Applied Sciences

Friedrich-List-Platz 1

01069 Dresden

Germany

sebastian.paufler@htw-dresden.de

+49 351-462 2631

Tab. S1: Assignment of the samples for the investigation of Mn release as a function of particle size and pH

No.	1	2	3	4	5	6	7	8	9
Weighed portion in g	25								
Grain size in mm	< 0.063 mm				< 4 mm				
pH of the water	6		5		6		5		6.9

Tab. S2: Chemical reagents and analytical conditions for the optimized BCR sequential extraction procedure after Rauret et al. (1999) / Sutherland & Tack (2002)

Step	Extracted phase	Chemical reagents*[1] and conditions
1	Acid extractable Exchangeable Carbonate	1 g aliquot, 40 ml 0.11 M CH_3COOH Shake for 16 h at 22±5 °C Separate extract from the solid by centrifugation at 3000 U/min for 20 min
2	Reducible	To step 1 residue: 40 ml 0.5 M $NH_2OH{\cdot}HCl$ (pH≈1.5) Shake for 16 h at 22±5 °C Centrifuge extract as per step 1
3	Oxidizable	To step 2 residue: 10 ml of 30 % H_2O_2 (pH 2–3) Keep at 85±2 °C for 1 h Add further 10 ml of 30 % H_2O_2 (pH 2–3) Keep at 85±2 °C for 1 h Add 50 ml; 1 M NH_4OAc (pH 2) Shake for 16 h at 22±5 °C Centrifuge extract as per step 1
4	Residual *[2]	To step 3 residue: 15 ml HNO_3 with 5 ml $HClO_4$ Keep at 70-80 °C for 1 h Add further 5 ml HNO_3 with 1 ml $HClO_4$ Keep at 120 °C for 1 h Centrifuge extract as per step 1

*[1] CH_3COOH (Acetic acid), $NH_2OH{\cdot}HCl$ (Hydroxylammonium-hydrochloride), H_2O_2 (Hydrogen peroxide), NH_4OAc (Ammonium acetate), HNO_3 (Nitric acid), $HClO_4$ (Perchloric acid)

*[2] Extraction of the residual phase differed slightly from Rauret et al. (1999) due to lab restrictions.

Note: Results were checked against a total extraction that was parallel conducted with separate samples by direct application of step 4.

Tab. S3: No. of taken samples for regular monitoring during the observation time

Infiltration						Extraction					
SIR cycles	V in m³	PW	OW 1	OW 2	OW 3	SIR cycles	V in m³	PW	OW 1	OW 2	OW 3
2	200	2	2	1	1	2	100	4	3	2	1
	2,000	2	2	1	1		1,000	4	4	4	4
	3,840	2	2	1	1		4,000	4	3	3	2
25	200	13	14	4	4	25	100	27	29	12	11
	2,000	9	9	5	5		1,000	11	12	9	8
	3,840	8	9	4	4		4,000	21	18	17	17
							8,840	5	3	3	5
							11,520	4	4	3	3
165	200	38	38	13	12	165	100	18	27	22	23
	2,000	65	64	69	68		1,000	9	24	24	26
	3,840	49	50	56	54		4,000	21	42	42	42
							8,840	21	40	40	40
							11,520	7	33	34	32
Shutdown for 100 d											
167	200	2	2	1	1	167	100	2	2	1	2
	2,000	2	2	2	2		1,000	1	1	1	2
	3,840	2	1	1	1		4,000	3	4	4	4
							8,840	1	2	2	2
							11,520	6	11	11	12
182	200	2	1	1	3	182	100	1	2	3	3
	2,000	4	5	5	4		1,000	1	3	3	3
	3,840	3	4	4	4		4,000	4	4	4	4
							8,840	3	3	3	3
							11,520	7	5	6	6
194	200	5	2	1	4	194	100	2	1	1	1
	2,000	7	11	9	9		1,000	8	4	3	3
	3,840	5	8	7	7		4,000	0	0	0	0
							8,840	0	0	0	0
							11,520	15	10	8	8

Tab. S4: Input and output data for the calculation of the saturation indexes of $MnCO_3$ and $FeCO_3$

		Input							Output
		V	O_2	pH	Ca	Mn	Fe	Alkalinity*	$Mn(II)_{eq}$
		m³	mg/l	-	mg/l	mg/l	mg/l	mg/l	mg/l
Infiltration	PW	200	24.9	7.98	25.0	0.05	0.02	76	0.84
	OW1	200	4.9	6.09	22.9	1.10	0.02	70	3.89
	OW2	200	0.0	6.04	17.9	0.90	0.09	54	5.46
	OW3	200	0.0	6.15	16.4	0.70	15.5	50	7.22
	PW	3,840	24.3	7.95	22.2	0.05	0.02	68	0.87
	OW1	3,840	22.3	7.21	21.5	0.50	0.02	65	0.94
	OW2	3,840	20.4	6.88	17.9	0.50	0.02	54	1.12
	OW3	3,840	4.8	6.22	10.4	0.50	8.45	32	3.91
Extraction	PW	100	23.0	7.59	22.9	0.05	0.02	70	0.89
	OW1	100	21.3	7.18	21.5	0.50	0.02	65	0.98
	OW2	100	9.7	6.69	17.9	0.60	0.02	54	1.52
	OW3	100	0.3	6.20	10.7	0.50	10.4	33	5.73
	PW	1,000	14.0	7.42	23.2	0.05	0.02	71	0.98
	OW1	1,000	10.8	6.89	18.2	0.60	0.02	56	1.32
	OW2	1,000	2.4	6.45	14.3	0.60	0.02	44	2.55
	OW3	1,000	0.0	6.16	10.7	0.60	11.4	33	6.31
	PW	4,000	0.1	6.07	22.9	0.60	0.02	70	5.22
	OW1	4,000	0.0	5.86	20.7	0.70	0.02	63	7.18
	OW2	4,000	0.0	5.84	17.9	0.70	0.10	54	7.26
	OW3	4,000	0.0	6.12	15.0	0.70	15.2	46	7.38
	PW	11,520	0.0	6.04	25.7	1.20	0.02	78	5.73
	OW1	11,520	0.0	6.08	25.0	0.90	0.02	76	5.39
	OW2	11,520	0.0	6.07	25.0	1.00	0.22	76	5.51
	OW3	11,520	0.0	6.17	17.9	0.80	17.9	54	7.75

* Alkalinity as HCO_3^-, gfw 61 g/mol

Tab. S5: Anion and cation concentration (n=1 for pH 6.9, mean of n=2 for pH 5& 6) in the mixing water and after 24 h incubation from the batch test

Parameter in mg/l	pH 6.9		pH 6			pH 5		
	Mixing water	<4mm after 24h incubation	Mixing water	after 24h incubation <0.063mm	after 24h incubation <4mm	Mixing water	after 24h incubation <0.063mm	after 24h incubation <4mm
F^-	0.01	<LOD	<LOD	0.15	0.15	<LOD	0.21	0.06
Cl^-	0.58	3.78	38.01	40.08	40.39	60.55	65.34	63.52
NO_2^-	<LOD	<LOD	<LOD	<LOD	<LOD	<LOD	<LOD	<LOD
Br^-	<LOD	<LOD	<LOD	<LOD	<LOD	<LOD	<LOD	<LOD
NO_3^-	0.45	<LOD	<LOD	<LOD	<LOD	<LOD	0.31	<LOD
SO_4^{2-}	1.38	2.47	0.64	12.14	1.98	0.31	14.36	1.11
PO_4^{3-}	<LOD	<LOD	<LOD	0.25	<LOD	<LOD	0.26	<LOD
Ca^{2+}	15.25	16.16	14.66	17.24	16.29	14.67	20.48	17.18
Mg^{2+}	5.35	5.38	5.21	5.34	5.39	5.20	5.80	5.52
Na^+	7.78	9.40	7.63	12.01	9.33	7.59	13.80	9.39
K^+	1.62	3.09	1.24	5.50	2.85	1.69	7.65	3.31
Sr	0.12	0.13	0.12	0.14	0.13	0.12	0.18	0.15
Ba^{2+}	0.02	0.02	0.03	0.08	0.03	0.02	0.11	0.04
Mn^{2+}	0.81	1.10	0.77	2.19	1.19	0.77	3.62	1.65
Fe^{2+}	0.09	0.05	0.02	0.02	0.01	0.04	0.05	0.02
Si	1.16	1.12	1.13	1.11	1.14	1.12	1.11	1.14

<LOD Limit of Detection

Tab. S6: Water quality of the inflow water with pH 5 and after the 0.5 m column SIII during the column experiment to evaluate a pH-dependent Mn release

	Inflow	PV					
		1	3	7	10	12	14
EC in µS/cm	195	202	230	206	199	197	198
O_2 in mg/l	1.5	0	0.63	0.7	1.08	1.18	1.32
pH	5.0	5.29	5.25	4.942	4.83	4.82	4.8
T in °C	14	20.8	21.1	21.3	22	22.4	22.7
Parameter in mg/l							
F^-	0.02	<LOD	<LOD	<LOD	<LOD	<LOD	<LOD
Cl^-	46.97	19.25	42.57	47.01	47.59	47.74	47.24
NO_2^-	<LOD	<LOD	<LOD	<LOD	<LOD	<LOD	<LOD
Br^-	<LOD	<LOD	<LOD	<LOD	<LOD	<LOD	<LOD
NO_3^-	<LOD	<LOD	<LOD	<LOD	<LOD	<LOD	<LOD
SO_4^{2-}	0.09	1.68	1.35	0.12	0.15	0.02	0.98
PO_4^{3-}	<LOD	<LOD	<LOD	<LOD	<LOD	<LOD	<LOD
Ca^{2+}	12.41	14.84	18.05	14.87	13.52	13.03	13.23
Mg^{2+}	4.24	5.27	6.41	5.07	4.57	4.39	4.37
Na^+	8.19	8.79	8.68	8.44	8.39	8.36	8.34
K^+	1.27	1.25	1.41	1.39	1.40	1.38	1.39
Sr	0.10	0.13	0.16	0.14	0.13	0.12	0.12
Ba^{2+}	0.05	0.04	0.05	0.06	0.06	0.06	0.07
Mn^{2+}	0.64	1.29	1.66	1.67	1.79	1.84	1.99
Fe^{2+}	0.25	0.06	0.09	0.11	0.04	0.08	0.04
Si	1.09	1.10	1.13	1.14	1.12	1.11	1.12

<LOD Limit of Detection

Tab. S7: Hydraulic properties of the columns

Column	Filling material	Grain size in mm	Length in m	Hydr. cond. in m/s	Darcy velocity in m/s	Pore velocity in m/s	Travel time in min.	Effective porosity
SI*[1]	Aquifer material*[3]	<4	2	1.1×10^{-5}	1.6×10^{-4}	5.5×10^{-4}	52	0.29
SII*[1]	Aquifer material*[3]	<4	2	1.1×10^{-5}	1.6×10^{-4}	5.4×10^{-4}	52	0.29
SIII*[2]	Aquifer material*[3]	<4	0.5	6.7×10^{-5}	1.3×10^{-4}	4.2×10^{-4}	17	0.32

*[1] Operated parallel to the phases of the PW (see section 2.3)
*[2] Operated for one day during the flow-through test (see section 2.4.2)
*[3] Natural aquifer material from core drillings at the depth of the actual filter screen, subsequently sieved to <4 mm

Tab. S8: Water quality along column SI and SII determined by ICP measurement, data represent median values of both columns if n≥2

		Ca^{2+} in mg/l	Mg^{2+} in mg/l	Na^{+} in mg/l	K^{+} in mg/l	Fe^{2+} in mg/l	Mn^{2+} in mg/l	Si in mg/l	Ba^{2+} in mg/l	Sr in mg/l	Cl^{-} in mg/l	NO_3^{-} in mg/l	NO_2^{-} in mg/l	SO_4^{2-} in mg/l	PO_4^{3-} in mg/l	Br^{-} in mg/l	F in mg/l
Extraction	Inflow (OW 1)	14.6	5.1	8.1	0.77	1.17	1.0	0.02	0.10	<LOD	<LOD	<LOD	<LOD	<LOD	<LOD	1.2	<LOD
		4	4	4	4	4	4	1	1	1	1	1	1	1	1	4	1
	P5	14.3	5.0	8.0	0.75	0.82	1.0	0.02	0.10	0.33	0.7	<LOD	1.7	<LOD	<LOD	1.2	<LOD
		10	10	10	10	10	10	4	4	1	1	1	1	1	1	10	1
	P4	14.5	5.1	8.1	0.78	0.83	1.0	0.03	0.10	0.33	<LOD	<LOD	1.7	<LOD	<LOD	1.2	0.01
		10	10	10	10	10	10	4	4	1	1	1	1	1	1	10	1
	P3	14.7	5.2	8.0	0.83	0.19	1.0	0.04	0.09	0.44	0.5	<LOD	1.6	<LOD	<LOD	1.2	<LOD
		10	10	10	10	10	10	4	4	1	1	1	1	1	1	10	1
	P2	14.6	5.1	7.9	0.83	0.05	1.0	0.05	0.09	0.29	0.4	<LOD	1.4	<LOD	<LOD	1.2	<LOD
		10	10	10	10	10	10	4	4	1	1	1	1	1	1	10	1
	P1	14.6	5.2	7.8	0.84	0.02	1.0	0.04	0.10	0.37	0.5	<LOD	1.4	<LOD	<LOD	1.2	<LOD
		10	10	10	10	10	10	4	4	1	1	1	1	1	1	10	1
Infiltration	Inflow (PW)	13.7	5.2	22.9	0.05	0.01	0.8	<LOD	<LOD	<LOD	<LOD	<LOD	<LOD	<LOD	<LOD	4.4	<LOD
		1	1	1	1	1	1	1	1	1	1	1	1	1	1	1	1
	P1	11.8	4.6	17.6	0.01	0.01	0.8	0.01	0.10	10.0	0.7	<LOD	3.9	<LOD	<LOD	1.9	<LOD
		4	4	4	4	4	4	1	1	1	1	1	1	1	1	4	1
	P2	11.8	4.6	18.0	0.03	0.01	0.8	0.02	0.10	9.9	0.5	<LOD	4.4	<LOD	<LOD	2.6	<LOD
		4	4	4	4	4	4	1	1	1	1	1	1	1	1	4	1
	P3	11.8	4.7	17.9	0.05	0.01	0.8	0.02	0.09	9.4	<LOD	<LOD	4.4	<LOD	<LOD	2.0	<LOD
		4	4	4	4	4	4	1	1	1	1	1	1	1	1	4	1
	P4	11.5	4.6	17.9	0.09	0.01	0.8	0.02	0.09	9.3	<LOD	<LOD	4.8	<LOD	<LOD	2.1	<LOD
		4	4	4	4	4	4	1	1	1	1	1	1	1	1	4	1
	P5	11.3	4.5	17.8	0.16	0.01	0.8	0.02	0.09	9.2	<LOD	<LOD	5.1	<LOD	<LOD	2.1	0.01
		4	4	4	4	4	4	1	1	1	1	1	1	1	1	4	1

<LOD Limit of Detection

Tab. S9: Median values for Eh and pH during infiltration and extraction at the PW and OW 1, 2 and 3

		PW				OW 1				OW 2				OW 3			
Infiltration	V	Eh		pH		Eh		pH		Eh		pH		Eh		pH	
	m³	mV	n	-	n	mV	n	-	n	mV	n	-	n	mV	n	-	n
	200	475	17	8.0	61	410	12	6.1	57	256	7	6.0	19	101	6	6.2	22
	2000	515	14	7.9	36	350	14	7.1	87	278	14	6.6	87	198	14	6.2	85
	3840	490	12	8.0	71	332	14	7.2	73	290	13	6.9	73	157	14	6.2	72
Extraction	100	282	30	7.6	106	320	31	7.2	105	224	14	6.7	74	176	13	6.2	72
	1000	232	18	7.4	76	226	19	6.9	75	153	16	6.5	65	106	15	6.2	65
	4000	215	27	6.1	105	208	26	5.9	101	196	25	5.8	100	98	23	6.1	98
	8840	179	5	6.0	77	206	5	6.0	77	200	5	6.0	77	98	5	6.2	75
	11520	174	15	6.1	72	194	14	6.1	76	184	13	6.1	76	94	14	6.2	75

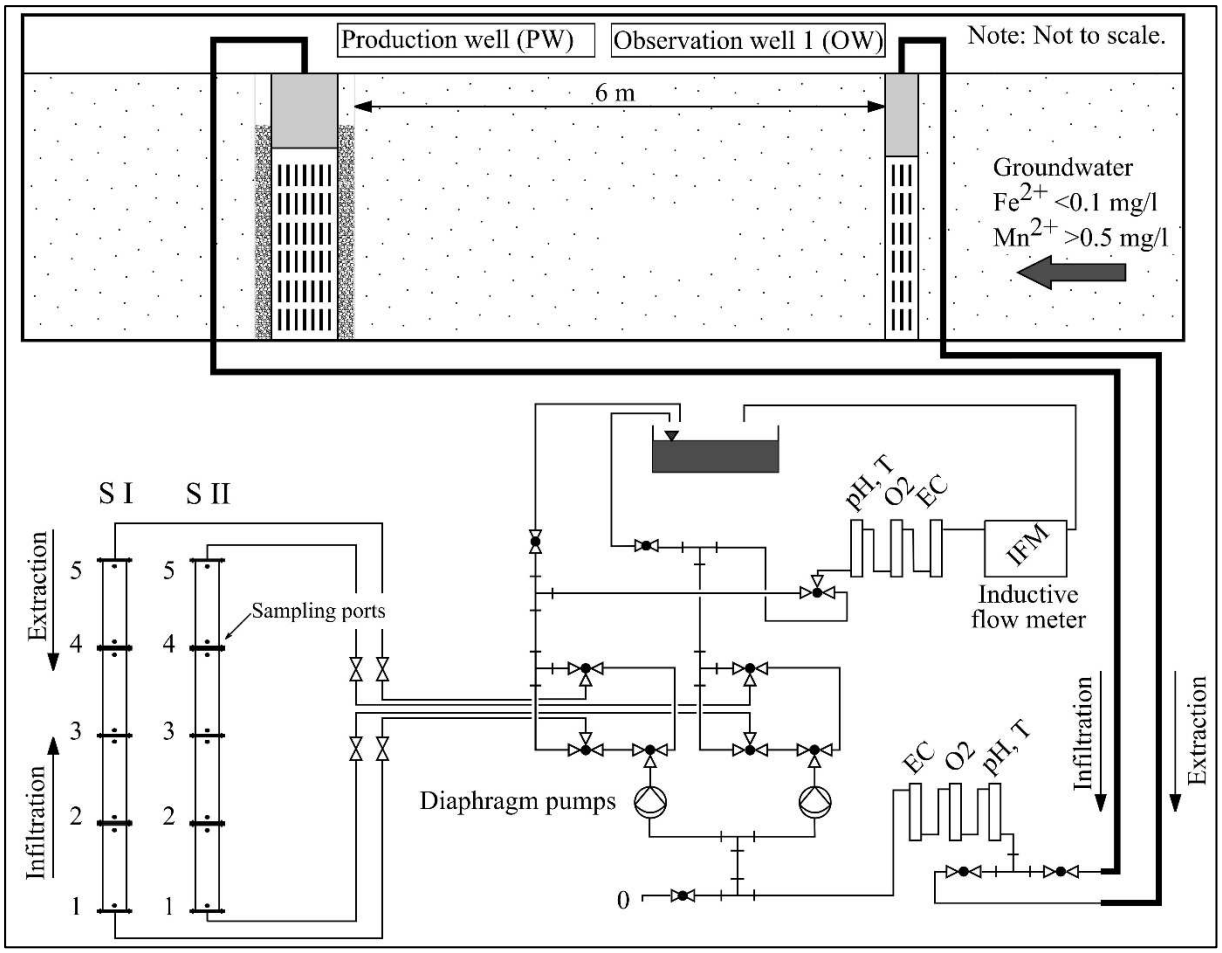

Fig. S1: Set-up of the column experiment at the production well in Khabarovsk

SIR cycles	V_{inf} in m³	PW	← 6 m →		OW 1	← 6 m →		OW 2	← 6 m →		OW 3
2	200										
	2,000	0.0	0.4	0.8	1.2	1.5	1.9	2.3	5.0	7.7	10.4
	3,840	0.0	0.2	0.4	0.6	1.4	2.2	3.1	5.0	6.8	8.7
25	200										
	2,000	0.0	0.0	0.0	0.0	0.6	1.2	1.7	6.7	11.7	16.8
	3,840	0.0	0.0	0.0	0.0	0.1	0.1	0.2	3.9	7.7	11.4
165	200										
	2,000	0.0	0.0	0.0	0.0	0.0	0.0	0.0	4.3	8.5	12.8
	3,840	0.0	0.0	0.0	0.0	0.0	0.0	0.0	2.7	5.4	8.1
167	200										
	2,000	0.0	0.0	0.0	0.0	0.0	0.0	0.0	3.6	7.2	10.8
	3,840	0.0	0.0	0.0	0.0	0.0	0.0	0.0	3.1	6.1	9.2
182	200										
	2,000	0.0	0.0	0.0	0.0	0.0	0.0	0.1	4.5	9.0	13.5
	3,840	0.0	0.0	0.0	0.0	0.0	0.0	0.0	2.6	5.2	7.8
194	200										
	2,000	0.0	0.0	0.0	0.0	0.0	0.0	0.1	4.7	9.3	13.9
	3,840	0.0	0.0	0.0	0.0	0.0	0.0	0.0	3.7	7.3	11.0

Fig. S2: Median Fe concentration in mg/l during infiltration between the PW and OW 3, diagonal lines mark the 100 d shutdown and split observation period 1 & 2 (see Fig. 2), intermediate values are calculated by linear interpolation (see Tab. S3 for no. of samples)

SIR cycles	V_{inf} in m³	PW	←	6 m	→	OW 1	←	6 m	→	OW 2	←	6 m	→	OW 3
2	200	7.7	7.5		7.2	6.9	6.7		6.5	6.4	6.3		6.3	6.3
	2,000	7.7	7.4		7.1	6.8	6.6		6.5	6.4	6.4		6.3	6.3
	3,840	7.8	7.4		7.1	6.7	6.6		6.5	6.4	6.4		6.4	6.4
25	200	7.9	7.3		6.7	6.1	6.1		6.1	6.1	6.2		6.2	6.2
	2,000	8.1	7.7		7.4	7.1	6.9		6.7	6.6	6.4		6.3	6.2
	3,840	7.9	7.7		7.5	7.3	7.2		7.1	7.0	6.7		6.5	6.3
165	200	8.0	7.4		6.7	6.1	6.1		6.0	6.0	6.1		6.1	6.1
	2,000	7.9	7.6		7.4	7.1	6.9		6.8	6.6	6.4		6.3	6.2
	3,840	8.0	7.7		7.5	7.2	7.1		7.0	6.9	6.7		6.4	6.2
167	200	7.9	7.3		6.7	6.1	6.1		6.0	6.0	6.1		6.1	6.2
	2,000	7.8	7.7		7.5	7.4	7.2		7.1	7.0	6.9		6.7	6.6
	3,840	7.1	7.2		7.2	7.3	7.2		7.1	7.0	6.8		6.6	6.3
182	200	8.3	7.6		6.9	6.2	6.2		6.1	6.1	6.1		6.1	6.2
	2,000	8.2	7.8		7.4	7.0	6.8		6.6	6.4	6.3		6.3	6.3
	3,840	8.1	7.8		7.5	7.2	7.1		6.9	6.8	6.6		6.4	6.2
194	200	8.0	7.5		7.0	6.5	6.3		6.2	6.1	6.1		6.1	6.1
	2,000	7.9	7.6		7.2	6.9	6.7		6.4	6.2	6.2		6.1	6.0
	3,840	8.0	7.7		7.3	7.0	6.9		6.7	6.5	6.4		6.2	6.1

Fig. S3: Median pH during infiltration between the PW and OW 3, diagonal lines mark the 100 d shutdown and split observation period 1 & 2 (see Fig. 2), intermediate values are calculated by linear interpolation (see Tab. S3 for no. of samples)

SIR cycles	V_{inf} in m³	PW	←	6 m	→	OW 1	←	6 m	→	OW 2	←	6 m	→	OW 3
2	200	175	169		164	159	149		140	131	148		165	182
	2,000	166	156		147	137	133		130	126	137		148	158
	3,840	166	157		147	137	130		123	116	125		135	144
25	200	182	171		159	148	154		160	167	181		196	211
	2,000	216	208		201	193	175		157	139	154		170	185
	3,840	197	190		182	175	169		164	159	161		163	166
165	200	201	187		174	160	158		155	153	165		177	189
	2,000	193	189		185	182	176		170	164	168		173	177
	3,840	189	185		182	178	174		170	166	165		164	163
167	200	178	167		156	145	151		157	163	177		191	206
	2,000	181	177		172	168	162		156	150	159		168	177
	3,840	198	195		193	190	185		180	175	170		164	158
182	200	199	180		161	141	147		152	158	175		193	211
	2,000	205	203		200	198	188		178	168	176		184	192
	3,840	192	193		193	194	188		183	177	175		173	171
194	200	200	187		175	162	161		159	158	176		194	212
	2,000	197	194		192	190	182		174	166	174		183	192
	3,840	216	212		208	205	196		187	179	176		173	170

Fig. S4: Median EC in µS/cm during infiltration between the PW and OW 3, diagonal lines mark the 100 d shutdown and split observation period 1 & 2 (see Fig. 2), intermediate values are calculated by linear interpolation (see Tab. S3 for no. of samples)

SIR cycles	V_{inf} in m³	PW	← 6 m →		OW 1	← 6 m →		OW 2	← 6 m →		OW 3
2	200	2.8	2.9	2.9	3.0	3.2	3.3	3.5	3.3	3.2	3.0
	2,000	2.6	2.3	2.0	1.8	1.5	1.2	0.9	1.0	1.1	1.2
	3,840	2.6	2.2	1.7	1.3	1.3	1.2	1.2	1.0	0.7	0.5
25	200	3.5	3.5	3.5	3.5	3.3	3.2	3.0	2.9	2.9	2.8
	2,000	3.2	3.1	3.1	3.0	2.7	2.5	2.2	1.9	1.7	1.4
	3,840	3.2	3.2	3.1	3.1	2.7	2.4	2.0	1.7	1.3	1.0
165	200	3.5	3.4	3.3	3.2	3.0	2.7	2.5	2.4	2.3	2.3
	2,000	3.0	2.9	2.8	2.7	2.6	2.5	2.4	2.1	1.9	1.6
	3,840	3.1	3.1	3.0	3.0	2.8	2.7	2.5	2.2	1.8	1.5
167	200	3.4	3.5	3.6	3.8	3.8	3.8	3.8	3.5	3.3	3.0
	2,000	3.7	3.5	3.4	3.3	3.0	2.8	2.6	2.3	2.1	1.9
	3,840	3.1	3.0	3.0	2.9	2.6	2.3	2.0	2.0	1.9	1.9
182	200	2.8	2.6	2.5	2.3	2.6	3.0	3.3	3.2	3.1	3.0
	2,000	3.0	2.9	2.9	2.8	2.6	2.3	2.1	2.2	2.4	2.5
	3,840	2.5	2.5	2.5	2.5	2.1	1.7	1.3	1.4	1.4	1.5
194	200	2.9	2.7	2.6	2.4	2.7	3.0	3.3	3.1	3.0	2.8
	2,000	3.2	3.1	3.1	3.0	2.6	2.3	1.9	2.3	2.8	3.2
	3,840	2.8	2.9	2.9	3.0	2.7	2.3	2.0	2.1	2.3	2.4

Fig. S5: Median hardness in °dH during infiltration between the PW and OW 3, diagonal lines mark the 100 d shutdown and split observation period 1 & 2 (see Fig. 2), intermediate values are calculated by linear interpolation (see Tab. S3 for no. of samples)

SIR cycles	V_{extr} in m³	PW	← 6 m →		OW 1	← 6 m →		OW 2	← 6 m →		OW 3
2	100	0.0	0.0	0.0	0.0	0.6	1.2	1.8	4.6	7.4	10.2
	1,000	0.0	0.0	0.0	0.1	0.8	1.6	2.4	6.4	10.4	14.4
	4,000	0.0	0.1	0.1	0.1	1.4	2.7	4.1	9.5	15.0	20.4
25	100	0.0	0.0	0.0	0.0	0.0	0.0	0.1	3.6	7.2	10.7
	1,000	0.0	0.0	0.0	0.0	0.0	0.1	0.1	4.2	8.3	12.4
	4,000	0.0	0.0	0.0	0.0	0.2	0.4	0.5	6.3	12.0	17.8
	8,840	0.0	0.0	0.0	0.0	0.0	0.0	0.0	6.1	12.3	18.4
	11,520	0.0	0.0	0.0	0.0	0.1	0.2	0.3	6.5	12.7	18.9
165	100	0.0	0.0	0.0	0.0	0.0	0.0	0.0	3.5	6.9	10.4
	1,000	0.0	0.0	0.0	0.0	0.0	0.0	0.0	3.8	7.5	11.3
	4,000	0.0	0.0	0.0	0.0	0.0	0.0	0.0	4.7	9.4	14.2
	8,840	0.0	0.0	0.0	0.0	0.1	0.1	0.1	5.2	10.3	15.4
	11,520	0.0	0.0	0.0	0.0	0.1	0.1	0.1	5.4	10.7	16.1
167	100	0.0	0.0	0.0	0.0	0.0	0.0	0.0	0.8	1.5	2.3
	1,000	0.0	0.0	0.0	0.0	0.0	0.0	0.0	3.5	7.0	10.5
	4,000	0.0	0.0	0.0	0.0	0.1	0.1	0.1	4.9	9.7	14.5
	8,840	0.0	0.0	0.0	0.0	0.1	0.2	0.3	5.6	11.0	16.4
	11,520	0.0	0.0	0.1	0.1	0.2	0.3	0.4	6.3	12.2	18.1
182	100	0.0	0.0	0.0	0.0	0.0	0.0	0.0	3.6	7.2	10.8
	1,000	0.0	0.0	0.0	0.0	0.0	0.0	0.0	4.3	8.5	12.8
	4,000	0.0	0.0	0.0	0.0	0.0	0.0	0.1	5.4	10.8	16.2
	8,840	0.0	0.0	0.0	0.0	0.1	0.1	0.2	6.2	12.2	18.2
	11,520	0.0	0.0	0.1	0.1	0.1	0.2	0.2	6.4	12.6	18.8
194	100	0.0	0.0	0.0	0.0	0.0	0.0	0.0	5.1	10.3	15.4
	1,000	0.0	0.0	0.0	0.0	0.0	0.0	0.0	4.7	9.5	14.2
	4,000										
	8,840										
	11,520	0.0	0.0	0.0	0.1	0.3	0.6	0.8	7.1	13.4	19.7

Fig. S6: Median Fe concentration in mg/l during extraction between the PW and OW 3, diagonal lines mark the 100 d shutdown and split observation period 1 & 2 (see Fig. 2), intermediate values are calculated by linear interpolation (see Tab. S3 for no. of samples)

SIR cycles	V_{extr} in m³	PW	←	6 m	→	OW 1	←	6 m	→	OW 2	←	6 m	→	OW 3
2	100	7.6	7.4		7.3	7.2	7.0		6.8	6.5	6.5		6.5	6.5
	1,000	7.4	7.2		7.1	6.9	6.7		6.6	6.4	6.4		6.4	6.5
	4,000	6.5	6.5		6.5	6.4	6.4		6.4	6.4	6.4		6.4	6.4
25	100	7.5	7.3		7.2	7.1	6.9		6.7	6.4	6.4		6.3	6.2
	1,000	7.2	7.0		6.9	6.7	6.5		6.4	6.2	6.2		6.2	6.2
	4,000	6.2	6.1		6.0	6.0	6.0		6.0	6.0	6.1		6.1	6.2
	8,840	6.1	6.1		6.1	6.1	6.1		6.1	6.1	6.1		6.2	6.2
	11,520	6.2	6.1		6.1	6.1	6.1		6.1	6.1	6.1		6.2	6.2
165	100	7.6	7.4		7.3	7.1	7.0		6.9	6.8	6.6		6.4	6.2
	1,000	7.3	7.1		7.0	6.9	6.8		6.7	6.6	6.4		6.3	6.1
	4,000	6.0	6.0		5.9	5.9	5.9		5.8	5.8	5.9		6.0	6.1
	8,840	6.0	6.0		6.0	6.0	6.0		6.0	6.0	6.1		6.1	6.2
	11,520	6.0	6.0		6.1	6.1	6.1		6.1	6.1	6.1		6.1	6.2
167	100	7.6	7.4		7.2	6.9	6.8		6.7	6.7	6.6		6.5	6.5
	1,000	7.8	7.6		7.4	7.1	7.0		6.9	6.7	6.6		6.6	6.5
	4,000	6.2	6.2		6.1	6.1	6.1		6.1	6.1	6.2		6.4	6.5
	8,840	6.7	6.6		6.5	6.5	6.5		6.5	6.5	6.6		6.6	6.7
	11,520	6.3	6.3		6.4	6.4	6.4		6.4	6.4	6.4		6.4	6.4
182	100	7.7	7.6		7.4	7.2	7.1		6.9	6.7	6.6		6.4	6.3
	1,000	7.8	7.4		7.1	6.8	6.6		6.5	6.4	6.3		6.2	6.1
	4,000	6.2	6.0		5.9	5.8	5.8		5.7	5.7	5.9		6.1	6.2
	8,840	6.0	6.1		6.3	6.5	6.5		6.5	6.5	6.5		6.5	6.6
	11,520	6.3	6.3		6.3	6.3	6.2		6.2	6.2	6.2		6.3	6.3
194	100	7.5	7.2		6.9	6.5	6.4		6.2	6.1	6.1		6.0	6.0
	1,000	7.5	7.2		6.9	6.7	6.5		6.3	6.1	6.0		6.0	6.0
	4,000													
	8,840													
	11,520	6.0	5.9		5.9	5.9	5.9		5.9	5.9	6.0		6.0	6.0

Fig. S7: Median pH during extraction between the PW and OW 3, diagonal lines mark the 100 d shutdown and split observation period 1 & 2 (see Fig. 2), intermediate values are calculated by linear interpolation (see Tab. S3 for no. of samples)

SIR cycles	V_{extr} in m³	PW	←	6 m	→	OW 1	←	6 m	→	OW 2	←	6 m	→	OW 3
2	100	168	163		159	155	144		134	124	130		136	142
	1,000	176	164		152	140	134		128	122	131		140	148
	4,000	145	140		134	128	130		131	133	138		143	148
25	100	189	184		178	173	172		171	170	170		171	171
	1,000	220	202		184	166	163		160	157	164		172	180
	4,000	146	141		137	132	138		143	149	169		189	209
	8,840	158	159		160	161	162		163	164	179		194	209
	11,520	164	163		161	160	162		163	165	180		195	211
165	100	193	185		178	170	164		157	150	152		154	156
	1,000	193	185		178	171	167		164	161	164		168	171
	4,000	175	157		140	122	118		115	111	135		158	182
	8,840	161	158		154	151	151		152	152	166		180	194
	11,520	167	164		160	156	156		156	156	169		182	195
167	100	181	177		173	170	168		166	165	166		167	169
	1,000	186	184		182	180	176		172	168	169		170	171
	4,000	159	145		131	117	112		107	102	134		166	199
	8,840	156	156		156	157	158		159	160	176		192	208
	11,520	172	170		168	166	166		166	165	180		195	211
182	100	198	193		189	185	180		176	171	169		166	164
	1,000	186	189		193	196	188		180	171	173		174	176
	4,000	157	141		125	110	103		96	89	125		160	196
	8,840	155	157		158	160	160		161	162	178		194	210
	11,520	174	171		168	165	165		165	165	181		197	213
194	100	195	202		208	215	191		167	143	156		169	181
	1,000	218	207		196	185	176		168	159	165		171	177
	4,000													
	8,840													
	11,520	173	169		165	161	161		162	163	179		196	213

Fig. S8: Median EC in µS/cm during extraction between the PW and OW 3, diagonal lines mark the 100 d shutdown and split observation period 1 & 2 (see Fig. 2), intermediate values are calculated by linear interpolation (see Tab. S3 for no. of samples)

SIR cycles	V_{extr} in m³	PW	← 6 m →		OW 1	← 6 m →		OW 2	← 6 m →		OW 3
2	100	3.1	3.0	3.0	2.9	2.3	1.8	1.2	1.0	0.7	0.5
	1,000	3.3	2.9	2.6	2.2	1.9	1.5	1.2	1.0	0.7	0.5
	4,000	2.8	2.5	2.3	2.0	1.7	1.3	1.0	0.9	0.7	0.6
25	100	3.2	3.1	3.1	3.0	2.7	2.5	2.2	2.0	1.7	1.5
	1,000	3.5	3.2	2.9	2.6	2.2	1.9	1.5	1.5	1.5	1.5
	4,000	3.4	3.0	2.5	2.1	1.9	1.7	1.5	1.3	1.2	1.0
	8,840	3.4	3.3	3.2	3.1	2.9	2.7	2.5	2.4	2.3	2.2
	11,520	3.5	3.5	3.5	3.5	3.5	3.6	3.6	3.3	2.9	2.6
165	100	3.5	3.1	2.8	2.5	2.3	2.2	2.0	1.8	1.5	1.3
	1,000	3.5	3.3	3.2	3.0	2.8	2.7	2.5	2.2	1.8	1.5
	4,000	3.5	3.3	3.2	3.0	2.8	2.7	2.5	2.4	2.2	2.1
	8,840	3.4	3.4	3.3	3.3	3.2	3.1	3.0	2.8	2.7	2.5
	11,520	3.5	3.4	3.4	3.3	3.2	3.1	3.0	2.8	2.6	2.5
167	100	3.9	3.6	3.3	3.0	2.9	2.7	2.6	2.6	2.6	2.7
	1,000	3.0	2.9	2.7	2.6	2.7	2.9	3.0	2.9	2.7	2.6
	4,000	3.5	3.3	3.0	2.8	2.6	2.4	2.2	2.4	2.5	2.7
	8,840	3.5	3.6	3.8	3.9	3.9	3.9	3.9	3.5	3.0	2.6
	11,520	4.0	4.0	4.0	4.0	4.2	4.3	4.5	3.9	3.2	2.6
182	100	2.9	2.8	2.7	2.6	2.4	2.3	2.2	2.3	2.4	2.5
	1,000	3.0	2.8	2.7	2.5	2.2	1.9	1.6	1.6	1.7	1.7
	4,000	3.5	3.0	2.6	2.1	1.8	1.4	1.1	1.4	1.7	2.0
	8,840	3.5	3.4	3.4	3.3	3.2	3.2	3.1	2.8	2.6	2.3
	11,520	3.6	3.5	3.5	3.4	3.5	3.6	3.8	3.2	2.6	2.0
194	100	3.4	2.7	2.1	1.5	1.8	2.2	2.5	2.5	2.5	2.5
	1,000	1.9	1.7	1.6	1.5	1.6	1.8	1.9	2.1	2.3	2.5
	4,000										
	8,840										
	11,520	4.0	3.8	3.7	3.5	3.7	3.8	4.0	3.5	3.1	2.6

Fig. S9: Median hardness in °dH during extraction between the PW and OW 3, diagonal lines mark the 100 d shutdown and split observation period 1 & 2 (see Fig. 2), intermediate values are calculated by linear interpolation (see Tab. S3 for no. of samples)

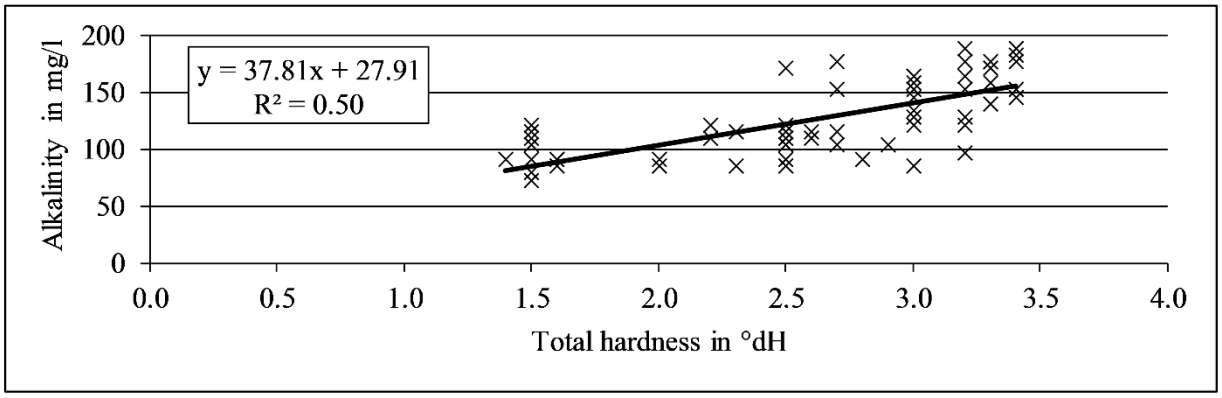

Fig. S10: Comparison of measured total hardness and measured alkalinity

SIR cycles	V_{inf} in m³	PW	←	6 m	→	OW 1	←	6 m	→	OW 2	←	6 m	→	OW 3
2	200	134	136	139		141	148	154		160	154	148		141
	2,000	126	116	105		94	83	71		60	64	69		73
	3,840	126	110	93		77	76	75		73	64	56		47
25	200	160	160	160		160	154	148		141	139	136		134
	2,000	149	146	144		141	131	121		111	101	91		81
	3,840	149	148	146		145	131	117		104	91	78		66
165	200	160	156	153		149	140	131		122	119	116		113
	2,000	139	136	132		128	125	122		119	109	98		88
	3,840	145	144	143		141	135	129		122	109	96		83
167	200	156	161	165		170	170	170		170	160	151		141
	2,000	166	161	156		151	142	133		124	116	108		100
	3,840	145	143	140		138	126	115		104	102	101		100
182	200	134	127	121		115	127	140		153	148	144		139
	2,000	139	138	136		134	125	116		107	112	117		122
	3,840	122	122	122		122	107	92		77	79	81		83
194	200	138	131	125		119	130	141		153	146	140		134
	2,000	149	146	144		141	127	114		100	116	133		149
	3,840	134	136	139		141	128	115		102	107	113		119

Fig. S11: Median HCO_3^- in mg/l during infiltration between the PW and OW 3, diagonal lines mark the 100 d shutdown and split observation period 1 & 2 (see Fig. 2), intermediate values are calculated by linear interpolation (see Tab. S3 for no. of samples)

SIR cycles	V_{extr} in m³	PW	←	6 m	→	OW 1	←	6 m	→	OW 2	←	6 m	→	OW 3
2	100	145	143	140		138	116	95		73	64	56		47
	1,000	151	138	124		111	98	86		73	64	56		47
	4,000	134	124	114		104	91	78		66	61	56		51
25	100	149	146	144		141	131	121		111	102	93		85
	1,000	158	147	136		124	111	98		85	85	85		85
	4,000	156	140	124		107	100	92		85	78	72		66
	8,840	156	153	149		145	138	130		122	119	115		111
	11,520	160	160	160		160	162	163		164	151	139		126
165	100	158	146	134		122	116	110		104	95	86		77
	1,000	160	154	148		141	135	129		122	110	97		85
	4,000	160	154	148		141	135	129		122	117	112		107
	8,840	156	155	153		151	147	143		139	134	128		122
	11,520	160	158	155		153	149	145		141	134	127		121
167	100	175	164	153		141	136	131		126	127	127		128
	1,000	141	136	131		126	131	136		141	136	131		126
	4,000	160	151	141		132	125	118		111	117	124		130
	8,840	160	165	170		175	175	175		175	159	143		126
	11,520	179	179	179		179	185	192		198	173	149		124
182	100	138	133	129		124	120	116		111	115	119		122
	1,000	126	121	115		110	100	90		81	82	83		84
	4,000	142	127	112		97	86	75		65	74	84		94
	8,840	142	140	138		136	134	131		129	121	112		103
	11,520	146	143	141		139	143	147		150	131	113		94
194	100	155	131	108		85	97	110		122	122	122		122
	1,000	98	93	88		83	88	94		100	107	115		122
	4,000													
	8,840													
	11,520	179	173	167		160	167	172.8		179	162	144		126

Fig. S12: Median HCO_3^- in mg/l during extraction between the PW and OW 3, diagonal lines mark the 100 d shutdown and split observation period 1 & 2 (see Fig. 2), intermediate values are calculated by linear interpolation (see Tab. S3 for no. of samples)

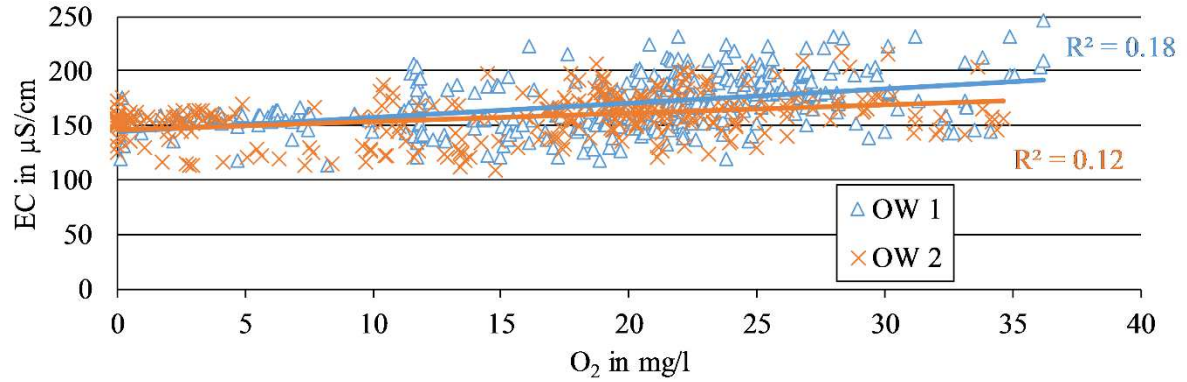

Fig. S13: Relation between O_2 and EC during infiltration phases at OW 1 and 2

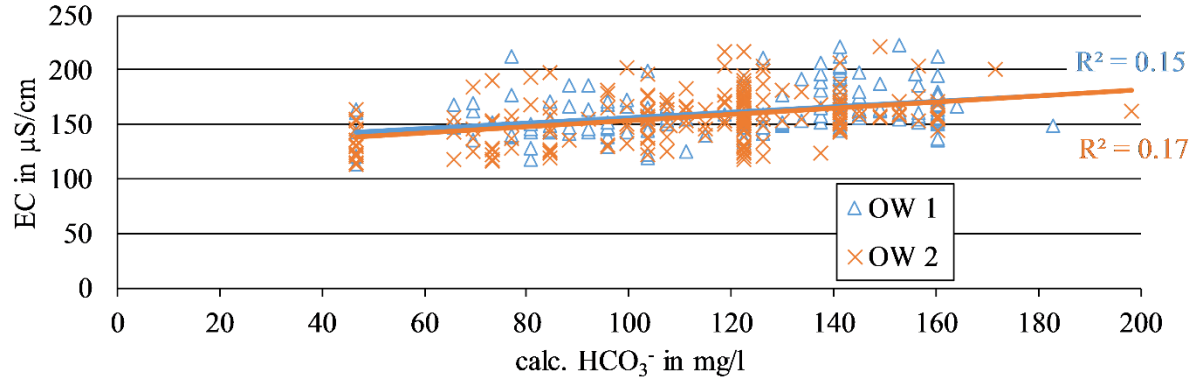

Fig. S14: Relation between HCO_3^- and EC during infiltration phases at OW 1 and 2

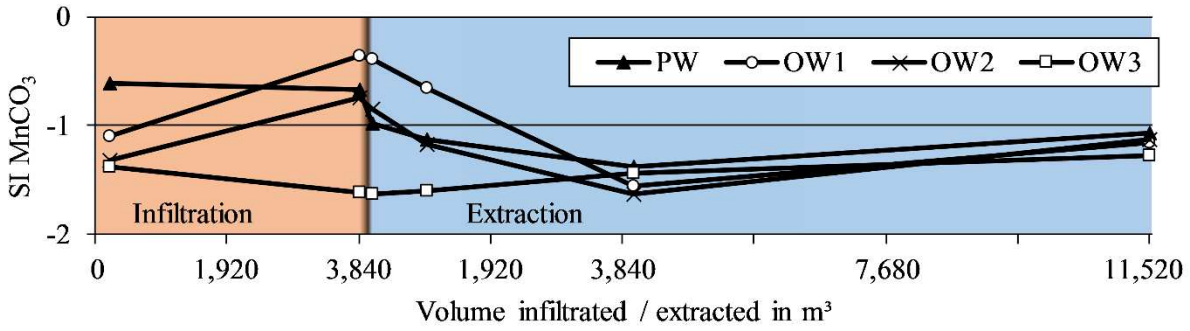

Fig. S15: Development of the saturation index for rhodochrosite during infiltration and extraction phases

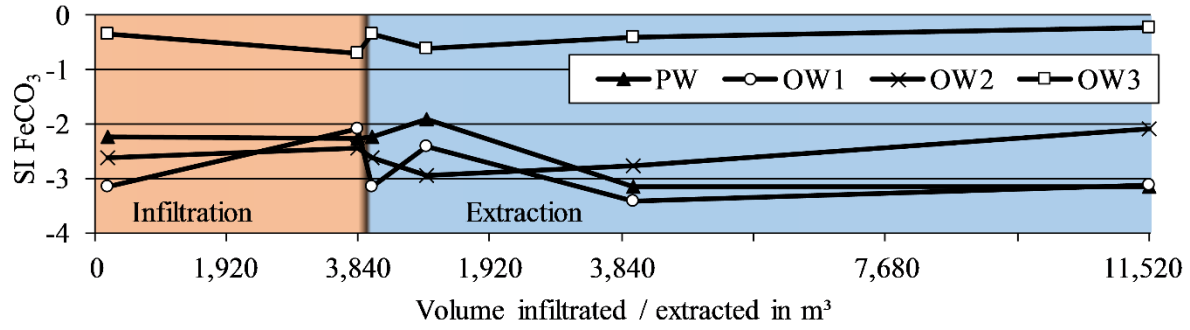

Fig. S16: Development of the saturation index for siderite during infiltration and extraction phases

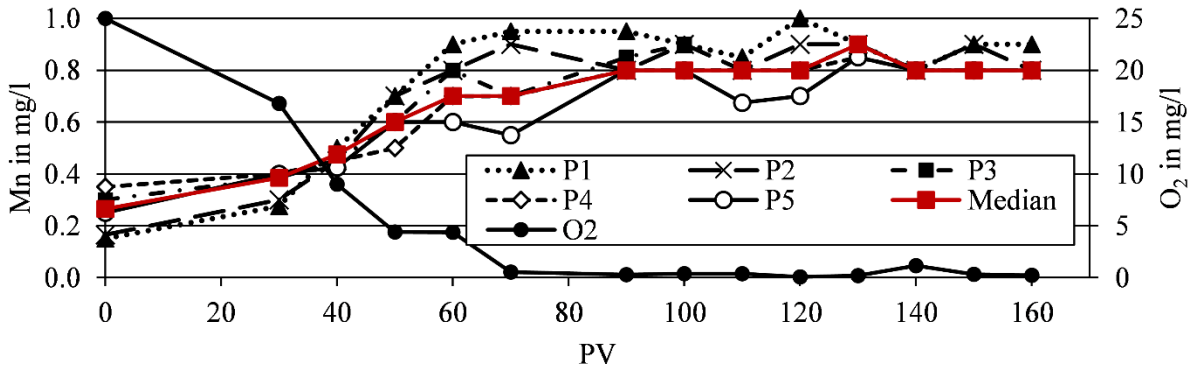

Fig. S17: Median Mn concentration along column SI for the entire observation period, each sampling port n=69, median of all five sampling ports n=345 (filled red boxes), Flow direction from P5 to P1 during extraction and vice versa during infiltration

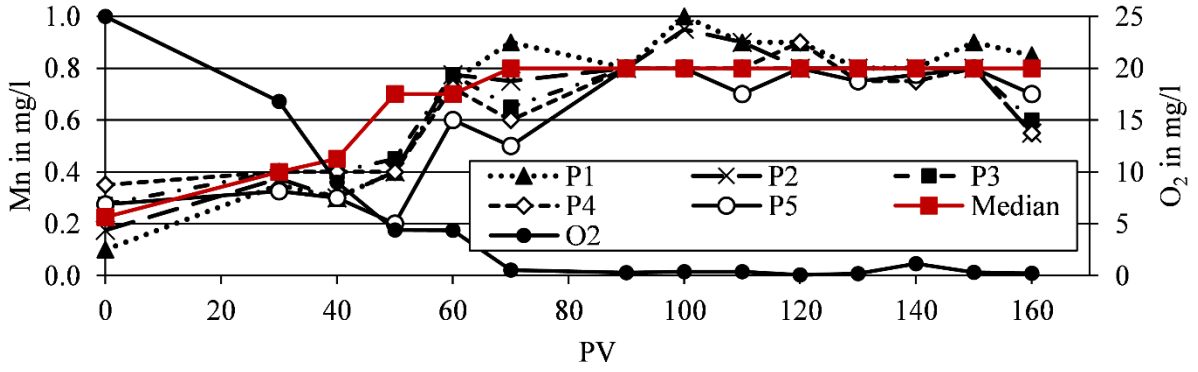

Fig. S18: Median Mn concentration along column SII for the entire observation period, each sampling port n=69, median of all five sampling ports n=345 (filled red boxes), Flow direction from P5 to P1 during extraction and vice versa during infiltration

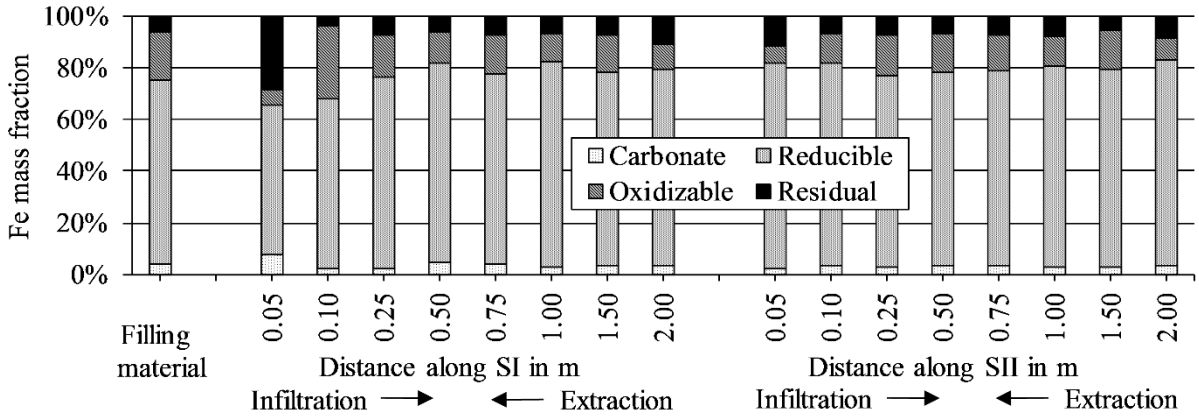

Fig. S19: Distribution of the Fe fractions along column SI & SII compared to the original filling material

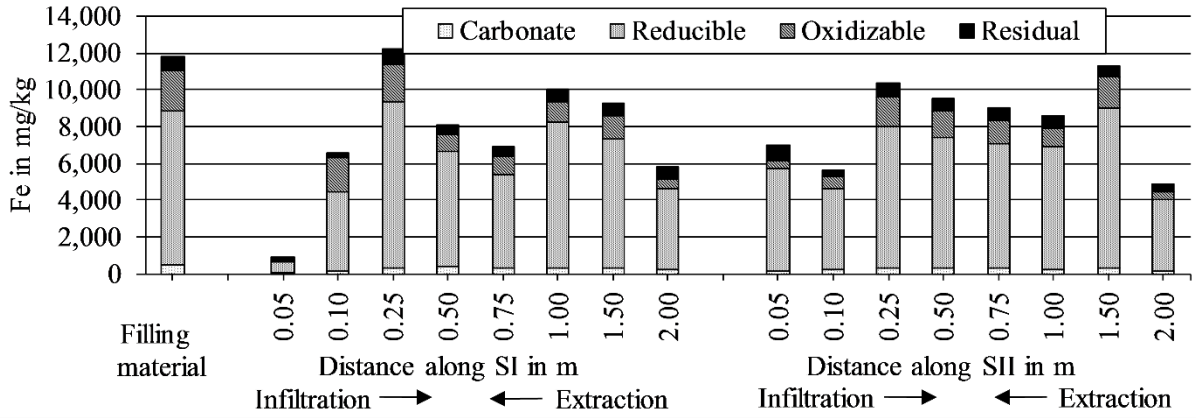

Fig. S20: Sum of the Fe fractions along column SI & SII compared to the unaffected filling material

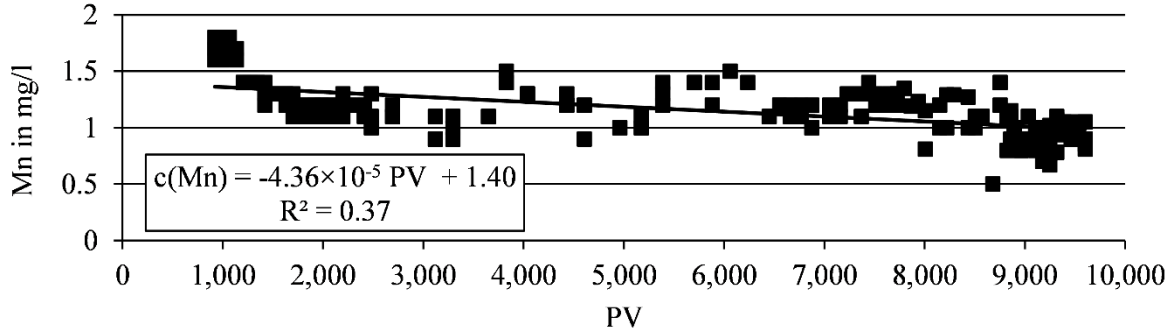

Fig. S21: Maximum Mn concentration at the end of extraction phases with $V_{EXT} \geq 9{,}000$ m³ (n=188), time after start-up is represented by total exchanged PV from OW 3 to the PW

Beiliegende Publikation 7

Paufler, S., Grischek, T., Adomat, Y., Herlitzius, J., Hiller, K., Metelica, Y. (2018) Effective range of chlorine transport in an aquifer during disinfection of wells: from laboratory experiments to field application. J. Hydrol. 559, 711-720. doi: 10.1016/j.jhydrol.2018.02.054.

Journal of Hydrology 559 (2018) 711–720

Contents lists available at ScienceDirect

Journal of Hydrology

journal homepage: www.elsevier.com/locate/jhydrol

Research papers

Effective range of chlorine transport in an aquifer during disinfection of wells: From laboratory experiments to field application

S. Paufler [a,*], T. Grischek [a], Y. Adomat [a], J. Herlitzius [b], K. Hiller [b], Y. Metelica [c]

[a] Dresden University of Applied Sciences, Friedrich-List-Platz 1, 01069 Dresden, Germany
[b] Arcadis Germany GmbH, EUREF-Campus 10, 10829 Berlin, Germany
[c] Vodokanal Khabarovsk, Topograficheskiy per. 12, 680000 Khabarovsk, Russia

ARTICLE INFO

Article history:
Received 10 January 2018
Received in revised form 14 February 2018
Accepted 16 February 2018
Available online 17 February 2018
This manuscript was handled by Huaming Guo

Keywords:
Well disinfection
Aquifer storage & recovery
Subsurface iron removal
1st-order consumption
Column experiments

ABSTRACT

Microbiological contamination usually leads to erratic operation of drinking water wells and disinfection is required after disasters and sometimes to restore proper well performance for aquifer storage and recovery (ASR) and subsurface iron removal (SIR) wells. This study focused on estimating the fate of chlorine around an infiltration well and improving the knowledge about processes that control the physical extent of the disinfected/affected radius. Closed bottle batch tests revealed low chlorine consumption rates for filter gravel and sand (0.005 mg/g/d) and higher rates for clay (0.030 mg/g/d) as well as natural aquifer material (0.054 mg/g/d). Smaller grain sizes <1 mm showed 10- to 70-times higher initial chlorine consumption rates within the first hour after contact compared to the median consumption rates. Initial chlorine concentration most likely does not impact disinfection ability at grain sizes >1 mm, but results in more effective disinfection for very fine material <0.063 mm. Column studies focused on the adaptation of the lab results to an actual SIR waterworks in Khabarovsk, Russia. Results reinforced the previous lab results with low 1st-order decay constants of 16 d^{-1} for filter material and much higher values of 254 d^{-1} for natural aquifer material. Application of the chlorine consumption rates to an example well consistently indicated that the filter gravel pack consumes <1% of infiltrated chlorine. The disinfection zone at the example well seems to extend to maximum 3.5 m into the aquifer. Excessive chlorine dosage of >10 mg/l would not further extend the disinfected radius. A preferable way to increase the range of chlorine application is to increase the total infiltrated volume and time. Three approaches are proposed for adapting lab results to actual infiltration wells, that are in principle applicable to any other site.

1. Introduction

During environmental disasters like the tsunami in Southeast Asia in 2004 or hurricane Katrina in 2005, thousands of (drinking) water wells were contaminated after surface water entered the wells (Copeland, 2005; Englande, 2008). Microbiological contamination caused by disasters like these usually leads to erratic operation of drinking water wells, requiring disinfection to restore proper well performance and water quality. Apart from clean-up in the aftermath of disasters, disinfection of wells can become necessary to maintain proper well performance during regular operation. Aquifer Storage and Recovery (ASR) has become a popular water management technique in Europe (Stuyfzand et al., 2005; Zuurbier, 2016, Sprenger et al., 2017), the US (Pyne, 2005), Australia (Dillon et al., 2016) and at many other sites in the world. ASR is intentionally used to store water in an aquifer during excess periods, and later recover water from the groundwater reservoir during periods of water shortage. If sediments of the target aquifer contain iron and/or manganese minerals and reductive dissolution of those minerals occurs during low O_2-concentrations (<0.5 mg/L) and low pH (<7.1) in the aquifer, elevated concentrations of dissolved iron (Fe) and manganese (Mn) may be observed in the recovered water (Stuyzand et al., 2005). Subsurface iron removal (SIR) is a widely used and approved pre-treatment technology for removing dissolved iron and manganese from groundwater (Hallberg and Martinell, 1976; Rott and Friedle, 2000). The principle of SIR is closely related to ASR: the injection of aerated water into an anoxic aquifer forms a so-called oxidation zone. Within this zone, dissolved and adsorbed Fe(II) and Mn(II) is oxidized to Fe(III) and Mn(IV) and deposited as metal(hydr)oxides. After a comparably short storage period of a few hours or days, the water can be recovered without containing dissolved iron or manganese.

* Corresponding author.
E-mail address: sebastian.paufler@htw-dresden.de (S. Paufler).

https://doi.org/10.1016/j.jhydrol.2018.02.054
0022-1694/

Nomenclature

25 %ile	25-percentile (First Quartile)
75 %ile	75-percentile (Third Quartile)
AM	Aquifer material
AMf	Aquifer material with a grain size <0.063 mm
ASR	Aquifer storage and recovery
C_0	Chlorine concentration at point 0 (mg/l)
$C_{Cl,0}$	Initial chlorine concentration in batch tests (mg/l)
$C_{Cl,Bl,0}$	Initial chlorine concentration in blind samples (mg/l)
$C_{Cl,Bl,j}$	Chlorine concentration after time interval j in blind samples (mg/l)
$C_{Cl,j}$	Chlorine concentration after time interval j (mg/l)
Cl	Chlorine, unspecified (mg/l)
$C_{t,i}$	Chlorine concentration at point i along the flow path (mg/l)
d_F	Filter screen diameter (m)
Δd_i	Distance from a well filter screen to point i (m)
EC	Electric conductivity (μS/cm)
Fe	Iron
FM	Filter material
FMf	Filter material with a grain size 0.01–1.00 mm
GW	Groundwater
IFM	Inductive flow meter
k	First order chlorine decay constant (d^{-1})
k_{Cl}	Mass related chlorine consumption rate (mg/g/d)
$k_{Cl,1h}$	Mass related chlorine consumption rate for the first hour after contact (mg/g/d)
l_F	Length of the well filter screen (m)
m_{aq}	Aquifer mass (kg)
$m_{Cl,PV}$	Chlorine mass within a certain pore volume (mg)
Mn	Manganese
$m_{S,d}$	Dry mass of a sample (g)
n	Number of samples
NaClO	Sodium hypochlorite
n_e	Effective porosity (−)
O_2	Dissolved oxygen (mg/l)
OW	Observation well
PV	Exchanged pore volumes (−)
PV_{Aq}	Exchanged PV of the aquifer (−)
PV_{Col}	Exchanged PV of the experimental columns (−)
PW	Production well
Q	Pumping rate (m^3/h)
qPCR	quantitative real-time Polymerase Chain Reaction
RMSE	Root-mean-square-error
SE	Standard error
SIR	Subsurface iron removal
T	Temperature (°C)
t_a	Travel time (min or d)
$t_{a,i}$	Travel time from point 0 to i (d)
Δt	Elapsed time after addition of chlorinated water (d)
V_{aq}	Aquifer volume (m^3)
V_{inf}	Infiltration volume (m^3)
V_{PV}	Pore volume of an aquifer section (m^3)
V_w	Volume of chlorinated water (l, liter)

Stuyfzand et al. (2005) and Zuurbier (2016) documented the potential benefits of using the principle of SIR during ASR.

Since the injection water for ASR and SIR sometimes contains undesirable bacterial agents and nutrients, problems can occur with the growth of both aerobic and anaerobic bacteria in surface equipment, pumps, downhole equipment and within the formation itself (Martin, 2013). If performance of an ASR well is declining and it is not clogged by fine particles or air bubbles, clogging is mostly biological in the form of bacterial cells and their extracellular polymeric substances forming slime on the wall of the well (Bouwer, 2002). Chlorination of the injection water is sometimes used as pretreatment because it helps to prevent well clogging and to control microbial fouling inside or around the injection/recovery well (Pavelic et al., 2005). In laboratory column experiments with tap water, Holländer et al. (2005) found biological clogging to be the main reason for a decreasing hydraulic conductivity and recommended adding chlorine to the infiltration water for ASR wells.

A wide span of recommended chlorine dosages are given in the literature on well disinfection. For "shock chlorination" after disasters, recommendations for chlorine dosages range from around 10 mg/l (NHDES, 2015) up to 50 and 200 mg/l (MDH, 2015). To control biological growth in ASR wells, a common approach is to keep the chlorine concentration between 1 and 3 mg/l in the infiltrating water during recharge (Bouwer, 2008). Additionally, it is advised to maintain a permanent trickle flow (0.5–1 m^3/h) of water with >1.5 mg/l chlorine into the well during periods of storage to preserve recharge-specific capacity and to avoid bacterial clogging (Pyne, 1995; Bouwer, 2008).

Most of the recommendations for well disinfection after disasters estimate the necessary chlorine dose based on the casing diameter and the water level in the well but do not consider additional chlorine depletion when the chlorinated waters enters the gravel pack and the aquifer. Furthermore, despite the great importance of a proper well disinfection in case of ASR and SIR wells that suffer from biological clogging, to the authors' knowledge no research has yet been carried out that focused on the actual disinfected/affected radius around the well. Therefore, the aims of this study were to estimate the fate of chlorine after injection into an infiltration well and improve the knowledge about processes that control the extent of the "disinfected" radius. In this paper the term "disinfection" will be used, but it is important to mention that complete disinfection can rarely be achieved when disinfectant is added to a natural sediment.

Chlorine consumption rates of filter gravel, filter sand, clay and natural aquifer material were determined in closed bottle batch tests. Additional column studies focused on the transfer of the lab results to an actual SIR waterworks in Khabarovsk, Russia. To simulate infiltration cycles, 3 columns filled with aquifer material and 1 column with filter gravel run in the SIR waterworks in Khabarovsk continuously parallel to the actual well cycles over a time period of 60 days. Three evaluation approaches showed consistent results for the application of lab and column test results to the actual operation of SIR wells in Khabarovsk. Based on this experience, general suggestions are given for the effective use of chlorine at infiltration wells.

2. Materials & methods

2.1. Field site Khabarovsk

The city of Khabarovsk is located in the Far East of Russia at the confluence of the Ussuri and Amur Rivers. To control elevated iron concentrations in the natural groundwater, SIR (Subterra-technique) is applied as a pre-treatment step (Herlitzius et al., 2012). The specific yield of the production wells (PW) started to decrease after a few months of operation and dropped to almost half of the initial value within one year. According to Herlitzius (2014), this decrease is mainly caused by accumulated biomass from iron-, manganese- and methane-oxidizing bacteria in the well

and filter gravel pack. To expand the oxidation zone, field trials with technical O_2 were carried out. Furthermore, sodium hypochlorite (NaClO) is added to the infiltration water to prevent further growth of biomass, but the chemical reactions after infiltration and the effects on the raw water quality are not yet fully understood.

Lab results were transferred to the PW that was used for water supply during the column studies. The actual well in the SIR waterworks in Khabarovsk had a casing diameter of 0.35 m, a 0.1-m-thick filter gravel pack and a filter screen height of 5 m. The infiltration time was 48 h at an infiltration rate of 80 m^3/h. The abstraction rate was 160 m^3/h over a time period of 72 h.

2.2. Set-up of the column experiments

Altogether 3 columns with aquifer material and 1 column with filter gravel were set up in the SIR waterworks in Khabarovsk (Tab. S1). The columns ran according to the infiltration (48 h) and pumping cycles (72 h) of a production well (PW). Two diaphragm pumps (delta opto-drive, ProMinent, Heidelberg, Germany) pumped infiltrate from the PW (infiltration cycles) or groundwater (GW, abstraction cycles) from an observation well (OW) into the columns. Flow direction in all columns was from bottom to top during infiltration and vice versa during abstraction. Since the OW was drilled at the inner edge of the oxidation zone of the PW, actual SIR processes were assumed to be completed and thus not simulated in the columns.

During infiltration, chlorine was measured before the columns and at sampling ports at 0.05 m and subsequently every 0.5 m along the columns (Fig. S1). Temperature (T), dissolved oxygen (O_2), pH and electrical conductivity (EC) were determined using WTW Multi 3430 and appropriate electrodes (WTW, Weilheim, Germany) in flow-through cells before and after the columns. Pressure was measured with digital pressure gauges (DM 01, BD Sensors, Germany). An inductive flow meter (IFM, MAG 5000, Siemens, Germany) was installed for flow measurements after the columns.

Each column had an inner diameter of 0.1 m and was made up of opaque PVC. For logistical reasons, the experiment was performed in two consecutive set-ups (Table S1). Chlorine consumption rates of filter gravel (grain size: 1–2 mm) from the local wells and of aquifer material obtained from a core drilling (sieved to grain size <4 mm) were determined within the first set-up. Subsequently, two additional columns were set-up with aquifer material from another core drilling. To enable higher flow rates and chlorine loads within an infiltration cycle while having the same travel time, columns of the second set-up were extended to a length of 2 m (Fig. S2).

During filling of the columns, the sediment mass was measured using a balance to calculate the bulk density and assess the compaction of the material in the columns. Mean travel time (t_a) and porosity (n_e) for both columns were determined from electrical conductivity (NaCl) breakthrough curves from tracer experiments performed before start-up. Flow rate and head loss were taken to calculate hydraulic conductivity by applying Darcy's law.

Water samples were taken 0.05, 0.5 and every 0.5 m along the columns. Free and total chlorine were determined for every sample with a photometer (AL200, Aqualytic, Germany). All data shown for chlorine in this study refer to free chlorine.

2.3. Closed bottle batch test

Chlorine consumption rates of filter gravel, filter sand, clay and natural aquifer material were determined in closed bottle batch tests. Altogether eight samples were studied: four grain sizes of filter material, two different clays and two grain sizes of natural aquifer material (Table S2). For each sample, chlorine consumption rates were determined for an initial chlorine concentration of 1.8 and 3.6 mg/l and for each concentration in triplicate in three independent 250 ml glass-stoppered conical flasks (Table 1). Blind chlorine consumption was determined in parallel using two additional 250 ml flasks without sediment. After filling the tested materials into the flasks, chlorinated water was added at a ratio of 1:10 (w/w dry mass). Chlorinated water was prepared by diluting 16% sodium hypochlorite solution (NaClO, Grade: GPR Rectapur®, VWR Chemicals, France) with distilled water. For airtight sealing of the flasks, water was slightly overflowing when the ground-glass stoppers were plugged in. All flasks were hand-shaken before storage. Storage temperature was 15 to 20 °C and the flasks were protected from incident light.

To examine time-dependent chlorine depletion by the material as well as the impact of multiple chlorine dosages on the depletion rate, residual chlorine was measured following two approaches (Table 1). In the first approach, samples were taken 1, 2, 4, 6, 8, 12, 24, 36, 48, 60 and 72 h after adding chlorinated water. For each measurement, 10 ml of water was sampled with a rinsed syringe and the residual chlorine concentrations (both free and total) were determined with a photometer (AL200, Aqualytic, Germany). The sample volume was replaced by distilled water, the flasks hand-shaken and returned to storage. Samples for the second approach were taken after 24, 48 and 72 h. Following the determination of residual chlorine on one sampling event, used water was removed from the flasks and replaced by fresh chlorinated water. Subsequently, the flasks were hand-shaken and returned to the storage. Since the used glass-stoppered conical flasks didn't fit into a centrifuge, water was removed by a syringe after making sure that the sediment settled down and the water showed no visible turbidity.

Evaluation of the batch experiments aimed to get a decay constant (Eq. (1)) to be applied to control the operation of the actual wells. Implementation of the blind consumption rate minimized a possible error from chlorine consumption by the glass-stoppered conical flasks themselves, and accounted for the change of chlorine mass due to sampling and replacement with distilled water.

$$k_{Cl} = \frac{(C_{Cl,0} - C_{Cl,j} - C_{Cl,Bl,0} + C_{Cl,Bl,j}) \times V_W}{m_{S,d} \times \Delta t} \quad (1)$$

with $C_{Cl,0}$ and $C_{Cl,Bl,0}$, being initial chlorine concentrations (mg/l) in the sample and the blind and $C_{Cl,j}$, and $C_{Cl,Bl,j}$ being measured chlorine concentration (mg/l) after time interval j, respectively. V_W represents the volume of added chlorinated water (l). $m_{S,d}$ and Δt referring to the dry mass of the sample (g) and the elapsed time (d) since adding chlorinated water. Hence, the derived decay constant k_{Cl} (mg/g/d) accounts for the mass being in interaction with chlorine as well as for the exposure time of chlorine to the material.

2.4. Adaptation of lab results to optimize operation of an actual infiltration well

Three approaches were taken to adapt the experimental results for practical application in the operation of an infiltration well in Khabarovsk. These can be used in principle for similar situations with infiltration wells anywhere in the world, and are described below.

2.4.1. 1st-order chlorine decay

Most models reported in the literature simulated chlorine decay in drinking water systems by using a first- or second-order kinetic expression (Vasconcelos et al., 1996; Boccelli et al., 2003; Warton et al., 2006). Since the flow path of a water molecule along the

Table 1
Experimental design of the batch experiments for each type of sediment and sample numbers.

Sediment	e. g. Aquifer material <4 mm							
Approach	Time-dependent chlorine consumption						Blind	Blind
Cl in mg/l	1.8			3.6			1.8	3.6
Sample	1	2	3	4	5	6	7	8
Approach	Impact of multiple chlorine dosage						Blind	Blind
Cl in mg/l	1.8			3.6			1.8	3.6
Sample	9	10	11	12	13	14	15	16

pores of an aquifer can be seen as flow along a very fine pipe, application of this existing approach was reasonable. To have as few unknown equation parameters as possible, a 1st-order chlorine decay model (Eq. (2)) was chosen to transfer the data obtained by column experiments to an actual well for predicting the fate of chlorine and the potential disinfection range within an aquifer:

$$C_{t,i} = C_0 \times e^{-k \times t_a} \quad (2)$$

with $C_{t,i}$ representing the chlorine concentration (mg/l) at point i after travel time t_a (d), C_0 is the initial chlorine concentration at point 0 (mg/l), and k is the first-order decay constant (d^{-1}). Decay constant k was derived by simulating the chlorine profiles along the columns with Eq. (2) and minimizing the difference between measured and simulated chlorine profiles. Root-mean-square-error (RMSE) was chosen as the best-fit indicator. Thus, each measured profile resulted in one value for k. Assuming a cylindrical distribution of infiltrate around the well (Eichhorn, 1985; Winkelnkemper, 2004), travel times $t_{a,i}$ from a well to point i within the aquifer can be calculated using Eq. (3):

$$t_{a,i} = \frac{\pi \times \Delta d_i^2 \times n_e \times l_F}{12 \times Q} \quad (3)$$

with Δd_i being the distance (m) from the well filter screen to point i within the aquifer, n_e and l_F representing effective porosity (−) and the length of the well filter screen (m). Q is the pumping rate (m^3/h) of the PW. Finally, Eq. (2) can be used to calculate $C_{t,i}$ as chlorine concentration (mg/l) in the aquifer with C_0 being the chlorine concentration (mg/l) in the infiltrating water, using k-values (d^{-1}) from the column experiments and replacing t_a in Eq. (2) by $t_{a,i}$ from Eq. (3).

2.4.2. Chlorine consumption related to mass and exposure time

To transfer the derived decay constant k_{Cl} (mg/g/d) from the batch tests to an aquifer section, total aquifer mass being in interaction with chlorine and the exposure time of chlorine to the aquifer material need to be determined. Assuming a cylindrical distribution of infiltrate around the well, aquifer volume V_{aq} between a well and point i within the aquifer can be calculated using Eq. (4):

$$V_{aq} = \pi \times l_F \times (\Delta d_i^2 - d_F^2) \quad (4)$$

with Δd_i being the distance (m) from the well filter screen to point i within the aquifer, d_F and l_F representing diameter (m) and length of the well filter screen (m). Multiplying Eq. (4) with the bulk density (kg/m^3) gives the total aquifer mass m_{aq} (kg) until point i. The pore volume (PV) of that section V_{PV} (m^3) results from multiplying Eq. (4) by the effective porosity n_e (−).

The theoretical chlorine mass within the pore volume ($m_{Cl,PV}$ in mg) is given by multiplying the PV by the chlorine concentration (mg/l) in the infiltrating water (5).

$$m_{Cl,PV} = V_{PV} \times C_0 \times 1000 \quad (5)$$

Finally, the calculated chlorine concentration $C_{t,i}$ (mg/l) at point i can be derived by Eq. (6). Travel time $t_{a,i}$ to point i is calculated according to Eq. (3).

$$C_{t,i} = \frac{(m_{Cl,PV} - k_{Cl} \times m_{aq} \times t_{a,i})}{V_{PV} \times 1000} \quad (6)$$

2.4.3. Correlation of chlorine concentration and exchanged pore volumes

Correlation of measured chlorine concentration along the three columns with aquifer material and the exchanged pore volumes (PV_{Col}) for a certain sampling point served as a third approach for chlorine transport range estimation. Linear regression resulted in three separate functions (Fig. S3). Eq. (7) represents the median slope of the three functions. The offset term of each function was not taken into account. An offset of Eq. (7) would avoid that $C_{t,i}$ could virtually become 0 mg/l.

$$C_{t,i} = 0.00077 \times PV_{Col} \quad (7)$$

Exchanged pore volumes within the aquifer (PV_{Aq}) can be calculated using Eq. (8), with V_{inf} representing the total infiltration volume (m^3). Other coefficients are stated above.

$$PV_{Aq} = \frac{V_{inf}}{\pi \times (\Delta d_i^2 - d_F^2) \times l_F \times n_e} \quad (8)$$

Assuming that the linear relation of Eq. (7) derived by the column experiments can be applied to an infiltration well, Eq. (7) was transformed to PV_{Col} and equated with Eq. (8). Finally, the resulting relation $PV_{Col} = PV_{Aq}$ was iteratively solved for a certain chlorine concentration within the aquifer $C_{t,i}$ with Δd_i as variable. The resulting Δd_i (m) represents the estimated range.

2.5. Solid material analysis following the column experiments

To assess the impact of chlorine to biological growth around a well, samples from filter sand (column 1, set-up 1) and aquifer material (columns 3 & 4, set-up 2) were further treated after completing the experiments. Samples were taken 0.05, 0.5 and every 0.5 m along the columns corresponding to water sampling port positions. The material was recovered by a rinsed scoop and immediately filled into sterile sample containers. Excavation was carried out wearing sterile laboratory gloves. Samples were stored at 4 °C before analysis.

Lab analysis aimed to take grown biomass as an indirect parameter for total existing DNA per gram aquifer material. The DNA quantity was determined by quantitative real-time Polymerase Chain Reaction (qPCR). Target organisms were for example *Rhodoferax* spp. and *Gallionella* sp. Further details about the applied primer and standards are described in Braun et al. (2016) and Herlitzius (2014).

3. Results

3.1. Chlorine consumption along the columns and derived rate constants for 1st-order chlorine decay

Within the 1st set-up, columns 1 (filter gravel) and 2 (aquifer material) ran over a time period of altogether 9 weeks, and 11

infiltration cycles were simulated. For the 2nd set-up with column 3 and 4 (both aquifer material), 11 infiltration cycles were simulated during 10 weeks of experimental time. Median chlorine concentration in the inflow water from the PW to the columns was 1.6 mg/l (n = 123 and 47) for set-up 1 and 2 (Table S3). Median pH in the inflow water was pH 8 (n = 126 and 61) for both set-ups and median temperature during set-up 1 and 2 was 7.3 °C (n = 126) and 7.9 °C (n = 60).

The inflow concentration of around 1.6 mg/l chlorine decreased within the first 1–2 min of travel time in column 1 (filter gravel) to around 1.58 mg/l (≈1% less) and dropped in columns 2, 3 and 4 with aquifer material to 0.54 (≈66% less), 1.17 (≈27% less) and 1.28 mg/l (≈23% less, Table S4). Fig. 1 shows that the chlorine concentration in column 1 decreased further to around 1.0 and 0.5 mg/l along the flow path. At the subsequent sampling point along columns 2–4 after 10–20 min travel time, chlorine concentrations further dropped to approx. 0.15 mg/l. For an observation period of one infiltration cycle, chlorine concentrations along column 1 increased at all three sampling points to >1 mg/l at the end of one cycle (1-1 to 1-3, Fig. S4). Along columns 2–4, a similar increase was noticed at the first measuring points (2-1, 3-1 and 4-1) but in none of the columns further along the flow path (Figs. S5–S7).

Simulation of the obtained chlorine profiles along column 1 led to a 1st-order decay constant of k = 16 d^{-1} (median, n = 34) for filter gravel (Table 2). Since most of the measured profiles along column 1 looked similar to the median graph (Fig. 1), application of a 0th-order function was tested and led to an equal median value. Median values of k for aquifer material derived from columns 2, 3 and 4 were k = 574 d^{-1} (n = 31), 224 d^{-1} (n = 28) and 223 d^{-1} (n = 28). Combining the results for aquifer material gave a median value of 256 d^{-1} (n = 79).

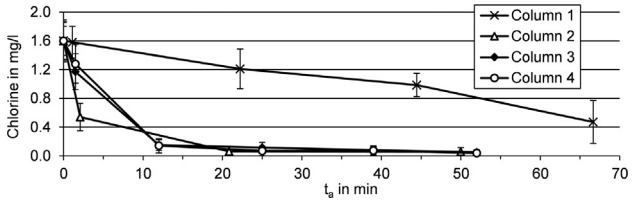

Fig. 1. Median values for chlorine along Column 1 (n = 34), 2 (n = 31), 3 (n = 28) and 4 (n = 28) over the total experimental time of each column, error bars indicating SE.

3.2. Mass-related chlorine consumption

Mass related chlorine consumption rate constants k_{Cl} (mg/g/d) of filter gravel, filter sand, clay and natural aquifer material were determined in closed-bottle batch tests (Table 3). The two largest grain size fractions 3.15–5.60 and 2.00–3.15 mm showed the lowest consumption rates with 0.003 mg/g/d (median, each n = 90). Median values of 0.004 and 0.011 mg/g/d (each n = 90) were determined for filter sand grain size fractions 1.00–2.00 and 0.10–1.00 mm. Both clay samples showed much higher rate constants of 0.031 and 0.030 mg/g/d (each n = 36). Since the clay samples consumed the chlorine much faster (Section 3.3), fewer samples were taken for time-dependent sampling. The highest chlorine consumption rates were determined for the natural aquifer material from Khabarovsk. The mixed sample (grain size <4 mm) showed a k_{Cl}-value of 0.039 mg/g/d (median, n = 102) and the highest rate constant of 0.156 mg/g/d (median, n = 96) was determined for the clay fraction of the aquifer material.

Median chlorine consumption rate constants for all grain size fractions of filter gravel & sand, clay and the natural aquifer material are 0.005 mg/g/d (n = 360), 0.030 mg/g/d (n = 72) and 0.054 mg/g/d (n = 198).

3.3. High chlorine consumption after initial contact

Chlorine consumption rates for the time period of 1 h after initial contact of the chlorine solution with the materials ($k_{Cl,1h}$) were determined for initial chlorine concentrations of 1.8 and 3.6 mg/l (Fig. 2). Because rate constants for grain size fractions >1 and <1 mm of filter gravel and sand as well as for clay 1 and 2 showed only minor variations, results are given as median for filter material (FM) >1 and <1 mm as well as for clay. Determined rate constants 1 h after contact for an initial chlorine concentration of 1.8 and 3.6

Table 2
1st-order decay constants k for chlorine derived from the column experiments.

Set-up	Column	Material	k in d^{-1}						
			Min.	25 %ile	Median	75 %ile	Max.	n	RMSE
1	1*	Filter gravel	0	12	16	24	36	34	0.18
	2	Aquifer material	124	334	574	820	1293	31	0.03
2	3		113	164	223	434	902	28	0.09
	4		56	130	224	255	1102	28	0.67
1&2	2–4	Aquifer material	56	178	256	649	1293	79	0.09

* Application of a 0th-decay ($C_{t,i} = C_0 - k \cdot t_{a,i}$) resulted in equal k-values, data not shown.

Table 3
Mass-related chlorine consumption rate constants k_{Cl} derived from batch tests.

Material	Grain size in mm	k_{Cl} in mg/g/d					
		Min.	25 %ile	**Median**	75 %ile	Max.	n*
Filter gravel & sand	3.15–5.60	0.000	0.002	0.003	0.007	0.264	90
	2.00–3.15	0.000	0.001	0.003	0.007	0.264	90
	1.00–2.00	0.000	0.003	0.004	0.009	0.258	90
	0.10–1.00	0.000	0.007	0.011	0.030	0.252	90
Clay 1	<0.063	0.012	0.020	0.031	0.067	2.112	36
Clay 2	<0.063	0.010	0.023	0.030	0.067	2.082	36
Aquifer material	<4.00	0.007	0.024	0.039	0.123	0.402	102
	<0.063	0.009	0.045	0.156	0.428	2.303	96

* Combined statistical data for time dependent sampling and multiple chlorine application.

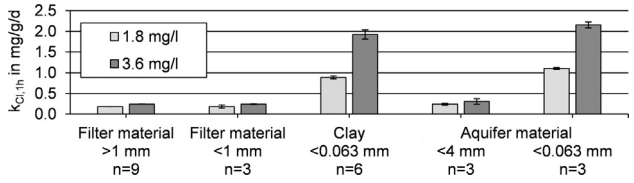

Fig. 2. Median values of mass-related chlorine consumption rate constants for the time period of 1 h after initial contact of the chlorine solutions with the materials, error bars indicating SE.

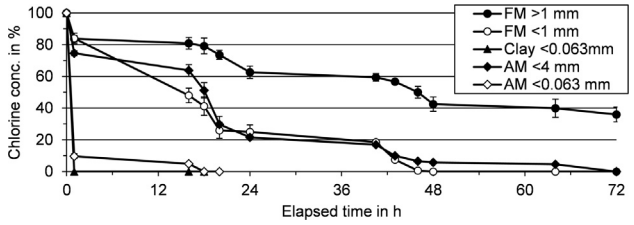

Fig. 3. Development of chlorine concentration over a time period of 72 h for initially 1.8 mg/l chlorine, median values for filter material >1 (n = 9) and <1 mm (n = 3), clay (n = 6), aquifer material <4 (n = 3) and <0.063 mm (n = 3), error bars indicating SE.

mg/l for filter material >1 and <1 mm were 0.18 and 0.24 mg/g/d. Mixed aquifer material (<4 mm) was in the same order of magnitude with $k_{Cl,1h}$-values of 0.24 and 0.30 mg/g/d. Clay and fine aquifer material (<0.063 mm) showed much higher consumption rates of 0.89 and 1.10 mg/g/d for an initial concentration of 1.8 mg/l chlorine as well as 1.93 and 2.15 mg/g/d for an initial concentration of 3.6 mg/l.

From initially 1.8 mg/l chlorine, filter material >1 mm consumed 16% within the first hour (Fig. 3). After 72 h, chlorine concentration was still 36% of the initial concentration. Filter material of smaller grain size <1 mm consumed also 16% within the first hour and after 46 h no residual chlorine was left. Aquifer material with grain size <4 mm showed a decrease in chlorine concentration of 25% within one hour and subsequently a behavior close to filter material <1 mm. Fine aquifer material <0.063 mm and clay consumed 90 and 100% of the initial chlorine within the first hour. For an initial 3.6 mg/l of chlorine, similar drops within the first hour were noted for filter materials and aquifer material <4 mm (Fig. S8). After 72 h, residual chlorine concentrations of 48, 27 and 9% were measured for samples with filter material >1 mm, <1 mm and aquifer material <4 mm. Clay and aquifer material <0.063 mm consumed 90% of initially 3.6 mg/l within the first hour and samples showed no residual chlorine after 16 h.

3.4. Partial disinfection by multiple chlorine application

The second sampling approach focused on the impact of multiple chlorine dosages to chlorine depletion. Results are given as median for filter material (FM) >1 and <1 mm as well as for clay (see above). Fig. 4 shows that 37% of the initial chlorine concentration of 1.8 mg/l was consumed by the filter material >1 mm after the first application. After the second and third application, absolute chlorine loss decreased to 19 and 16%. Filter material <1 mm consumed 64, 48 and 29% after the first, second and third application. After the first two applications, clay consumed 100% of initial concentration of 1.8 mg/l and 90% after the third. 39, 35 and 18% of initially 1.8 mg/l chlorine were consumed by the mixed aquifer material (<4 mm). The grain size fraction <0.063 mm of the aquifer material consumed 100, 84 and finally 62% of initially 1.8 mg/l chlorine. From an initial chlorine concentration of 3.6 mg/l, 29%

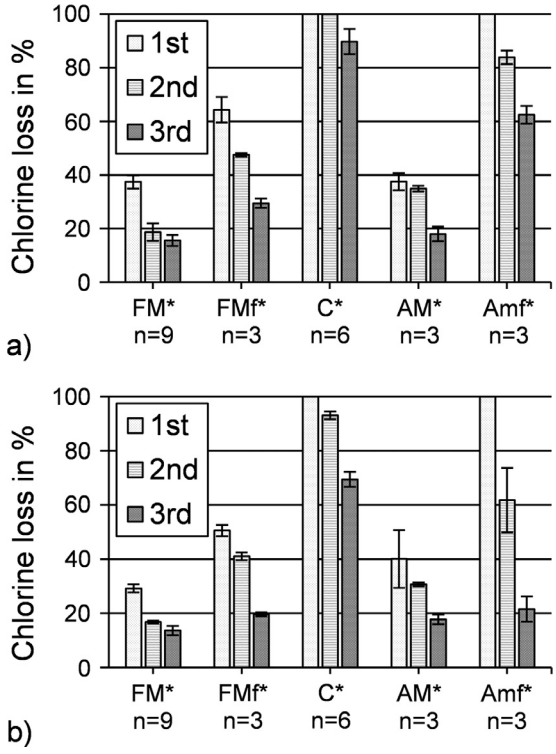

Fig. 4. Decreasing chlorine consumption (median) within 24 h for multiple chlorine application with an initial concentration of 1.8 mg/l (a) and 3.6 mg/l (b), error bars indicating SE. *FM = Filter material >1 mm, FMf = fine Filter material <1 mm, C = Clay, AM = Aquifer material <4 mm, AMf = fine AM <0.063 mm.

were consumed by filter material >1 mm after the first application, 17 and 14% after the two subsequent steps. Filter material <1 mm consumed 51, 41 and finally 20%. Clay consumed 100, 93 and 69% of initially 3.6 mg/l across the three steps. 40, 31 and 18% from 3.6 mg/l chlorine were consumed by the mixed aquifer material (<4 mm). With 100% chlorine loss after the first step, 62 and 22% after the two following steps the grain size fraction <0.063 mm of aquifer material showed the largest drops between each addition. Absolute chlorine consumption rates k_{Cl} decreased similarly after each chlorine addition (Fig. S9).

3.5. Microbiological growth in the columns

Accumulated biomass along column 1 with filter sand (set-up 1) and columns 3 & 4 with aquifer material (set-up 2) was indirectly determined using qPCR measurements (Fig. 5). At the inlet of column 1 with filter sand 4.1×10^5 DNA-copies/g were determined. Further along the column, the No. of copies decreased to 4.1×10^4 DNA-copies/g and remained around 1×10^5 DNA-copies/g until the outlet. Aquifer material from columns 3 & 4 showed 1.3×10^6 and 6×10^5 DNA-copies/g at the inlet. The No. of copies

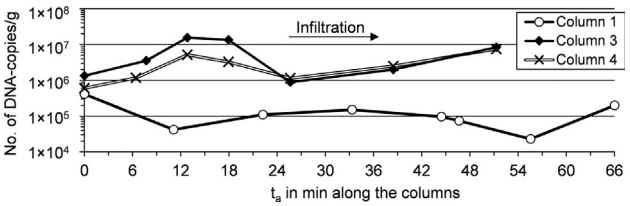

Fig. 5. Accumulated biomass indicated as DNA-copies/g along column 1 (filter sand) and columns 3 & 4 with aquifer material.

increased along both columns to 1.6×10^7 and 5×10^6 DNA-copies/g ($t_a \approx 12$ min) and dropped after a travel time of 26 min to around 1×10^6 DNA-copies/g. In both columns the No. of copies showed an increase towards the outlet to 8×10^6 DNA-copies/g. Former column experiments in Khabarovsk showed that around 1×10^6 DNA-copies/g are probably the low, non-critical threshold for biological clogging and 1×10^9 DNA-copies/g indicate severe biological clogging (Herlitzius, 2015).

3.6. Transport range of chlorine around an infiltration well

Three approaches were used to adapt the results from lab experiments to operate an SIR infiltration well at the field site in Khabarovsk (Fig. 6). 1st-order chlorine decay was applied with median k-values of 16 d^{-1} for filter material and 256 d^{-1} for natural aquifer material (see 2.4.1). Results from batch tests were applied with median k_{Cl}-values of 0.005 and 0.054 mg/g/d for filter and natural aquifer material (2.4.2). Correlation of exchanged pore volumes was used as a third estimation approach (2.4.3). A cylindrical distribution of the infiltrate was assumed for the well having a 0.1-m-thick filter pack and an infiltration rate of 80 m^3/h (see 2.1).

Application of the results from the batch tests led to an estimated range of 1.3 m and the 1st-order decay approach resulted in an estimated range of 2.2 m (Fig. 6). Because the applied constants for both approaches are median values over each experimental time, resulting estimations can be considered as median chlorine transport range. Both approaches rely on travel time along the flow path to calculate changes in chlorine concentration. Because correlation of PV also accounted for the infiltrated volume (V_{inf}), estimated ranges can be obtained over the time of an infiltration cycle. For an infiltration time of 48 h in Khabarovsk (V_{inf} = 3.840 m^3), the estimated chlorine range becomes maximum 3.2 m (Fig. 7). Regular monitoring of the closest OW, 6 m apart from the PW, proved that no chlorine reaches the OW during regular well operation. During a field test with equal infiltration volume and an initial chlorine concentration of about 10 mg/l only traces of chlorine were observed at the OW (data not shown).

4. Discussion

4.1. Evaluation of the determined consumption rates to estimate chlorine ranges

To validate results from the batch tests (Section 3.2), determined median values of mass-related chlorine consumption rates for filter and aquifer material (0.0005 and 0.054 mg/g/d) were used to calculate chlorine profiles along columns 1–4 (Fig. S10). Applied rate constants resulted in an underestimation of measured chlorine profiles. The experimental approach of the closed bottle batch tests entailed that the entire material surface made contact with chlorinated water. Along the columns, however, the porous soil matrix prevented the entire grain surface from coming into contact with the chlorine. Moreover, on a macro-scale, preferential flow

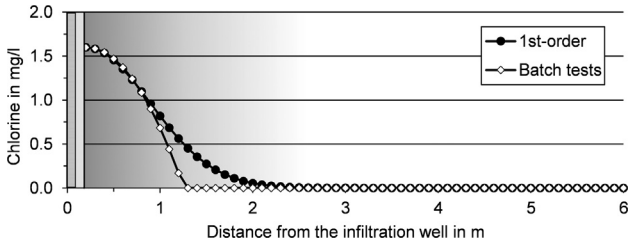

Fig. 6. Estimated range of chlorine around an infiltration well as a function of travel time within the aquifer.

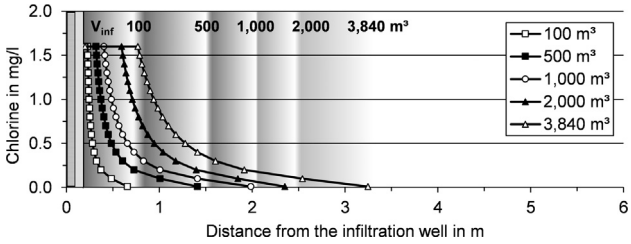

Fig. 7. Estimated range of chlorine around an infiltration well as a function of infiltration volume.

paths may have been established, leading to "dead-end" pores that further reduced the reactive surface. Considering a surface dependency of chlorine decay (Vasconcelos et al., 1996), chlorine consumption rates derived by closed bottle batch tests represent the upper threshold value for a certain material. Hence, the rates of chlorine consumption estimated here can be considered as worst-case. Additionally, the given median values included the high chlorine consumption rates after initial contact with the material (Section 3.3). Excluding those high rates would result in minimal smaller k_{Cl}-values and wider transport ranges.

For further validation, 1st-order decay constants for filter material, clay and natural aquifer material were calculated based on the results of the closed bottle batch tests (Table S5). The calculated constants from the closed bottle batch tests are much smaller (e.g. median values of 0 and 3 d^{-1} for filter and aquifer material <4 mm) in comparison to the 1st-order decay constants derived from the column experiments (median values of 16 and 256 d^{-1} for filter and aquifer material). Maximum calculated k-values from the batch tests were slightly higher (e.g. 10 and 12 d^{-1}), and consistently represented values for the first hour after initial contact with chlorine solution. The strong deviations can be explained by the time scale for both approaches. Results from the column experiments indicated that filter material consumed >50% of the infiltrated chlorine within the travel time of ≈1 h (Fig. 1). Moreover, natural aquifer material consumed >90% within only 20 min of travel time. Because the residual chlorine concentration after 1 h during the batch tests with filter material was >80% of the initial concentration, the calculated maximum k-values for filter material from the batch tests are approx. in the same order of magnitude like from the column experiments. For subsequent time intervals, calculated k-values from the batch tests were based on the elapsed time up to a certain sample (up to 4 days) and thus, showed a higher deviation. Considering the fast chlorine consumption by aquifer material, calculated maximum k-values from the batch tests (1 h after initial contact) virtually included the high consumption rates, but failed to account for the actual maximum rates within <20 min after the initial contact. Thus, the calculated 1st-order decay constants from the batch experiments are not comparable to those derived from the column experiments. Shorter sampling intervals within the first hour after initial contact would probably allow a more accurate calculation of 1st-order decay constants from batch tests.

Median 1st-order chlorine decay constants for filter material (16 d^{-1}) and natural aquifer material (256 d^{-1}) were used to compute chlorine profiles along the columns. Since k was originally derived from the measured profiles, large errors were not expected. Nonetheless, Fig. S10 suggests that k-values of 16 d^{-1} and 256 d^{-1} are representative for simulating chlorine decay in the filter material and the aquifer material, respectively. A sensitivity analysis showed that k-values between the 25-percentile and the median would still deliver accurate results (Figs. S11 and S12). Higher k-values up to the 75-percentile may cause larger errors for subsequent transport range estimation.

Application of lab results to operation of an actual SIR infiltration well in Khabarovsk resulted in an estimated chlorine range of 1.2 m derived from batch experiments (Fig. 6). Since the applied k_{Cl}-values represent the worst-case for chlorine consumption, the estimated range of 1.2 m can be considered the minimal transport range. Because the applied 1st-order decay model reproduced the measured chlorine profiles along the columns accurately within a wide span of k-values, the estimated chlorine range of 2.2 m probably represents the closest approximation to the actual range. A limitation of the 1st-order model is the sole dependence on the initial chlorine concentration and that it does not take into account other species which react with the chlorine (Warton et al., 2006). Haas and Karra (1984) developed a parallel first-order model that is perhaps more representative of true chlorine consumption (Eq. (9)).

$$C_{t,i} = C_0 \times \left[(Y \times e^{-k_1 \times t_a}) + (1 - Y) \times e^{-k_2 \times t_a})\right] \quad (9)$$

The model used two kinetic terms occurring at the same time, one representing rapid decay and the other slower decay. A coefficient (Y) split chlorine into a rapid- and a slow-reacting fraction. The determination of two separate kinetic chlorine fractions was not possible with the obtained results of this study. Further studies that focus on the actual chlorine consumption reaction would improve the estimation process.

Fig. 7 shows an increasing range of chlorine at larger infiltration volumes. This observation is supported by the results of the batch tests (3.4) that suggest that filter and aquifer material could be partially disinfected by multiple applications of chlorinated water. Thus, the continuous delivery of chlorinated water at an infiltration well may slowly extend the disinfected zone.

4.2. Factors controlling the chlorine consumption

In modeling residual chlorine concentrations in drinking water networks, pipe walls are usually considered active surfaces that react with chlorine (Vasconcelos et al., 1996). Hence, in this study a surface dependency of chlorine consumption was assumed. The specific surface for each grain size was calculated assuming an ideal sphere with mean diameters of 4.38, 2.58, 1.50 and 0.55 mm for filter materials, 0.58 mm for aquifer material <4 mm (Seifert, 2013) and 0.063 mm for clay and aquifer material <0.063 mm. Correlation clearly showed that materials with a large specific surface (smaller grain size) lead to less residual chlorine after one hour of contact (Table S6). K_{Cl}-values for the first hour after contact reflected this dependency. Residual chlorine after 72 h was not at all dependent on grain size for an initial chlorine concentration of 1.8 mg/l, and only weakly dependent for initial 3.6 mg/l. Fig. 4 indicated a strong dependency of the ability to disinfect the material on the grain size (specific surface). Correlation confirmed that chlorine loss after a second and third application compared to the first one was less for smaller grain sizes. Grain size becomes a major factor impacting the chlorine consumption after the initial contact but gets less important with longer contact time. Furthermore, disinfection by multiple chlorine applications has a larger impact on small grain sizes.

Blum (1989) concluded that the loss of chlorine after initial contact with the material also depends on the initial chlorine concentration. In this study, only samples with a grain size of <0.063 mm showed much lower $k_{Cl,1h}$-values at an initial 1.8 mg/l of chlorine and increased rates at 3.6 mg/l (Fig. 2). In samples with an initial 1.8 mg/l of chlorine, no residual chlorine was measured after the first hour. The available chlorine mass at 1.8 mg/l was less than the potential chlorine consumption by those materials. Hence, the lower consumption rates observed for the initial concentration of 1.8 mg/l represent a lower threshold value but are not necessarily correlated to the initial chlorine concentration itself. Fig. 4 indicated that multiple chlorine applications at an initial 3.6 mg/l of chlorine lead to lower chlorine losses compared to multiple applications with an initial 1.8 mg/l. Thus, disinfection of smaller grain sizes <0.063 mm benefits from higher initial chlorine concentrations.

Chlorine consumption rates within the first hour after initial contact of the chlorine solution with the materials (Fig. 2) were 10–70-times higher than the median k_{Cl}-values (Table 3). If particulate or dissolved organic matter (OM) and inorganic substances, such as ammonium, iron or manganese are present, additional chlorine at the beginning of the infiltration would be consumed before being able to carry out the intended disinfection (Deborde and von Gunten, 2008). Blum (1989) found dissolved NH_4^+ to be responsible for up to 57% of the initial chlorine consumption. Since the examined aquifer material originated from an SIR plant and groundwater contained dissolved manganese and ammonium, adsorbed cations could have caused high initial chlorine consumption. This assumption is in line with the observation that smaller grain sizes had the highest consumption rates after first contact and consumed less chlorine after multiple application at higher initial chlorine concentrations.

Both filter material and natural aquifer material showed decreasing chlorine consumption at longer contact times and were partially disinfected by multiple chlorine applications. Nevertheless, the chlorine front in the columns did not move along the flow path, neither within one infiltration cycle nor after multiple infiltration cycles. Results from qPCR analysis after the column experiments showed maximum biomass accumulation after around 15 min along the flow path in columns with aquifer material. Exactly at this distance, no chlorine was measured anymore and simulated chlorine profiles indicated a similar disinfection range (Fig. S13). Rinck-Pfeiffer et al. (2000) investigated clogging processes for ASR-wells by laboratory columns and measured the highest amounts of accumulated biomass at the inlet, followed by a decreasing trend in the flow direction of the columns. This supports the results of this study. Taking the reversed flow direction during abstraction cycles into account, when chlorine-free groundwater was sent through the columns, high amounts of biomass accumulated at the inlet. For flow direction during infiltration, chlorine inhibited microbiological growth at the inlet and biomass accumulated after the chlorine was consumed. Since along column 1 with filter sand chlorine remained above the detection limit until the outlet, accumulation of biomass was suppressed along the entire column. Hence, results of qPCR analysis further confirm the estimated transport range of chlorine along the columns. Despite the observed accumulation of biomass, no decrease in hydraulic conductivity of the columns was observed (data not shown). Thus, results of this study confirm the observation that around 1×10^6 DNA-copies/g are uncritical for biological clogging under the given site conditions (Herlitzius, 2015). Taking into account, that bacteria may need >60 days (11 cycles) to adapt in the transitional milieu, the measured values pointing towards a progressive biological growth (Chapelle, 1993).

4.3. Practical implication

This study aimed to estimate the transport range of chlorine around an infiltration well and to improve knowledge about processes that control the extent of the disinfected radius. Results of closed bottle batch tests (Section 3.2) showed a very low chlorine consumption rate k_{Cl} of 0.005 mg/g/d for filter material. The infiltrating water at the example well in Khabarovsk passes the approx. 950 kg (Eq. (4)) heavy filter gravel pack within about 14 s (1.6×10^{-4} d, Eq. (3)). Hence, 1 PV of the filter gravel pack is exchanged within 14 s and 0.75 mg chlorine are consumed by the entire filter

gravel pack during this time. Considering a PV of the filter gravel pack to be 141 L (n_e = 0.3) and the infiltration concentration of 1.6 mg/l chlorine, around 226 mg of chlorine are theoretically flowing through that 1 PV. Thus, only 0.33% of the infiltrating chlorine will be consumed by the filter gravel pack and > 99% will enter the aquifer.

To assess the impact of increased chlorine concentrations in the infiltrating water on the transport range of chlorine within the aquifer, the 1st-order approach and determined mass-related chlorine consumption rates were further applied. The results highlight that an increase of the infiltration concentration up to 10 mg/l chlorine would still lead to a disinfected range of <3 m (Figs. S14 and S15). Moreover, a chlorine concentration in the order of magnitude for shock chlorination, up to 100 mg/l, would still result in a chlorine transport range of <4 m (data not shown). The main reason is most likely that the volume of the chlorinated aquifer and thus the consumption capacity increases quadratically with an increasing radius. Furthermore, several manuals for well disinfection (e.g. Holben and Gaber, 2003) suggest that at increased chlorine concentrations, biofilms as well as their metabolites could develop a hard, protective crust and can be less effectively removed. Hence, it seems clearly not advisable to disinfect a well with excessively high chlorine concentrations. The perhaps minimally larger chlorine transport range would not justify the increased costs for disinfection. A preferable approach to increase the effect of chlorination is most likely to increase the total infiltrated volume and the infiltration time (Fig. 7).

Although the obtained consumption rates and the proposed modeling approaches were applied to a single infiltration well only in this study, this strategy may be applicable to other sites. Results of this study indicate that chlorine consumption in the filter gravel pack is almost negligible and only needs to be considered at sites where very fine filter sand with grain sizes <1 mm is used. To estimate the effective transport range of chlorine within the adjacent aquifer, two different approaches can be taken: 1) closed bottle batch tests with natural aquifer material and/or 2) column experiments. Closed bottle batch tests can be conducted within two weeks and the derived chlorine transport ranges probably represent a minimum. More accurate results can be expected from column experiments, but the much higher sampling and maintenance effort must be taken into account.

5. Conclusion

Microbiological contamination usually leads to erratic operation of wells used for water supply, such that disinfection is required to reestablish abstraction capacity and ensure microbiologically safe water. Besides clean-up in the aftermath of disasters, disinfection of wells can be necessary to maintain proper well performance for ASR and SIR wells. This study focused on estimating the fate of chlorine around an infiltration well and improving the knowledge about processes that control the extent of the disinfected radius or volume of aquifer. Closed bottle batch tests revealed low chlorine consumption rates for filter gravel and sand (0.005 mg/g/d) and higher rates for clay (0.030 mg/g/d) as well as natural aquifer material (0.054 mg/g/d). Smaller grain sizes <1 mm showed 10–70-times higher chlorine consumption rates within the first hour after contact compared to median values. Grain size becomes less important for longer contact times. Initial chlorine concentration most likely does not impact disinfection ability at grain sizes >1 mm but can lead to a more effective disinfection of grain sizes <1 mm, especially for very fine materials <0.063 mm. Results from column studies reinforced the previous lab results with low 1st-order decay constants of the filter material (16 d^{-1}) and much higher values of 254 d^{-1} for natural aquifer material. Adaptation of the chlorine consumption rates to the SIR well in Khabarovsk showed consistently that the filter gravel pack of a well consumes <1% of infiltrated chlorine. The disinfection zone at the example well extended around 2 m (>90% of the chlorine mass), maximum 3.5 m into the aquifer. Excessive chlorine dosage of >10 mg/l would not necessarily increase the disinfected radius. A preferable approach to increase the efficiency of chlorine dosage is most likely the increase of the total infiltrated volume and the infiltration time. The three proposed approaches to adapt lab tests to field sites are applicable to other sites with only moderate effort for lab and possibly field tests.

Acknowledgements

The work was performed as cooperation between the Arcadis Germany GmbH, Vodokanal Khabarovsk and the Division of Water Sciences at the University of Applied Sciences Dresden. The authors are grateful to the ESF for the financial support to S. Paufler (grant no. 200031585).

Appendix A. Supplementary data

Supplementary data associated with this article can be found, in the online version, at https://doi.org/10.1016/j.jhydrol.2018.02.054.

References

Blum, E., 1989. Investigations into chemical reactions of the disinfection with hydrogen peroxide and chlorine for drinking water treatment PhD Thesis. Institute for Radiochemistry, University Karlsruhe, Karlsruhe, Germany, p. 158 (In German).

Boccelli, D.L., Tryby, M.E., Uber, J.G., Summers, R.S., 2003. A reactive species model for chlorine decay and THM formation under rechlorination conditions. Water Res. 37, 2654–2666. https://doi.org/10.1016/S0043-1354(03)00067-8.

Bouwer, H., 2002. Artificial recharge of groundwater: hydrogeology and engineering. Hydrogeol. J. 10 (1), 121–142. https://doi.org/10.1007/s10040-001-0182-4.

Bouwer, H. (ed.), 2008. Design, Operation, and Maintenance for Sustainable Underground Storage Facilities. 1st ed., Denver: AWWA Research Foundation, 268 p. ISBN: 978-1-60573-041-7.

Braun, B., Schröder, J., Knecht, H., Szewzyk, U., 2016. Unraveling the microbial community of a cold groundwater catchment system. Water Res. 107, 113–126. https://doi.org/10.1016/j.watres.2016.10.040.

Chapelle, F.H., 1993. Ground-Water Microbiology and Geochemistry. 1st ed., New York: John Wiley & Sons Inc, 424 p. ISBN: 978-0471348528.

Copeland, C., 2005. Hurricane Damaged Drinking Water and Wastewater Facilities: Impacts, Needs, and Response. CRS Report for Congress, p. 6.

Deborde, M., von Gunten, U., 2008. Reactions of chlorine with inorganic and organic compounds during water treatment - kinetics and mechanisms: a critical review. Water Res. 42 (1–2), 13–51. https://doi.org/10.1016/j.watres.2007.07.025.

Dillon, P.J., Vanderzalm, J., Page, D., Barry, K., Gonzalez, D., Muthukaruppan, M., Hudson, M., 2016. Analysis of ASR clogging investigations at three australian ASR sites in a bayesian context. Water 8 (10), 442. https://doi.org/10.3390/w8100442.

Eichhorn, D., 1985. Contribution to the theory of subsurface iron removal. PhD Thesis, Department of Water Sciences, TU Dresden, Dresden, Germany. (In German).

Englande, A.J., 2008. Katrina and the thai tsunami - water quality and public health aspects mitigation and research needs. Int. J. Environ. Res. Public Health 5 (5), 384–393.

Haas, C.N., Karra, S.B., 1984. Kinetics of wastewater chlorine demand exertion. J. Water Pollut. Control Fed. 56 (2), 170–173.

Hallberg, R.O., Martinell, R., 1976. Vyredox - in situ purification of ground water. Ground Water 14 (2), 88–93. https://doi.org/10.1111/j.1745-6584.1976.tb03638.x.

Herlitzius, J. (ed.), 2014. Microbiological researches to elaborate control methods of the microbiological situation and actions to prevent a possible performance loss of wells from the first section of the Tunguska reservoir in Khabarovsk. Scientific-technical report, Arcadis Germany GmbH, unpublished, 219 p.

Herlitzius, J. (ed.), 2015. Conditions for the formation of biofilm and technical solutions for the prevention of biofilm formation on the technological equipment of the water catchment in the Tunguska reservoir in Khabarovsk: Evaluation of the results of the quantitative determination of microorganisms until 15.07.2015. Scientific-technical report, Arcadis Germany GmbH, unpublished, 24 p.

Herlitzius, J., Sumpf, H., Grischek, T., 2012. German-Russian cooperation for clean drinking water. Int. J. Water Manag., bluefacts, 76–81.

Holben, R.R.S., Gaber, M.R.S., 2003. Water Well Disinfection Manual. Michigan Department of Environmental Quality. Online available: www.michigan.gov/documents/deq/deq-wb-dwehs-wcu-disinfectmanual_221334_7.pdf, last accessed 10.11.2017.

Holländer, H.M., Boochs, P.W., Billib, M., Panda, S.N., 2005. Laboratory column experiments to investigate clogging effects in an aquifer – impact of physical deposition, gas bubbles and biological activity. Grundwasser 4 (10), 205–315. https://doi.org/10.1007/s00767-005-0102-y. (In German).

Martin, R. (ed.), 2013. Clogging issues associated with managed aquifer recharge methods. IAH Commission on Managed Aquifer Recharge, Australia, 214 p. ISBN 978-0-646-90852-6.

MDH, 2015. Well Disinfection. Minnesota Department of Health, Environmental Health Division, Brochure, 8 p. Online available: www.health.state.mn.us/divs/eh/wells, last accessed 17.11.2017.

NHDES, 2015. Disinfecting a Private Well. New Hampshire Department of Environmental Services, Environmental Fact Sheet, 2 p. Online available: http://des.nh.gov/organization/-divisions/water/ dwgb/index.htm, last accessed 17.11.2017.

Pavelic, P., Nicholson, B.C., Dillon, P.J., Barry, K.E., 2005. Fate of disinfection by-products in groundwater during aquifer storage and recovery with reclaimed water. J. Contam. Hydrol. 77, 119–141. https://doi.org/10.1016/j.jconhyd.2004.12.003.

Pyne, R.D.G., 1995. Ground water Recharge and Wells: A Guide to Aquifer Storage Recovery. 1st ed., Boca Raton, Florida, USA: CRC Lewis Publishers, 400 p. ISBN: 978-1566700979.

Pyne, R.D.G., 2005. Aquifer storage recovery: a guide to groundwater recharge through wells. 2nd ed., Gainesville, Florida, USA: ASR Systems, 608 p. ISBN: 978-0977433704.

Rinck-Pfeiffer, S., Ragusa, S., Sztajnbok, P., Vandevelde, T., 2000. Interrelationships between biological, chemical, and physical processes as an analog to clogging in aquifer storage and recovery (ASR) wells. Water Res. 34 (7), 2110–2118. https://doi.org/10.1016/S0043-1354(99)00356-5.

Rott, U., Friedle, M., 2000. Eco-friendly and cost-efficient removal of arsenic, iron and manganese by means of subterranean ground-water treatment. Water Supply 18, 632–636.

Seifert, J., 2013. Investigations into the reaction zones of a subsurface iron removal plant in Khabarovsk Diploma Thesis. Division of Water Sciences, HTW Dresden, Dresden, Germany, p. 61 (In German).

Sprenger, C., Hartog, N., Hernández, M., Vilanova, E., Grützmacher, G., Scheibler, F., Hannappel, S., 2017. Inventory of managed aquifer recharge sites in Europe: historical development, current situation and perspectives. Hydrogeol. J. 25, 1909–1922. https://doi.org/10.1007/s10040-017-1554-8.

Stuyfzand, P., Wakker, J.C., Putters, B., 2005. Water quality changes during Aquifer Storage and Recovery (ASR): results from pilot Herten (Netherlands), and their implications for modeling. Proc. 5th Int. Symp. on Managed Aquifer Recharge, 10-16 June 2005, Berlin, 164-173.

Vasconcelos, J.J., Boulos, P.F., Grayman, W.M., Kiene, L., Wable, O., Biswas, P., Bhari, A., Rossman, L.A., Clark, R.M., Goodrich, J.A., 1996. Characterization and Modeling of Chlorine Decay in Distribution Systems. American Water Works Association Research Foundation, Denver, CO.

Warton, B., Heitz, A., Joll, C., Kagi, R., 2006. A new method for calculation of the chlorine demand of natural and treated waters. Water Res. 40 (15), 2877–2884. https://doi.org/10.1016/j.watres.2006.05.020.

Winkelnkemper, H., 2004. Subsurface iron and manganese removal. wwt. Wasserwirtschaft Wassertechnik 4, 38–41 (In German).

Zuurbier, K., 2016. Increasing freshwater recovery upon aquifer storage: A field and modelling study of dedicated aquifer storage and recovery configurations in brackish-saline aquifers. PhD Thesis, Department of Geo-Engineering, TU Delft, Delft, The Netherlands, 10.4233/uuid:4631f3d2-14ff-4505-bcba-0c21956c460f.

Supplementary material

Effective range of chlorine transport in an aquifer during disinfection of wells: from laboratory experiments to field application.

Paufler, S[a], Grischek, T[a], Adomat, Y[a], Herlitzius, J[b], Hiller, K.[b], Metelica, Y.[c]

[a] Dresden University of Applied Sciences, Friedrich-List-Platz 1, 01069 Dresden, Germany

[b] Arcadis Germany GmbH, EUREF-Campus 10, 10829 Berlin, Germany

[c] Vodokanal Khabarovsk, Topograficheskiy per. 12, 680000 Khabarovsk, Russia

Corresponding author:

S. Paufler

Dresden University of Applied Sciences

Friedrich-List-Platz 1

01069 Dresden

Germany

sebastian.paufler@htw-dresden.de

+49 351-462 2631

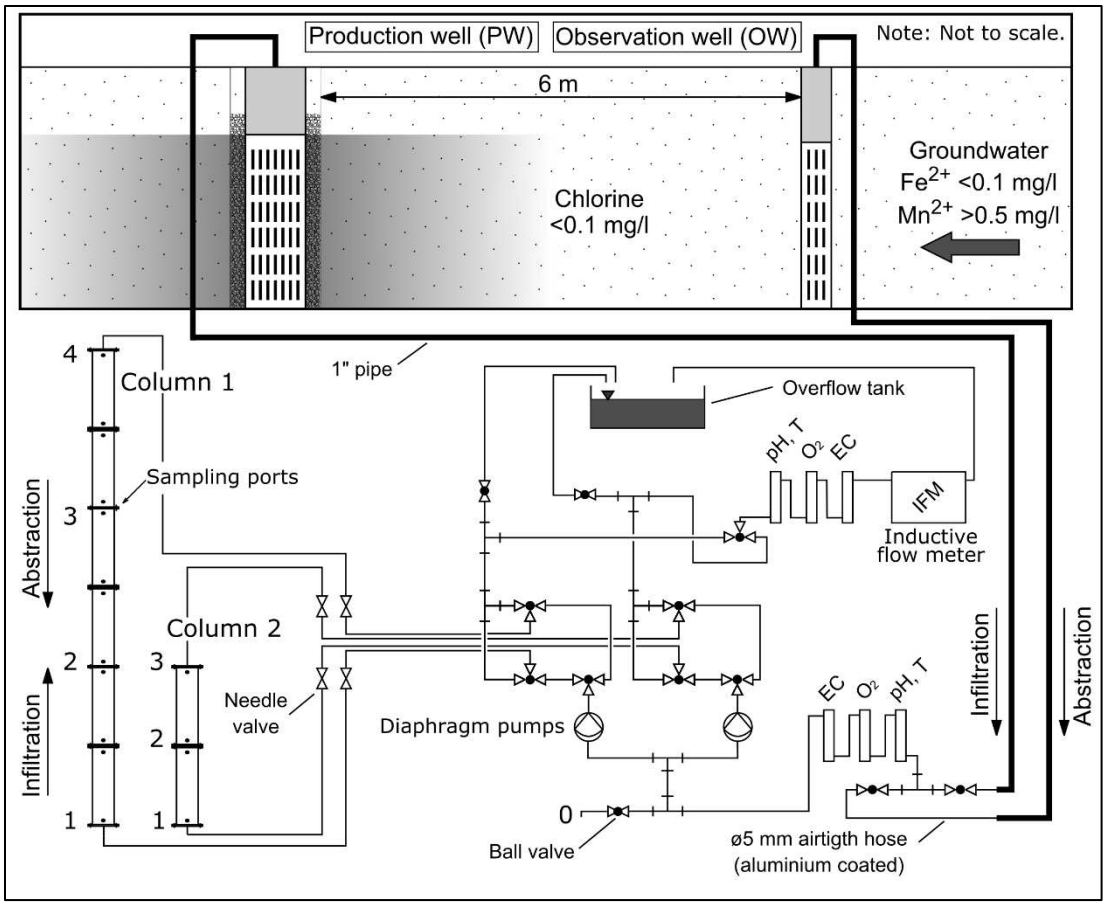

Fig. S1: Flow scheme for set-up 1 of the column experiments

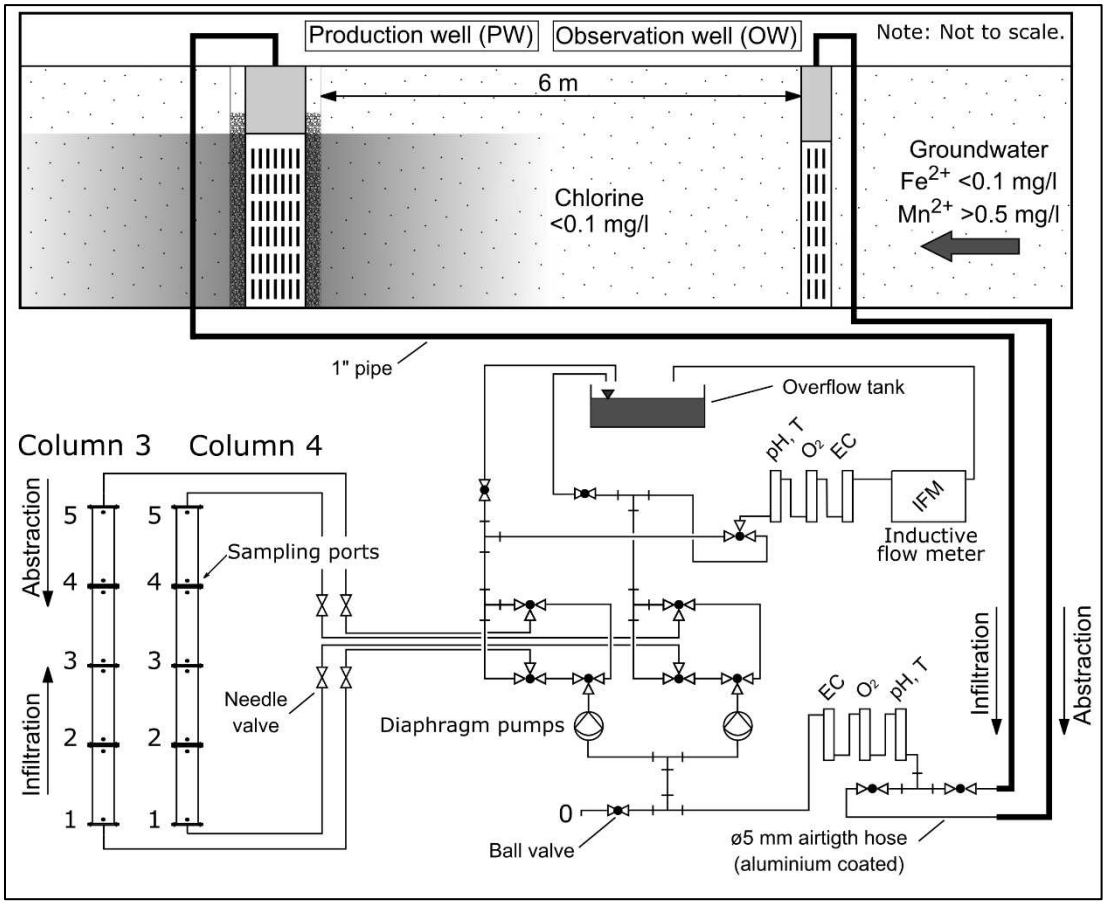

Fig. S2: Flow scheme for set-up 2 the of column experiments

Tab. S1: Filling material and hydraulic properties of the columns

Set-up	Column	Filling material	Grain size in mm	Length in m	Hydr. cond. in m/s	Darcy velocity in m/s	Pore velocity in m/s	Travel time in min	Effective porosity
1	1	Filter gravel*1	1…2	3	$3.2 \cdot 10^{-3}$	$2.1 \cdot 10^{-4}$	$7.5 \cdot 10^{-4}$	66	0.28
	2	Aquifer material*2	<4	1	$1.8 \cdot 10^{-4}$	$1.3 \cdot 10^{-4}$	$4.0 \cdot 10^{-4}$	50	0.32
2	3	Aquifer material*2	<4	2	$1{,}1 \cdot 10^{-5}$	$1.6 \cdot 10^{-4}$	$5{,}5 \cdot 10^{-4}$	52	0.29
	4	Aquifer material*2	<4	2	$1{,}1 \cdot 10^{-5}$	$1.6 \cdot 10^{-4}$	$5{,}4 \cdot 10^{-4}$	52	0.29

*1 Obtained as bagged goods

*2 Natural aquifer material from core drillings at the depth of the actual filter screen, subsequently sieved to <4 mm

Tab. S2: Investigated grain size fractions and sources of the raw material

Material	Grain size in mm	Source
Filter gravel & sand *1	3.15 to 5.60	Bagged goods Quarzwerke GmbH, Frechen, Germany
	2.00 to 3.15	
	1.00 to 2.00	
	0.10 to 1.00	
Clay 1 *1	<0.063	Bagged goods Quarry Plessa II, Keraton, Germany
Clay 2 *1	<0.063	Bagged goods Quarry Ruppach, Börkey Teratech, Germany
Aquifer material *2	<4.00	SIR plant in Khabarovsk (Russia) Lifted by core drilling Grain size derived from sieve analysis
	<0.063	

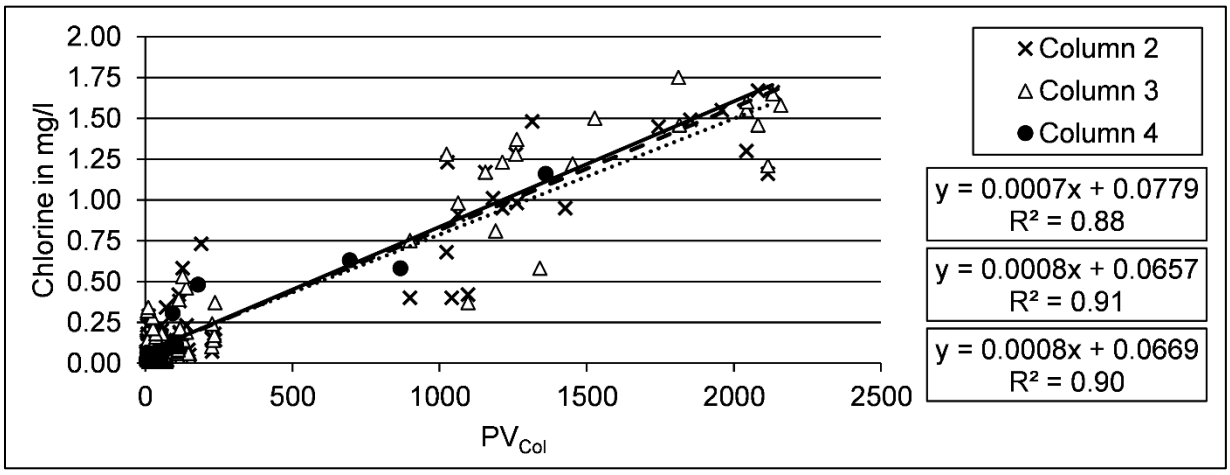

Fig. S3: Chlorine concentration as a function of exchanged pore volumes (PV) for all three columns filled with aquifer material

Tab. S3: Water quality of the inflow waters for the column experiments during set-up 1 and 2

	Set-up		**Chlorine**	**pH**	**O_2**	**EC**	**T**	**$Fe_{dissolved}$**	**Fe_{total}**	**Mn**	**NH_4^+**	**NO_2^-**	**NO_3^-**	**SiO_2**	**Hardness**
			mg/l	-	mg/l	µS/cm	°C	mg/l	mg/l	mg/l	mg/l	mg/l	mg/l	mg/l	°dH
Production well (PW) (Inflow during infiltration cycles)	1	Min	0.0	6.2	10	156	6.1	0.02	0.01	0.02	0.01	<0.01	<1	12	0.5
		25 %ile	1.2	7.8	23	172	6.8	0.02	0.01	0.05	0.05	0.01	<1	14	2.5
		Median	1.6	8.0	27	187	7.3	0.02	0.02	0.05	0.05	0.01	<1	14	2.9
		75 %ile	2.0	8.0	32	205	7.8	0.02	0.03	0.08	0.05	0.01	<1	14	3.5
		Max	3.2	8.7	41	260	9.1	0.41	0.44	0.50	0.4	0.01	3.00	20	3.7
		n	123	126	127	126	126	128	128	128	113	109	110	111	109
	2	Min	0.0	6.3	15	151	6.0	0.02	0.01	0.02	0.01	<0.01	<1	10	2.1
		25 %ile	1.4	7.6	22	186	6.9	0.02	0.01	0.06	0.05	<0.01	<1	14	3.0
		Median	1.6	8.0	24	197	7.9	0.02	0.02	0.10	0.05	<0.01	<1	14	3.2
		75 %ile	1.9	8.2	27	209	8.4	0.02	0.03	0.11	0.05	<0.01	1.00	16	3.5
		Max	2.6	8.5	33	232	10.2	0.07	0.09	0.50	0.50	0.01	4.00	18	4.5
		n	47	61	60	60	60	64	64	64	62	62	62	47	62
Observation well (OW) (Inflow during abstraction cycles)	1	Min		5.6	0	105	5.4	0.02	0.01	0.05	0.1	<0.01	<1	12	0.5
		25 %ile		5.9	0	125	5.7	0.02	0.01	0.60	0.4	0.01	<1	14	2.4
		Median		6.0	0	154	6	0.02	0.02	0.70	0.6	0.01	<1	14	3.0
		75 %ile		6.7	8	160	6.7	0.02	0.03	0.90	0.7	0.01	<1	16	3.2
		Max		7.5	29	219	8.7	0.76	0.96	1.40	2.2	0.01	2.00	22	3.7
		n		228	231	229	229	239	238	239	153	150	150	150	149
	2	Min		5.4	0	89	5.3	0.02	0.01	0.05	0.2	<0.01	<1	10	1.2
		25 %ile		5.9	0	154	5.5	0.02	0.02	0.50	0.6	<0.01	<1	16	3.0
		Median		6.2	0	162	5.7	0.02	0.03	0.80	0.8	<0.01	<1	16	3.5
		75 %ile		6.4	0	166	6.2	0.12	0.18	0.82	0.9	<0.01	<1	18	4.0
		Max		7.7	25	215	8.6	1.62	1.48	1.10	1.4	0.10	<1	28	6.4
		n		105	106	106	106	106	106	106	105	105	105	104	105

Note: Water quality data were provided by Arcadis Germany GmbH.

Tab. S4: Chlorine concentration in mg/l and travel time t_a in min along columns 1 to 4

Set-up	Column	Sampling port	Min	25 %ile	Median	75 %ile	Max	n	t_a
1	1	Inflow	0.00	1.16	1.59	2.02	3.18	123	0
		1-1	0.41	0.96	1.58	1.74	3.00	35	1.1
		1-2	0.10	0.83	1.21	1.51	1.91	19	22.0
		1-3	0.03	0.37	0.99	1.31	1.55	21	44.4
		1-4	0.07	0.17	0.47	1.00	1.86	31	66.7
	2	Inflow	0.00	1.16	1.59	2.02	3.18	123	0
		2-1	0.11	0.31	0.54	0.91	1.56	34	2.1
		2-2	0.00	0.04	0.06	0.11	0.65	35	20.8
		2-3	0.00	0.02	0.06	0.08	0.10	12	50.1
2	3	Inflow	0.03	1.42	1.60	1.86	2.62	47	0
		3-1	0.15	0.82	1.17	1.38	1.67	28	1.5
		3-2	0.03	0.09	0.15	0.26	0.71	28	12.0
		3-3	0.03	0.07	0.12	0.14	0.23	28	25.2
		3-4	0.02	0.06	0.08	0.12	0.18	28	38.9
		3-5	0.01	0.03	0.05	0.07	0.13	28	52.0
	4	Inflow	0.03	1.42	1.60	1.86	2.62	47	0
		4-1	0.10	1.08	1.28	1.53	1.82	28	1.5
		4-2	0.00	0.09	0.14	0.26	0.50	28	12.0
		4-3	0.01	0.05	0.07	0.12	0.34	28	25.2
		4-4	0.01	0.05	0.08	0.11	0.32	28	38.9
		4-5	0.01	0.03	0.04	0.06	0.21	28	52.0

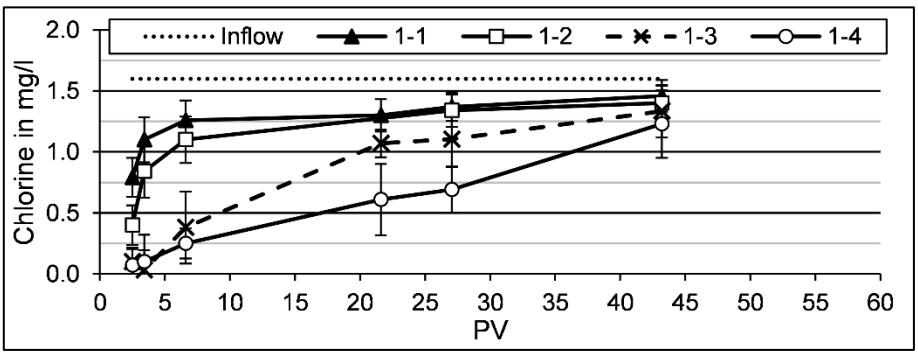

Sampling port	t_a in min
1-1	1.1
1-2	22.0
1-3	44.4
1-4	66.7

Fig. S4: Median chlorine concentration along column 1 during one infiltration cycle, error bars indicating SE

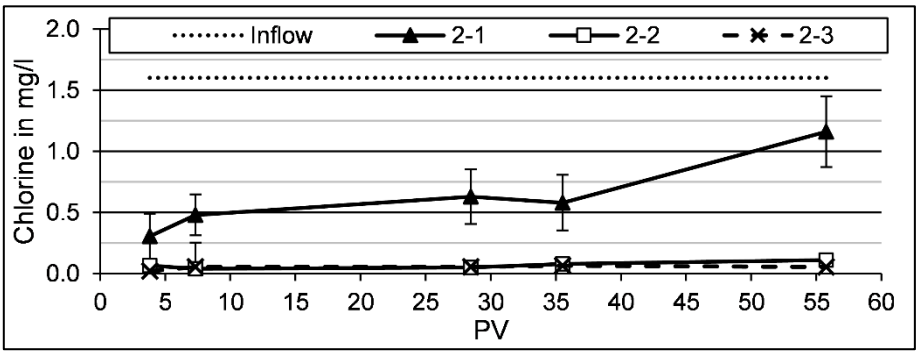

Sampling port	t_a in min
2-1	2.1
2-2	20.8
2-3	50.1

Fig. S5: Median chlorine concentration along column 2 during one infiltration cycle, error bars indicating SE

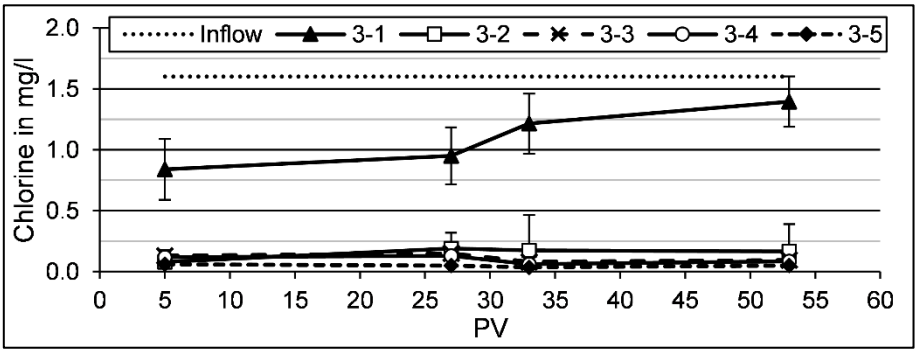

Sampling port	t_a in min
3-1	1.5
3-2	12.0
3-3	25.2
3-4	38.9
3-5	52.0

Fig. S6: Median chlorine concentration along column 3 during one infiltration cycle, error bars indicating SE

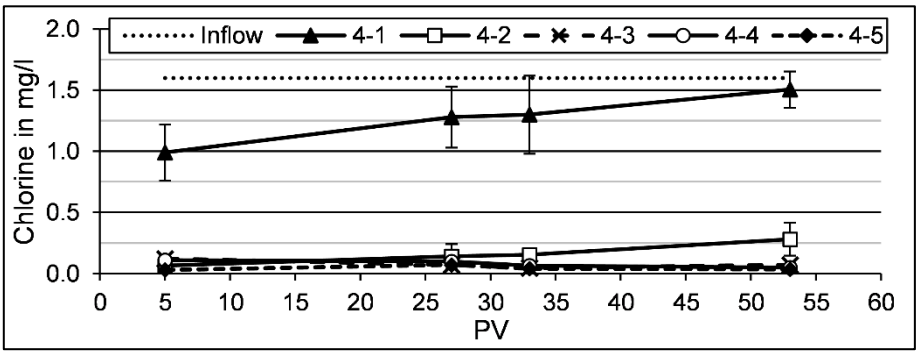

Sampling port	t_a in min
4-1	1.5
4-2	12.0
4-3	25.2
4-4	38.9
4-5	52.0

Fig. S7: Median chlorine concentration along column 4 during one infiltration cycle, error bars indicating SE

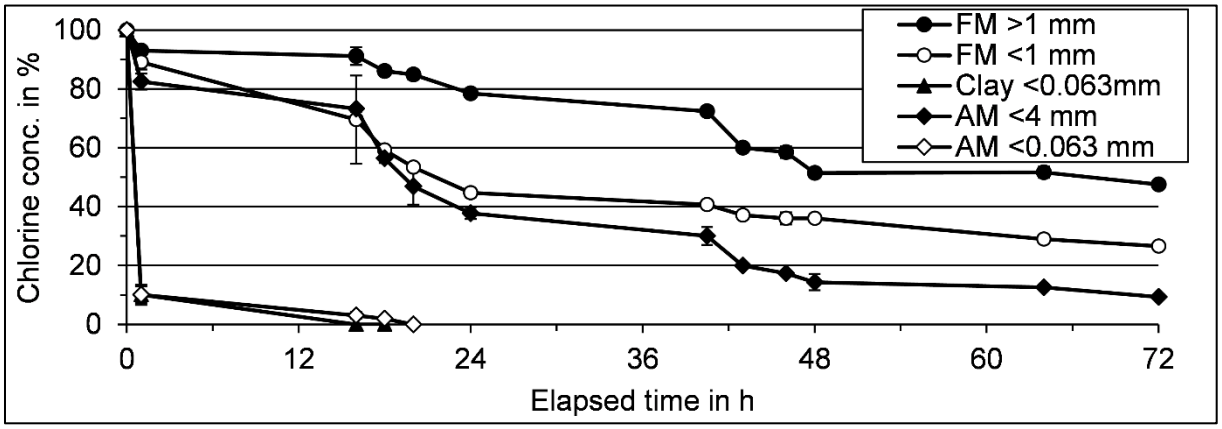

Fig. S8: Development of chlorine concentration over a time period of 72 h for initially 3.6 mg/l chlorine, median values for filter material >1 (n=9) and <1 mm (n=3), clay (n=6), aquifer material <4 (n=3) and <0.063 mm (n=3), error bars indicating SE

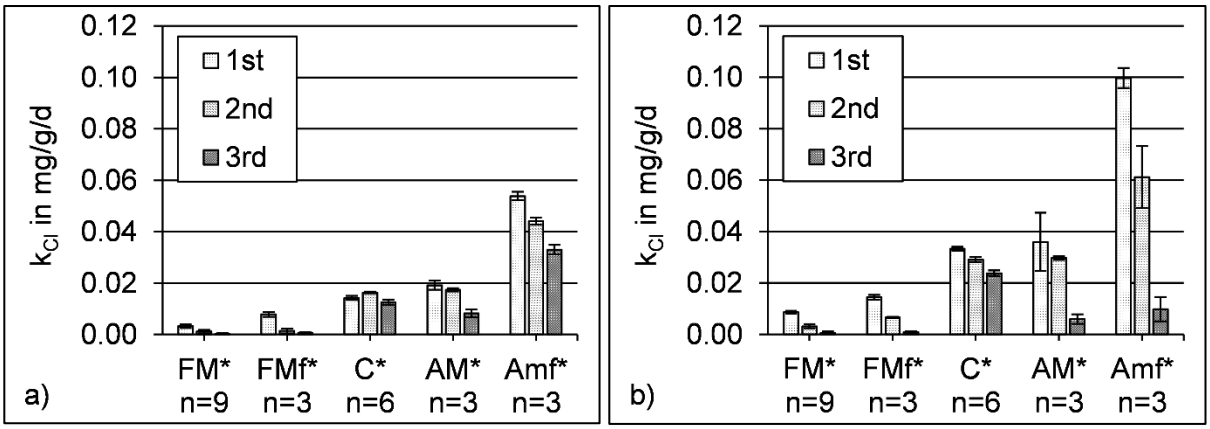

Fig. S9: Decreasing chlorine consumption rate (median) within 24 h for multiple chlorine application with an initial concentration of 1.8 mg/l (a) and 3.6 mg/l (b), error bars indicating SE

* FM=Filter material >1 mm, FMf= Filter material <1 mm, C=Clay, AM=Aquifer material <4 mm, AMf=fine AM <0.063 mm

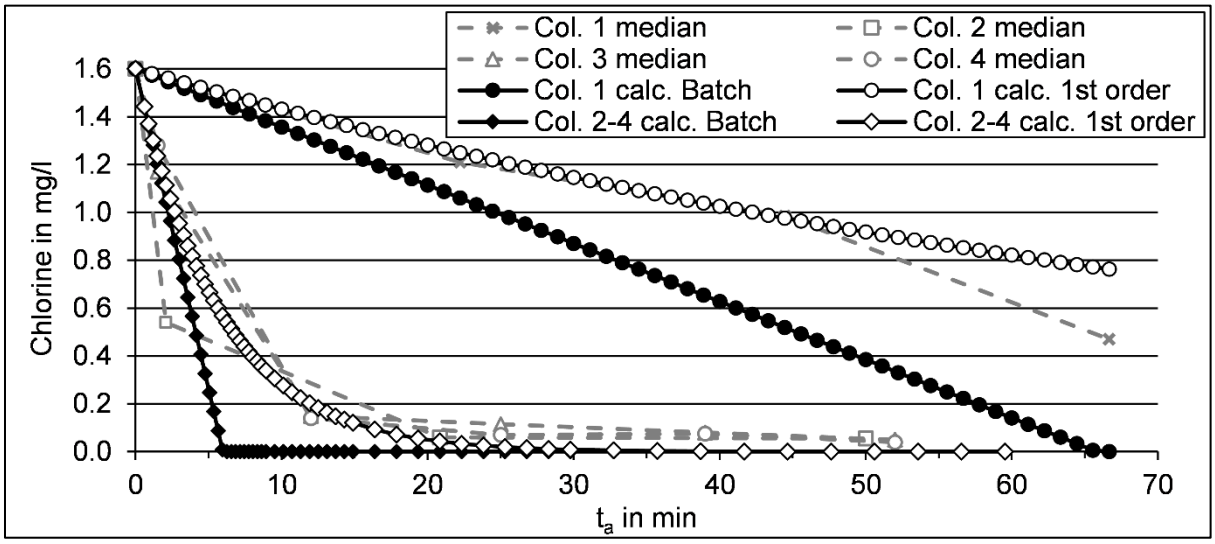

Fig. S10: Calculated vs. measured chlorine profiles along column 1 and columns 2-4

Tab S5: Calculated 1st-order decay constants from closed bottle batch tests

Inital chlorine concentration	Material	Filter material		Clay	Aquifer material	
	Grain size	>1 mm	<1 mm	<0.063 mm	<4 mm	<0.063 mm
1.8 mg/l	Min	0	0	0	0	0
	Median	0	0	1	3	7
	Max	5	10	288	12	55
	n	38	12	7	12	5
3.6 mg/l	Min	0	0	0	0	0
	Median	0	1	9	1	27
	Max	3	4	70	10	54
	n	38	12	7	12	5

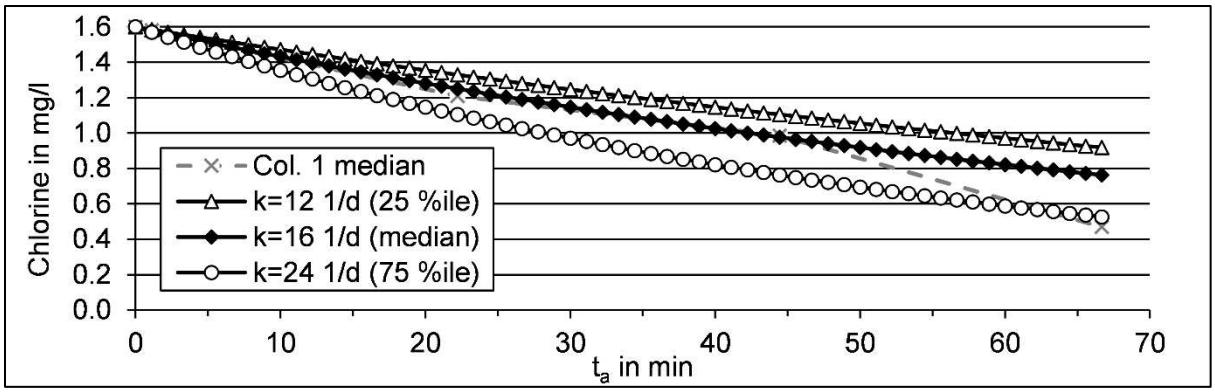

Fig. S11: Sensitivity analysis for derived 1st-order chlorine decay constants for filter material

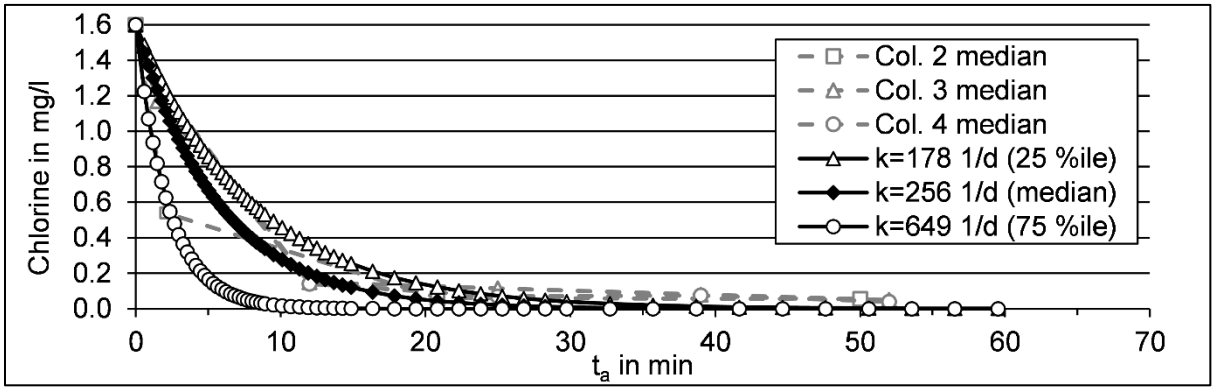

Fig. S12: Sensitivity analysis for derived 1st-order chlorine decay constants for aquifer material

Tab. S6: Correlation coefficients for test of parameter dependency to grain surface

Parameter	Section	Initial chlorine concentration	r	R^2	p
Chlorine consumption rates k					
Median	3.2	1.8 and 3.6 mg/l	0.62	0.38	<0.05
k-value for 1st hour	3.3	1.8 mg/l	0.97	0.95	<0.05
		3.6 mg/l	0.99	0.99	<0.05
Residual chlorine					
after 1 h	3.3	1.8 mg/l	-0.99	0.97	<0.05
		3.6 mg/l	-1.00	1.00	<0.05
after 72 h		1.8 mg/l	-0.65	0.42	<0.05
		3.6 mg/l	-0.85	0.73	<0.05
Loss of chlorine after multiple applications					
1st	3.4	1.8 mg/l	0.97	0.94	<0.05
2nd			0.97	0.93	<0.05
3rd			0.96	0.91	<0.05
1st		3.6 mg/l	0.98	0.96	<0.05
2nd			0.93	0.87	<0.05
3rd			0.78	0.61	<0.05

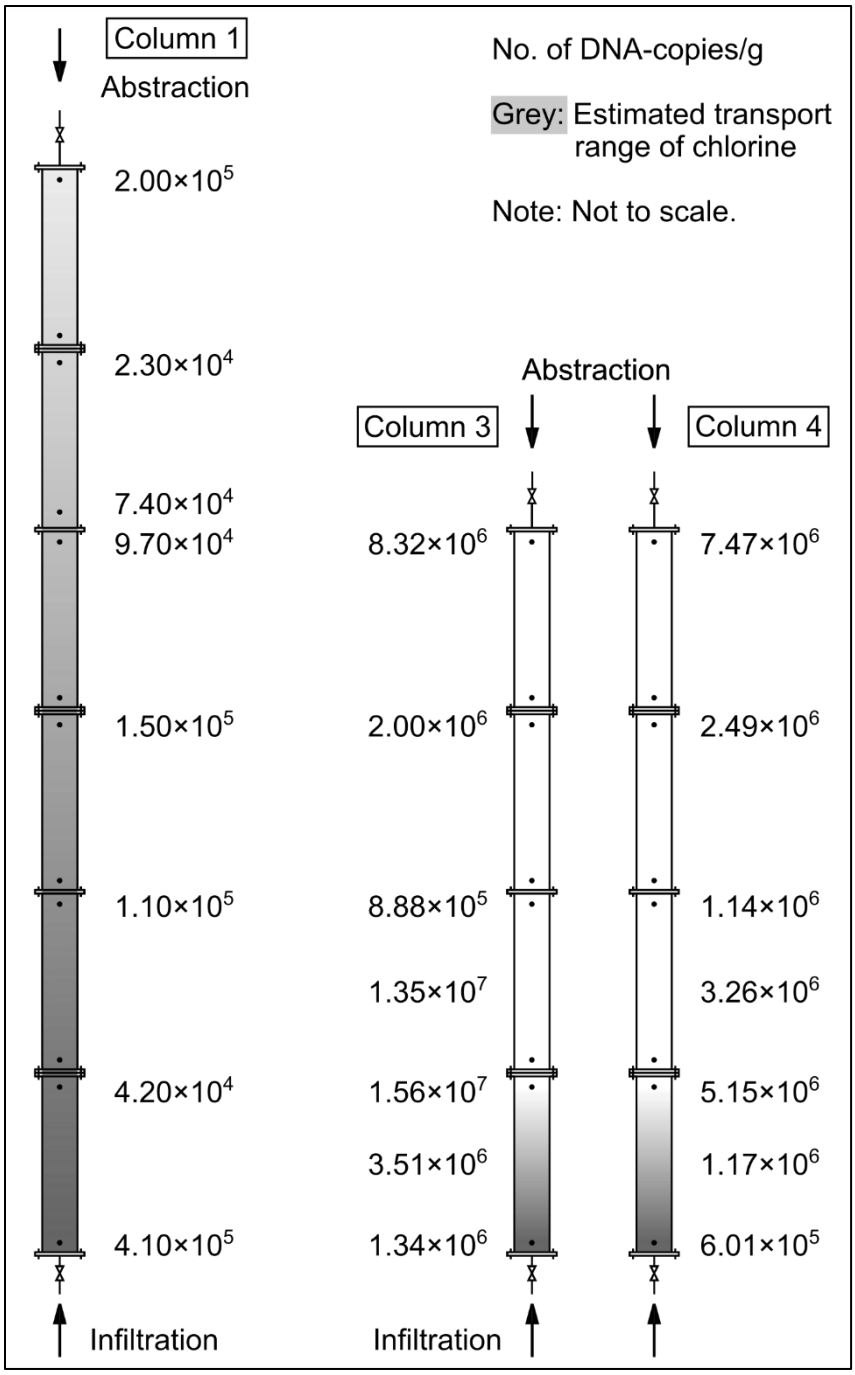

Fig. S13: Accumulated biomass indicated as DNA-copies/g along column 1 (filter sand) and columns 3 & 4 with aquifer material compared to the estimated transport range of chlorine

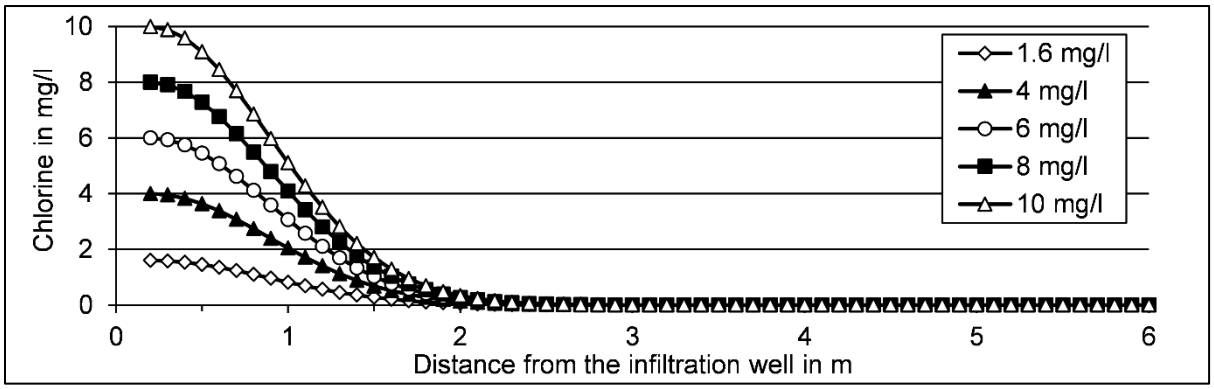

Fig. S14: Estimated range of chlorine at increased chlorine concentrations in the infiltrate, 1st-order chlorine decay with k=254 d^{-1}

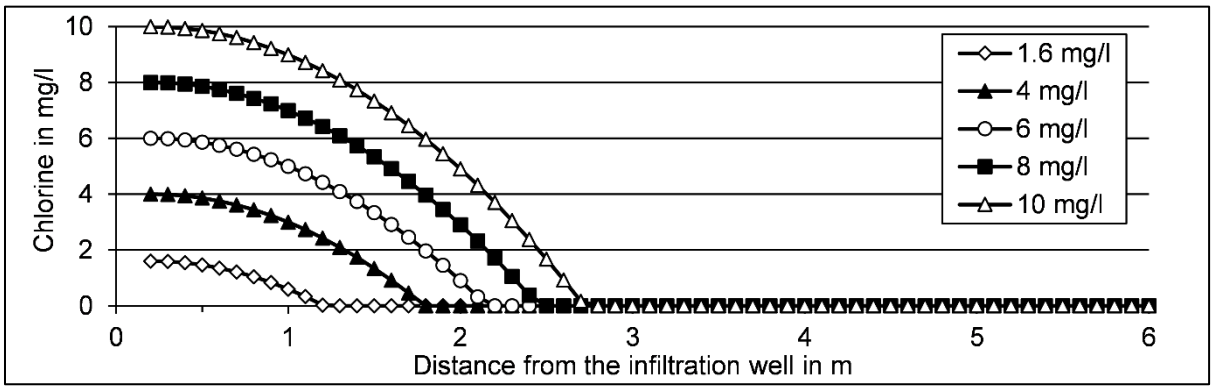

Fig. S15: Estimated range of chlorine at increased chlorine concentrations in the infiltrate, mass related chlorine consumption with k_{Cl}=0.054 mg/g/d

Beiliegende Publikation 8

Paufler, S., Grischek, T., Ruppert, M. (2019) Freisetzung von Mangan nach Umstellung von Brunnen mit unterirdischer Enteisenung auf Dauerbetrieb. gwf Wasser / Abwasser 1(160), 55-65.

Freisetzung von Mangan nach Umstellung von Brunnen mit unterirdischer Enteisenung auf Dauerbetrieb

Sebastian Paufler, Thomas Grischek, Martin Ruppert

Eingereicht: 13.07.2018
Begutachtet im Peer-Review-Verfahren: 03.09.2018

Brunnen, unterirdische Enteisenung und Entmanganung, Brunnenbetrieb, Mangan

Das Wasserwerk Eggersdorf soll nach etwa 40-jährigem Betrieb saniert werden. Bisher bereiteten 16 Brunnen eisen- und manganhaltiges Grundwasser unterirdisch auf. Um die Auswirkungen einer Umstellung von unterirdischer Enteisenung auf kontinuierliche Förderung und oberirdische Enteisenung zu untersuchen, wurde über 250 Tage ein Feldversuch durchgeführt. Die Mangankonzentration im Förderwasser stieg ab einem Ergiebigkeitskoeffizienten (EGK) von 30 bis zum Versuchsende bei EGK 65 auf bis zu 0,72 mg/L an und war damit etwa 3,5-mal höher als die Hintergrundkonzentration im Grundwasser. Die Desorption von Mn^{2+} und die chemische Reduktion von abgeschiedenen Mangan(Hydr-)oxiden durch Fe^{2+} werden als Ursache der Mn-Freisetzung vermutet.

Release of manganese at subsurface iron removal wells after transition to continuous operation

The waterworks Eggersdorf has to be modernized after about 40 years of operation. In total, 16 vertical production wells have been operated as both infiltration and abstraction wells for subterrestrial removal of iron and manganese from groundwater, also known as subsurface iron removal (SIR). To test the transition from SIR to common above-surface iron removal, a well was continuously pumped in a field test over a period of 250 days. The manganese concentration in the pumped water started to increase at an efficiency coefficient of 30 and reached 0.72 mg/L at the end of the field test at an efficiency coefficient of 65, which was about 3.5 times higher than the background concentration in groundwater. Desorption of Mn^{2+} and chemical reduction of deposited manganese(hydr-)oxides by Fe^{2+} were probably the source for the Mn release.

1. Einleitung

Das Wasserwerk (WW) Eggersdorf des Wasserverbandes Strausberg-Erkner (WSE) ist seit etwa 40 Jahren in Betrieb und soll saniert werden. Bei Bedarf fördert das Wasserwerk ca. 16.000 m^3/d (max. 19.500 m^3/d). Die 16 Brunnen werden nach dem UNEIS-Verfahren [1] als Infiltrations- und Förderbrunnen betrieben, um eisen- und manganhaltiges Grundwasser unterirdisch aufzubereiten (allgemein: unterirdische Enteisenung/Entmanganung, UEE). Die inzwischen erforderliche Nutzung als Spitzenlast-WW führt zu einer ungleichmäßigen Auslastung und Nutzung der Brunnen und ist für die Anwendung der UEE ungünstig. Nach der Sanierung kommen für den Betrieb zwei Varianten in Frage: die weitere Nutzung der UEE mit dem UNEIS-Verfahren oder die Umstellung des Brunnenbetriebs auf ausschließliche Grundwasserförderung mit nachgeschalteter oberirdischer Aufbereitung.

Kölle [2] warnt, dass eine Umstellung auf Normalbetrieb (dauerhafte Grundwasserförderung) zu einem erheblichen Anstieg der Mangankonzentration führen kann, die über

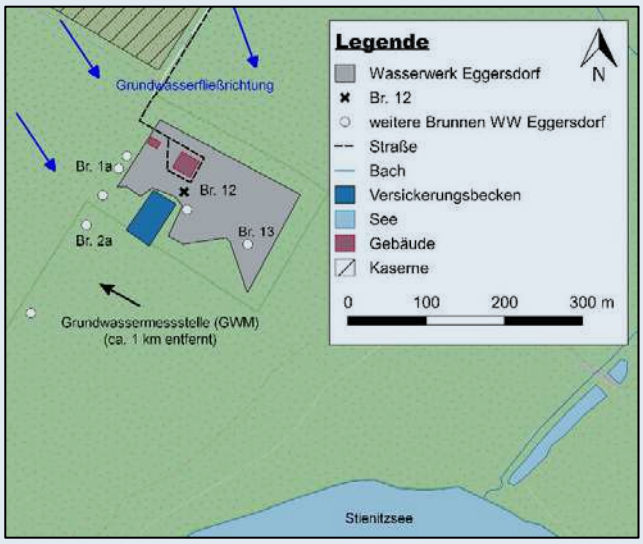

Bild 1: Lage des Untersuchungsgebietes

den Werten des natürlichen Grundwassers (GW) liegt. An einigen UEE-Standorten wurde ein Anstieg der Mn-Konzentration beobachtet, nachdem die unterirdische Aufbereitungskapazität deutlich überschritten wurde [3, 4]. Nach Kenntnis der Autoren sind in der Literatur keine Standortbeispiele für die dauerhafte Umstellung von UEE-Brunnen auf kontinuierliche Förderung dokumentiert, welche die Abschätzung einer möglichen Freisetzung von Mn oder anderen Schwermetallen erlauben.

In der vorliegenden Studie werden die Ergebnisse eines Feldversuchs für die Umstellung eines UNEIS-Brunnens auf eine dauerhafte Förderung von eisen- und manganhaltigem GW vorgestellt. Über einen Zeitraum von 250 Tagen förderte ein Brunnen des WW Eggersdorf kontinuierlich Grundwasser zu einem Containerwasserwerk (CWW), in dem das GW oberirdisch aufbereitet wurde. Während des Versuchs kam es zu einer Freisetzung von Mn aus der ehemaligen Reaktionszone der UEE. Die Mn-Konzentration im Rohwasser war bis zu 3,5-mal höher als die Hintergrundkonzentration im GW. Auf Grundlage der Ergebnisse werden Ursachen der Freisetzung diskutiert.

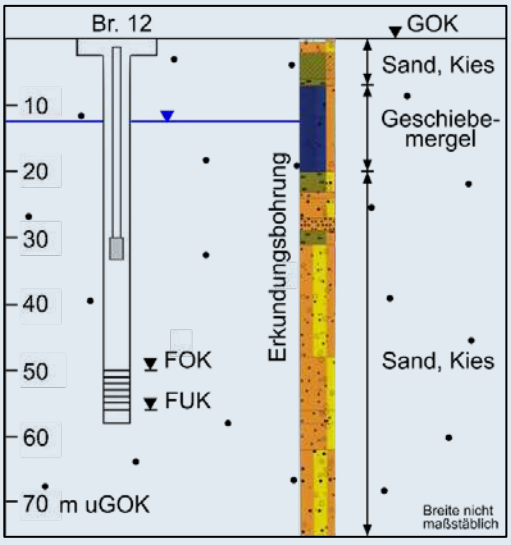

Bild 2: Ausbau des Br. 12 und Ergebnisse der Erkundungsbohrung

2. Material & Methoden

2.1 Standortbeschreibung

Das WW Eggersdorf liegt südlich von Eggersdorf in einem Waldstück am Stienitzsee (**Bild 1**). Für den Testbetrieb wurde der Brunnen 12 genutzt (**Bild 2**). Der Filterbereich des Br. 12 befindet sich im tieferen von 2 Grundwasserleitern (GWL). In den oberen GWL schneidet der Stienitzsee ein. Aufgrund der schwer durchlässigen Trennschicht zwischen beiden GWL strömt dem Brunnen kein Uferfiltrat zu. Basierend auf einem Stufenpumpversuch nach der Inbetriebnahme von Br. 12 (Daten nicht gezeigt) und mithilfe der Software AQTESOLV [5] wurde der k_f-Wert des GWL mit $1{,}4 \cdot 10^{-3}$ m/s ermittelt (Lösung nach Theis [6]). Das geförderte GW hat ein Alter von 20 bis 30 Jahren und fließt landseitig von Nordwest zum Stienitzsee. Das GW enthält ca. 1 mg/L Fe, 0,2 mg/L Mn und ist mit einer Säurekapazität ($K_{S4,3}$) von 3-4 mmol/L gut gepuffert (Grundwassermessstelle etwa 1 km nordwestlich, **Tabelle 1**). Der Vergleich der el. Leitfähigkeit und der Chloridkonzentration zu Versuchsende (496 µS/cm bzw. 15 mg/L) mit der GW-Beschaffenheit (**Tabelle 1**) zeigt, dass sich die Beschaffenheit des Förderwassers den Messwerten der GWM OP nähert. Dies gilt auch für die Sulfatkonzentration. Aufgrund der ähnlichen Filterpositionen des Br. 12 und des OP der GWM war dies zu erwarten – die Grundwasserbeschaffenheit im OP kann für den Vergleich mit der Entwicklung der Förderwasserbeschaffenheit genutzt werden.

Br. 12 ist bis in eine Teufe von 58 m unter Geländeoberkante (uGOK) ausgebaut (**Bild 2**). Der Filterkies wurde von 49 m bis zur Endteufe von 58 m uGOK eingebracht. Filteroberkante (FOK) und -unterkante (FUK) des 6 m langen Stahlschlitzbrückenfilters liegen bei 50 bzw. 56 m uGOK. Zwischen 6 und 18 m uGOK sowie zwischen 46 und 48 m uGOK befinden sich zwei Tonsperren. Bei der Inbetriebnahme im November 2002 wurde der Wasserspiegel um 2,02 m abgesenkt bei einer Förderrate von 100 m^3/h. Daraus ergibt sich eine spezifische Ergiebigkeit von 49,5 $m^3/(h \cdot m)$ bei Betriebsbeginn.

Bei der UEE mit dem UNEIS-Verfahren werden die Brunnen abwechselnd für Infiltration und Förderung genutzt. Für die Infiltration in den Br. 12 wurde Trinkwasser mit einem Sauerstoffgehalt von ca. 10 mg/L O_2 verwen-

Tabelle 1: Beschaffenheit des Grundwassers im Zustrom der Brunnen und des Mischreinwassers aller Brunnen, N = 7 für GWM, N = 5 für Mischreinwasser

Parameter	Grundwasser		Mischreinwasser WW Eggersdorf
	GWM OP 62…64 m uGOK	GWM UP 86…88 m uGOK	
Temperatur in °C	10,3	10,4	11,0
el. Leitfähigkeit in µS/cm	443	383	539
pH-Wert	7,8	7,6	7,5
O_2 in mg/L	0,19	0,20	10,12
DOC	2,17	2,36	2,73 (TOC)
Ca^{2+} in mg/L	79	62	88
Mg^{2+} in mg/L	6,9	7,7	6,8
K^+ in mg/L	1,0	1,3	1,1
Na^+ in mg/L	7,5	9,2	9,3
Fe_{ges} in mg/L	0,69	1,10	0,03
Mn in mg/L	0,19	0,16	<0,002
NH_4^+ in mg/L	0,24	0,5	<0,05
Al in mg/L	<0,005	0,2	<0,005
Cl^- in mg/L	24,9	7,3	18,3
SO_4^{2-} in mg/L	52,6	4,4	54,7
NO_3^- in mg/L	<0,1	<0,1	<0,1
$K_{S4,3}$ in mmol/L	3,04	3,80	3,93
$K_{B8,2}$ in mmol/L	0,15	0,23	0,42
Härte (Ca+Mg) in °dH	12,7	10,5	13,8

det. Das Infiltrationsvolumen betrug 2.000 m³, die Infiltrationsrate lag bei ca. 30 m³/h. Das Fördervolumen betrug 14.000 m³ bei einer Förderrate von 60 bis 70 m³/h. Daraus ergibt sich ein Ergiebigkeitskoeffzient von EGK = 7 (EGK = Fördervolumen $V_{För}$/Infiltrationsvolumen V_{Inf}).

2.2 Versuchsaufbau

Versuchsweise wurde der Br. 12, der bisher als UNEIS-Brunnen (Wechsel von Infiltration und Förderung) betrieben wurde, nur noch als Förderbrunnen genutzt. Die notwendige oberirdische Enteisenung des Grundwassers wurde in einem Containerwasserwerk durchgeführt. Das CWW hatte eine Aufbereitungskapazität von 40-50 m³/h. Bei einer Umstellung auf einen dauerhaften Förderbetrieb soll der Br. 12 mit einer Förderrate von ca. 60 m³/h betrieben werden. Um den dauerhaften Förderbetrieb zu simulieren, wurde die Förderrate zu Versuchsbeginn mit 45 m³/h möglichst hoch gewählt (Maximalkapazität des CWW). Die Förderrate musste nach 13 Tagen auf 25 m³/h und nach 139 Tagen auf 15 m³/h gedrosselt werden, um die Kapazität eines Versickerungsbeckens für das aufbereitete Wasser nicht zu überschreiten. Um die Auswirkung der Förderrate auf die Mn-Konzentration zu bewerten, wurde der Br. 12 zum Versuchsende über 72 h mit einer Förderrate von 60 m³/h betrieben.

In dem CWW wurde über einen Kompressor Luftsauer-

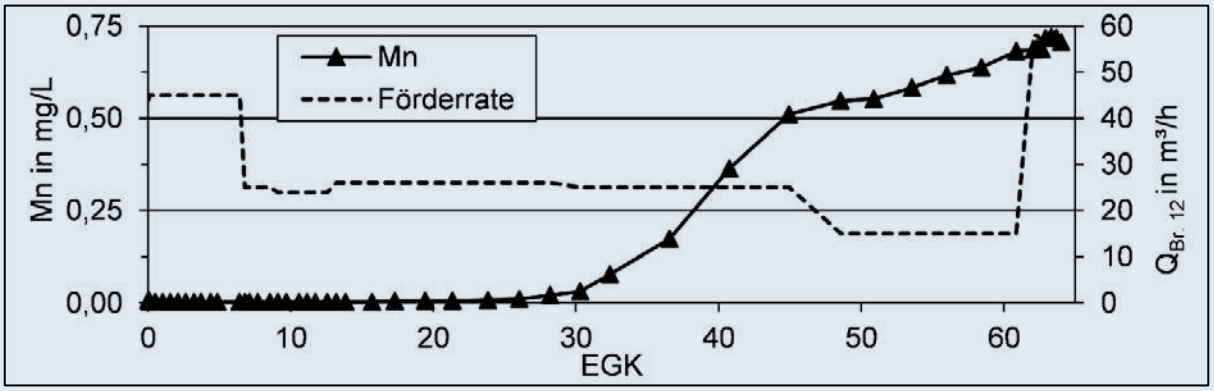

Bild 3: Mn-Konzentration im Förderwasser; Anstieg ab einem EGK von ca. 30 (Fördervolumen ≈ 60.000 m³)

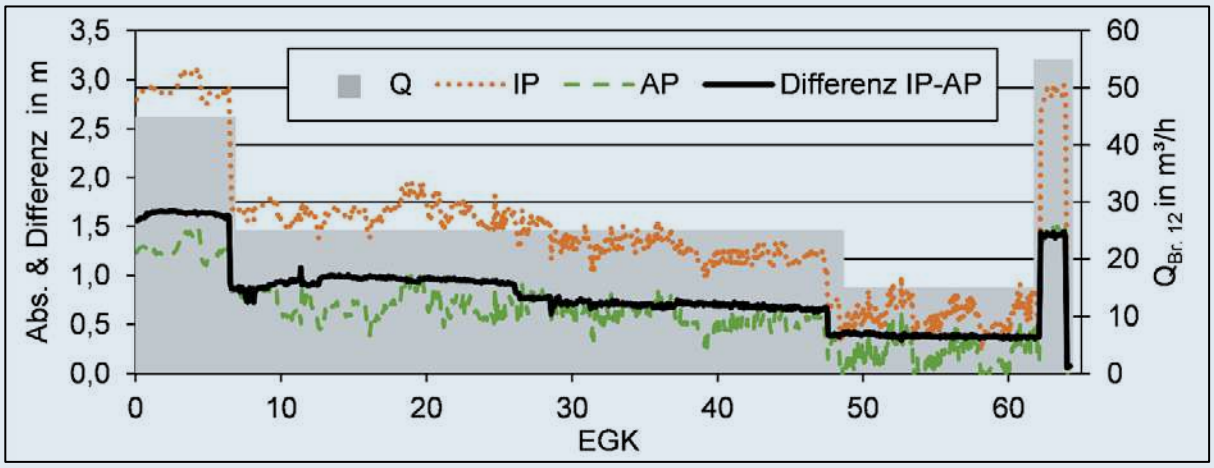

Bild 4: Absenkung im IP und AP des Br. 12 und Darstellung der Förderrate

stoff in das Grundwasser eingemischt. Für die folgende Enteisenung sorgten zwei Filterbehälter mit jeweils 1.300 kg Filtermaterial (1.000 kg CaO/MgO basiertes „Magno-Filt" von Akdolit + 300 kg Quarzsand, je 1-2 mm). Die manuell gesteuerte Rückspülung der zwei Filter erfolgte zu Versuchsbeginn nach etwa vier Wochen (Einfahren der Filter) und wurde auf eine regelmäßige, wöchentliche Rückspülung angepasst. Der Differenzdruck vor dem Rückspülen betrug 0,2-0,3 bar. Das Rückspülwasser wurde in ein zweites Versickerungsbecken neben dem CWW geleitet.

2.3 Probennahme und Analytik

Die Sofortparameter (pH-Wert, O_2, el. Leitfähigkeit, Temperatur) wurden mit einem WTW 3430i (Xylem Analytics Germany, Weilheim) in einer Durchflussmesszelle am Eingang des CWW gemessen. Die Wasserprobenahme erfolgte an der Steigleitung des Br. 12 vor dem CWW. Während der ersten 48 h des Testbetriebs (Rückförderung des letzten Infiltrats) wurden täglich zwei Proben genommen. Anschließend wurde die Probenahmehäufigkeit auf eine tägliche und nach 14 Tagen auf eine wöchentliche Probenahme verringert und ereignisbasiert angepasst. Während der Probenahme wurden die Sofortparameter gemessen und parallel dazu kontinuierlich aufgezeichnet. Außerdem wurde die Säurekapazität $K_{S4,3}$ durch Titration im Feld bestimmt, da die Pufferkapazität des Wassers die Enteisenung/Entmanganung stark beeinflusst.

Die Proben wurden über einen 0,45 µm PTFE Spritzenfilter filtriert. Die Hauptkationen Ca^{2+}, Mg^{2+}, Na^{+}, K^{+} und die gelösten Schwermetalle Al, As, Cr, Cu, Fe, Mn, Pb und Zn wurden mittels ICP-OES gemessen (Optima 4300 DV, PerkinElmer, Waltham, MA, USA). Br^{-}, F^{-}, Cl^{-}, NO_2^{-}, NO_3^{-}, PO_4^{3-} und SO_4^{2-} wurden mittels Ionenchromatografie gemessen (Dionex: Autosampler AS50, Eluens-Generator EG50, Gradientenpumpe GP50, Elektrochemischer Detektor ED50, Separationssäule AS19). Der SAK_{254} und der DOC-Gehalt wurden stichprobenweise bestimmt.

Für die Bewertung einer möglichen Änderung der Leistungsfähigkeit des Brunnens wurden die Absenkungs- und Förderdaten aufgezeichnet. Im Brunnen wurde jeweils ein Datenlogger (Mini Diver, Van Essen Instruments B.V., Delft, Niederlande) im Innen- und Außenpegel installiert. Die Durchflussmessung erfolgte mit einem fest installierten magnetisch-induktiven Durchflussmesser (IDM) am Brunnen.

3. Ergebnisse

3.1 Anstieg der Mangankonzentration und des pH-Werts

Im regulären UNEIS-Betrieb wurde der Br. 12 mit einem EGK von 7 betrieben. Das Förderwasser der letzten UNEIS-Zyklen enthielt nach dem üblichen Fördervolumen von 14.000 m³ etwa 0,02 mg/L Fe und < 0,002 mg/L Mangan (jeweils Median, N = 25). Während des Versuchs über insgesamt 250 Tage wurden rund 120.000 m³ Grundwasser gefördert. Dies entspricht einem EGK von 65. Die Mn-Konzentration stieg nach einem EGK von ca. 30 stetig von 0 auf bis zu 0,72 mg/L an und blieb auch bei der kurzzeitigen Steigerung der Förderrate auf diesem Wert (**Bild 3**).

Der pH-Wert stieg kontinuierlich über die gesamte Versuchsdauer von etwa pH 6,9 auf bis zu pH 7,6 an. Eine Überprüfung der Messreihen nach dem Versuch zeigte eine zunehmend schlechter werdende Messgenauigkeit der verwendeten pH-Sonde. Da der Fehler nachträglich nicht quantifiziert werden konnte, werden die Ergebnisse für den pH-Wert im Weiteren nicht betrachtet.

Nachdem die infiltrierten 2.000 m³ zurückgefördert waren (EGK = 1), schwankten der Sauerstoffgehalt, die Wassertemperatur und die el. Leitfähigkeit nur geringfü-

gig um die jeweiligen Medianwerte von 0,01 mg/L, 10,5 °C und 497 µS/cm. Keiner der weiteren Sofortparameter zeigte einen ähnlichen Trend wie der pH-Wert.

3.2 Verhalten weiterer ausgewählter hydrochemischer Parameter

Nach dem Überschreiten von EGK 7 begannen die Eisen-Konzentration von < 0,01 auf max. 0,15 mg/L und die Ammonium-Konzentration von ca. 0,1 auf max. 0,2 mg/L anzusteigen. Nach dem kurzzeitigen Anstieg blieben Eisen mit ca. 0,08 mg/L und Ammonium mit ca. 0,15 mg/L annähernd konstant. Die Medianwerte betrugen 0,12 bzw. 0,08 mg/L (**Tabelle 2**). Der $K_{S4,3}$-Wert lag stabil bei etwa 3,9 mmol/L (Median, N = 50). Die Nitrat-Konzentration stieg ab einem EGK von 16 für etwa 50 Tage von < 0,2 auf > 3 mg/L an. Im gleichen Zeitraum ging die Ammonium-Konzentration von 0,15 … 0,20 mg/L auf < 0,1 mg/L zurück. Die Konzentrationen der Hauptkationen Ca, Mg, Na und K schwankten nur geringfügig um die jeweiligen Medianwerte im gesamten Versuchszeitraum. Mit dem Anstieg der Mn-Konzentration stieg die Ca-Konzentration temporär an (+ 10 mg/L), blieb aber in der Größenordnung der vorhergehenden Messwertstreuung. Aufgrund des Anstiegs der Mn-Konzentration wurde das Analysespektrum um Al, As, Cr, Cu, Pb und Zn erweitert. Fast alle analysierten Schwermetalle zeigten durchgängig Messwerte unter der jeweiligen Bestimmungsgrenze (BG, **Tabelle 2**). Nur Zn überstieg mit einem Medianwert von 0,005 mg/L und maximal 0,22 mg/L die BG. Die in **Tabelle 2** angegebenen Schwankungsbreiten zeigen, dass fast alle Beschaffenheitsparameter während des Versuchs annähernd konstant waren.

3.3 Hydraulische Kenngrößen des Brunnens

Während des Versuchs wurden die Wasserstände im Innen- und Außenpegel (IP, AP) des Br. 12 kontinuierlich erfasst und die Absenkung im Vergleich zum Ausgangswasserstand berechnet (**Bild 4**). Im IP wurde der Wasserstand um maximal 3,1 m abgesenkt und im AP um max. 1,5 m. Die Differenz zwischen der Absenkung im IP und AP schwankte in Abhängigkeit von der Förderrate. Bei einer Förderrate von 45 m³/h betrug die Differenz 1,55 m, bei 25 m³/h 0,8 m, bei 15 m³/h 0,38 m und bei 60 m³/h 1,32 m. In den Zeiträumen konstanter Förderraten blieb die Differenz zwischen IP und AP annähernd gleich bzw. zeigte einen leichten Abwärtstrend. Der Medianwert der berechneten spez. Ergiebigkeit ($Q_{spez.}$ = Förderrate/ Absenkung) für den IP betrug 19 m³/(h·m) mit einer Schwankungsbreite von 16-23 m³/(h·m) (1. & 3. Quartil, N = 934, **Bild 5**). Die berechnete spez. Ergiebigkeit stieg für IP und AP im Versuchszeitraum leicht an.

4. Diskussion

4.1 Ursache der Manganfreisetzung

Bei der unterirdischen Aufbereitung wird das im GW gelöste Eisen und Mangan während der Förderphase durch Adsorption an Tonminerale oder die bereits abgeschiedenen Fe- oder Mn(Hydr-)oxide immobilisiert. Während der Infiltrationsphasen wird das adsorbierte Fe^{2+} und Mn^{2+} oxidiert. Die Oxidation des adsorbierten Mangans findet vorwiegend im brunnennahen Raum statt, während Eisen weiter entfernt vom Brunnen oxidiert wird (**Bild 6**, [7]).

Im regulären UNEIS-Betrieb wurde der Br. 12 mit einem EGK von 7 betrieben und förderte 14.000 m³ fast eisen- und manganfreies Grundwasser. Während des

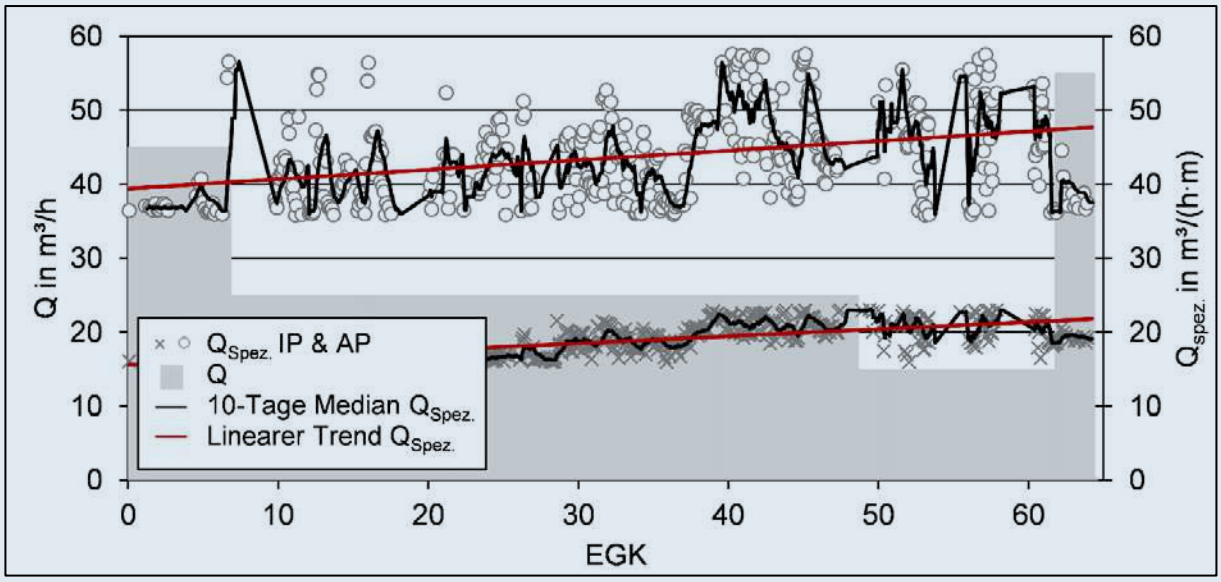

Bild 5: Spezifische Ergiebigkeit für die Absenkungen im IP und AP des Br. 12

Tabelle 2: Statistische Kennwerte aller analysierten Parameter über den Versuchszeitraum

Parameter	Einheit	Min	P_{10}*	Q_1*	Median	Q_3*	P_{90}*	Max	N
Wst. IP	m uROK	11,3	12,3	12,9	13,1	14,3	14,3	14,9	51
Wst. AP	m uROK	11,2	11,7	12,0	12,2	12,7	12,9	13,0	51
$Q_{spez.}$	$m^3/(h \cdot m)$	11	14	15	16	17	20	31	50
pH-Wert	-	6,96	7,11	7,13	7,23	7,52	7,63	7,67	50
O_2 gelöst	mg/L	0,00	0,01	0,01	0,01	0,02	0,02	1,07	50
el. Leitf.	µS/cm	493	495	496	497	498	501	575	50
T	°C	10,3	10,4	10,4	10,5	10,6	10,71	13,4	50
$K_{S4,3}$	mmol/L	3,8	3,8	3,9	3,9	3,9	3,9	4	50
Ca^{2+}	mg/L	80	80	86	88	92	96	106	48
Mg^{2+}	mg/L	6,41	6,46	6,65	6,94	7,20	7,40	7,47	48
Na^+	mg/L	7,79	7,88	7,98	8,71	8,83	9,10	9,22	48
K^+	mg/L	1,06	1,08	1,15	1,21	1,26	1,32	7,06	48
Fe	mg/L	0,005	0,009	0,044	0,076	0,087	0,118	0,421	50
Mn	mg/L	0,003	0,003	0,003	0,006	0,538	0,688	0,720	50
Si	mg/L	0,40	0,40	0,44	0,56	0,57	3,86	3,88	30
Al	mg/L	<0,005	<0,005	<0,005	<0,005	<0,005	<0,005	<0,005	13
As	mg/L	<0,001	<0,001	<0,001	<0,001	<0,001	<0,001	<0,001	12
Pb	mg/L	<0,001	<0,001	<0,001	<0,001	<0,001	<0,001	<0,001	13
Cu	mg/L	<0,001	<0,001	<0,001	<0,001	<0,001	0,0026	0,035	13
Cr	mg/L	<0,0005	<0,0005	<0,0005	<0,0005	<0,0005	<0,0005	0,0005	13
Zn	mg/L	0,003	0,003	0,004	0,005	0,022	0,074	0,220	12
NH_4^+	mg/L	0,025	0,025	0,09	0,12	0,15	0,16	0,2	43
F-	mg/L	0,06	0,08	0,08	0,14	0,17	0,22	0,49	45
Cl-	mg/L	14,6	15,4	15,8	16,4	17,3	18,3	19,2	45
Br-	mg/L	0,1	0,1	0,1	0,1	0,1	0,1	0,1	45
NO_3^-	mg/L	0,02	0,05	0,05	0,16	0,37	3,33	3,42	45
NO_2^-	mg/L	0,025	0,025	0,025	0,025	0,025	0,025	0,025	45
SO_4^{2-}	mg/L	45	46	47	48	49	52	81	45
PO_4^{3-}	mg/L	0,5	0,5	0,5	0,5	0,5	0,5	0,5	45
SAK_{254}	1/m	2,8	2,8	2,9	3,0	3,2	3,2	3,3	3
DOC	mg/L	2,8	2,8	2,9	3,0	3,2	3,2	3,3	3
TOC	mg/L	1,9	3,1	3,3	3,6	4,0	4,4	4,6	11
GH	°dH	12,6	12,7	13,6	14,0	14,5	15,0	16,5	48
KH	°dH	0,2	7,5	10,9	10,9	10,9	10,9	11,2	48
NKH	°dH	1,7	1,8	2,7	3,1	3,7	7,0	16,3	48

* P_{10} & P_{90} = 10- & 90-Perzentil; Q_1 & Q_3 = 1. & 3. Quartil

Versuchs wurde ein Anstieg der Mn-Konzentration ab einem EGK von etwa 30 beobachtet (**Bild 3**). Mit dem Anstieg auf bis zu 0,72 mg/L überstieg die Mn-Konzentration den Hintergrundwert im GW von 0,19 mg/L um bis zu 0,53 mg/L. Rott et al. [4] beobachteten einen Anstieg der Mn-Konzentration bei einem "Crashtest" einer UEE. Bereits ab einem EGK von 2 stieg die Mn-Konzentration auf etwa 0,4 mg/L an und überstieg damit die Konzentration im GW von 0,35 mg/L geringfügig. Die Anstiegskurve der Mn-Konzentration flachte bis zum Versuchsende bei einem EGK von 23 ab, ohne ein Plateau zu erreichen, Fe und Arsen (As) wurden nicht frei-

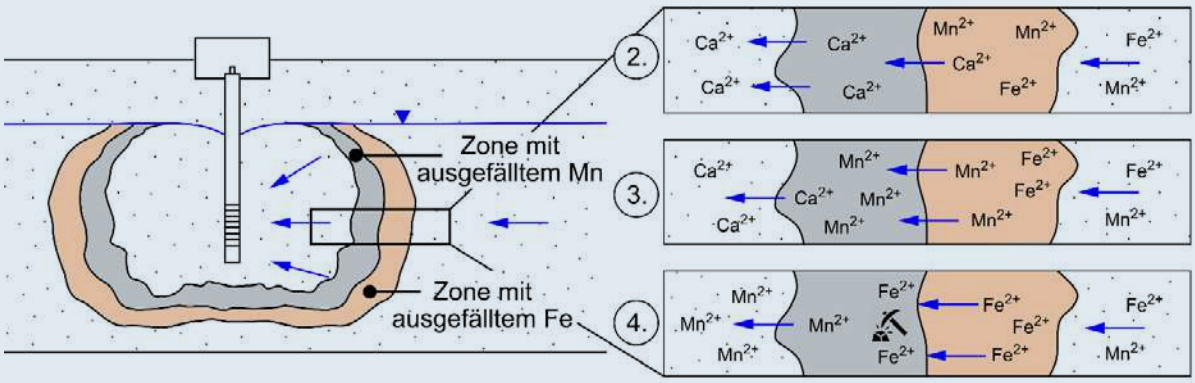

Bild 6: Vermuteter Reaktionsmechanismus der Mn-Freisetzung aus der Oxidationszone, Ausbildung der Reaktionszone geändert nach [21]

gesetzt. Als Ursache der Mn-Freisetzung wurde die Remobilisierung von Mn(Hydr-)oxiden benannt. Der „Crashtest" von Rott et al. [4] wurde durchgeführt, nachdem die Anlage die ersten 23 Infiltrationszyklen durchlief. Außerdem setzte die Entmanganung erst kurz vor dem „Crashtest" ein, sodass bis zum Zeitpunkt des Tests wahrscheinlich nur geringe Mengen Mangan im GWL abgeschieden wurden.

Rössner et al. [3] beobachteten bei der Inbetriebnahme einer UEE einen Anstieg der Mn-Konzentration, nachdem der EGK von 3-4 auf 5 angehoben wurde. Die Mn-Konzentration im Förderwasser war mit 0,8-1,1 mg/L etwa 2,5-3,5-mal höher als die Konzentration im GW (0,3 mg/L). Oren et al. [8] beobachteten den Anstieg der Mn-Konzentration im Förderwasser von Brunnen einer Soil-Aquifer-Treatment-Anlage nach 25 Jahren Betrieb mit geringen Mn-Konzentrationen. Wahrscheinlich führte die Reduktion von Mn-Oxiden im GWL zur Mobilisierung von Mn^{2+}. Durch den stetigen Betrieb wurden die Adsorptionsplätze im GWL in Grundwasserfließrichtung allmählich belegt, wodurch sich eine „Front" erhöhter Mn-Konzentration in Richtung der Brunnen bewegte.

Im WW Eggersdorf war zusammen mit dem Anstieg der Mn-Konzentration ein temporärer Anstieg der Ca-Konzentration um 10 mg/L messbar. Die Fe-Konzentration blieb davon unbeeinflusst (**Bild 3**). Eine mögliche Ursache ist der Kationenaustausch, bei dem im GW gelöstes Fe^{2+} adsorbiert und Ca^{2+} desorbiert [9].

Nach Henning [10] ist auch die Adsorption von Mn^{2+} reversibel und kann durch den Austausch mit anderen Kationen rückgängig gemacht werden. Canfield et al. [11] zeigten an Sedimentproben im Labor, dass die Adsorption von Mn^{2+} nur von unvollständig oxidierten Mn-Oxiden (MnO_x, x<2) umkehrbar ist. Von vollständig oxidierten Manganoxiden war die Adsorption irreversibel und Mn^{2+} konnte nur durch die Reduktion der Manganoxide mobilisiert werden. Da immobilisiertes Mn bei der UEE teilweise nicht als Oxid vorliegt [12] bzw. vorhandene Mn-Oxide meist nicht vollständig oxidiert sind [13], ist die Adsorption von Mn^{2+} häufig umkehrbar. Deshalb kann die Desorption von Mn^{2+} eine Ursache für den beobachteten Anstieg des Mangans sein.

Die Adsorption von Fe^{2+} und Mn^{2+} an Eisen- und Manganoxiden ist vor allem von der jeweiligen Konzentration und vom pH-Wert abhängig [14, 15]. Sharma [15] zeigte für eine Mn-Konzentration von 0,5 mg/L, dass bei pH 7,5 etwa 15-mal mehr Mn an Eisenoxiden adsorbierte als bei pH 6. Bei 1,5 mg/L Mn adsorbierte etwa 40-mal mehr bei pH 7,5 als bei pH 6. Die Adsorptionskapazität der Eisenoxide für Fe^{2+} stieg um den Faktor 3 bei einem Anstieg des pH-Wertes von pH 6 auf pH 7,5. Dabei war die Menge an adsorbiertem Fe^{2+} unabhängig von der Mangankonzentration. Auch bei einer Mn-Konzentration von bis zu 1,5 mg/L adsorbierten 100 % der gelösten 4 mg/L Eisen. Die steigende Adsorptionskapazität bei steigendem pH-Wert wurde auch für die Adsorption von Mn^{2+} an Manganoxiden nachgewiesen [14].

Die Adsorption von Fe^{2+} an Mn-(Hydr)oxiden im inneren Bereich des Reaktionsraumes ist unwahrscheinlich. Manganoxide wirken als Oxidationsmittel für Fe^{2+} und würden durch in den inneren Reaktionsraum eindringendes Eisen reduziert werden (Gl. 1). Henning [10], Kölle [2] und Meyerhoff [7] weisen für den störungsfreien Betrieb einer UEE explizit auf die Gefahr der Mn-Remobilisierung durch ein zu weites Vordringen von Fe^{2+} in den Reaktionsraum hin (z. B. bei zu hohen EGK).

$$MnO_2 + 2Fe^{2+} + 4H_2O \rightarrow Mn^{2+} + 2Fe(OH)_3 + 2H^+ \qquad (1)$$

Aufgrund der Passivierung der Mn-Oxid-Oberflächen

durch das entstehende $Fe(OH)_3$ verläuft die Reaktion am Anfang schnell und wird mit steigender Reaktionsdauer langsamer [16]. Nach Villinski et al. [17] kann die Reaktionsgeschwindigkeit durch die Passivierung langfristig bis zu 1.000-fach geringer sein als zu Beginn. Postma & Appelo [18] zeigten in Säulenversuchen zur Untersuchung der Reaktionskinetik von Gl. 1, dass sich entlang des Fließweges eine Reaktionsfront mit erhöhten Mn^{2+}- und H^+-Konzentrationen ausbildet. Nachdem die Mn-Konzentration ein Maximum erreichte, flachte die Kurve ab und die Mn-Konzentration wurde geringer. Die Fe^{2+}-Konzentration stieg an, bevor das Mangan vollständig ausgetragen wurde und erreichte ein Maximum, nachdem die Mn-Konzentration etwa 0 mg/L betrug [18].

Falls im zuströmenden Grundwasser gelöste biologisch abbaubare Kohlenstoffverbindungen (BDOC) vorhanden sind, ist die Reduktion von zuvor abgeschiedenen Mn-(Hydr)oxiden eine mögliche Ursache der Manganfreisetzung (Gl. 2). Der DOC am OP der GWM beträgt etwa 2,17 mg/L (Median, N = 7, **Tabelle 1**). Während des Versuches wurden im Förderwasser etwa 3 mg/L DOC gemessen (N = 3, **Tabelle 2**). Da es entlang des Fließweges durch den ehemaligen Reaktionsraum nicht zum Abbau des DOC kommt, ist die mikrobielle Reduktion nach (2) unwahrscheinlich. Aufgrund des Alters des GW von Jahrzehnten ist kein BDOC-Anteil zu erwarten, der zu einer Mn-Reduktion und der beobachteten Manganfreisetzung führen könnte.

$$\{CH_2O\} + 212MnO_2(s) + 438H^+ \rightarrow 106CO_2 + 212Mn^{2+} + 16NH_4^+ + HPO_4^{2-} + 318H_2O \quad (2)$$

mit $\{CH_2O\} = (CH_2O)_{106}(NH_3)_{16}(H_3PO_4)$ *[19], vereinfacht BDOC*

Auf Grundlage der Ganglinien der Ca-, Fe- und Mn-Konzentration kann die beobachtete Manganfreisetzung wie folgt erklärt werden (**Bild 6**):

- Am Ende der Infiltration bzw. vor Beginn der Förderung war das Korngerüst innerhalb der Reaktionszone mit einer Schicht aus Fe- und Mn-Oxiden mit einer hohen Adsorptionskapazität überzogen [1, 14]. Da das Infiltrat weitestgehend eisen- bzw. manganfrei war, waren die freien Adsorptionsplätze vor allem durch Ca^{2+}, Mg^{2+} oder K^+ besetzt.
- Mit dem Beginn der Förderung wurde das Infiltrat zurückgepumpt und eisen- und manganreicheres GW drang in die Reaktionszone ein. Entlang des Fließweges zum Brunnen konnte gelöstes Mn zwar adsorbieren, wurde aber zunächst durch Fe^{2+} verdrängt, bis der Bedarf an freien Adsorptionsplätzen für Eisen gedeckt war [11].
- Entlang des Fließweges nahm die Adsorptionskapazität ab und eine Sättigungsfront für Fe^{2+} und Mn^{2+} wanderte nach innen.
- Fe^{2+} erreichte den inneren Bereich der Reaktionszone, in dem vorher vorwiegend Mn abgeschieden wurde. Durch das Fe^{2+} wurden die Mn-Oxide reduziert und Mn^{2+} freigesetzt (Gl. 1). Aufgrund der anfangs hohen Reaktionsgeschwindigkeit stieg die Mn-Konzentration schnell an (**Bild 3**). Durch die Desorption von Ca^{2+} von den Mn-Oxiden stieg die Ca-Konzentration im Förderwasser zeitgleich an.
- Das Abflachen der Mn-Ganglinie kann auf die fortschreitende Passivierung zurückgeführt werden. Aufgrund der Passivierung durch Fe-(Hydr)oxide verringerte sich die reaktive Oberfläche der Mn-Oxide und weniger Mn^{2+} wurde freigesetzt [16, 17]. Darüber hinaus kann der anhaltende Austrag zum Abflachen der Kurve beitragen [18]. Da davon ausgegangen werden kann, dass die Mn-(Hydr)oxide im Überschuss im

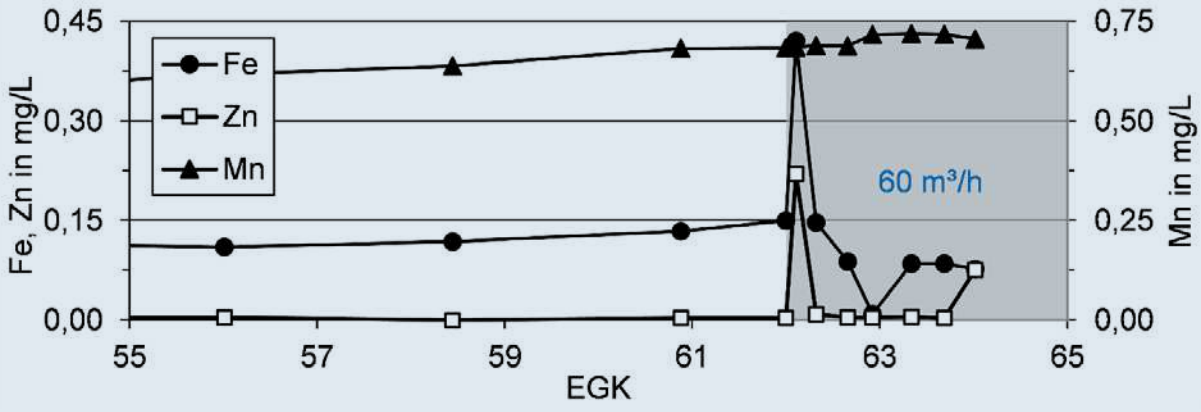

Bild 7: Kurzzeitiger Anstieg von Fe und Zn nach der Steigerung der Förderrate von 15 auf 60 m^3/h

Tabelle 3: Maximale Konzentrationen ausgewählter Schwermetalle im Vergleich zum Trinkwassergrenzwert, alle Angaben in mg/L

Parameter	Grenzwert [30]	max. Konz. während des Versuchs
Al	0,2	<0,0005
As	0,01	<0,001
Cr	0,05	<0,0005
Cu	2,0	0,035
Pb	0,01	<0,001
Zn	-	0,22

Vergleich zu Fe^{2+} vorhanden waren, war bis zum Versuchsende kein Durchbruch von Fe^{2+} messbar.

4.2 Entwicklung der Wasserbeschaffenheit bei dauerhafter Förderung

4.2.1 Freisetzung von Eisen und Mangan

Mit der Annahme, dass der o. g. Reaktionsmechanismus ( ) die Hauptursache der Mn-Freisetzung ist, kann die Entwicklung der Mn-Konzentration mithilfe der Fe-Konzentration im GW abgeschätzt werden. An der GWM im GW-Zustrom wurden zwischen 0,7 mg/L (OP) und 1 mg/L Fe (UP) gemessen. Bei annähernd gleichen Molmassen von Fe und Mn könnten gemäß Gl. 1 max. 0,35-0,5 mg/L Mn^{2+} zur Hintergrundkonzentration von ca. 0,2 mg/L freigesetzt werden. Dies entspricht etwa 0,6-0,7 mg/L. Das gemessene Maximum von 0,72 mg/L (**Tabelle 2**) entspricht diesem Wert bzw. liegt leicht darüber. Eine mögliche Erklärung ist die Kumulation des freigesetzten Mn^{2+} entlang des Fließweges zu einer „Welle" [8, 18]. Das heißt, wenn die maximale Hintergrundkonzentration etwa 1 mg/L Fe beträgt (OP), sollte die Mn-Konzentration bei dauerhafter Förderung nicht über 0,7 mg/L ansteigen und der zuletzt gemessene Wert stellte wahrscheinlich das Maximum dieser Welle dar.

Seit seiner Inbetriebnahme im November 2002 förderte der Br. 12 insgesamt $2{,}35 \cdot 10^6$ m^3 GW. Mit der Annahme, dass das Förderwasser manganfrei war und damit stets ca. 0,2 mg/L Mn ($c(Mn_{GW})$ im GWL verblieben, wurden seit der Inbetriebnahme insgesamt ca. 470 kg Mn abgeschieden. Falls die Mn-Konzentration nach der Umstellung in der Größenordnung von 0,7 mg/L bleibt, werden ca. 0,5 mg/L zusätzlich zur Mn-Konzentration im zuströmenden GW (ca. 0,2 mg/L) ausgetragen. Bei einer kontinuierlichen Förderung von 60 m^3/h mit 0,7 mg/L Mn würden fast zwei Jahre vergehen, bis die abgeschiedenen 470 kg Mn vollständig ausgetragen sein würden. Das komplexe Zusammenwirken der Sorptions-, Auflösungs- und Passivierungsprozesse lässt jedoch eine genaue Prognose zur Dauer der Freisetzung nicht zu. Es ist davon auszugehen, dass der größte Teil des bei der UEE in den vergangenen 15 Jahren zurückgehaltenen Mangans nicht mehr desorbierbar bzw. schwer reduzierbar ist. Bei Berücksichtigung eines geringer werdenden Mn-Austrages würde sich im Förderwasser innerhalb von zwei Jahren eine deutlich geringere Mn-Konzentration einstellen als im Versuch. Aufgrund der fortschreitenden Passivierung der Mn-(Hydr)oxide wird sich die Mn-Konzentration langfristig vermutlich wieder der Konzentration im GW von ca. 0,2 mg/L nähern.

Eine Freisetzung von Fe und ein Anstieg der Fe-Konzentration über die Hintergrundkonzentration im zuströmenden GW sind unwahrscheinlich. Da die mikrobielle Reduktion der Mn-(Hydr)oxide als unwahrscheinlich bewertet wurde und die mikrobielle Reduktion von Fe-(Hydr)oxiden theoretisch erst nach der Manganreduktion stattfindet [20], ist nicht mit einer mikrobiellen Reduktion der Fe-(Hydr)oxide zu rechnen. Aufgrund der hohen Affinität von Fe^{2+} für Fe-(Hydr)oxide [15] sind auch eine Desorption bzw. ein Kationenaustausch, bei dem Fe^{2+} freigesetzt wird, unwahrscheinlich.

4.2.2 Keine Freisetzung weiterer Schwermetalle

Da Eisen- und Mangan(hydr)oxide, ähnlich wie organisches Material, eine hohe Bindungskapazität für Schwermetalle besitzen, können diese bei der Auflösung der (Hydr)oxide ebenfalls freigesetzt werden [22, 23]. Schwermetalle mit einer hohen Affinität zu Eisen- bzw. Mangan(hydr)oxiden sind beispielsweise Kupfer (Cu), Blei (Pb), Cobalt (Co), Zink (Zn), Nickel (Ni) [18, 24, 25]. Blei, Kupfer und Zink besitzen die höchste Adsorptionsfähigkeit [26, 27]. Außerdem werden erhöhte Konzentrationen von Arsen (As) und Chrom (Cr) häufig mit der Auflösung von Fe- oder Mn-(hydr)oxiden in Verbindung gebracht [28, 29]. Um eine mögliche Freisetzung von Schwermetallen infolge der beobachteten Mn-Freisetzung zu bewerten, wurden mit dem Beginn des Anstieges von Mn auch Al, As, Cr, Cu, Pb und Zn in das Überwachungsprogramm aufgenommen. **Tabelle 2** zeigt, dass Al, As, Cr, Cu und Pb in fast allen Proben unterhalb der Bestimmungsgrenze lagen. Mit der Steigerung der Förderrate von 15 auf 60 m^3/h zu Versuchsende war nur ein kurzzeitiger Anstieg von Fe und Zn messbar (**Bild 7**).

Die Konzentrationen von Mn sowie Al, As, Cr, Cu und Pb blieben von der Steigerung der Förderrate unbeeinflusst. **Tabelle 3** zeigt außerdem, dass die Konzentrationen der zusätzlich analysierten Schwermetalle deutlich unterhalb der Trinkwassergrenzwerte lagen [30]. Da die kurzzeitigen Konzentrationsspitzen von Fe und Zn nur Einzelwerte waren, wird nicht von einer Freisetzung ausgegangen. Durch

die plötzliche Steigerung der Förderrate und höhere Fließgeschwindigkeiten wurde möglicherweise partikuläres Eisen aus der unmittelbaren Umgebung des Brunnens mobilisiert. Auf Grundlage der Ergebnisse wird das Risiko eines zusätzlichen Aufbereitungsaufwandes für andere Schwermetalle auch bei einer anhaltenden Mn-Freisetzung als sehr gering eingeschätzt.

4.3 Hydraulische Auswirkungen einer dauerhaften Förderung

Bild 4 zeigt, dass der Eintrittsverlust (vereinfacht als Different IP-AP) während der Zeiträume gleicher Förderraten des Br. 12 nur geringfügig schwankte bzw. einen leichten Abwärtstrend zeigte. Dies deutet darauf hin, dass die dauerhafte Förderung bisher keinen negativen Einfluss auf den Zustand des Filterrohres hatte. Die gleich verlaufenden, leicht ansteigenden Trends der berechneten spez. Ergiebigkeit für IP und AP bestätigen dies (**Bild 5**). Da sich der AP in der Filterkiesschüttung befindet, sind keine Aussagen zu einer möglichen Verockerung der Kiesschüttung möglich. Weil die O_2-Konzentration im Förderwasser nach der Rückförderung des Infiltrats dauerhaft bei ≤ 0,02 mg/L lag, ist eine Verockerung unwahrscheinlich. Ein Vergleich der spezifischen Ergiebigkeit von 49,5 $m^3/(h{\cdot}m)$ nach Inbetriebnahme des Br. 12 im Jahr 2002 mit der aus dem Jahr 2018 von 19 $m^3/(h{\cdot}m)$ (IP) weist auf eine Brunnenalterung im Bereich der Filterschlitze und/oder der Filterschüttung hin. Bei Berücksichtigung des Anstiegs der Fe-Konzentration, unmittelbar nach dem Überschreiten des jahrelangen Betriebspunktes bei EGK 7, deutet dies auf ein mögliches Optimierungspotenzial des Brunnenbetriebes hin.

5. Zusammenfassung

Das Wasserwerk Eggersdorf soll nach 40 Jahren Betrieb saniert werden. Aufgrund der ungleichmäßigen Auslastung bzw. Nutzung der 16 UEE-Brunnen (UNEIS-Verfahren) und möglichen wirtschaftlichen Vorteilen werden für die geplante Sanierung zwei Varianten betrachtet. Eine Variante ist die Sanierung und anschließende Umnutzung der UEE-Brunnen für die ausschließliche Grundwasserförderung mit einer oberirdischen Enteisenung / Entmanganung. Um die mögliche Umstellung zu simulieren, förderte der Br. 12 kontinuierlich vom 30.08.2017 bis 20.04.2018 Grundwasser zu einem Containerwasserwerk. Auf Grundlage der Ergebnisse sollten die Auswirkungen dieser Variante hydrochemisch und hydraulisch bewertet werden. Für die Planung der nach der Umstellung notwendigen oberirdischen Aufbereitung sollte die zu erwartende Eisen- und Mangankonzentration im Förderwasser abgeschätzt werden.

Im Verlauf des Testbetriebs stieg die Mn-Konzentration ab etwa EGK 30 kontinuierlich an. Aus der ehemaligen Reaktionszone wurden bis zu 0,5 mg/L Mangan freigesetzt, so dass die Mn-Konzentration im Förderwasser mit ca. 0,7 mg/L die Konzentration im GW-Zustrom (ca. 0,2 mg/L) um den Faktor 3,5 überstieg. Auf Grundlage der Ganglinien der Ca-, Fe- und Mn-Konzentration und unter Berücksichtigung des Verlaufs des pH-Werts sind die Desorption von Mn^{2+} und die chemische Reduktion von abgeschiedenen Mn-(Hydr)oxiden durch Fe^{2+} als Ursache der Mn-Freisetzung zu vermuten. Mit der Annahme, dass mit dem GW max. etwa 1 mg/L Fe zuströmen, sollte die Mn-Konzentration bei dauerhafter Förderung nicht über 0,70-0,75 mg/L ansteigen. Aufgrund einer zu erwartenden fortschreitenden Passivierung der Mn-(Hydr)oxide durch Fe-Verbindungen und das komplexe Zusammenwirken der Sorptions- und Auflösungsprozesse kann die Dauer der Freisetzung schwer prognostiziert werden. Eine Abschätzung zeigt, dass sich die beobachtete Mn-Konzentration von ca. 0,7 mg/L innerhalb von zwei Jahren deutlich verringern wird. Langfristig wird sich die Mn-Konzentration wieder der Hintergrundkonzentration im GW von 0,2 mg/L nähern.

Eine Freisetzung von Fe und ein Anstieg der Fe-Konzentration auf Werte über der Hintergrundkonzentration im zuströmenden GW sind nicht zu erwarten. Trotz Freisetzung von Mangan kommt es nicht zu einer Belastung des Förderwassers durch andere Schwermetalle wie Aluminium, Arsen, Blei, Chrom, Kupfer und Zink. Die Konzentrationen der analysierten Schwermetalle lagen deutlich unter den Grenzwerten der Trinkwasserverordnung.

Danksagung

Diese Arbeit wurde als Kooperation zwischen dem Wasserverband Strausberg-Erkner (WSE) und dem Lehrgebiet Wasserwesen der HTW Dresden durchgeführt. Die Autoren danken dem ESF für die finanzielle Unterstützung von S. Paufler (Stipendium-Nr. 200031585).

Literatur

[1] *Eichhorn, D.*: Beitrag zur Theorie der Eisenelimination bei der Untergrundwasseraufbereitung. Dissertation, Fakultät für Bau-, Wasser- und Forstwesen, Technische Universität Dresden (1985).

[2] *Kölle, W.*: Aufbereitung im Aquifer unter Verwendung von nitrathaltigem Wasser. Stuttgarter Berichte zur Siedlungswasserwirtschaft 115 (1991), 89-108.

[3] *Rössner, U, Sailer, C, Langert, J, Plaßmann, C.*: Einfahrbetrieb der Unterirdischen Enteisenung und Entmanganung an der Wassergewinnung Kaldenkirchen (Niederrhein). ewp Energie-Wasser-Praxis 12 (2017), 92-95.

[4] *Rott, U., Meyer, C., Friedle, M.*: Residue-free removal of arsenic, iron, manganese and ammonia from groundwater. Wat. Sci. Technol. - Water Supply 2 (2002) Nr. 1, 17-24.

[5] *Duffield, G.M.*: AQTESOLV for windows version 4.5 user's guide. HydroSOLVE, Inc., Reston (2007).

[6] *Theis, C.V.*: The relation between the lowering of the piezometric surface and the rate and duration of discharge of a well using

groundwater storage. Am. Geophys. Union Trans. 16 (1935), 519-524. doi: https://doi.org/10.1029/TR016i002p00519.

[7] *Meyerhoff, R.*: Entwicklung von Planungs- und Anwendungskriterien für die in-situ-Aufbereitung eisen- und manganhaltiger Grundwässer. Dissertation, Stuttgarter Berichte zur Siedlungswasserwirtschaft 139 (1996), 233 S.

[8] *Oren, O., Gavrieli, I., Burg, A., Guttman, J., Lazar, B.*: Manganese mobilization and enrichment during soil aquifer treatment (SAT) of effluents, the Dan Region Sewage Reclamation Project (Shafdan), Israel. Environ. Sci. Technol. 41 (2007) Nr. 3, 766-772. doi: 10.1021/es060576+.

[9] *van Halem, D., Moed, D.H., Verberk, J.Q.J.C., Amy, G.L., van Dijk, J.C.*: Cation exchange during subsurface iron removal. Water Research 46 (2012) Nr. 2, 307-315. doi: 10.1016/j.watres.2011.10.015.

[10] *Henning, A.-K.*: Biologische Mechanismen bei der unterirdischen Aufbereitung von Grundwasser am Beispiel des Mangans. Dissertation, Stuttgarter Berichte zur Siedlungswasserwirtschaft 176 (2004), 149 S.

[11] *Canfield, D.E., Thamdrup, B., Hansen, J.W.*: The anaerobic degradation of organic matter in Danish coastal sediments: Iron reduction, manganese reduction, and sulfate reduction. Geochim. Cosmochim. Acta 57 (1993) Nr. 16, 3867-3883. doi: https://doi.org/10.1016/0016-7037(93)90340-3.

[12] *Mettler, S., Abdelmoula, M., Hoehn, E., Schoenenberger, R., Weidler, P., von Gunten, U.*: Characterization of iron and manganese precipitates from an in situ ground water treatment plant. Ground Water 39 (2001) Nr. 6, 921-930. doi: 10.1111/j.1745-6584.2001.tb02480.x.

[13] *Riedel, E., Janiak, C.*: Anorganische Chemie. Walter de Gruyter, Berlin, New York, 961 S., 2003.

[14] *Morgan, J.J., Stumm, W.*: Colloid-chemical properties of manganese dioxide. J. Colloid Interface Sci. 19 (1964) Nr. 4, 347-359.

[15] *Sharma, S.K.*: Adsorptive iron removal from groundwater. Dissertation, Wageningen University, 200 S., 2001.

[16] *Postma, D.*: Concentration of Mn and separation from Fe in sediments - I. Kinetics and stoichiometry of the reaction between birnessite and dissolved Fe(II) at 10°C. Geochim. Cosmochim. Acta 49 (1985) Nr. 4, 1023-1033. doi: https://doi.org/10.1016/0016-7037(85)90316-3.

[17] *Villinski, J.E., Saiers, J.E., Conklin, M.H.*: The Effects of Reaction-Product Formation on the Reductive Dissolution of MnO_2 by Fe(II). Environ. Sci. Technol. 37 (2003) Nr. 24, 5589-5596. doi: 10.1021/es034060r.

[18] *Postma, D., Appelo, C.A.J.*: Reduction of Mn-oxides by ferrous iron in a flow system: column experiment and reactive transport modeling. Geochim. Cosmochim. Acta 64 (2000) Nr. 7, 1237-1247. doi: https://doi.org/10.1016/S0016-7037(99)00356-7.

[19] *Jacobs, L.A., von Gunten, H.R., Keil, R., Kuslys, M.*: Geochemical changes along a river-groundwater infiltration flow path: Glattfelden, Switzerland. Geochim. Cosmochim. Acta 52 (1988) Nr. 11, 2693-2706. doi: https://doi.org/10.1016/0016-7037(88)90038-5.

[20] *Stumm, W., Morgan, J.J.*: Aquatic chemistry. Chemical equilibria and rates in natural waters. Wiley, New York, 1.003 S., 1996.

[21] *Hartmann, U., Wingrich, H.*: Untersuchungen zur Enteisenung und Entmanganung im Grundwasserleiter. Wasserwirtschaft Wassertechnik 33 (1983) Nr. 8, 280-285.

[22] *Davranche, M., Bollinger, J.C.*: Heavy metals desorption from synthesized and natural iron and manganese oxyhydroxides: Effect of reductive conditions. J. Colloid Interface Sci. 227 (2000a) Nr. 2, 531-539. doi: https://doi.org/10.1006/jcis.2000.6904.

[23] *Davranche, M., Bollinger, J.C.*: Release of metals from iron oxyhydroxides under reductive conditions: Effect of metal/solid interactions. J. Colloid Interface Sci. 232 (2000b) Nr. 1, 165-173. doi: 10.1006/jcis.2000.7177.

[24] *von Gunten, H.R., Karametaxas, G., Krähenbühl, U., Kuslys, M., Giovanoli, R., Hoehn, E., Keil, R.*: Seasonal biogeochemical cycles in riverborne groundwater. Geochim. Cosmochim. Acta 55 (1991) Nr. 12, 3597-3609. doi: https://doi.org/10.1016/0016-7037(91)90058-D.

[25] *von Gunten, H.R., Kull, T.P.*: Infiltration of inorganic compounds from the Glatt river, Switzerland, into a groundwater aquifer. Wat. Air Soil Poll. 29 (1986) Nr. 3, 333-346. doi: https://doi.org/10.1007/BF00158764.

[26] *Nicholson, K., Eley, M.*: Geochemistry of manganese oxides: metal adsorption in freshwater and marine environments. In: Nicholson et al. (eds.) Manganese Mineralization: Geochemistry and Mineralogy of Terrestrial and Marine Deposits, Geological Society Special Publication 119 (1997), 309-326. doi: https://doi.org/10.1144/GSL.SP.1997.119.01.20.

[27] *Gilkes, R.I., McKenzie, R.M.*: Geochemistry and Mineralogy of Manganese in Soils. In: Graham et al. (eds.) Manganese in Soils and Plants, 344 S., Kluwer Academic Publishers, Dordrecht, Boston, London, 1988.

[28] *Ho, C.P., Hseu, Z.Y., Iizuka, Y., Jien, S.H.*: Chromium Speciation Associated with Iron and Manganese Oxides in Serpentine Mine Tailings. Environ. Eng. Sci. 30 (2013) Nr. 5, 241-247. doi: 10.1089/ees.2012.0046.

[29] *Postma, D., Mai, N.T.H., Lan, V.M., Trang, P.T.K., Sø, H.U., Nhan, P.Q., Larsen, F., Viet, P.H., Jakobsen, R.*: Fate of Arsenic during Red River Water Infiltration into Aquifers beneath Hanoi, Vietnam. Environ. Sci. Technol. 51 (2017) Nr. 2, 838-845. doi: 10.1021/acs.est.6b05065.

[30] TrinkwV: Trinkwasserverordnung in der Fassung der Bekanntmachung vom 10. März 2016 (BGBl. I S. 459), die zuletzt durch Artikel 1 der Verordnung vom 3. Januar 2018 (BGBl. I S. 99) geändert worden ist, 45 S., 2018.

Autoren:

Sebastian Paufler
(Korrespondenzautor)
sebastian.paufler@htw-dresden.de
Hochschule für Technik und Wirtschaft Dresden
Friedrich-List-Platz 1
01069 Dresden

Thomas Grischek
Hochschule für Technik und Wirtschaft Dresden
thomas.grischek@htw-dresden.de
Friedrich-List-Platz 1
01069 Dresden

Martin Ruppert
Wasserverband Strausberg-Erkner
Am Wasserwerk 1
15344 Strausberg